Journal of Double Star Observations

Speckle Interferometry of Close Visual Binaries

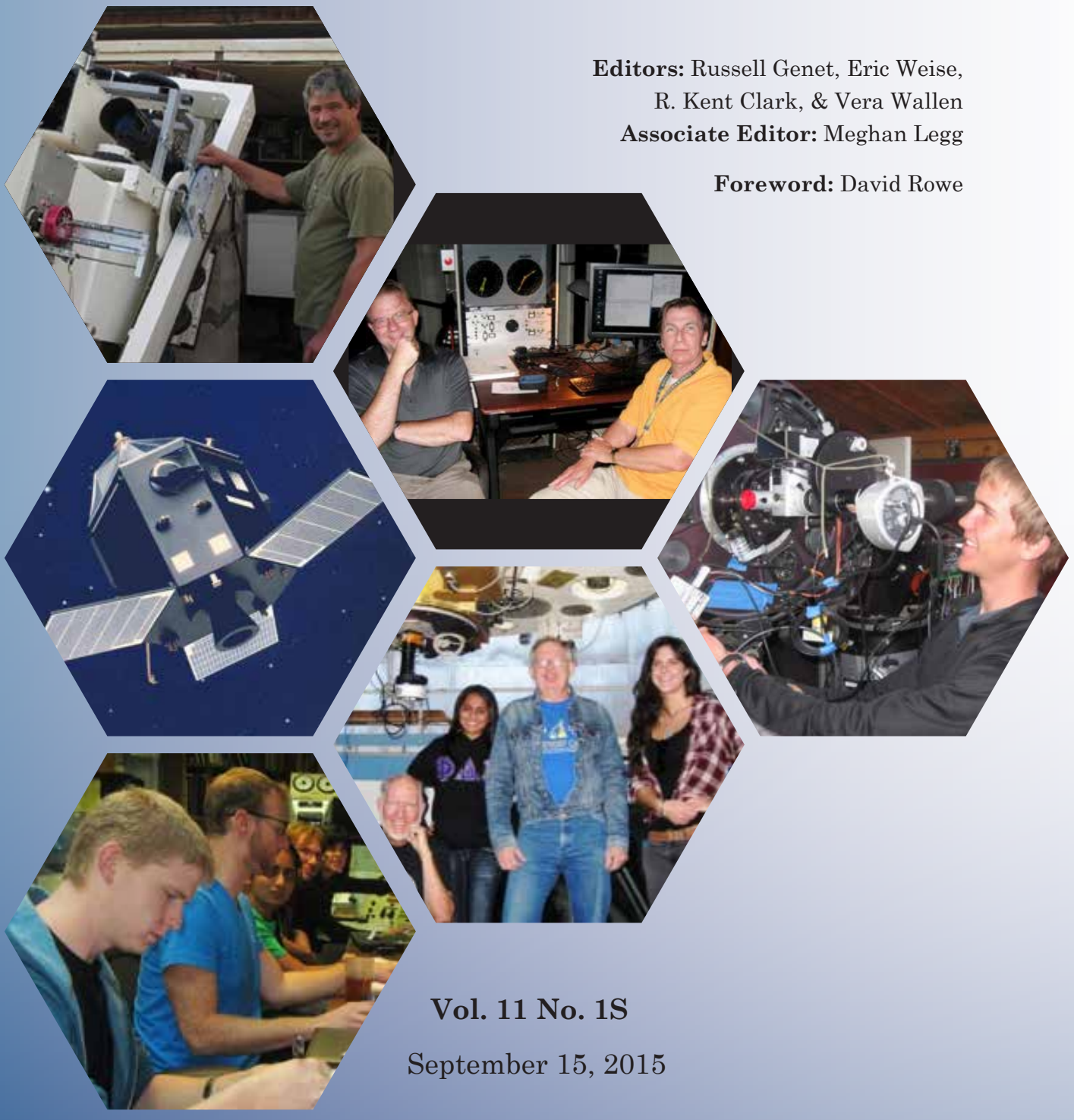

Editors: Russell Genet, Eric Weise, R. Kent Clark, & Vera Wallen
Associate Editor: Meghan Legg

Foreword: David Rowe

Vol. 11 No. 1S

September 15, 2015

Contents

Editorial

This is a special issue of the *Journal of Double Star Observations.* Special issues bring related papers together. This promotes ease of access for readers, since the related papers are not spread throughout a number of different issues. Special issues also facilitate additional dissemination as a book.

This special issue of the Journal of Double Star Observations is being published simultaneously as a book entitled Speckle Interferometry of Close Visual Doubles, published by the Collins Foundation Press. We thank the Society for Astronomical Sciences for permission to reprint the papers starting on pages 226, 234, & 343. The paper starting on page 340 previously appeared in the Journal of Double Star Observations.

Special issues may be a set of papers on a single topic, such as speckle interferometry, or may be a set of papers resulting from a conference or a seminar. While the bulk of the papers in a single-topic special issue are original papers, some papers from earlier issues of the *JDSO* or other journals may be included to round out a topic or provide proper credit to earlier work.

Regular, quarterly issues of the *JDSO* are edited and formatted by the *JDSO* editors. This allows papers to be submitted in almost any format. On the other hand, special issues of the *JDSO* are formatted following very specific instructions that allow the merging of the papers together with minimal effort, as well as easing their additional publication as a book when desired.

To simplify the preparation of special issue papers, the papers may be prepared in Google Docs, Pages, or MS Word, following special issue Instructions to Authors. Papers prepared in Google Docs or Pages are submitted as MS Word.docx papers, using the "save as" function, for final merging and editing. An additional simplification that eases author preparation is the use of single instead of two-column format.

Detailed Instructions to Authors for writing and formatting special issue papers will be provided in the next special issue of the *JDSO*. Many of these instructions have been borrowed from the Instructions to Authors for the *Astronomical Journal* and the *Astrophysical Journal.* We thank the *AJ* and *ApJ* for permission to adopt many of their instructions.

Editors

R. Kent Clark and Russell Genet

Special Issue Guest Editors

Eric Weise, Vera Wallen, Meghan Legg, and Cheryl Genet

Foreword

I received an email in late spring 2012 from Russ Genet. Russ had become interested in speckle interferometry as an outgrowth of his many years of teaching astronomical research by way of at-the-eyepiece measurements of double stars. He had just acquired a Luca-S emCCD camera and needed a telescope to try it on. The email described the camera and the observing program and asked if I knew of "a telescope in the 0.5 to 2 meter range" that could be used to make speckle observations. Russ knew that I had an operational PlaneWave Instruments CDK20 at my observatory deep in the Mojave desert. It has an aperture of 20" which satisfied his lower cutoff limit. I was also aware that Russ knew far more than I did about the availability of telescopes in this size range. Clearly, he was on a fishing expedition.

I took a brief look into speckle interferometry and, like Russ, became fascinated with the subject. A long sequence of short exposure images is taken of an object, most often a double star, and the collection is processed in the Fourier domain, where the average power spectrum is computed. The power spectrum retains all of the high-spatial-frequency information available from the full aperture of the telescope, and upon taking the inverse Fourier transform, one finds the sub-arcsecond double star sparkling within the symmetric sidelobes of the autocorrellelogram, defiantly disobeying our well-known seeing-limited aphorism. Of course, I was hooked.

So, Russ and I began planning an observing run at Pinto Valley Observatory (PVO) for mid-November. PVO is a small facility with a cabin, a bunkhouse, and an observatory. It is completely off-grid, with energy from solar panels and water from a well. It had old batteries that no longer held a complete charge. The 20" corrected Dall-Kirkham telescope and its German Equatorial mount were original prototypes. The telescope worked well but the mount was a bit cranky. The RA gear had 50 arcseconds of periodic error that repeated 15 times per rotation.

Speckle interferometry sounds simple: Center a double star on a high-speed, low-noise camera. Take a thousand 20-millisecond images. Process the subsequent "FITS cube" using free software. However, in order to take advantage of the resolution that one can achieve with the technique, the full-resolution diffraction disk must be oversampled by a factor of 5 to 10 times. In practice, this means stacking Barlows before the camera until the effective focal ratio of the telescope is something around f/50 and the field of view is less than an arcminute. The old mount with its large backlash and periodic error was not going
to work.

I called my old friend Dan Gray, the man behind Sidereal Technology, and he said that he would be delighted to come down from Portland and volunteered to put high resolution on-axis encoders on the mount. Dan and I had worked together for many years on direct-drive motors and on-axis encoders, and Dan's new controller was capable of using measurements from encoders mounted directly on the axis, thus bypassing the problems in the gear train. This would solve the problem of finding the double stars, or so we thought.

Russ asked if he could bring an assistant and I said that was fine. On the Saturday night of a star party in the desert, I have always make cedar-planked salmon on the Baja-grill, and in order to size the chunk of salmon, about a week before the run I asked Russ if he was bringing a student. Yes, he said. In fact, he said, he had invited 8 students and expected all of them to join us. Russ is very enthusiastic and sometimes, in his excitement, he forgets the usual courtesies. Anyway, the cabin and its infrastructure can't support such a large group, and so, after threatening to cancel the run, Russ grudgingly capitulated into bringing only one student, Joe Richards, a brilliant and hardworking young man with a love of telescopes, astronomy, and image processing.

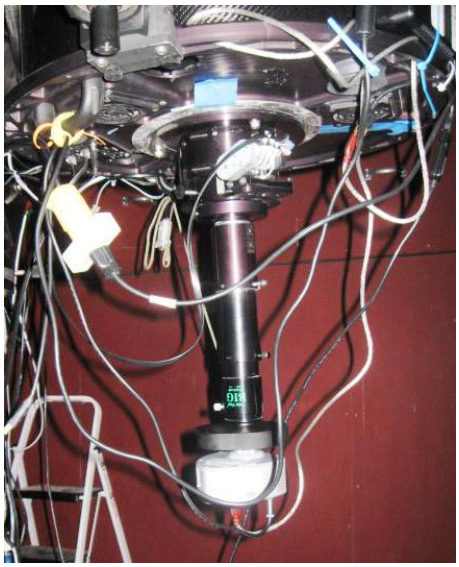

A stack of Barlows was used to increase the focal ratio of the telescope from its native f/6.8 to approximately f/50. The stack was followed by a filter wheel and the Andor Luca-S camera. As this image demonstrates, careful planning for cables and wire is a must on modern equipment.

A day before the run, Dan arrived with a new controller, encoder readheads, and encoder tape. The idea was to fasten the readheads to a mount that was not designed for readheads, and to mount the tape on the aluminum housing of the GEM that was not machined to the accuracy needed to hold the tape. As it turns out, the high-resolution tape encoder technology requires rather exacting placement of the readhead with respect to the tape, including tip, tilt, yaw, and spacing.

Dan had machined the mounting brackets for the readheads from photographs of the mount that we had taken six months earlier, and they worked remarkably well considering the circumstances. Dan tweaked the brackets with a hand file in order to get the readheads aligned properly, and mounted the tape in an ingenious way that eliminated the problem of differential thermal expansion between the aluminum housing and the stainless steel encoder tape. Only one problem remained. The distance between the tape and the readhead changed as the mount was rotated about the RA axis because the outside of the housing had a few thousandths of an inch of runout. Nobody cares about the accuracy of the *outside* of a housing, right?

Dan asked for Scotch Tape. We were out of luck in the cabin so I drove to the nearest neighbor and borrowed a roll, all the while thinking that this is crazy. Dan then spent the next eight hours applying and removing the sticky tape, filing the brackets, and tweaking the position of the readheads while observing the behavior of the encoders as the axes were rotated. I would have given up in an hour, realizing the problem was hopeless, especially without an indicator. Hopeless? Not! In the end, after a long day of seemingly Sisyphean persistence, Dan got both encoders to work flawlessly. Good thing.

My friend Jonah Hare had spent the previous day upgrading and checking software and hardware on the telescope, and installing and testing a wireless network between the cabin and observatory, a run of about 100 meters. For the first time at PVO we had full control of the telescope, camera, and mount without being in the observatory. November evenings get cold in the high desert, and it was a joy to operate the equipment from the cabin where a hot fire in the stove kept us all warm.

Dan installing high-resolution on-axis encoders on the Pinto Valley Observatory's telescope mount. In the end it took hand files and Scotch tape to get them to work.

Russ and Joe arrived Friday evening and we installed the long Barlow stack and the camera. The practical problems were quickly apparent. The very small field of view made it impossible to find a star to focus the system, and the out of focus images made it impossible to find a star. Anyone that's tried it will immediately know what I'm talking about. The solution was to remove the science camera and put the main imaging camera back on, do a full mount model using Sitech and PointXP, then swap the main camera for the science camera and start hunting for a bright star. With luck and persistence, a star was found to focus with, an offset initialization was performed, and we were off and running…

…until we tried to find the first target double. Nothing. The field of view was indeed very small. The Barlow stack was flexible and the telescope had other un-modeled errors, all of which conspired to lower the chances of finding the target to something close to zero. We all sat around the small kitchen table staring at the laptop, trying various unsuccessful search strategies by hand, and arguing a bit about the best course of action. Finally, Dan took his laptop and sat in the chair by the fire and wrote a square spiral search in VB Script. In a couple of hours he had it working. After a normal, but unsuccessful, GoTo, the search script was started and the real-time image from the science camera was watched very carefully. When the target was detected by eye, the Stop Search button was clicked. Because the search space was so large, the search speed needed to be quite high, and the target would fly by and was often outside of the field of view by the time the operator hit the Stop button. So Dan wrote a routine that allowed the square spiral search to be played slowly backwards, and the target would gently drift back into view.

Late that evening we acquired our fist FITS cube of a known double. Russ opened the data in Florent Losse's REDUC software and processed it. I still remember the moment vividly. It was magic. A double star having a separation much less than the seeing limit was fully resolved in the autocorrellelogram. In fact, as someone said at the time, "You could drive a truck through it". In the end, it all worked and we went to bed.

The next night was mostly about logistics and data recording. As simple as it sounds, there's a lot to it. A massive spreadsheet was created to record all the camera settings, the object designations, the time of observation, the reference star information, and the dozen other things that might be needed in the future when details have been forgotten. Dan, Jonah, and I left it to Russ and Joe to work out.

Dan, Dave, Joe, and Russ passionately discussing the problems and potential solutions for finding the science targets. The telescope and science camera were being controlled via a wireless network and remote desktop software from the warmth and comfort of the cabin.

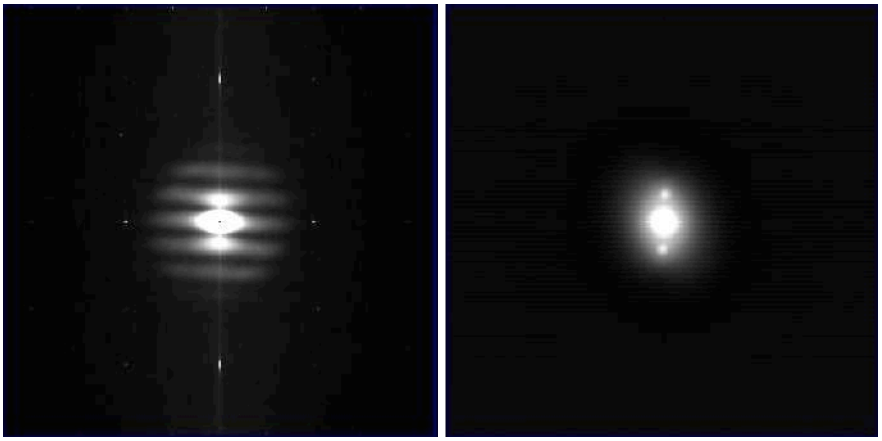

One of the first double star reductions from Pinto Valley Observatory. It was pure magic. The image on the left is the averaged power spectrum showing fringes from the double. The image on the right is the Fourier transform of the power spectrum, known as the autocorrellelogram. The sidebands clearly show that the object is double. In speckle interferometry the autocorrelation will always have two sidebands. There are techniques, including bispectrum analysis, that can be used to create a true image.

The third and final night was the science run. Even with only five people, the cabin, observatory, and bunkhouse require a surprising amount of electrical energy over the course of four days. It's easy to forget to turn off lights; and laptops, cameras, fans, and mount consume lots of energy over the long days and longer nights. The electric coffee percolator, toaster, and 240 Volt water pump are also demanding loads. For 11 year old batteries, it was too much. On the evening of the science run, I noticed the batteries were a bit on the low side and I warned the team that under no circumstances should the batteries be allowed to drop below 23.8 Volts, the point at which battery life is harmed. Dan and I went to bed early while Russ and Joe recorded FITS cubes, measurements for entries on the long spreadsheet list of science doubles. Due to the quirky design of the cabin, to get to the voltmeter that measures the battery voltage one must go through the bedroom where I was sleeping. I remember Russ sneaking through the room several times in the middle of the night. In the end, the batteries failed a little after midnight.

Joe, Dan, Dave, and Russ at Pinto Valley Observatory in the Mojave desert; CDK20 in the background.

In spite of the difficulties, Russ and Joe acquired useful FITS cubes for 42 double stars that evening, and many of the subsequent reductions yielded improved orbits for the gravitationally bound binaries. Two of the observations even led to the discovery of two new triple stars. But the real value of that long weekend in November was the confidence gained by that small group on a modest budget, who realized that they could materially add to the scientifically important field of double star observations using the techniques of speckle imaging. Russ and I went on to have a total of three observing runs at Pinto Valley Observatory. Each run had its own difficulties and each set of difficulties in turn causes advancements. Russ greatly improved the instrumentation from run to run, and I wrote speckle reduction code that overcame interference in the camera and allowed semi-automatic processing of large data sets. These improvements were very important to much larger runs on much larger telescopes, as you will hear about in subsequent chapters. Enjoy the adventure.

David Rowe / August 2015

Speckle Interferometry of Close Visual Binaries

Russell M. Genet[1,2,3,4]

1. California Polytechnic State University, San Luis Obispo
2. Concordia University, Irvine, California
3. Cuesta College, San Luis Obispo, California
4. University of North Dakota, Grand Forks

Abstract Speckle interferometry circumvents atmospheric seeing limitations, facilitating astrometric observations of visual binaries with small separations. Some of these closely-spaced binaries have short periods, allowing complete orbits to be obtained in just a few years. Speckle observations of close visual binaries have been made by an eclectic group of student, amateur, and professional astronomers with an EMCCD camera on two smaller telescopes and then on both 2.1- and 0.8-meter telescopes at Kitt Peak National Observatory. Advanced technologies to increase the reach of speckle interferometry are also being pursued by this group, which includes a number of engineering faculty and students. These technological advances include full automation to increase the quantity of observations in an economical manner, and masks adapted from exoplanet imaging to disperse the bright primary starlight away from "discovery zones" so that faint secondary stars can be detected. Consideration is being given to the development of a large, four-meter-class, dedicated automatic sparse-aperture telescope for high spatial-resolution speckle interferometry. This sparse-aperture telescope may only cost about one-hundredth the cost of an equivalent filled-aperture telescope.

Close Visual Binaries and Speckle Interferometry

Astrometric orbits can be used to establish the "dynamical mass" (the sum of the two individual stellar masses) of a binary if the distance to the binary is also known. Knowing this distance allows an angular separation—the semi-major axis of the elliptical orbit—to be translated into an actual physical separation. Kepler's Third Law can then be applied to determine the dynamical mass sum.

However, what is needed to develop and refine stellar evolutionary models is the individual component masses, not the combined dynamical mass. Astrometric orbits, when combined with radial velocity curves, allow the summed dynamical mass to be parsed into individual stellar masses. Most of the visual binaries' orbits established prior to 1980 had periods of many decades or even centuries. Thus there was little overlap between these astrometric binaries, with their long periods and slow movements, and the radial velocity curves of spectroscopic binaries, with their short periods and high velocities.

What was needed were more astrometric orbits of shorter-period, faster-moving binaries so that spectroscopic radial velocity curves would be available for the same binaries to provide complete, individual-mass solutions. Unfortunately, most such short-period binaries have angular separations that are less than the seeing disk. With normal imaging, atmospheric jitter causes these binaries to jump about at high speed, hopelessly smearing images of binaries with separations below the typical seeing limit of about one arc second or more. This causes them to appear as a single star.

In 1970, Anton Labeyrie, a French astronomer, beat the seeing limit by taking hundreds of very short-exposure images of close double stars with a high-speed film camera (Labeyrie 1970). Each exposure contained many distinct binary star images randomly superimposed on each other. Although atmospheric jitter caused the images to radically change from one exposure to the next, Labeyrie found that as long as both stars were within the "isoplanatic patch" (which typically has a diameter of about five arc seconds), their jitter was correlated. By taking the Fourier transform of each image and processing many images in Fourier space, the most frequent position angles and separations in the images became apparent.

These were, of course, the position angles and separations of the double star being observed, although there was an inherent 180° ambiguity in the position angle. By the end of the 1970s, Harold McAlister and his associates were making high speed film camera observations of very close binaries on the 2.1- and 4.0-meter telescopes at Kitt Peak National Observatory (McAlister 1985). They obtained, for the first time, astrometric orbits on many spectroscopic binaries with existing radial veracity curves, thus yielding individual stellar masses for those all too few binaries that also had known distances. High-speed Tri-X film was not an easy medium to use, however. With the advent of early microcomputers and intensified CCD (ICCD) cameras, observations were made from the warm room at the 4-meter telescope instead of the Cassegrain cage as shown in Figure 1.

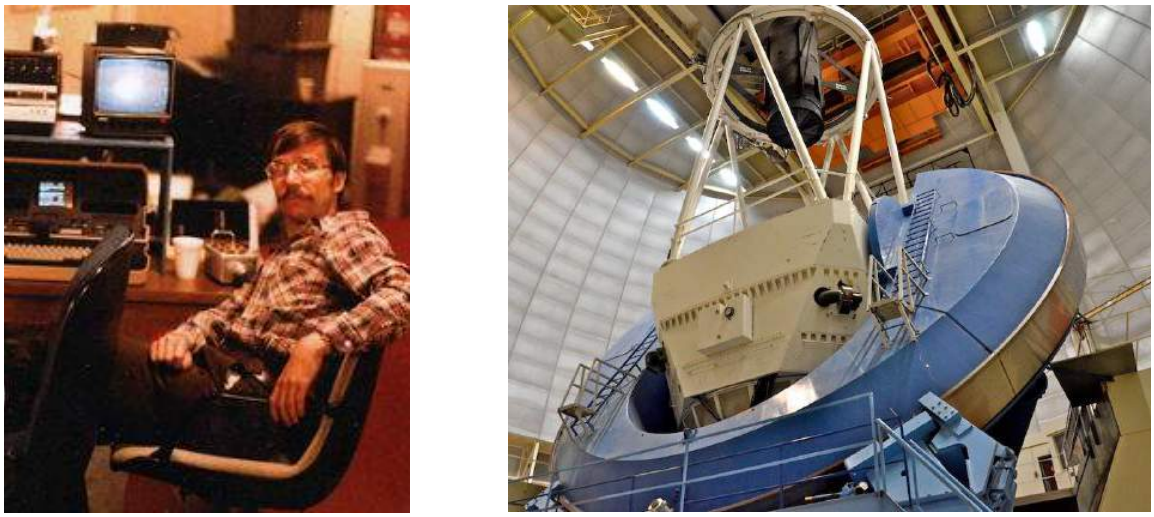

Figure 1. A young William Hartkopf (left) captures high-speed frames with an early Osborn portable computer from an intensified CCD (ICCD) camera located at the Cassegrain focus of the 4-meter telescope at Kitt Peak National Observatory (right). Similar observations were also made on the 2.1-meter telescope at Kitt Peak.

The European Space Agency launched the Hipparcos astrometric satellite in 1989 (Figure 2). At the time of its launch, the most capable computers on the planet did not have sufficient computational power to analyze the expected data. Trusting Moore's Law, they had the requisite capability when it came time, a few years later, to reduce and analyze their data (Perryman 2010).

Hipparcos provided accurate distances of about 100,000 stars, most for the first time. Binaries with astrometric (angular separation) orbits based on observations patiently built up over the decades and centuries, but previously at unknown distances, immediately became more valuable since the known distances finally allowed dynamical masses to be calculated. Hipparcos discovered large numbers of new binaries, suspected binaries, and close double stars, a rich source we are still actively mining decades later (Perryman 2012).

When, in the near future, the results from the European Space Agency's latest astrometric telescope, Gaia (Figure 3), become available, we will know the distances to many additional binaries. Furthermore, the already known distances to binaries will be refined by about a factor of ten (Eyer et al. 2013). Since distance uncertainty is often the major error source, recomputation of dynamical masses will significantly improve their accuracy. Not only will Gaia provide accurate distances, but, similar to Hipparcos, Gaia should discover a large number of binaries, suspected binaries, and close double stars. We may find this rich source of close binaries difficult to effectively follow up on unless we significantly improve our ability to obtain astrometric orbits of a large number of close visual binaries.

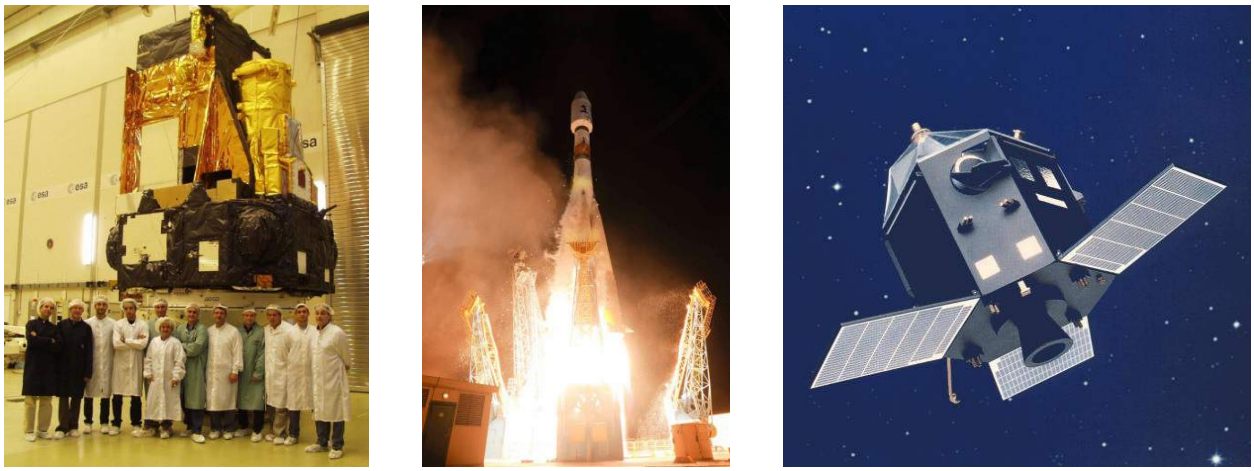

Figure 2. The European Space Agency's Hipparcos astrometric satellite.

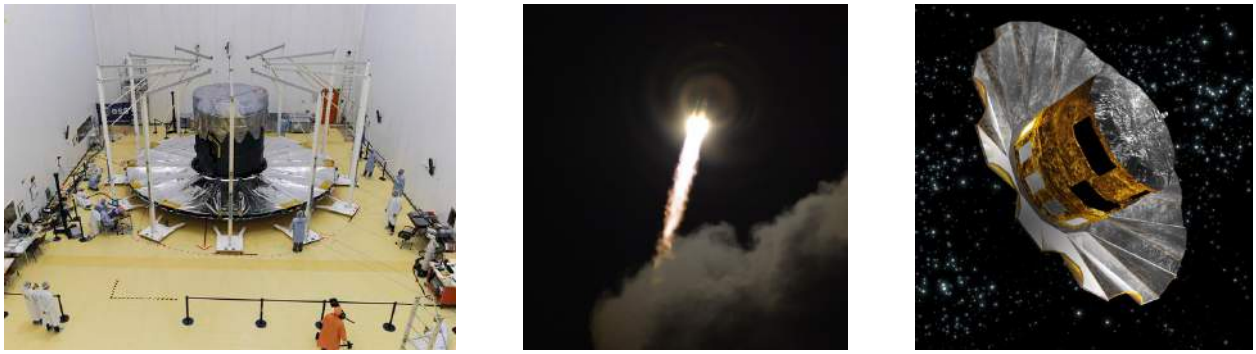

Figure 3. The European Space Agency's Gaia astrometric satellite.

Amateurs and Students Carry On with Wide Visual Binaries

With professional astronomers concentrating on speckle interferometry observations of close visual binary stars, continuing the observations of wide visual binaries (and other double stars) fell on the shoulders of amateur and student astronomers (Argyle 2012). Many amateurs and students have used an astrometric eyepiece with a ruler and protractor etched into a reticle to observe wide, bright double stars (Genet et al. 2010), while others have used CCD cameras to reach fainter magnitudes and somewhat closer separations.

An astrometric eyepiece is a self-contained, easy-to-use astronomical instrument that costs less than $200 USD (Figure 4). These eyepieces have been used by well over 100 students in an Astronomy Research Seminar offered by Cuesta College every fall for the past eight years and a summer-camp version of the seminar at the University of Oregon's Pine Mountain Observatory. The student teams' observations ended up as published papers, including over two dozen papers published in the *Journal of Double Star Observations*.

Recently, Cuesta College's Astronomy Research Seminar was expanded as a hybrid online/in-person course that included 38 students from 10 different schools. The overall seminar instructor, Genet, was aided by 14 assistant instructors (primarily local high school science teachers) and a number of advanced amateur astronomers and other professional astronomers. Most of the students were high school students, taking the seminar as their first college course. One team observed double stars with an astrometric eyepiece, while most of the others used CCD cameras—some in person and others remotely at robotic observatories (Figure 5). Although most of the teams observed wider double stars, two teams were involved with speckle interferometry observations of close double stars.

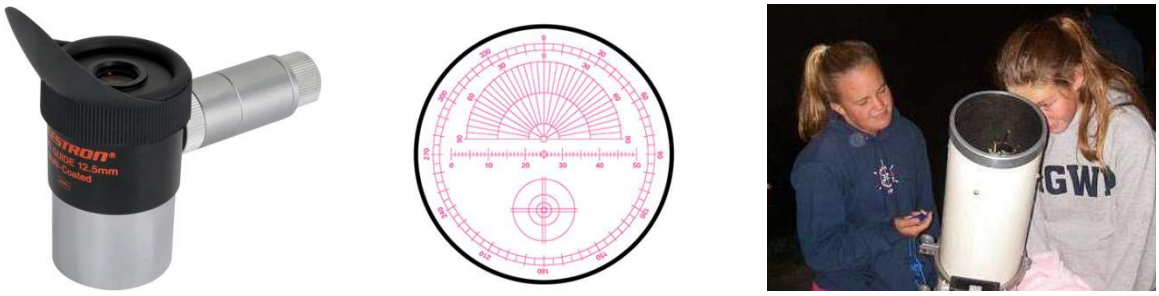

Figure 4. Astrometric eyepieces with a laser-etched reticle were used by Arroyo Grande High School students taking Cuesta College's Astronomy Research Seminar.

Figure 5. Cadet teams at the Army and Navy Academy in Carlsbad, California, made remote observations using iTelescope's network of robotic telescopes (left). A student team in Pearl City, Hawaii, used a CCD camera on the 0.5-meter telescope at Leeward Community College for their observations (right).

Speckle Interferometry Moves to Smaller Telescopes

Florent Losse, an amateur astronomer in France, was a key pioneer of small-telescope speckle interferometry (Figure 6, left). Because he did not have access to an intensified CCD (ICCD) camera or an electron multiplying CCD (EMCCD) camera, the read noise on regular CCD cameras would have been very high at fast readout speeds. Thus Florent patiently took the time for slow readouts, one frame at a time for hundreds of frames on each double star.

Losse's speckle observations of close visual binaries began appearing in the 6th Orbit Catalog, and were right in line with speckle observations made by professional astronomers with larger telescopes. Florent also extended his user-friendly, well-documented double star reduction software, REDUC, to include speckle interferometry, paving the way for other amateur astronomers to also make speckle interferometry observations of close binaries on their telescopes.

Several years ago, Genet and one of his Cuesta College students, Jo Johnson, joined Brian Mason for a night during one of Mason's speckle interferometry runs on the 4-meter telescope at Kitt Peak National Observatory (Figure 6, right). Genet wanted to see, in person, how speckle interferometry observations were made by professional astronomers on large telescopes. The U.S. Naval Observatory has two identical, intensified CCD (ICCD)-based speckle cameras. One is permanently mounted on their 26-inch refractor in Washington, while the other is used for "off campus" observing runs at various telescopes such as the 4-meter telescopes at Kitt Peak National Observatory and Cerro Tololo Interamerican Observatory. Although sizeable, the speckle camera system and supporting electronics and computer fit within a check-in bag so they can be flown to observing sessions.

Figure 6. Florent Losse and his 0.4-meter telescope (left). Genet, Mason, and Johnson in the Casseigrain cage of the 4-meter telescope at Kitt Peak National Observatory with USNO's ICCD camera (right).

Some time ago, a number of companies began manufacturing electron-multiplying CCD (EMCCD) cameras using back-illuminated CCD chips made by e2v. These cameras were quite expensive (typically $40,000 USD), large, and heavy, and they required a fairly short cable to connect them to a PC plug-in card. They were not small-telescope-friendly cameras! However, Andor Technologies eventually began making a much smaller, lower cost ($14,000 USD) EMCCD camera based on a front-illuminated chip made by Texas Instruments. These "Luca" cameras were USB-based, and were compact enough to be easily mounted on smaller telescopes. Genet acquired one of these cameras, thanks to a grant from the American Astronomical Society and a sizeable discount from Andor Technologies, and made it the heart of a portable speckle interferometry camera system (Genet 2013).

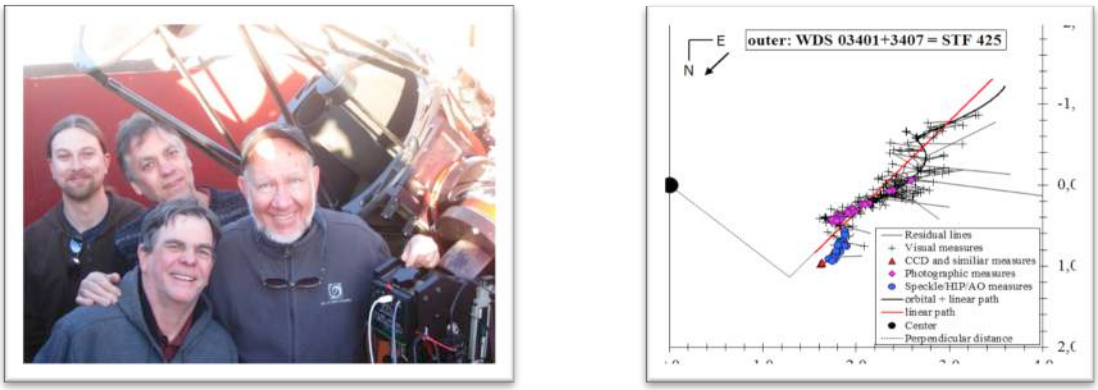

Figure 7. Joe Roberts, Dan Gray, Dave Rowe, and Russ Genet with the PlaneWave Instruments CDK-20 telescope at the Pinto Valley Observatory (left). New triple star discovered during their observing run at the Pinto Valley Observatory (right).

David Rowe (Figure 7) kindly offered the use of his PlaneWave Instruments 0.5-meter Corrected Dall-Kirkham (CDK) telescope at his Pinto Valley Observatory in the Mojave Desert Reserve for the first speckle interferometry run using this portable speckle camera system. Although the first two nights of the run were engineering evaluations of various sorts, speckle interferometry of close double stars began in earnest on the last night. Some 42 doubles (including two new triple stars discovered during subsequent analysis) were observed before solar power for this remote observatory ran out at midnight. This observing run and its results are described in "Two New Triple Star Systems with Detectable Inner Orbital Motions and Speckle Interferometry of 40 Other Double Stars" (Genet et al. 2015a). A few months later, other observers joined in for second and then third speckle observing runs on the 0.5-meter telescope at the Pinto Valley Observatory (Figure 8).

Figure 8. Eric Weise installs speckle interferometry camera on the CDK-20 telescope at the Pinto Valley Observatory (left). The eight observers on the third Pinto Valley Observatory run (right).

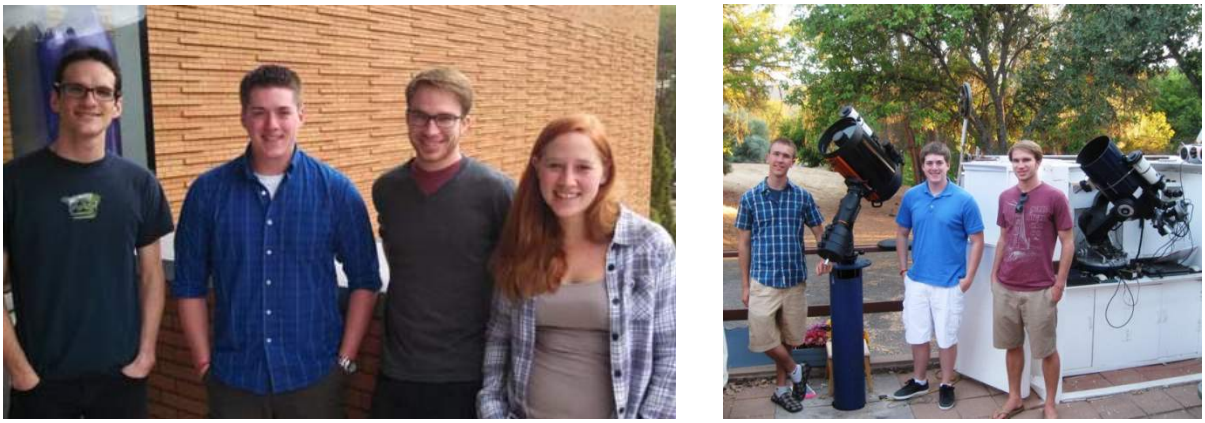

Figure 9. Cal Poly student observers Jason Goad, Cameron Allen, Ryan Morshead, and Katilin McArdle (left). Eric Weise, Cameron Allen, and Ryan Morshead with two of the telescopes at the Orion Observatory (right). The Cal Poly students used the 10-inch telescope on the right for their observations.

Speckle observations were also made at the Orion Observatory, Genet's private observatory near Santa Margarita Lake that is often used by students from California Polytechnic State University, Cuesta College, and local high schools for their research projects (Figure 9). An example of such a project is "Research of Double Stars with Speckle Interferometry" (Allen et al. 2015).

Another example of speckle interferometry at the Orion Observatory was the observations of ten close double stars by two visiting astronomers from Shanghai Astronomical Observatory, Yuanyuan Ding and Chaoyan Wang, along with Weise and Genet (Figure 10). Calibration of the pixel scale was made with a slit mask with uniformly spaced slits. Half of a focus mask was used for these observations, with the other half masked off. This form of calibration is similar to the famous Young "double slit" experiment (Weise et al. 2015).

There are over 2000 binaries with published orbits and accompanying plots. Some of the plots show observations falling almost exactly on the published orbit like a "string of pearls," while others show that recent observations have deviated from the previously published orbit, suggesting the orbit may need revision at some point. Recent observations of some binaries suggest that the published orbits are way off, i.e. "bad orbits." To aid observers in selecting binaries to observe, Weise and Genet (2015) developed a binary orbit classification scheme.

Figure 10. Eric Weise, Chaoyan Wang, Yuanyuan Ding, and Russ Genet (left). They made speckle interferometry observations of double stars with the 0.25-meter telescope at the Orion Observatory. The slit mask used for pixel scale calibration (right).

Speckle Interferometry Observations at Kitt Peak

Elliott Horch, an astronomer at Southern Connecticut State University, kindly invited Genet to join him on a two-night run on the 3.5-meter WIYN telescope at Kitt Peak National Observatory. Elliott's two-channel speckle interferometry camera, shown in Figure 11, is arguably the most advanced of all cameras (Horch 2012). A dichroic splits the beam into R- and I-band wavelengths with the speckles imaged on two high-end Andor EMCCD iXon cameras. Because the special cables to the plug-in PC cards had to be kept short, a PC was fastened to the bottom of the speckle camera. Two instances of the Andor Solis camera control screens can be seen on Genet's PC in Figure 11.

Figure 11. Elliott Horch and his speckle camera on the 3.5-meter WIYN telescope. One of the Andor EMCCD cameras can be seen. The other is out of view on the other side. The black PC can be seen fastened to the bottom of the system (left). Russ Genet operates the two cameras from the warm room while Elliott operates the log (right).

The 3.5-meter WIYN telescope is somewhat complex to operate as it requires controlling the shape of the primary mirror. The many actuators which control the shape of the mirror can be seen in Figure 12 (left). Dave Summers, one of the most experienced telescope operators on the mountain, operated the telescope for Elliott and Genet (Figure 12, right).

During a break, Genet stopped by the 2.1 meter telescope to visit Catherine Pilachowski (Figure 13). Pilachowski and a graduate student were using the Phoenix near-infrared spectrograph, which can be seen on the bottom of the telescope in Figure 13. It was clear that this would be a good telescope to use for speckle interferometry. During the day Genet also visited Matthew Penn at the McMath-Pierce solar telescope facility, as one of these three telescopes might be usable for nighttime speckle observations.

Figure 12. The many actuators on the back of the 3.5-meter WIYN telescope (left). Dave Summers controls the telescope (right).

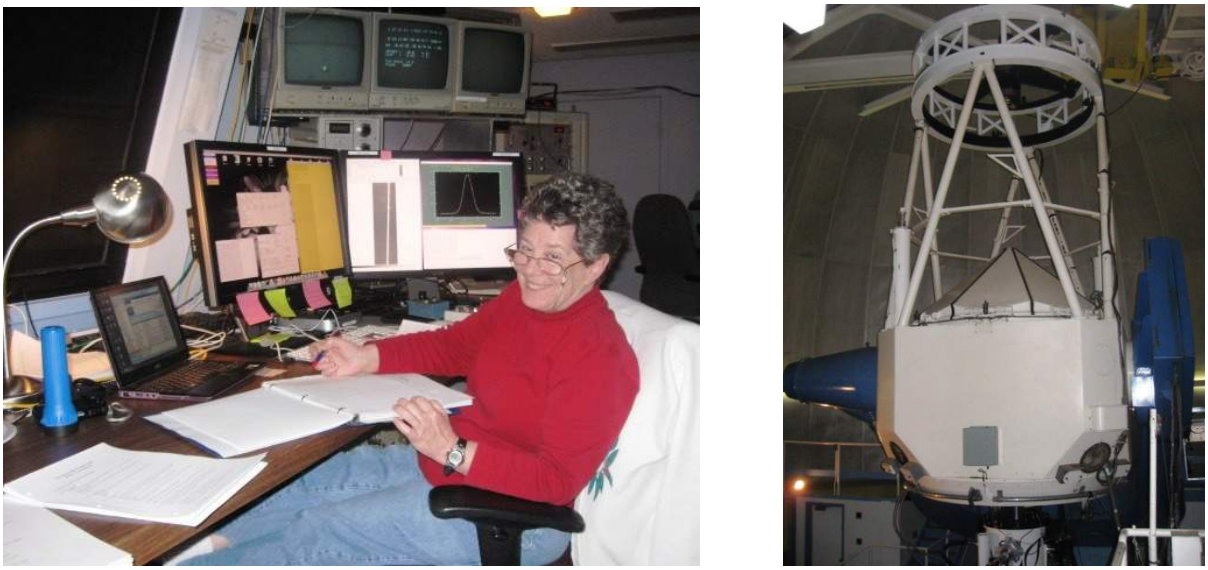

Figure 13. Catherine Pilachowski in the warm room of the 2.1-meter telescope controlling (left) the near-infrared spectrograph on the bottom of the telescope (right).

A spring visit was made to the National Optical Astronomy Observatory's headquarters in Tucson to discuss possible speckle observations on the 2.1-m telescope. Richard Joyce kindly pulled out drawings of the telescope and suggested how a speckle camera might be interfaced to the 2.1-meter telescope in terms of physical mounting, cabling, and software.

It was decided that the telescope's acquisition/guider unit should be left in place and an aluminum interface plate should go between Genet's small, portable speckle camera and the large, almost two-foot diameter opening at the bottom of the acquisition/guider unit. Heather Mathis located, in a remote corner of the 2.1-meter dome, an instrument interface plate that had not been used for many years, and it was adopted as the interface.

To make sure that everything worked properly, a single night of engineering checkout time was made available at the end of July 2013 (Genet et al. 2015c). The engineering checkout team consisted of Genet, Tom Smith, Kent Clark, and Paul Wren. When they arrived, Mathis had already removed the massive Phoenix spectrograph and was adding the lead counterweights needed to compensate for the lightweight speckle camera. Smith mounted the EMCCD camera to the interface plate, and the team connected up the cables (Figure 14).

Figure 14. Mathis installed counterweights (left), Smith fastened the EMCCD camera to the interface plate (center), and Mathis and Genet fastened down the cables (right).

Dave Summers trained the team on opening and closing the observatory, operating the telescope, loading up the telescope computer's cache with a target list, etc. (Figure 15). The 2.1-meter is a complex system, with a thick manual that describes its operation.

Figure 15. Genet at the telescope operator's station (left). Crew in the warm room: (left to right) Dave Summers, Kent Clark, Tom Smith, and Paul Wren.

Knowing that the speckle interferometry camera would work on the telescope, a proposal was prepared and submitted which requested seven nights for observations preceded by one night of engineering checkout. Obtaining time on the telescopes at Kitt Peak National Observatory is very competitive, and the team was fortunate to be awarded the eight nights.

As it would have been difficult for students and others to stay for the entire eight-night run, the run was split into "A" and "B" teams, with a smaller "weekend" team sandwiched in between. Genet stayed for the entire run, as did Smith. Joining Genet and Smith from the A Team were: Mark Trueblood, Winer Observatory; Eric Weise, Univ. of Calif., San Diego; Alex Teiche, California Polytechnic State University; Dan Wallace, Univ. of North Dakota; Josh Plummer, Univ. of South Alabama; and Kent Clark, Univ. of South Alabama.

The Weekend Team consisted of John Kenny, Kayla Chaney, and Rikita Patel, all from Concordia University, Irvine. The B Team consisted of Paul Wren (in addition to Genet and Smith).

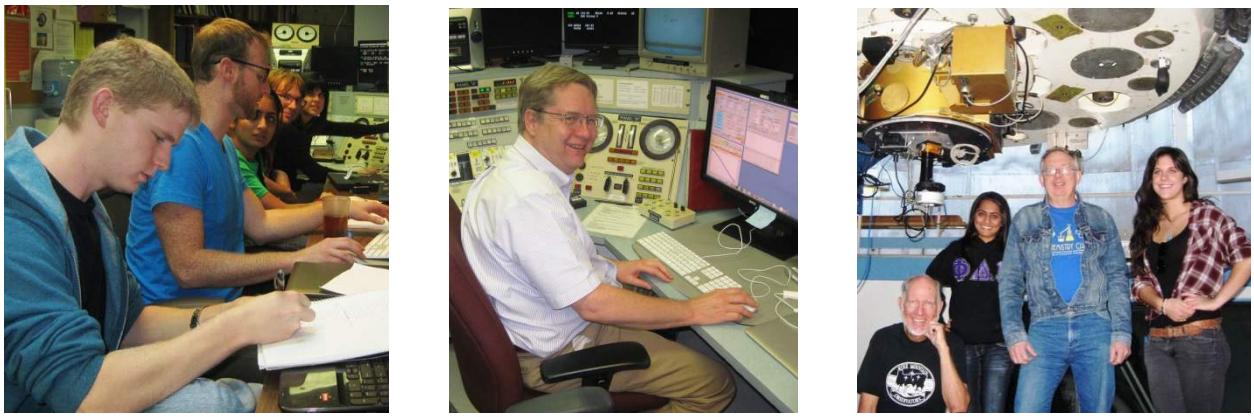

Figure 16. Students in the warm room: Josh Plumer, Dan Wallace, Rikita Patel, Alex Teiche, and Kayla Chaney (left). JDSO Editor Kent Clark at the controls (center). Russell M. Genet, Rjikita Patel, John Kenney, and Kayla Chaney under the telescope (right).

As luck would have it, the first seven nights were totally clear without even a hint of clouds. The eighth night was cloudy for the last half of the night. Speckle observations were made of over 1000 close double stars, many of them binaries, as well as several hundred single stars for use in deconvolution. Over a terabyte of data was gathered. The run is described in some detail in "Kitt Peak Speckle Interferometry of Close Visual Binary Stars" (Genet et al. 2015d).

Just a couple of weeks after the run, two high school teams taking Genet's Astronomy Research Seminar (Figure 17) used data from the Kitt Peak run as the basis for their research seminar papers. See "First Speckle Interferometry Observations of Binary BU 1292" (Adam et al. 2015a), and "Speckle Interferometry Observation of Binary WDS 01528-0447" (Adam et al. 2015b).

While reducing the data for just a few close binary stars observed on the 2.1-meter telescope at Kitt Peak using Florent Losse's REDUC was not a problem, doing this for over a thousand double stars, matching up single deconvolution stars to the doubles, and including deconvolution in the reduction was problematic. Not being an approach anyone would want to repeat on another run, three major efforts were launched to solve this problem.

First, the results from the first Kitt Peak run were not well organized. Not only was there a problem matching single deconvolution stars to double stars, but identifiers had been entered by hand by the various camera operators, and over 100 of them had entry errors. It took a Cal Poly student, Alex Teiche, several months to square away the data base. He developed a spreadsheet that pointed to both the double stars and their matching single deconvolution stars in a uniform manner. See "Kitt Peak Speckle Interferometry Program Database Generation" (Teiche 2015).

Second, Dave Rowe and Russ Genet decided that to reduce the large Kitt Peak data set and to prepare for future runs of this size, a new reduction program was needed. To this end, Rowe wrote the software, while Genet tested it out on the Kitt Peak data organized by Teiche. Over 30 versions of the program were written by Rowe and tested by Genet during January and February of 2014. A user's guide was developed in parallel with programming and testing. See "User's Guide to PS3 Speckle Interferometry Reduction Program" (Rowe & Genet 2015).

Rowe's speckle interferometry program, an addition to his Plate Solve 3 program, has many advanced features. All the observations can be preprocessed automatically (making all the Fourier transforms). This reduces the file size and subsequent reduction times by about a factor of one thousand.

The program, PS3, can run in either of two modes. The first is a manual mode where one selects a double, one at a time, from a data base, and, optionally, a matching single deconvolution star. The second mode is semi-automatic, using the Teiche spreadsheet as a pointer to both the double and single stars.

In the semi-automatic mode, PS3 automatically generates solutions and displays autocorrelograms, although the user can override an automatic solution and provide a manual solution.

PS3 has many other features, including adjustable Gaussian high and low pass filters, an axes interference filter, display of both the autocorellogram and the power spectral density, and automatic recording of all the reduction parameters and any user's comments.

Figure 17. One of the high school research teams (left), their autocorellogram (center), and their observational plot (right) that compared the point predicted from the ephemeris and the observed (calculated) point from Kitt Peak.

Third, to avoid difficult-to-use observational results in the future, an observational/data-flow process was defined. Standard formats were established to match the observational results to the PS3 reduction program, thus allowing observations to be reduced in a semi-automatic fashion. The specifications included instructions and formats for pre-run preparation, choosing targets and recording observations during runs, and post-run reduction. See "The Double Star Speckle Interferometry Observation and Reduction Process" (Genet 2015).

With a well-defined observational process, data formats, and a semiautomatic, well-documented reduction program in hand, the group was ready for another major speckle interferometry run. They applied for and were granted another week of observing at Kitt Peak in April of 2014 to observe doubles on the other half of the sky (Figure 18).

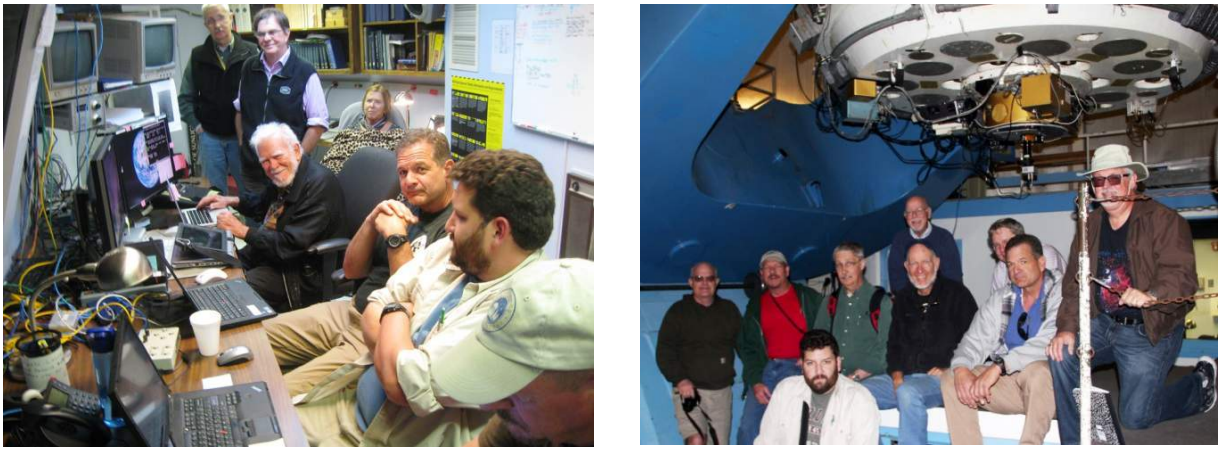

Figure 18. Observers in the warm room (left): Wayne Green, Dave Rowe, special guest Keith Hege (and his wife under the books), Reed Estrada, and Chris Estrada. Observers under the telescope at the second Kitt Peak run (right): Greg Jones, Tom Smith, Chris Estrada (front), Wayne Green, Ed Wiley (rear), Russ Genet (front), Kent Clark (rear), Reed Estrada (front), and Richard Harshaw.

Figure 19. Detrick Branston makes a measurement on the north port of the 1.6-meter Main telescope of the McMath-Pierce Telescope Facility, while Pat Boyce, Richard Harshaw, and Ed Wiley provide advice (left). Pat Boyce and Richard Harshaw assemble the speckle camera system for observations on the 0.8-meter East Auxiliary Telescope (right).

As in the first Kitt Peak run, the observers were split into two teams, one for the first half of the run, and the other for the last half. Genet and Smith, again, stayed for the entire run. The observers on the 2.1-meter telescope included Kent Clark, Reed Estrada, Chris Estrada, Tom Frey, John Ridgely, Dave Rowe, Alex Teiche, Nathalie Haurberg, Cassie Hollman, Izak McGieson, Rafel Ramos, Don Westergen, Grady Boyce, Tom Smith, and Russ Genet.

Simultaneous with the speckle interferometry observations on the 2.1-meter telescope, another team of observers evaluated the suitability of the Main 1.6-meter and Auxiliary East 0.8-meter telescopes at the McMath-Pierce solar telescope facility for nighttime speckle interferometry observations of close double stars (Figure 19). The McMath team included Richard Harshaw, Greg Jones, Ed Wiley, Pat Boyce, Jimmy Ray, David Douglass, Lri Prause, Detrick Branston, and Russ Genet (who split his time between telescopes).

Pointing tests on the 1.6-meter telescope suggested that it could make useful speckle observations. See "Potential of the McMath-Pierce 1.6-Meter Solar Telescope for Speckle Interferometry" (Hashaw et al. 2015a). However, efforts were concentrated on the 0.8-meter East Auxiliary telescope. Several optical. configurations were evaluated, and one was used to make useful speckle operations of several close double stars. For the papers on the McMath-Pierce research, see "Testing of the McMath-Pierce 0.8-Meter East Auxiliary Telescope's Acquisition and Slewing Accuracy" (Harshaw et al. 2015b), "Close Binary Star Speckle Interferometry on the McMath-Pierce 0.8-Meter Solar Telescope" (Wiley et al. 2015), and "Speckle Interferometry with the McMath-Pierce East Auxiliary Telescope" (Harshaw et al. 2015c).

The 2.1-meter telescope facility at Kitt Peak includes a separate and independently-controlled 1.0-meter telescope that feeds the large spectrographs in the basement below the 2.1-meter telescope. During our observing run at Kitt Peak, Wayne Green and John Kenney observed a number of short-arc, very long-period binaries with the high-resolution Echelle spectrograph to obtain radial velocities (Figure 20).

After the Kitt Peak second run, Greg Jones compared the performance of a number of low cost, high speed CCD and CMOS cameras. Richard Harshaw purchased one of these cameras (the Celestron Skris CCD camera) and began making speckle interferometry observations of brighter, close double stars. Harshaw compared a number of calibration procedures for these low cost cameras and concluded that drifts were best for camera angle, and slit masks were best for pixel scale. See "Calibrating a CCD Camera for Speckle Interferometry" (Harshaw 2015d).

Figure 20. Wayne Green and John Kenney at the top, slit end of the spectrograph (left). The light from the slit then enters the basement room which contains several spectrographs including a high resolution Echelle (right).

Advanced Technology Developments

Although stellar masses in the middle of the main sequence have been accurately established through the combination of astrometric and spectroscopic observations of binaries, the masses of stars on both ends of the main sequence, as well as those evolved off of the main sequence, are not well known. Only recently, the masses of late-M dwarfs were found to be off by a factor or two (Dupuy et al. 2012). Astrometric observations of short-period binary stars, with one of these needed stars as a component, are required to establish their masses in a fundamental manner. Once individual masses are determined, stellar evolutionary models can be refined.

Three technologies, discussed below, have the potential to extend the reach of binary-star speckle interferometry. A program of potential observations and advanced hardware and software engineering developments has been suggested. See "Speckle Interferometry of Short-Period Binary Stars" (Genet et al. 2015b).

Hipparcos, the European Space Agency's astrometric space telescope, discovered thousands of potential short-period binary stars—many of which, over two decades later, have not yet been confirmed, while others have not been sufficiently followed to establish good orbits. The short periods of some of these close visual binaries allow the establishment of high quality orbits within a reasonable time frame. Furthermore, their components have sufficient orbital velocities to allow radial velocity curves to be obtained. The combination of accurate astrometric orbits and radial velocity curves can provide individual component stellar masses in a very fundamental manner.

In the future, we expect that the number of potential close binaries discovered by the European Space Agency's recently launched Gaia astrometric telescope, the Large Synoptic Survey Telescope (LSST), and other survey telescopes will, literally, suggest millions of short-period binary candidates worth pursuing. The first challenge will be to determine, through astrometric observations, which of these many potential candidates actually are short-period binaries. The second challenge, by way of differential, multi-band photometry, will be to determine, in turn, which of the actual binaries have at least one component that is a star that is not in the middle of the main sequence, and hence have poorly known masses.

Although the survey telescopes, such as Gaia and LSST, will provide a virtual flood of binary star possibilities, the number of observers and the telescope observational time required to follow up on them is well beyond our current capabilities. One approach to solving this dilemma is automation. A workshop on the automation of speckle interferometry was held at the U.S. Naval Observatory in June of 2014 (Figure 21).

Figure 21. Attendees at the U.S. Naval Observatory Workshop on the Automation of Speckle Interferometry gather under the historic 26-inch refractor. Reed Riddle, Merlene Clark, Bill Hartkopf, Jerry Hubbell, Kent Clark, Brian Mason, and Russ Genet (left). Brian Mason and Bill Hartkopf at the 26-inch refractor's control station (right).

Following the USNO workshop, an undergraduate Electrical Engineering student at California Polytechnic State University, Alex Teiche, spent the summer writing over 10,000 lines of code to fully automate speckle interferometry observations on the 10-inch telescope at the Orion Observatory. See Figure 22 and "Automated Speckle Interferometry of Double Stars" (Teiche et al. 2015).

Figure 22. Alex Teiche checks the equipment automation setup at the Orion Observatory (left). Alex watches the telescope run automatically from the observatory's warm room (right).

For his Master's thesis in Mechanical Engineering at California Polytechnic State University, Ed Foley is developing masks with various geometric shapes to disperse the light of bright primary stars away from "discovery zones." This will allow fainter secondary stars to be observed than would be possible without the masks. Shaped aperture masks for space telescopes have been under development at Princeton University for quite some time. Neil Zimmerman, a post-doc at Princeton, designed a mask specifically for Celestron C-11 telescopes such as the one at the Orion Observatory and also at Jimmy Ray's observatory in Arizona. See "Observations of Large Delta-Magnitude Close Binaries with Shaped Aperture Masks" (Foley et al. 2015) and Figure 23.

The time available on 4-meter and larger telescopes for speckle interferometry of close binary stars is insufficient to follow up on currently known close binaries, let alone sort through new short-period binary candidates to determine which ones actually are binaries, and then follow these long enough to establish high-quality orbits. The solution to this difficulty is the development of low cost, large aperture telescopes that could be devoted, in a fully-automated fashion, entirely to close binary star speckle interferometry.

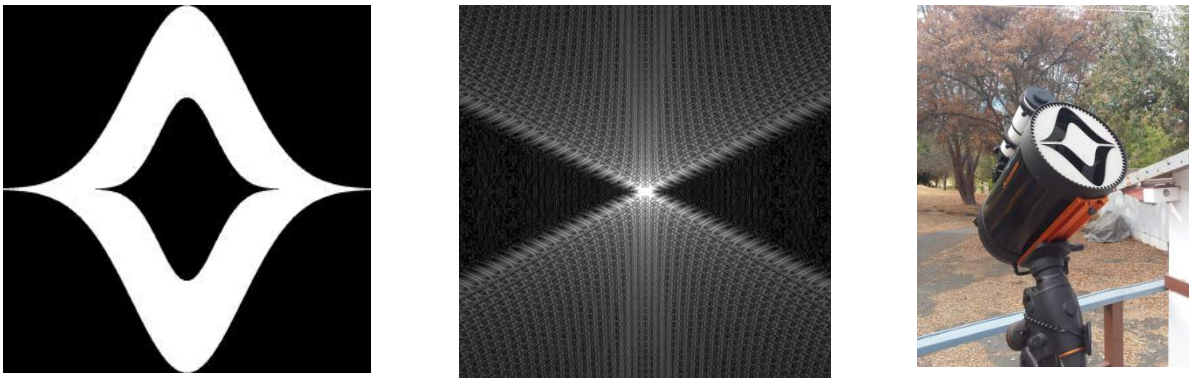

Figure 23. A mask designed by Ed Foley. The central portion of the mask covers the telescope's secondary mirror (left). The Fourier transform of the mask reveals the two discovery zones on the left and right (center). The mask on the Celestron C-11 telescope at the Orion Observatory (right).

A number of workshops and meetings have been held to explore various possibilities. In September 2014 at the Mt. Wilson workshop, participants decided to concentrate on the development of sparse-aperture speckle interferometry telescopes (Figure 24). As envisioned at this workshop, such telescopes will have multiple spherical mirrors (with closely matched focal lengths) arranged to conform to the (sparse) surface of a larger (virtual) spherical mirror. Spherical aberration will be reduced by way of an aspheric secondary (such as Pressman-Carmichael) for a Cassegrain configuration, or refractive optics for a prime focus configuration.

Figure 24. Attendees at Mt. Wilson Workshop on the Speckle Interferometry of Double Stars. John Kenney, Brian Mason, Nils Turner, Russ Genet, Dave Rowe, Alex Teiche, and Reed Estrada. Chris Estrada was behind the camera (left). Dave Rowe explains the basics of bispectrum analysis (right).

At the Mt. Wilson Workshop, Dave Rowe presented simulation results for a 2-meter sparse-aperture telescope with seven 0.5-meter mirrors (Figure 25). The results looked promising. Since then, a rough cost estimate suggests that a 4.0-meter sparse aperture telescope might only cost about $500,000 to build, about 1/100th of the cost of a 4.0-meter filled-aperture such as the recently built Discovery Channel Telescope at Lowell Observatory.

Matthew Clause, a Master's student in Mechanical Engineering, designed a servomechanism to position the multiple mirrors with the high precision required for phasing. Michael Niditz, a Senior majoring in Architectural Engineering, designed a stiff test stand to evaluate a three-mirror sparse-aperture system. The three spherical mirrors were made by Tong Liu at Hubble Optics.

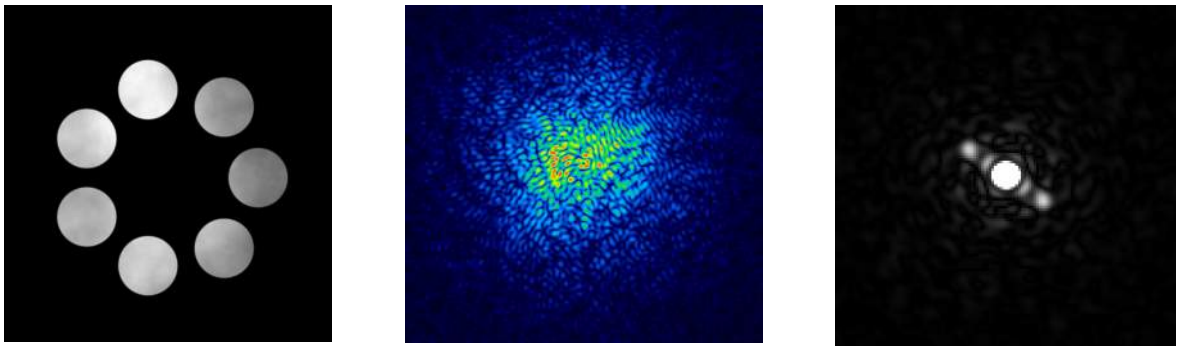

Figure 25. Simulation of two-meter sparse-aperture speckle interferometry telescope.

Acknowledgments

Genet thanks California Polytechnic State University Office of Research and Economic Development for support through their Extramural Funding Initiative and the W. M. Keck Foundation for support through the Concordia University Undergraduate Education Program.

References

Adam, M., Roberts, S., Schenk, M., VanRonk, C., Loayza, C., Genet, R. M., Johnson, B., Smith, C., & Wren, P. 2015a. First speckle interferometry observation of binary BU 1292. *Journal of Double Star Observations,* 1S, 67.

Adam, M., Weise, E., Johnson, B., Lutes, B., Huck, K., Patel, A., and Genet, R. M. 2015b. Speckle interferometry observation of binary WDS 01528-0447. *Journal Double of Star Observations,* 1S, 75.

Allen, C., Goad, J., Morshead, R., McArdle, K., & Weise, E. 2015. Double star research with speckle interferometry. *Journal of Double Star Observations,* 1S, 19.

Argyle, R. 2012. *Observing and Measuring Visual Double Stars*. London: Springer-Verlag.

Dupuy, T., Liu, M., & Ireland, M. 2012. Testing theory with dynamical masses and orbits of ultracool binaries. *ASP Conference Series*, 16. In preparation.

Eyer, L., Holl, B., Pourbaix, D., Mowlavi, N., Siopis, C., Barblan, F., Evans, D.W., & North, P. 2013. The Gaia mission. arXiv:1303.0303v1 [astro-ph.IM].

Foley, E. L., Genet, R. M., Ridgely, J.R., Rowe, D., & Zimmerman, N. T. 2015. Observation of large delta-magnitude close binaries with shaped aperture masks. *Journal of Double Star Observations,* 1S, 173.

Genet, R. M. 2013. Portable speckle interferometry camera system. *Journal of Astronomical Instrumentation*, 2, 134008.

Genet, R. M. 2015. The double star speckle interferometry observation and reduction process. *Journal of Double Star Observations,* 1S, 101.

Genet, R. M., Johnson, J., & Wallen, V. 2010. One-semester astronomical research seminars. In *Small Telescopes and Astronomical Research*. Santa Margarita, CA: Collins Foundation Press.

Genet, R. M., Zirm, H., Rica, F., Richards, J., Rowe, D., & Gray, D. 2015a. Two new triple star systems with detectable inner orbital motions and speckle interferometry of 40 other double stars. *Journal of Double Star Observations,* 1S, 1.

Genet, R. M., Ridgely, J. R., Teiche, A., Foley, E., Christiansen, C., Rowe, D., Zimmerman, N., Knox, K., Hege, K., Kenney, J., Clark, R. K., Holenstein, B., Mohanan, K., & Armstrong, J. 2015b. Speckle interferometry of short-period binary stars. *Journal of Double Star Observations,* 1S, 151.

Genet, R. M., Smith, T., Clark, R. K., Wren, P., Mathis, H., Summers, D., & Hansey, B. 2015c. Portable speckle interferometry camera checkout at Kitt Peak. *Journal of Double Star Observations,* 1S, 47.

Genet, R. M., Rowe, D., Smith, T. C., Teiche, A., Harshaw, R., Wallace, D., Weise, E., Wiley, E., Boyce, G., Boyce, P., Branston, D., Chaney, K., Clark, R. K., Estrada, C., Estrada, R., Frey, T., Green, W., Haurberg, N., Jones, G., Kenney, J., Loftin, S., McGieson, I., Patel, R., Plummer, J., Ridgely, J., Trueblood, M., Westergren, D., & Wren, P. 2015d. Kitt Peak speckle interferometry of close visual binary stars. *Journal of Double Star Observations,* 1S, 55.

Harshaw, R., Jones, G., Wiley, E. O., Boyce, P., Branston, D., Rowe, D., & Genet, R. M. 2015a. Potential of the McMath-Pierce 1.6-meter solar telescope for speckle interferometry. *Journal of Double Star Observations,* 1S, 113.

Harshaw, R., Ray, J., Prause, L., Douglass, D., Branston, D., & Genet, R. M. 2015b. Testing of the McMath-Pierce 0.8-meter east auxiliary telescope's acquisition and slewing accuracy. *Journal of Double Star Observations,* 1S, 127.

Harshaw, R., Ray, J., Douglass, D., Prause, L., & Genet, R. M. 2015c. Speckle interferometry with the McMath-Pierce east auxiliary telescope. *Journal of Double Star Observations,* 1S, 133.

Harwhaw, R. 2015d. Calibrating a CCD camera for speckle interferometry. *Journal of Double Star Observations,* 1S, 141.

Horch, E., Howell, S., Everett, M., & Ciardi, D. 2012. Observations of binary stars with the differential speckle survey instrument IV: observations of Kepler, CoRoT, and Hipparcos stars from the Gemini North Telescope. *AJ,* 144, 165.

Labeyrie, A. 1970. Attainment of diffraction limited resolution in large telescopes by Fourier analyzing speckle patterns in star images. *A&A,* 6, 85.

McAlister, H. 1985. High angular resolution measurements of stellar properties. *ARA&A,* 23, 59.

Perryman, M. 2012. Astronomical applications of astrometry: ten years of exploitation of the Hipparcos satellite data. Cambridge: Cambridge Univ. Press.

Perryman, M. 2010. *The Making of History's Greatest Star Map.* New York: Springer.

Rowe, D. & Genet, R. M. 2015. User's guide to PS3 speckle interferometry reduction program. *Journal of Double Star Observations,* 1S, 89.

Sérot, J. 2015. Measurements of double stars using a 280 mm reflector and an EM-CCD. *Journal of Double Star Observations,* 1S, 191.

Teiche, A. S. 2015. Kitt Peak speckle interferometry program database generation. *Journal of Double Star Observations,* 1S, 85.

Teiche, A. S., Genet, R. M., Rowe, D., Hovey, K. C., & Gardner, M. 2015. Automated speckle interferometry of double stars. *Journal of Double Star Observations,* 1S, 169.

Weise, E., Ding, Y., Wang, C., & Genet, R. M. 2015. International speckle interferometry collaboration. *Journal of Double Star Observations,* 1S, 127.

Weise, E. & Genet, R. M. 2015. A novel system for collating binary orbital solutions. *Journal of Double Star Observations,* 1S, 39.

Wiley, E. O., Harshaw, R., Jones, G., Branston, D., Boyce, P., Rowe, D., Ridgely, J., Estrada, R., & Genet, R. M. 2015. Close binary star speckle interferometry on the McMath-Pierce 0.8-meter solar telescope. *Journal of Double Star Observations,* 1S, 127.

Two New Triple Star Systems with Detectable Inner Orbital Motions and Speckle Interferometry of 40 Other Double Stars

Russell Genet[1,2,3,4], Henry Zirm[5], Francisco Rica[6], Joseph Richards[3], David Rowe[7], and Daniel Gray[8]

1. California Polytechnic State University, San Luis Obispo
2. Concordia University, Irvine, California
3. Cuesta College, San Luis Obispo, California
4. University of North Dakota, Grand Forks
5. Markt Schwaben, Germany
6. Agrupación Astronómica de Mérida, Mérida (Badajoz), Spain
7. PlaneWave Instruments, Rancho Dominguez, California
8. Sidereal Technology, Portland, Oregon

Abstract Speckle interferometry observations of 42 double stars with a separation between 0.5″and 2.0″ were made at Pinto Valley Observatory with a 0.5-meter PlaneWave Instruments CDK20 telescope equipped with a portable Andor Luca-S EMCCD-based speckle camera. STF162 AB / CHR4 Aa, Ab and STF 425, both without previously published orbits, were found to be triple systems. We provide orbits of the inner pairs.

Introduction

Observations were made of 42 relatively close (0.4 to 2.5 arcseconds) double stars. Two were found to be triple systems, and we provide orbits for the inner pairs of these newly discovered systems. Of the remaining 41 doubles, 18 were known binaries with published orbits, while the remaining 19 doubles were without published orbits and many were probably just optical doubles.

All observations were made with a portable speckle camera system that featured an Andor Luca-S EMCCD camera, which has 10 μ square pixels in a 658x496 pixel array, and x8 magnification (Genet 2013). All integrations were 15 ms in length taken through a Johnson V filter. Observations were made with 1x1 binning and 128x128 Regions of Interest (RoIs) that were read out in the "Kinetic" frame-transfer mode at approximately 67 frames/second.

The camera was mounted on a 0.5-meter PlaneWave Instruments CDK20 corrected Dall-Kirkham Cassegrain telescope equipped with a Sidereal Technology (SiTech) Servo Controller and high-resolution, on-axis encoders. This telescope is located at David Rowe's Pinto Valley Observatory located in the heart of the Mojave National Preserve in Southern California.

Calibration

By observing binaries in the Sixth Catalog of Orbits of Visual Stars (Hartkopf & Mason 2012), 17 independent estimates were obtained of the camera angle and pixel scale. For the night of observation, the predicted separations and position angles were calculated based on the ephemerides in the catalog. These values were used as inputs to the double star reduction program REDUC (Losse 2012) in its "Calibration" (as opposed to "Measure") mode, to determine the camera's position angle and pixel scale via "Autocorrelation" (Figure 1).

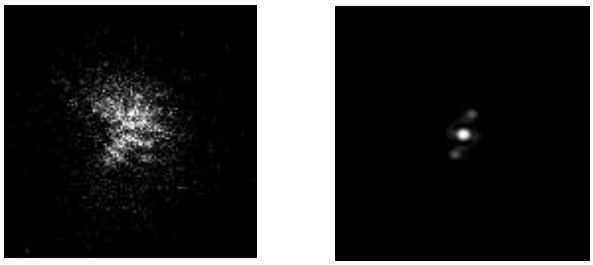

Figure 1. Typical single speckle image (left) and autocorellogram (right). These were for STT20, a binary with a separation of 0.584″. Integration times for 2000 frames were 15 ms with a Johnson V filter.

Calibration results from 17 binaries are summarized in Table 1. The camera angle is in degrees from north, while the pixel scale is in arcseconds/pixel with 10 micron pixels. The negative camera angle is a rotation west of north, i.e., 337.54°. Variances include both measurement errors and discrepancies between the predicted and actual (but unknown) true values.

	Camera Angle	Pixel Scale
Mean	-22.46	0.0538
Standard Deviation	1.54	0.0020
Standard Error of the Mean	0.37	0.0005

Table 1. Calibration results from 17 binaries.

Five east-west drifts of two relatively bright stars, 58 And and psi Per, were obtained. “Synthesis Drift” in REDUC performed the analysis by fitting linear least squares lines through the centroids to provide the camera angles, with results shown in Table 2. The standard errors of the mean are just indicators of internal precision within the repeated drift runs on each star. If measurements for 17 different single drift stars had been obtained, as was the case for 17 different binaries, then it could have been determined if there were systematic differences between various drifts. With only two drift stars, however, there was no way to reliably estimate the magnitude of any such systematic errors.

Camera Angle (°)	58 And	psi Per
Mean	-23.13	-22.9
Standard Deviation	1.04	0.71
Standard Error of the Mean	0.47	0.35

Table 2. Camera angle from five drift stars.

Drifts, with their larger internal errors and unknown external errors, were not used in the final calibration. Total reliance was placed on the mean camera angle and pixel scale derived from 17 binaries with known orbits. These values and their standard errors of the mean were, respectively, -22.46 ± 0.37° and 0.0538 ± 0.0005 ″/pixel.

Repeatability and Accuracy

Once the camera angle and pixel scale were derived, an estimate was made of the internal precision (i.e., internal consistency) and external (overall) error of the observations, using 18 binaries that were in the *Sixth Catalog of Orbits of Visual Stars* (Hartkopf & Mason 2012).

Each observation, which consisted of 2000 frames (each with 15 ms integration), was recorded as a data cube. Each cube was then broken up into four sub-cubes of 500 frames each, providing four samples that allowed an average solution to be calculated together with its corresponding standard error of the mean. Admittedly a sample of only four is small, but even a rough estimate of internal precision (repeatability) can be useful.

There is, of course, a degree of circularity in using the same set of binaries to not only determine the camera angle and pixel scale, but to also make an accuracy estimate (regression toward the mean). Thus the accuracy estimate may be an underestimate (Mendenhall et al. 1990). On the other hand, since the accuracy estimate includes both observational errors and errors in the orbital position predictions, it may be an over-estimate. It should also be noted that all observations were made within a single night, thus night-to-night variances are not represented.

Table 3 summarizes the results of the internal precision and external accuracy analysis. All values are in milli-arcseconds (mas). The values for the position angle, θ, are the "rotational" error distances in mas. The conversion of the position angle errors to tangential distance errors (simply the product of θ and ρ) allowed them to be compared on a one-to-one basis with the separation errors. At its heart, double star astrometry is the determination of the positions of centroids in an x/y plane.

	Precision	Accuracy
θ	1.1	16.0
ρ	3.4	24.8
RSS	3.6	29.5

Table 3. Internal precision and external accuracy estimates in milli arcseconds (mas).

The internal precision errors were less than the external accuracy errors by a factor of eight. It might be noted that, if instead of considering the variance within single data cubes, precision had been estimated by comparing the repeatability of observations of the same binaries across several nights (not possible in our one-night run), the internal precision would have been somewhat poorer and thus there would not have been as large a difference between internal precision and external accuracy. Also, if only binaries with high grade orbits had been used, the accuracy would have been better, further reducing the difference. The θ and ρ errors were root-sum-squared together for final, single error values for internal precision and external errors, as shown in Table 3. Thus the overall estimate of accuracy for this run was about 30 mas.

Observational Results

Observations were made over four hours on the evening of November 19, 2012, with a midpoint of almost exactly 21:00 Pacific Standard Time (UT+8). This corresponds to 07:00 UT November 20, 2012, to JD 2456251.792, and to the Besselian epoch of 2012.8880. All observations were made through a Johnson V filter with 15 ms integrations. The electron-multiplying gain was adjusted to roughly half well (half full scale) or, where that could not be reached, set at near maximum gain.

Each double star took four minutes, on average, to observe. With 15 ms integration time for each of 2000 frames in a data cube and the camera operating in the frame transfer mode, each observation took about 30 seconds. Thus the duty cycle was about 12.5%. The remaining 210 seconds were used to look up the next double to observe, command the telescope to go to that double, slew to the double, acquire the double (often using a spiral search routine written on the spot by Gray), roughly center the double on the camera display with the telescope controls, move (with the mouse) the Region of Interest (RoI) over the double, set the camera's electron-multiplying gain, check to make sure everything was okay, and, finally, start the integration.

Observational results are provided in Table 4. A Johnson V filter (540 nm center wavelength, 90 nm FWHM) was used for all observations. The first four columns (WDS Designation, Discoverer Designation, Primary Magnitude, and Secondary Magnitude) were copied straight from the Washington Double Star Catalog (Mason et al. 2013). The fifth column is the Besselian epoch. The measured values for θ and ρ (observational epoch) were determined with REDUC in the "Measure" mode, using the camera angle (Δ) and pixel scale (E) from the calibration discussed above as inputs.

WDS Designation	Discoverer	Primary	Secondary	Date	θ	ρ	O-C	O-C	Orbit	Orbit	Note
α, β (2000)	Designation	Magnitude	Magnitude	Besselian	(°)	(″)	(θ)	(ρ)	Grade	Reference	
00063+5826	STF 3062	6.42	7.32	2012.8876	352.8	1.521	0.6	-0.031	2	Kiyaeva et al. (2001)	
00546+1911	STT 20AB	6.12	7.19	2012.8876	179.5	0.584	0.2	0.016	3	Docobo & Ling (2007)	
00550+2338	STF 73AB	6.12	6.54	2012.8876	326.7	1.067	0.1	-0.024	2	Muterspaught et al. (2010)	
01095+4715	STT 515AB	4.59	5.61	2012.8877	118.2	0.495	0.1	-0.022	4	Muterspaught et al. (2010)	
01097+2348	BU 303	7.32	7.56	2012.8877	292.5	0.603					
01106+5101	BU 235AB	7.54	7.82	2012.8877	139.0	0.827	1.8	-0.028	4	Seymour et al. (2002)	
01283+4247	AC 14	8.29	8.88	2012.8878	91.9	0.765					
01401+3858	STF 141	8.28	8.61	2012.8878	303.4	1.666					
01493+4754	STF 162AB	6.47	7.22	2012.8877	198.8	1.946	0.5	-0.017	L+9	Genet et al. (this work)	b
01532+1526	BU 260	8.75	8.97	2012.8878	259.6	1.120	-0.7	0.027	5	Cvetkovic & Novakovic (2006)	
02062+2507	STF 212	8.35	8.71	2012.8878	161.8	1.904					
02140+4729	STF 228	6.56	7.21	2012.8877	295.6	0.749	0.0	-0.015	2	Soderhjelm (1999)	
02331+5828	STF 272	8.33	8.36	2012.8880	216.9	1.911					
02388+3325	STF 285	7.48	8.14	2012.8880	162.7	1.708					
02422+4242	STT 44AB	8.46	8.96	2012.8880	55.9	1.387					
02529+5300	STF 314AB,C	6.95	7.26	2012.8879	315.7	1.549					
02589+2137	BU 525	7.47	7.45	2012.8879	272.4	0.537	-2.1	0.043	4	Costa (1978)	
02592+2120	STF 333AB	5.17	5.57	2012.8879	209.9	1.381	0.4	0.025	4	Rica et al. (2012)	
03054+2515	STF 346AB	6.21	6,19	2012.8879	254.1	0.421	-3.2	-0.055	3	Heintz (1997)	
03058+4342	BU 1175	7.23	8.80	2012.8879	273.3	0.683					
03177+3838	STT 53	7.73	8.50	2012.8880	237.1	0.617	-1.0	0.016	3	Alzner (1988)	
03233+2058	STF 381	7.56	8.75	2012.8880	107.9	1.056					
03250+4013	HU 1058	8.22	8.83	2012.8880	113.8	0.840					
03285+5954	STF 384AB	8.13	8.85	2012.8880	272.4	1.953					
03302+5922	STF 389AB	6.42	7.89	2012.8879	71.5	2.523					
03312+1947	STF 403	8.71	8.92	2012.8880	172.3	2.290					
03344+2428	STF 412AB	6.60	6.86	2012.8879	353.1	0.742	0.8	0.001	3	Scardia et al. (2002)	
03401+3407	STF 425	7.52	7.60	2012.8879	60.8	1.898	0.7	-0.020	L+9	Genet et al. (this work)	b
03407+4601	STT 59	7.90	8.85	2012.8880	355.6	2.819					
03454+4952	HU 103AB	8.70	8.86	2012.8879	202.2	1.158					
04064+4325	A 1710	8.16	8.27	2012.8879	311.9	0.618	1.5	-0.001	3	Heintz (1982)	
04069+3327	STT 71AB	6.86	8.66	2012.8879	229.2	0.743					
04182+2248	STF 520	8.26	8.46	2012.8880	78.8	0.632	-2.5	0.039	3	Hartkopf & Mason (2001)	
04227+1503	STT 82AB	7.31	8.63	2012.8880	332.6	1.210	-1.2	-0.017	3	Mason et al. (2004)	
04233+1123	STF 535	6.95	8.29	2012.8878	270.5	1.054	0.8	0.002	5	Hartkopf & Mason (2000)	
04422+3731	STF 577	8.38	8.45	2012.8880	337.5	0.723				Mason et al. (2004)	
04478+5318	HU 612	7.06	8.54	2012.8880	0.3	0.699	-0.4	0.030	5	Novakovic (2007)	
05055+1948	STT 95	7.02	7.56	2012.8880	296.4	0.926	-0.6	-0.033	4	Jasinta (1996)	
05103+3718	STF 644AB	6.96	6.78	2012.8880	222.6	1.647					
05167+1826	STF 670AB	7.72	8.28	2012.8880	165.1	2.520					
05188+5250	STF 657	8.30	8.81	2012.8880	310.5	0.952					
05240+2458	STF 694AB	8.65	8.54	2012.8880	14.2	1.379					

Table 4. Double star speckle measures.

Notes:
[a] In close agreement with recent speckle observations in θ, but off in ρ. See orbital plot below.
[b] Our analysis suggests this is a gravitationally bound triple system.
[c] Similar to "a" above, in close agreement in ρ, but other θ speckle observations were about 242°.
[d] Significant trend in past speckle interferometry observations confirmed by our observation.
[e] As above, significant trend confirmed by our observation.

The observed minus calculated (O-C) values for θ and ρ were calculated by comparing observed values with those interpolated from the Sixth Catalog of Orbits of Visual Stars ephemerides to the night of observation.

Two New Triple Star Systems with Detectable Inner Orbital Motions

Table 5 provides fundamental information on the two systems we suspected to be triple star systems. We found that the superimposed movements are clearly reflected in the measurements, especially in the position angles, so we calculated the orbital elements for the inner systems. We did not calculate orbits for the presumably very long period outer systems, simply assuming that their path over a short time scale was linear. Meaningful orbital calculations of the outer pairs may only be possible after further measurements from coming decades. Lists of measurements and resulting residuals used can be obtained by request.

Washington Double Star catalogue	WDS 01493+4754	WDS 03401+3407
Discoverer Designation	STF162 AB | CHR 4 Aa,Ab	STF 425
Aitkens Double Star catalogue Nr.	ADS 1438	ADS 2668
Henry Draper catalogue Nr.	HD 11031	HD 22692
Hipparcos catalogue Nr.	HIP 8475	HIP 17129
Coordinates α_{2000} / δ_{2000}	27.°31 / +47.°90	55.°03 / +34.°12
Parallax (van Leeuwen 2007)	0.”00784 ± 0.”00102	0.”02173 ± 0.”00084
Distance to Sun (in Parsecs)	$127.6^{+19.0}_{-14.7}$	$46.0^{+1.9}_{-1.7}$
Combined visual magnitude (V in mag)	5.82	6.82
Differential visual magnitude (dV in mag)	0.8 | ~3 estimated	0.1
Combined spectral and luminosity class	A3V	F9 V

Table 5. Designations, coordinates, and other properties.

WDS 01493+4754 = STF162 AB / CHR4 Aa,Ab = ADS 1438

Located in Perseus, this system is at least triple. The notes entry for this system in the Washington Double Star Catalog contains the following information: “Although this new component is indicated as Aa,Ab, we have not firmly established whether it is associated with the A or B component of the wide pair. B is a spectroscopic binary. The system appears to be quintuple” (McAlister et al. 1987).

We considered whether the combined and overlaid movement sequences (the three proven components) are visible and predictable. For the inner pair CHR4 Aa,Ab measurements exist from 1984 to 1994. These cover an arc of about 60 degrees and show a well-defined orbital arc. After 1994, the inner system unfortunately could not be resolved. But this suborbital motion is detectable in the residuals of the outer system STF162 AB (Figure 2), so we determined a provisional period of the internal system. The measurements for STF162 AB covers nearly 180 years; the first successful separation of the main components are from J.F.W. Hershel in 1828.

We began our analysis with a weighted fit, calculating only the linear motion parameters in Cartesian coordinates. The general form was adopted from Debehogne and de Freitas Mourao (1977). The resulting residuals (in arcseconds) are plotted against time as shown in Figure 2.

Clearly visible is the expected “wobble”, induced by the overlaid motion of the inner pair CHR4 Aa,Ab. A first tentative period of nearly 35 years was assumed from the residuals in Figure 2. A first combined differential correction fit with zero eccentricity and the preliminary period was made. The resulting period for CHR4 Aa,Ab is P_{inner} = 36.9 years with an uncertainty of ±0.6 years. The other tentative (circular) elements are T_{inner} = 2004.6, α_{inner} = 0.056 arcseconds and a node of $\Omega_{2000\ inner}$ = 16 degrees. With these tentative elements it is possible to calculate an independent visual orbit for the inner pair based on the available speckle measurements for CHR4 Aa,Ab. A differential correction routine in rectangular coordinates was used (van den Bos 1926, also see Heintz 1978). On this basis, the correction factors for the elements ΔT_{inner}, Δe_{inner}, ΔA_{inner}, ΔB_{inner}, ΔF_{inner} and ΔG_{inner} are calculated. The period was assumed to be known (P_{inner}=36.9 years), thus fixed and not corrected. After several iterations, a new independent visual orbit for the inner pair was found (Table 6). Subsequently, the linear path and the inner photo centric semi-major axis based on the new visual orbits were calculated, based on the combination of differential correction for linear and orbital motion in rectangular coordinates. All final elements are collected in Table 6. The ephemerides for the inner and outer components are collected in Table 7. Additional figures for the final outer combined linear and photo centric solution and the inner visual orbital solution can be found in Figures 3 and 4.

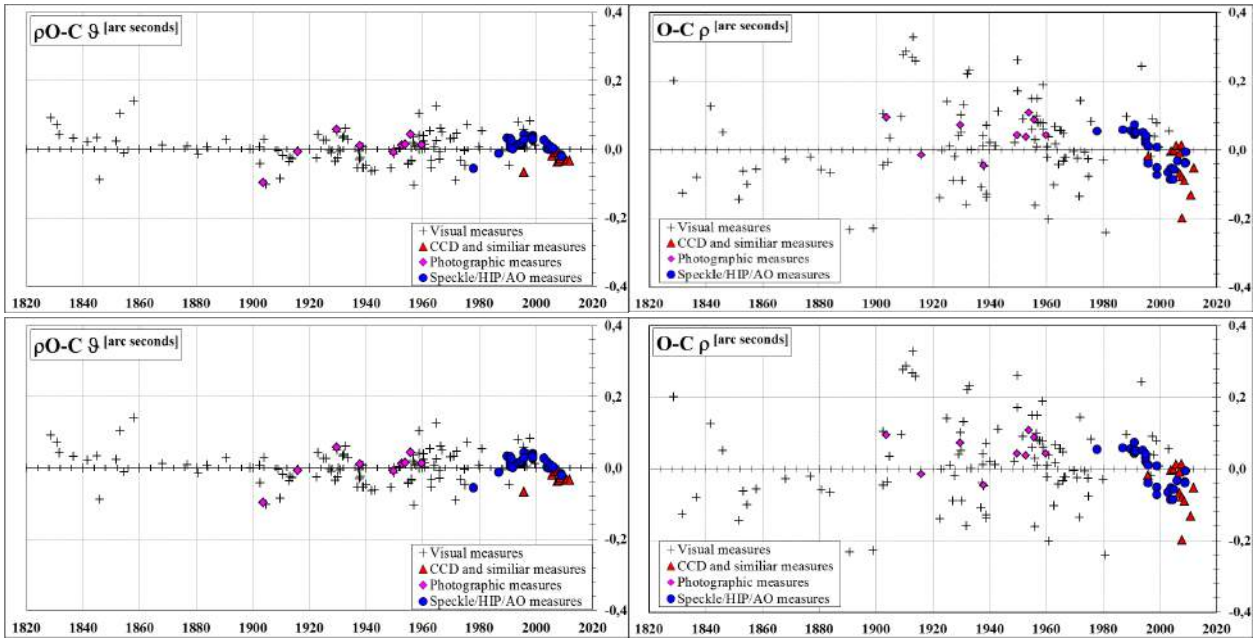

Figure 2. Residual plots for STF 162 AB, only linear motion assumed.

linear solution main components (outer)				new visual orbit (inner) with photo centric amplitude, calculated from linear motion residuals from STF 162 AB			
$X_0 = \Delta\delta$	-1.663	± 0.029	arcseconds	P_{inner}	36.9	± 0.6 (adopted, see text)	years
$\mu_X = \mu_\delta$	-0.00241	± 0.00015	arcseconds / year	T_{inner}	2004.8	± 3.8	years
$Y_0 = \Delta\alpha_{cos\delta}$	-0.957	± 0.050	arcseconds	e_{inner}	0.234	± 0.069	-
$\mu_Y = \mu_{\alpha cos\delta}$	0.00418	± 0.00012	arcseconds / year	α_{inner}	0.040	± 0.003	arcseconds
t_0	1937.8	± 12.5	years	a_{inner}	0.122	± 0.027	arcseconds
ϑ_0	209.9	± 1.7	degrees	i_{inner}	34.4	± 15.5	degrees
ρ_0	1.919	± 0.004	arcseconds	$\omega_{secondary\ inner}$	348.6	± 43.8	degrees
μ_{XY}	0.00482	± 0.00019	arcseconds / year	$\Omega_{2000\ inner}$	32.0	± 40.5	degrees

Table 6. Final combined linear + orbital results for STF 162 AB and CHR 4 Aa,Ab.

The mass sum for the innerpair CHR 4 Aa,Ab is $\Sigma M = 2.8 \pm 1.2\ M_{Sol}$, the errors in mass resulting from orbit and parallax uncertainties. With the relation from Equation 1, it is not possible to estimate the individual masses for the single members of CHR 4 Aa,Ab. The value $f\text{-}\beta = 0.33 \pm 0.03$ was obtained. However, since the difference in brightness is not known (no measurements are available), a preliminary estimate must be made. A luminosity ratio β can be calculated if we estimate a tentative assumed brightness difference dV. If dV = 3 ± 1 mag assumed, a mass ratio f = 0.39 ± 0.06 was calculated. This results in individual masses for $Mass_{CHR\ 4\ Aa} = 1.7 \pm 0.8\ M_{Sol}$ and for $Mass_{CHR\ 4\ Ab} = 1.1 \pm 0.5\ M_{Sol}$.

Ephemerides	Combined motion		Linear path only		Photo centric orbit only		Visual orbit inner pair CHR 4 Aa,Ab	
	ϑ_{2000} [°]	ρ ["]	ϑ_{2000} [°]	ρ ["]	Δδ ["]	Δα ["]	ϑ_{2000} [°]	ρ ["]
2013.0	198.3	1.964	199.2	1.953	-0.021	0.026	128.6	0.103
2015.0	198.1	1.979	198.9	1.955	-0.032	0.019	148.7	0.114
2017.0	198.0	1.991	198.7	1.957	-0.040	0.011	165.1	0.126
2019.0	198.0	2.001	198.4	1.958	-0.045	0.001	178.7	0.137
2021.0	197.9	2.008	198.1	1.960	-0.047	-0.009	190.5	0.145
2025.0	197.9	2.012	197.6	1.964	-0.042	-0.026	211.6	0.150
2030.0	197.7	2.001	196.9	1.970	-0.022	-0.038	240.2	0.132
2035.0	197.1	1.976	196.2	1.975	0.009	-0.031	285.7	0.097
2040.0	195.8	1.953	195.5	1.981	0.029	-0.001	358.7	0.089

Table 7. Ephemerides for STF 162 AB and CHR 4 Aa,Ab.

These mass values are only preliminary, but they could help determine the parameters of the individual components. It is important to obtain new and accurate measurements of the positions and brightness differences of the inner components. By using lucky imaging, it may be possible to determine the assignment of the inner system to STF 162 A or STF 162 B.

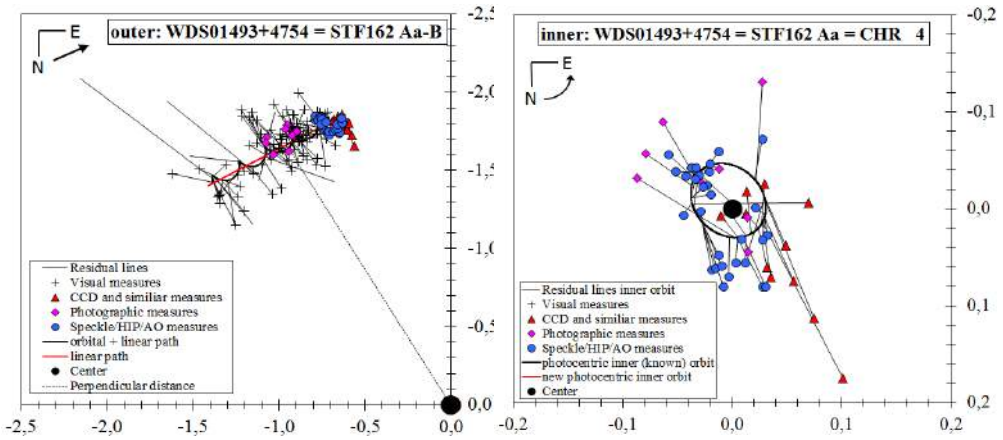

Figure 3. Outer combined Linear + orbital solution (left), and inner photo centric orbital solution only, visual measures not shown (right).

WDS 03401+3407 = STF 425 = ADS 2668

The double star STF 425, located in constellation Perseus, was first discovered by William Herschel in 1783. However, he only measured the position angle. Only 40 years later, J. South obtained the first complete measurement. The two main visible stars currently have a separation of about 2 arcseconds. These stars have almost the same brightness and are yellow main sequence stars with the common spectral class F9. Basic information on STF 425 is provided above in Table 5. Rica noted that STF 425 shows an interesting trend as can be seen in Figure 6. A preliminary Cartesian plot of the secondary's x and y positions showed an "S" shaped wobble, suggesting a triple system. The speckle interferometry observations prior to ours were made by McAlister et al. (1987), Scardia et al. (2007), Prieur et al. (2008), Castets and Tregon (2009), Scardia et al. (2011), and Mason et al. (2012b). Past observations for the analysis were supplied by the US Naval Observatory to which we added our recent speckle observation.

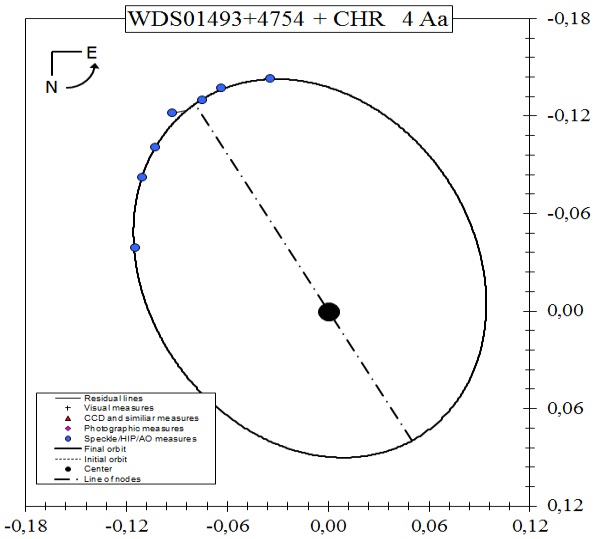

Figure 4. Inner visual orbital solution for CHR 4 Aa,Ab.

Andre Tokovinin pointed out to us that STF 425 was observed in 2012 with Robo-AO on the 1.5-meter telescope at Palomar Observatory, and he saw no companion around A or B.

We initiated our analysis with a weighted fit, calculating only linear motion parameters in Cartesian coordinates. The general form was adopted from Debehogne and de Freitas Mourao (1977). The resulting residuals (in arcseconds) are plotted against time and shown in Figure 5.

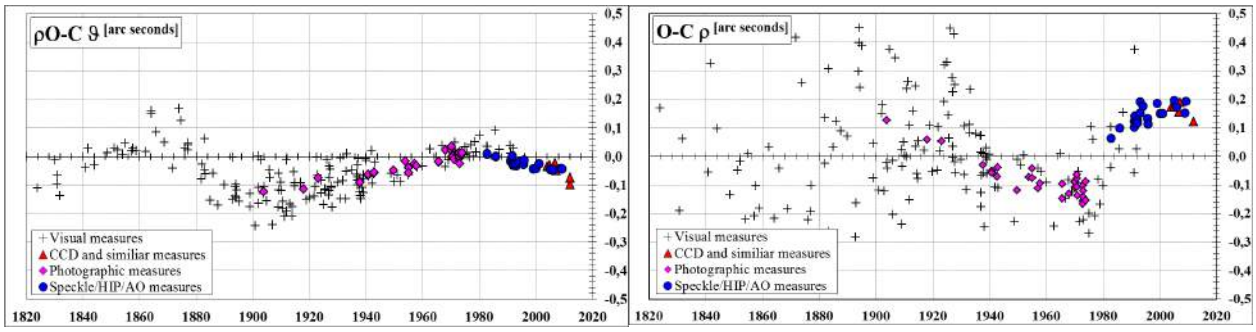

Figure 5. Trend plots for STF 425, only linear motion assumed.

Clearly visible in the position angle (θ) and separation (ρ) rho residuals in Figure 5, based on a preliminary linear fit, is remarkable "wobble" of about 0.1 arcseconds. This is a very clear indication of a suborbital movement caused by a possible invisible companion. We performed a combined calculation of the linear (for the outer orbit) and the orbital (for the inner orbit) movement in Cartesian coordinates, based on the combination of differential correction for 7 orbital elements (van den Bos, 1926) and the 4 parameters from linear motion (see above).

This differential correction fit was made based on the first linear elements and an assumed fixed period of ~110 years. For simplification, zero eccentricity was assumed, and thus only A_{inner}, B_{inner}, F_{inner}, G_{inner} and the four linear elements had to be calculated.

Subsequently, we applied a reweighting procedure as described by Irwin, Walker, and Young (1996). A combined linear and orbital fit based on the initial outer (linear) and inner (orbital) fit was made by freeing the correction parameters for eccentricity and periastron passage, with final results as shown in Table 8.

We did not assume that only orbital motion was detectable in the inner pair. We performed a combined orbital-orbital solution (for both the outer and inner orbits) in Cartesian coordinates (with maximum 14 possible unknowns) following van den Bos (1926). The final weights from the linear and orbital fits were used. For the outer orbit, zero eccentricity was assumed, thus differential corrections were only for A $_{outer}$, B $_{outer}$, F $_{outer}$, G $_{outer}$ and a period fixed with a preliminary period of P outer = 2000 years. The inner orbit was, at first, adopted from a linear orbital solution and was not differential corrected at first. But it turned out that the orbit calculation is only possible if the period is fixed and the orbit is assumed at circular. Thus differential corrections were performable only for A_{outer}, B_{outer}, F_{outer}, G_{outer}. In this case, different fixed periods can be calculated for an orbit, but it is clear that an orbital curvature was barely recognizable and therefore a simplistic circular orbit calculation was vague. Thus the preferred solution is the linear + orbital solution, provided in Table 8.

Linear solution main components (outer)				New photo centric orbit (inner)			
$X_0 = \Delta\delta$	1.141	± 0.021	arcseconds	P_{inner}	106.5	± 1.7	years
$\mu_X = \mu_\delta$	0.00933	± 0.00011	arcseconds / year	T_{inner}	1980.19	± 0.94	years
$Y_0 = \Delta\alpha_{cos\delta}$	1.287	± 0.019	arcseconds	e_{inner}	0.612	± 0.050	-
$\mu_Y = \mu_{\alpha cos\delta}$	-0.00827	± 0.00025	arcseconds / year	α_{inner}	0.179	± 0.008	arcseconds
t_0	2045.3	± 2.6	years	i_{inner}	106.8	± 2.4	degrees
ϑ_0	48.4	± 0.9	degrees	$\omega_{1\ inner}$	77.8	± 3.4	degrees
ρ_0	1.719	± 0.006	arcseconds	$\Omega_{2000\ inner}$	65.5	± 2.6	degrees
μ_{XY}	0.01247	± 0.00027	arcseconds / year				

Table 8. Final combined linear + orbital results for STF 425.

The final linear + orbital fit produces residuals with rms and MA values in position angle (θ) of 0.50/0.32 degrees, the rms/MA values in separation (ρ) are 0.043 and 0.026 arcseconds. The ephemerides up to 2040 are shown in Table 9.

Ephemerides	Combined motion		Linear path only		Photo centric orbit only		Estimated visual orbit inner pair a = 0.59 arcseconds assumed	
	ϑ_{2000} [°]	ρ ["]	ϑ_{2000} [°]	ρ ["]	Δδ ["]	Δα ["]	ϑ_{2000} [°]	ρ ["]
2013.0	60.1	1.918	61.6	1.766	0.117	0.109	223.0	0.520
2015.0	59.3	1.907	60.8	1.760	0.117	0.102	221.0	0.506
2017.0	58.4	1.896	60.0	1.755	0.117	0.094	218.9	0.490
2019.0	57.5	1.885	59.2	1.750	0.116	0.086	216.6	0.473
2021.0	56.7	1.874	58.4	1.746	0.115	0.078	214.1	0.454
2025.0	54.9	1.851	56.8	1.738	0.112	0.061	208.5	0.415
2030.0	52.8	1.823	54.8	1.730	0.106	0.038	199.9	0.366
2035.0	50.5	1.796	52.7	1.724	0.097	0.015	188.5	0.319
2040.0	48.3	1.770	50.6	1.721	0.086	-0.009	173.8	0.283

Table 9. Ephemerides for STF 425 to 2040.

Although it was not possible to assign the movement of the invisible companion to either component A or B, for simplification we assigned it tentatively to component A. If it is detectable, only further observations are likely to provide the assignment of the invisible companion to the appropriate component. The apparent motion of the linear and orbital paths, the measurements, and the corresponding residual lines are displayed in Figure 6; the axis units are in arcseconds.

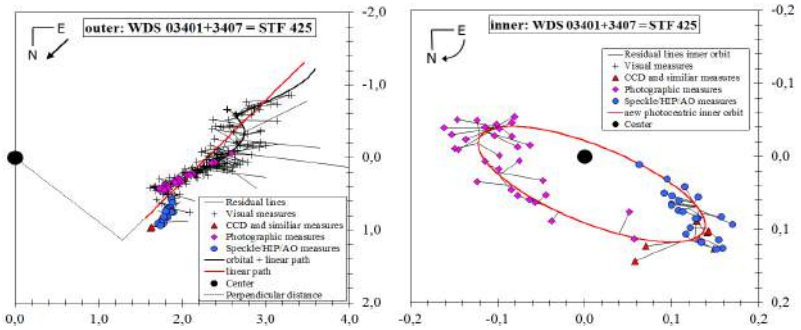

Figure 6. Outer combined Linear + orbital solution (left), and inner photo centric orbital solution only, visual measures are not shown (right).

Summarizing, the inner orbit has a period of about 107 years. The eccentricity seems to be large (e~0.6) and the photo centric half axis is α = 0.18 arcseconds. Both visible members of this system are nearly equal in brightness, color, and absolute magnitude. Thus it can be assumed that each component is a late F main sequence star with a mass of M_{SOL} ~1.2 (Schmidt-Kaler, 1982). With this result, one can try to estimate the mass of the invisible companion. For this estimate we need some formulas, described below.

To determine the total mass (ΣM) of a visual binary system, the period (P in years), the great semi major axis (a in arcseconds), and the parallax (π in arcseconds) are required, given in Equation 1.

$$\Sigma M = M_{VC} + M_{IC} = a^3 \cdot \pi^{-3} \cdot P^{-2} \qquad \textit{Eq. 1}$$

The total mass (ΣM) of the sub system is composed by the mass one of the visible component (M_{VC} in units of Sol mass) and the mass of the invisible component (M_{IC} in units of Sol mass). Further, we require an estimate of the mass ratio (B). In the present case, this is simply taken as the ratio of the photo centric semi major axis (α in arcseconds) of the visible component to the semi major axis (a in arcseconds) of the orbital path of the both components:

$$B = \frac{\alpha}{a} = \frac{M_{IC}}{M_{VC} + M_{IC}} \qquad \textit{Eq. 2}$$

The reorganization and combination of Equation 1 and Equation 2 leads to the following relations:

$$\alpha \cdot \frac{M_{VC} + M_{IC}}{M_{IC}} = \alpha \cdot \frac{a^3 \cdot \pi^{-3} \cdot P^{-2}}{M_{IC}} = a = \left[\left(M_{VC} + M_{IC} \right) \cdot \pi^3 \cdot P^2 \right]^{1/3} \qquad \textit{Eq. 3}$$

As a result we only have two unknowns; the mass of the invisible component (M_{IC}) and the semi major axis a. The mass of the visible component (M_{VC}) we can adapt from Schmidt-Kaler (1982) tables for physical parameters of main sequence stars. Within reasonable limits we estimate a theoretical value for the mass of the invisible companion.

With Equation 4 we can derive the theoretical (visible) half axis of the inner orbit and the theoretical mass of the visible primary iteratively, until this value is the same as the initial mass for an late F type main sequence star: M_{VC} = 1.2 M_{SOL}.

$$M_{VC} = \frac{M_{IC}}{\alpha} \left[\left(M_{VC} + M_{IC} \right) \cdot \pi^3 \cdot P^2 \right]^{1/3} - M_{IC} \qquad \textit{Eq. 4}$$

If the calculated mass value coincides with the theoretical value, the value of the visual semi major axis (a in arcseconds) can be calculated via:

$$a = \left[\left(M_{VC} + M_{IC} \right) \cdot \pi^3 \cdot P^2 \right]^{1/3} \qquad \textit{Eq. 5}$$

The calculated value for the photo centric half axis, is α_{calc} = 0.18 arcseconds. If the Mass for the invisible companion matches with 1.2 M_{SOL}, then we obtain the result of 0.53 M_{SOL} for the invisible companion. The theoretical, visible half axis is ~ a_{inner} = 0.586 arcseconds. A star with a mass of 0.5 M_{SOL} is possible for an early M dwarf star, with a corresponding large difference in brightness. This may be the reason that this companion is not resolvable in visual pass bands.

Comparison with Previous Observations

To compare the 20 binaries observed with all previously reported observations, plots from ORB6 were opened in Microsoft Paint and the coordinates of the "fixed" primary star and the plot scale (graphic pixels/arc second) determined. These three values—two for the primary star coordinates, and one for scale—were entered into a spread sheet for each binary along with the measured θ and ρ values for the binaries.

The graphic pixel location on each plot for each observation was calculated and a large "+" sign, centered on the location of the current observation, was then "penciled" in. To see how well observations matched the predicted time along the orbit for the night of observation, the time along each orbit, based on interpolated θ and ρ values from ORB6 ephemerides, was marked with a long, thin line. The observational sequence number was added to the plots in the lower left corner. Past observations that are **green +** are visual (micrometer) observations, **violet *** are photographic, while **blue** filled circles are speckle interferometry. A **red +** is Hipparcos, while a **red T** is Tycho.

Near or on the Line

The first set of 12 observations, shown below, was very near or essentially on the lines of the predicted elliptical paths.

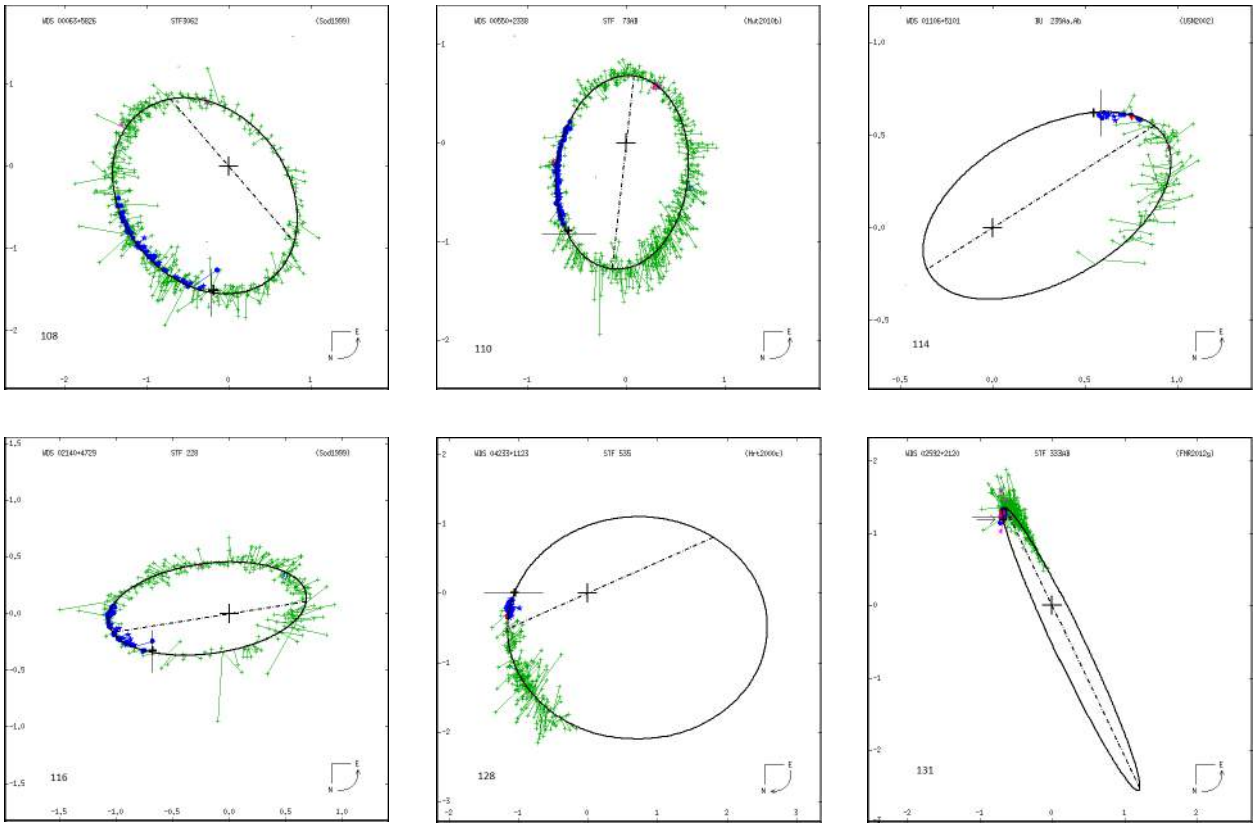

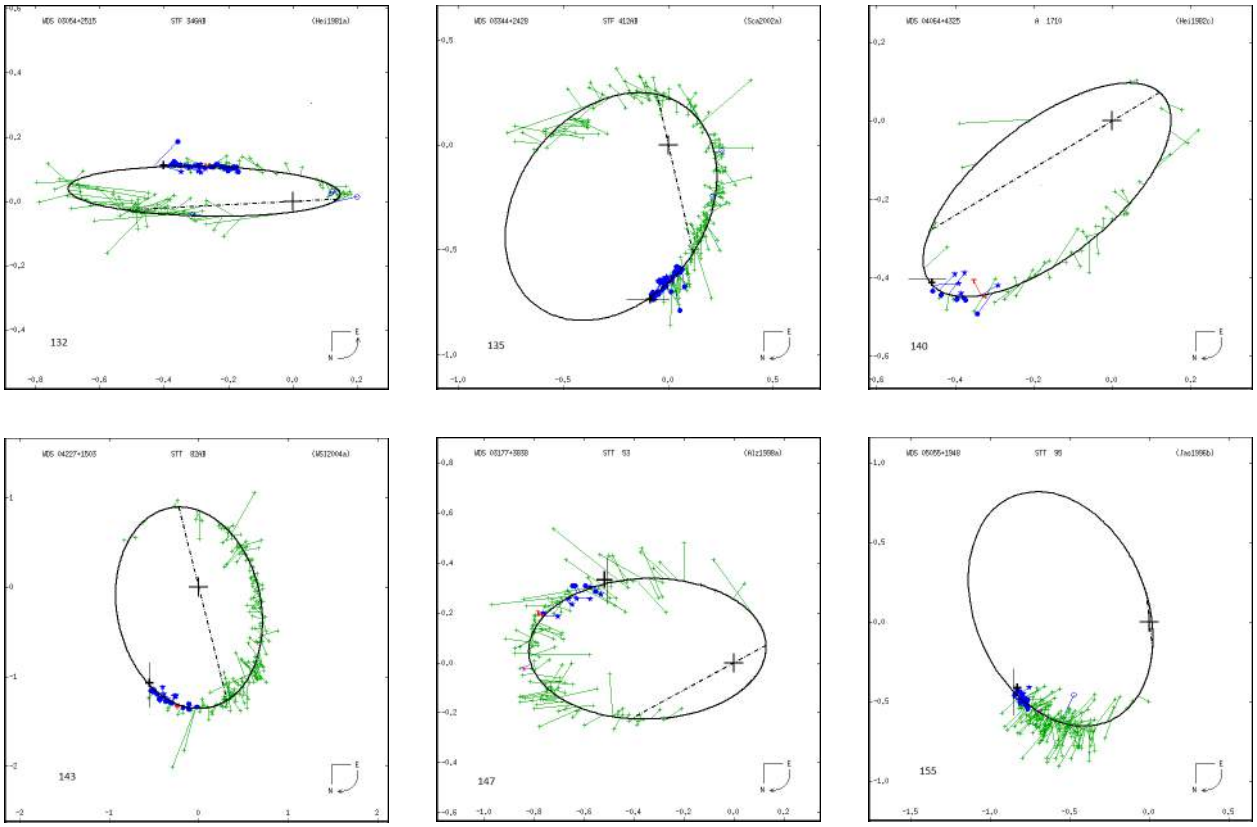

Not on the Line (but perhaps that was all right)

Although observations were not on the line for six of the 20 binaries, they were near other inteferometric measures that were also off the line (or headed off the line). This may suggest that these orbits were off and a recalculation of the orbit would have put observations on the line. Many of these orbits were just provisional (Grade 5) orbits, so it may not be worthwhile to recalculate them until further speckle interferometric observations are made. The O-C "errors" from these orbits may over-represent actual external errors.

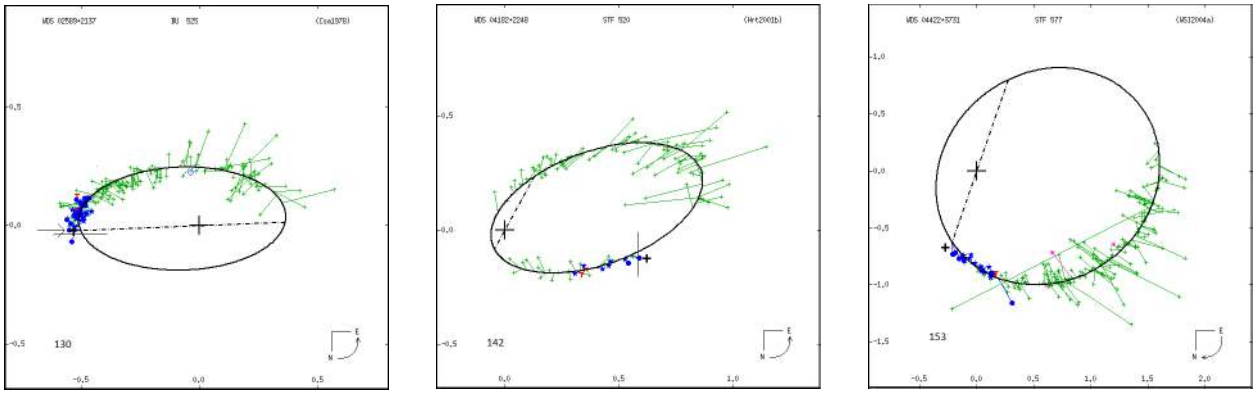

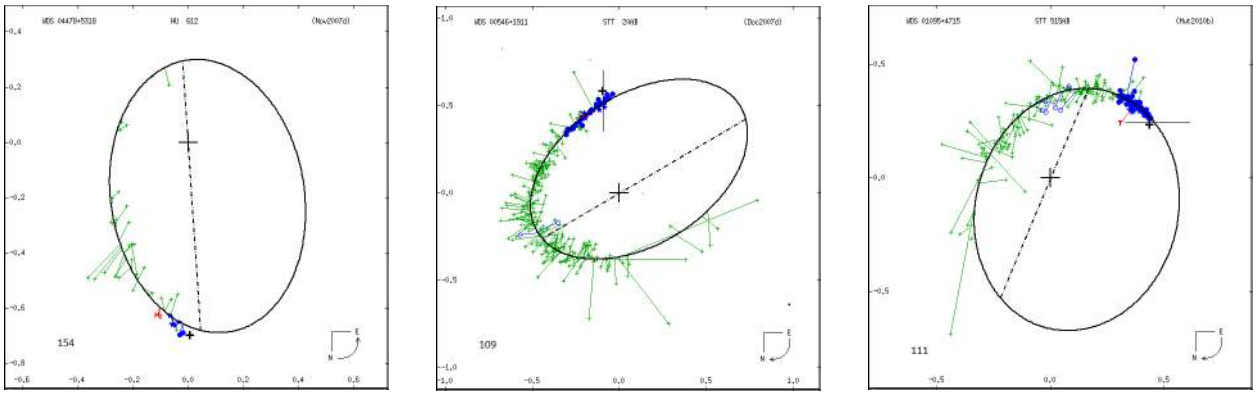

Off the Line (but not way off)

Finally, there were two cases where the plots suggested that the observations were further off than many other interferometric measurements. Perhaps such points might be expected to happen on occasion, since the 0.5-meter telescope had significantly less aperture than many of the other telescopes reporting speckle interferometry observations. Alternatively, perhaps these points are the start of a new "trend" or direction for speckle observations. This could be the case for BU 260, although STF 202 is clearly both off the orbit and also discordant with respect to other speckle observations. The autocorrelogram for STF 202 was by far the poorest of the 20 binaries, but BU 260's looked quite normal.

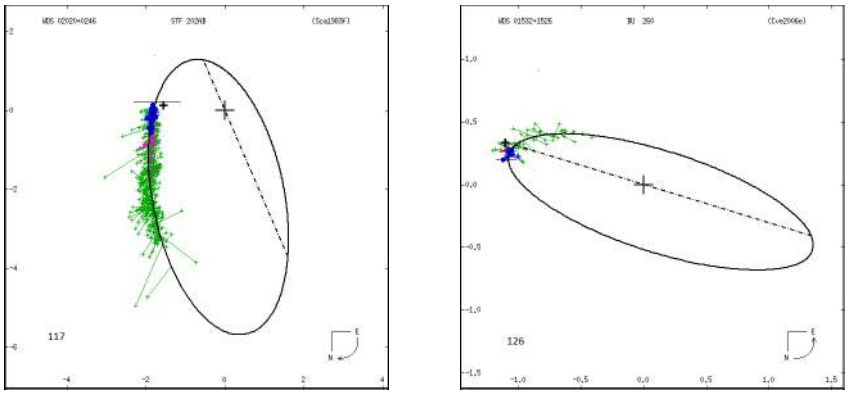

Conclusion

We measured the position angles and separations of 42 fairly close double stars over four hours with a portable speckle interferometry camera system on a 0.5-meter telescope. We reduced our data with REDUC, a program written by Florent Losse. We discovered two new triple star systems and derived orbits for the inner pairs.

Acknowledgments

We thank the American Astronomical Society for funding the Andor Luca-S EMCCD camera and also Andor for making a demonstration unit available at a reduced price. We also thank the US Naval Observatory for extensive use of the *Washington Double Star Catalog*, the *Sixth Catalog of Orbits of Visual Binary Stars*, and the *Forth Interferometric Catalog*. A special thanks goes to Brian Mason for past observations and to Robert Buchheim for help with orbital plots. Finally, we thank the reviewers of this paper for their helpful suggestions: Robert Buchheim, Joseph Carro, Jerry Foote, Thomas Frey, Jolyon Johnson, Brian Mason, Thomas Smith, Vera Wallen, and Ed Wiley.

References

Alzner, A. 1998. *A&AS*, 132, 253.
Castets, M. & Tregon, B. 2009. *El Observador de Estrellas Dobles*, 3, 7.
Costa, J. M. 1978. *Inf. Circ.*, 75.
Cvetkovic, Z. & Novakovic, B. 2006. *Ser AJ*, 173, 73.
Debehogne, H. & de Freitas Mourao, R. R. 1977. *Astronomy and Astrophysics*, 61, 453-457.
Docobo, J. A. & Ling, J. F. 2007. *AJ* 133, 1209.
Genet, R. M. 2013. *Journal of Astronomical Instrumentation.* In preparation.
Hartkopf, W. I. & Mason, B. D. 2012. *Sixth Catalog of Orbits of Visual Binary Stars,* Washington: US Naval Observatory.
Hartkopf, W. I. & Mason, B. D. 2000. *IAUC*, 142.
Hartkopf, W. I. & Mason, B. D. 2001. *IAUC*, 145.
Heintz, W. D. 1978. *Double Stars (revised edition).* Ed. Dordrecht, D. *Geophysics and Astrophysics Monographs*, 15.
Heintz, W. D. 1982. *IAUC*, 88.
Heintz, W. D. 1997. *ApJS* 111, 335.
Irwin A. W., Yang S. L. S., & Walker G. A. H. 1996. *PASP*, 108, 580.
Jasinta, D. M. D. 1996. *A&AS*, 118, 381.
Kiyaeva, O. V., Kisselev, A. A., Polyakov, E. V., & Rafal'Skii, V. B. 2001. Pisma Astron. *Zhur*, 27, 456.
Losse, F. 2012. REDUC V4.7. http://www.astrosurf.com/hfosaf/Reduc/Tutorial.htm
Mason, B. D., Hartkopf, W. I., Wycoff, G. L., Pascu, D., Urban, S. E., & Hall, D. M. 2004. *AJ*, 127, 539.
Mason, B. D., Wycoff, G. L., & Hartkopf, W. I. 2012a. *The Washington Double Star Catalog*, Washington: US Naval Observatory.
Mason, B. D., Henry, T. J., Soderblom. D. R., Hartkopf, W. I., Holdenreid, E. R., Rafferty, T. J., & Urban, S. E. 2012b. In preparation.
McAlister, H. A., Hartkopf, W. I., Hutter, D. J., & Franz, O. G. 1987. *AJ*, 93, 688.
Mendenhall, W., Wackerly, D. D., & Shara, M. M., 1990. *Mathematical Statistics with Applications*, 4. Boston: PWS-Kent.
Muterspaugh, M. W., Hartkopf, W. I., Lane, B. F., O'Connell, J., Williamson, M., Kulkarni, S. R., Konacki, M., Burke, B. F., Colavita, M. M., Shao, M., & Wiktorowicz, S. J. 2010. *AJ*, 140, 1623.
Novakovic, B. 2007. *ChJAA*, 7, 415.
Prieur, J. L., Scardia, M., Pansecchi, L., Argyle, R. W., Sala, M., Ghigo, M., Koechlin, L., & Aristidi, E. 2008. *MNRAS*, 387, 772.
Rica, F. M., Barrena, R., Vazquez, G., Henriquez, J. A., & Hernandez, F. 2012. *MNRAS*, 419, 197.
Scardia, M., Prieur, J. L., Koechlin, L., & Aristidi, E. 2002. *IAUC*, 147.
Scardia, M., Prieur, J. L., Pansecchi, L., Argyle, R. W., & Sala, M. 2011. *AN*, 332, 508.
Scardia, M., Prieur, J. L., Pansecchi, L., Argyle, R. W., Basso, S., Sala, M., Ghigo, M., Koechlin, L., & Aristidi, E. 2007. *MNRAS*, 374, 965.
Schmidt-Kaler, T. H. 1982. Physical parameters of the stars. In *Landolt-Bornstein New Series*, 2b, astronomy and astrophysics – stars and star cluster. Eds. Schaifers, K. & Voigt, H. H. New York: Springer.
Seymour, D., Mason, B. D., Hartkopf, W. I., & Wycoff, G. L. 2002. *AJ*, 123, 1023.
Soderhjelm, S. 1999. *A&A*, 341, 121.
van den Bos, W. H. 1926. *CiUO*, 68, 352.
Van Leeuwen, F. 2007. *Hipparcos, the New Reduction of the Raw Data.* Astrophysics & Space Science Library. Berlin: Springer, 350.

Double Star Research with Speckle Interferometry

Cameron Allen[1], Jason Goad[1], Ryan Morshead[1], Kaitlin McArdle[1], and Eric Weise[2]

1. California Polytechnic State University, San Luis Obispo
2. University of California, San Diego

Abstract Six double stars were recorded and analyzed using speckle interferometry. Results were generally in accordance with previous observations provided by the Washington Double Star Catalog.

Introduction

Observations were made by several students (Figure 1) on two separate dates, the first on Saturday, August 31, 2013 (B2013.665), a still, cloudless night. This run gathered data on five stars: STF2404, STF 2492AB, STF2613AB, STF2725AB, and STF2978. The second run was conducted on Friday, September 13, 2013 (B2013.700), also a still, cloudless night, where data was gathered on STF2848 and STF2727AB. Through these observations and the experiences that they offered, new students were provided an introduction to double star research and the recording of scientific data, and experience in the process of writing and publishing research papers.

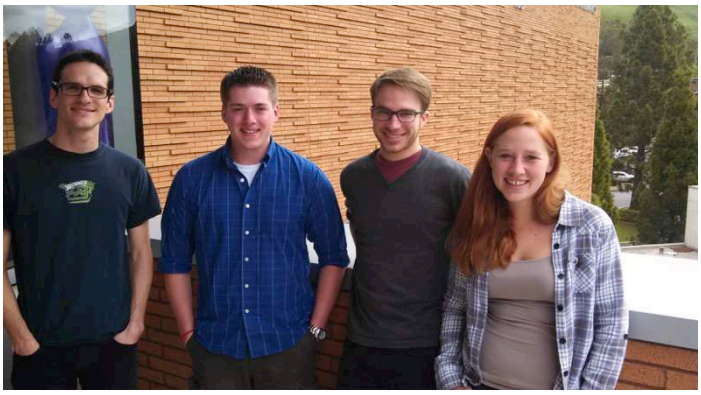

Figure 1. Cal Poly students left to right:
Jason Goad, Cameron Allen, Ryan Morshead, and Kaitlin McArdle.

Equipment

For observations, a 10 inch f/10 Meade Schmidt-Cassegrain equatorially mounted telescope was used with a x5 Barlow lens, yielding a 500 inch effective focal length. This telescope is the primary instrument used at the Orion Observatory in Santa Margarita, CA. The control system was made by Sidereal Technology (SciTech) based in Portland, Oregon. The SciTech control system was interfaced with TheSky6 for quick slewing to stars.

The equipment used for our speckle observations was a camera and optical system designed for portability and use on a wide range of telescopes (Genet et al. 2013). In the past, this system had been taken to a variety of telescopes, including the Pinto Valley Observatory's 0.5 meter and to the Kitt Peak National Observatory's 2.1 meter telescopes. At the heart of this portable speckle imaging system is an Andor Luca-S front illuminated EMCCD camera.

This camera has a 658x496 pixel CCD chip with 10 micron square pixels. Andor's electron multiplication system allows for very fast exposures to be taken at a very high signal to noise ratio. The optical system also included a slide mirror which allowed a wide-field CCD acquisition camera to be attached. We used an SBIG 402. The slider was modified by Reed and Chris Estrada, who attached a linear stepper motor, allowing the mirror to be moved with no external torque being applied to the telescope.

The last piece of equipment on the portable speckle system is a Nautilus Controller filter wheel. This motorized wheel has seven removable filter positions. In our system we had Cousins R, I, B, and V, Sloan R and V, and a narrow-band Hα filter. For our observations we used the Cousins R filter to observe double stars and drift calibrations, and we used the Hα filter for slit mask calibrations (Figure 2).

Methods

All integration times in this experiment were 15 milliseconds and stored in .fits format. Our data was analyzed using REDUC, a software developed by the French double star observer Florent Losse. The data acquisition and analysis were accomplished using the built-in functions in this software.

At the beginning of our run we calibrated the camera using Altair. First we took seven 2,000 frames using a slit mask and a Hα filter. For the first three of these, the slit mask was not rotated, but the last four we rotated the mask by an arbitrary angle to mitigate any systematic bias introduced by having only one mask orientation. The angular distance from the central to first order diffraction peaks was found to be z = 7.914 arc seconds by the formula:

$$\frac{206{,}265\lambda}{d}$$

(Maurer 2012), where λ is the central wavelength of the Hα filter (656.281 nanometers) and d is the spacing between the centers of the slits (17.1 millimeters). Using z, we found the pixel scale to be 0.2537±0.0010 arc seconds per pixel.

We then did five drifts using Altair and a Cousins R filter. The drift integration times were 15 milliseconds long and took 250 frames to cross the entire field of view. Using the “Synthetic Drift” feature in REDUC, we found our camera angle to be -3.35 degrees, with a standard deviation of 0.19 degrees. A total of five drifts were taken with Altair.

For observing our target stars, we used the Cousins R filter. Six runs of 2,000 images each were taken for each double star system (seven runs were done for STF2725AB). Each of these runs was then analyzed using the “Autocorrelation” function in REDUC. This function runs each image through a series of ten distinct Fast Fourier Transforms (FFT) to produce ten ‘masks’ (S0-S9) that compress the frames into a single image with varying contrasts (Figure 3). From this image, we reduce the data by selecting our points, and after inputting our pixel scale (E) and camera angle (Δ), we found our position angle (Θ) and separation (ρ). There is a 180° ambiguity in the position angle measurement when using autocorrelation. To resolve the issue, we compared our position angles to recent measurements catalogued in the Washington Double Star Catalog, and chose the value that agreed with recent measurements. Due to the slow-moving nature of the observed systems, rapidly changing position angles were not an issue.

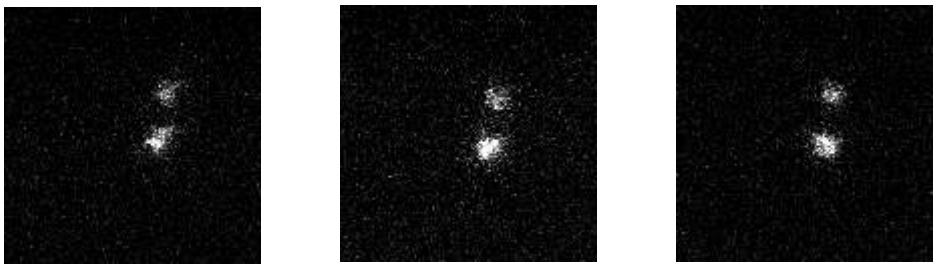

Figure 2. Three of 2000 initial frames of STF2725 showing the "speckles" that are present before undergoing speckle interferometry.

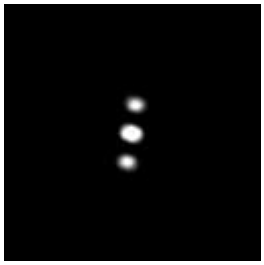

Figure 3. Autocorrelogram image of STF2613.

Data

One auxiliary goal of this project was to provide the observers with an estimate of the limits of speckle interferometry and, specifically, of the limitations of our equipment. To this end we allowed STF 2492AB to remain on our observing list, even though it has a delta magnitude of 3. Normally such egregious stars would be overlooked. When we reduced the data on this star, only two of our six observations yielded any measurable results. Because we could not do any statistical analysis with only two data points, we did not report the position angle and separation for this star (Table 1).

In addition, when looking at the WDS data for STF2727AB, we averaged the last ten data points, excluding two that had position angles that were off by 2-3 standard deviations where the average was inclusive, and between 15-16 standard deviations where the average was exclusive. The observations excluded were observed on 2012.8 and 2011.778.

	PA (°)	Sep. (")	Date	N	WDS PA (°)	WDS Sep. (")	Note
STF2404	180.745	3.639	B2013.665	6	181.34	3.407	a
STF2613AB	355.198	3.591	B2013.665	6	354.26	3.568	b
STF2725AB	11.670	6.153	B2013.665	7	10.82	6.059	c
STF2727AB	265.85	8.986	B2013.700	6	266.20	8.921	d
STF2848	123.750	10.894	B2013.700	6	123.99	10.839	e
STF2978	144.73	8.424	B2013.665	6	144.31	8.351	f

Table 1: Our data in left columns and average of the past ten observations reported to the WDS.

Notes: Standard deviations of our observations and the past ten observations in the WDS.
[a]Our Data: PA 0.22°; sep. 0.017" WDS: PA 1.50°; sep. 0.221"
[b]Our Data: PA 0.01°; sep. 0.001" WDS: PA 0.26°; sep. 0.111"
[c]Our Data: PA 0.01°; sep. 0.002" WDS: PA 0.29°; sep. 0.067"
[d]Our Data: PA 0.03°; sep. 0.019" WDS: PA 0.76°; sep. 0.114"
[e]Our Data: PA 0.04°; sep. 0.026" WDS: PA 0.40°; sep. 0.052"
[f]Our Data: PA 0.20°; sep. 0.201" WDS: PA 1.03°; sep. 0.193"

Analysis

We compared our data to the last ten measurements in the WDS provided by Brian Mason and William Hartkopf to see whether our measurements were similar or awry. The reason for utilizing only ten measurements as opposed to linear trends or larger data sets is because the stars themselves are slower moving and the previous ten measurements are from recent years. This provides a stable subset of data that we could compare against, which would not be possible if the star was moving much faster or erratically.

For STF2404, the average separation in the last 10 recorded measurements was calculated to be 3.407", while we recorded an average of 3.639". Given the WDS standard deviation of 0.221", our measurements are just over one standard deviation of difference. When comparing the position angles, the WDS average is 181.34° ± 1.5°, while our measurements show a position angle of 180.75°, which is well within one standard deviation. Overall, our recorded data is in agreement with previous observations.

For STF2613AB, the WDS reports an average separation of 3.57 ± 0.11", while our results average out to 3.59". Our separation is therefore within one standard deviation of the WDS values. For position angle, the WDS average is 354.26° ± 0.26° while our data shows the position angle to be 355.20°. Our recorded position angle is nearly 4 standard deviations off of the mean, and thus not in agreement with other recently recorded measurements. Because of this difference, we cannot say that our observations are in agreement with the WDS mean.

For STF2725AB, the WDS reports an average separation of 6.059 ± 0.067", while our results average out to 6.153". Our separation is just over one standard deviation away from the mean value. For position angle, the WDS average is 10.82° ± 0.29° while our data shows the position angle to be 11.67°. The discrepancy between our value and the WDS mean puts our position angle at just under 3 standard deviations off, and therefore is not in agreement with other recent measurements.

For STF2727AB, the WDS reports an average separation of 8.921 ± 0.114", while our results average out to 8.986". Our separation is therefore within one standard deviation of the WDS values, although on the far end. For position angle, the WDS average is 266.20° ± 0.76° while our data shows the position angle to be 265.85°. This too is within the standard deviation of the WDS mean, but again on the far end of the deviation. We can then say that our observations for this star system are in agreement with previous measurements.

For STF2848, the WDS reports an average separation of 10.839 ± 0.052", while our results average out to 10.892". Our separation is just barely over one standard deviation, differing by 26 ten-thousandths of an arc second. For position angle, the WDS average is 123.99° ± 0.40° while our data shows the position angle to be 123.75°. Our measured position angle is well within one standard deviation of the WDS average. Based on these differences, our observations can be said to be in agreement with previous values.

For STF2978, the WDS reports an average separation of 8.351 ± 0.193", while our results average out to 8.424". Our separation is therefore well within one standard deviation of the WDS values, and in agreement. For position angle, the WDS average is 144.31° ± 1.03° while our data shows the position angle to be 144.73°. Our data is well within the standard deviation of the WDS average, and thus also in agreement.

Conclusion

Overall, this research fulfilled its goal of introducing students to double star research, the use of speckle interferometry, and the process of writing and publishing a research paper.

Acknowledgments

We thank Russ Genet for the use of Orion Observatory and guidance over the course of the research. We also thank Brian Mason and William Hartkopf for providing past observations of the stars we observed. A final thanks to Vera Wallen, Mark Brewer, and Robert Buchheim who gave time to reviewed our paper.

References

Genet, R.M. et al. 2013. Close double star speckle interferometry program. In *Proceedings for the 32nd Annual Conference of the Society for Astronomical Sciences*. Eds. Warner, B. D., Buchheim, R. K., & Foote, J. L., 61.

Maurer, Andreas. 2012. The diffraction grating micrometer. In *Observing and Measuring Visual Double Stars, Second Edition.* Ed. Argyle, R.W. New York: Springer, 185.

A Novel System for Classifying Binary Orbital Solutions

Eric D. Weise[1] and Russell M. Genet[2,3,4,5]

1. University of California, San Diego
2. California Polytechnic State University, San Luis Obispo
3. Concordia University, Irvine, California
4. Cuesta College, San Luis Obispo, California
5. University of North Dakota, Grand Forks

Abstract A new system for classifying binary star orbital solutions is presented. This system is comprised of seven groups. Stars in a group share a common trait which make the stars interesting targets. The method has aided in the creation of target lists which focus more on improving the grades of orbital solutions published by the Washington Double Star Catalog. The methods are still in their infancy, however the system has been useful for the authors for their recent observation runs.

Introduction

While preparing for several observation runs, we developed a set of categories which partition a large set of binary star systems. These categories have been included in the authors' target lists. The process began while the authors were reviewing possible targets for an upcoming session at Kitt Peak National Observatory. While looking through the Washington Double Star Catalog for interesting systems, there were several factors which piqued our interest, so we decided to make a list of binary star systems categorized by which of these interesting factors was the most prevalent in each system.

As of yet, this classification of orbits is moderately subjective; the authors' judgments have been made by visual inspection of the orbital plots included in the *Sixth Catalog of Orbits of Visual Binary Stars* maintained by the United States Naval Observatory. It is our hope that this method will become standardized and more rigidly defined. Eventually, perhaps a computer code could be developed which would use past observations and the parameters of the orbital solution as inputs to determine which category any binary star belonged to.

Motivations for Classifying Orbital Solutions

The motivations for our method of classifying the orbital solutions were twofold. Our first concern was maximizing the number of targets on an observation list which would most benefit knowledge of double stars. For instance, the category “Bad Orbit” indicates that recent observations of the system deviated from the orbital ephemerides, and one or two more observations could be used to calculate a more accurate orbital solution. It may be a more efficient use of time to observe systems in the “Bad Orbit” category than to observe stars with good agreement between the orbital ephemerides and the subsequent observations.

Our second goal was to streamline the observation process. As seasoned observers know, an observation run is never guaranteed to turn out useful results, no matter the amount of time or effort given to preparation. An effective observer needs to be able to think on his or her feet. By categorizing our targets before an observation run, we were able to modify our target list quickly during observations and still maintain a healthy ratio of calibration stars to scientifically interesting systems. For instance, if an observer does not have time to observe all of the systems in a target list, the observer can easily truncate the list by eliminating the less interesting systems.

Overview of Orbital Categories

In a first cut at a classification scheme for binary orbits, we came up with the seven categories below:

CB Calibration Binaries
BO Bad Orbits
FS Few Speckles
NS No Speckles
SP Strings of Pearls
LC Late Component
SR Special Request

Calibration Binaries – CB

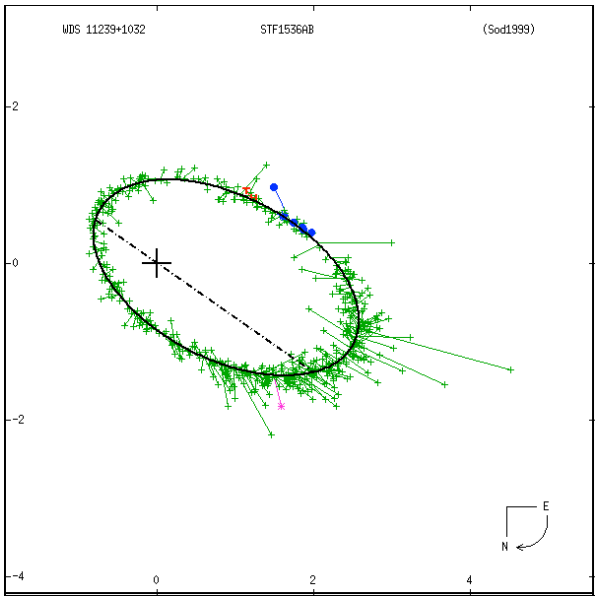

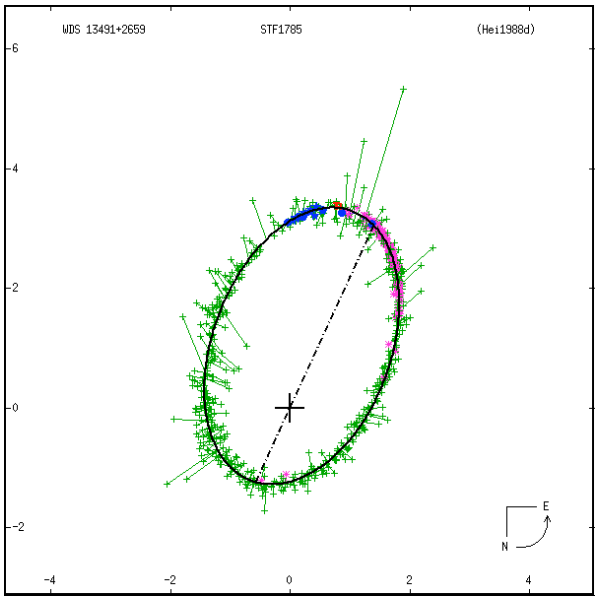

Above left is a Grade 2 system. Speckle observations suggest it is decently on track. Current separation is about 2 arc seconds, perhaps a bit close for smaller telescopes with wider fields-of-view. Other things being equal, it is good to have the separation approaching half of the camera's fov, perhaps not so wide that it won't fit in a 256x256 pixel RoI. The components are bright, 4.0 and 6.7 magnitude. Bright is good for calibration (high S/N), but the delta mag of this binary is really too great, 2.7, for it to be a good calibration binary.

Above right is another Grade 2 calibration binary. Recent speckles appear right on orbit. This one is wider. Other calibration doubles that could be observed could be systems with published rectilinear elements, although most tend to be too wide for use in calibration. Also, somewhat lower grade binaries could be used where plenty of recent speckles right on the orbit really pin things down, but there is not enough orbital coverage to give the system a high grade.

Bad Orbits – BO

Most of the "BO" binaries are Grade 4 or 5, and as such are prime candidates for additional observations, especially speckle, moving them up to Grade 3 or better where they can then be used in evolutionary models. BOs are especially fun. One can often see how an original orbit with visual observations is often brought into serious question with recent, more accurate speckle observations. One is tempted to add another speckle observation or so and calculate a new orbit.

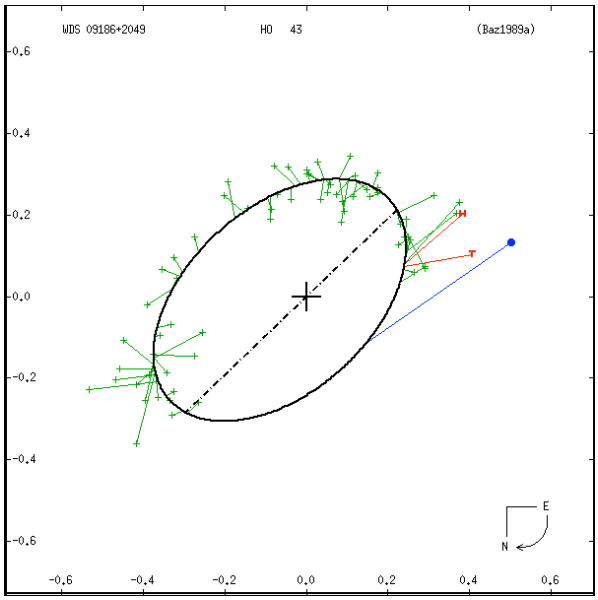

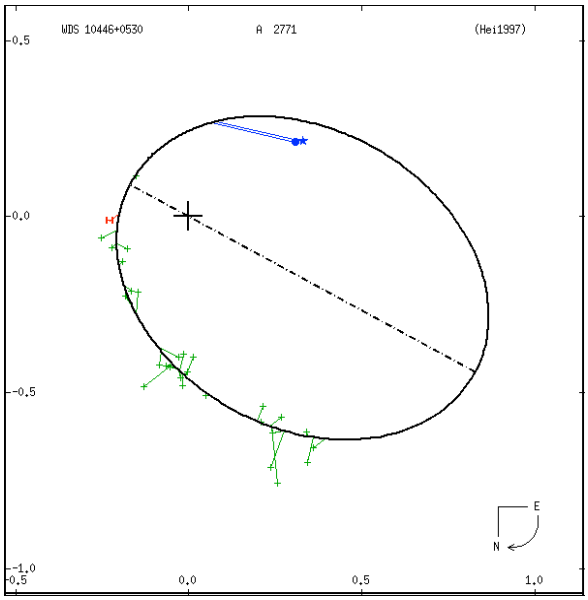

The original orbit on the left was thrown off by several of the last visual points, while other visual observations which, at the time, must have looked errant, are supported by Hipparcos and Tyco and one lone speckle observation made by Jay Farihi with a 2.4-m telescope. On the right, two speckle observations, one by the USNO, suggest the actual orbit may be quite different.

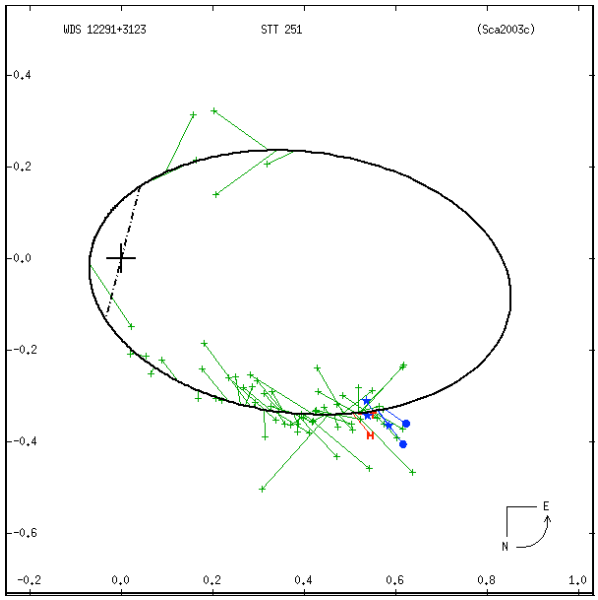

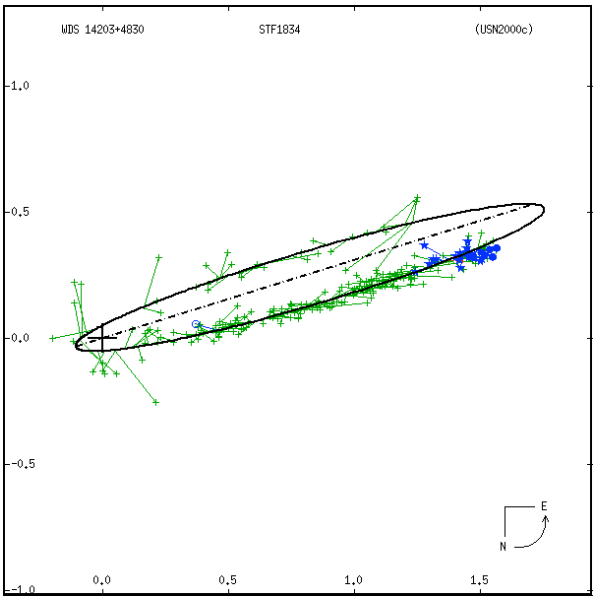

The observations on the left appear to be headed off the orbit, while the ones on the right are only doing so modestly.

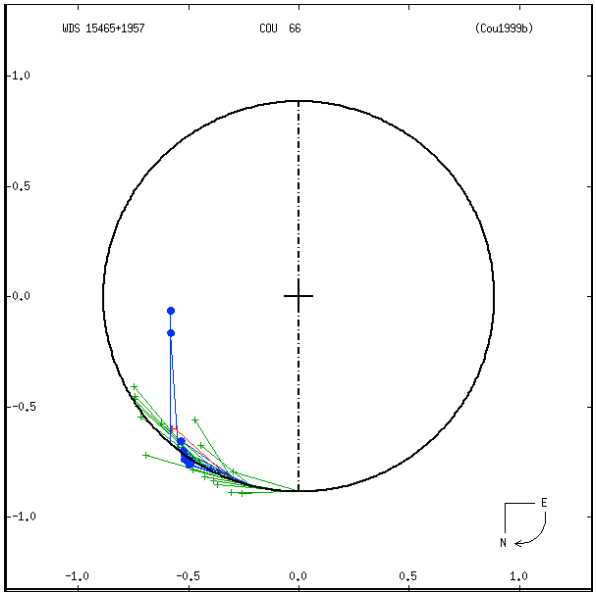

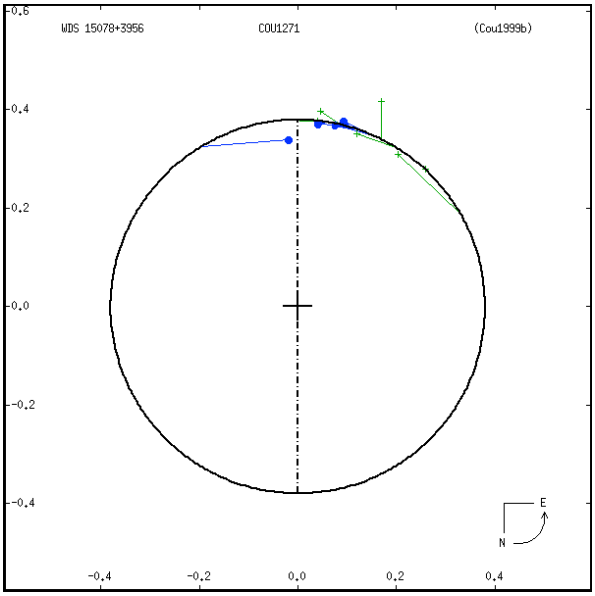

Perhaps the system on the left isn't a binary at all, just an optical double? On the right, the observations may appear to be on orbit at first glance, but clearly their timing is way off and the true orbit may be highly elliptical.

Few Speckles – FS

Orbits with few speckle, FS, observations tend to be Grade 4 and 5, mostly 5. The primary difference between them and "Bad Orbits" is that while the orbits are low grade, they do not appear to be grossly off. Adding accurate speckle observations can up their grade, especially if the period is short enough for the added observation(s) to be somewhat spaced out.

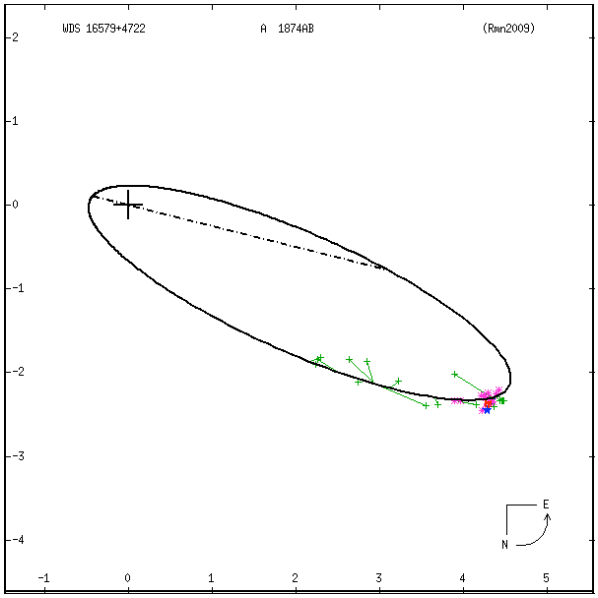

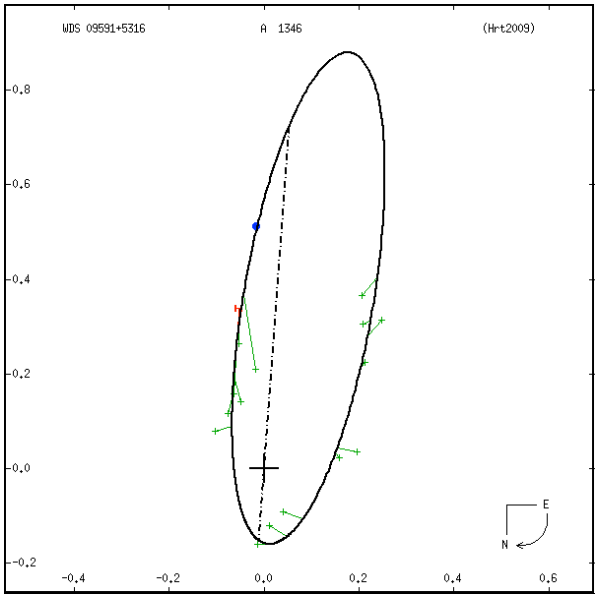

No Speckles – NS

These binaries tend to be Grade 4 or 5, perhaps mainly 5. Speckle observations could upgrade their orbit. Shorter periods are likely to be more amenable to upgrading.

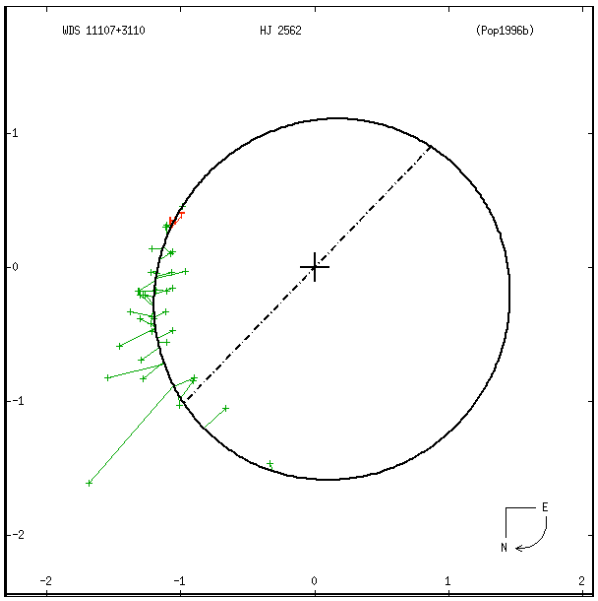

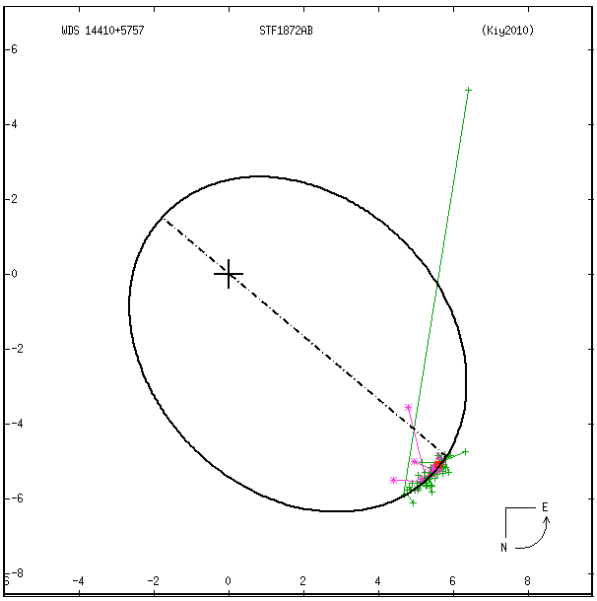

Strings of Pearls – SP

Like their namesakes, these are beautiful orbital plots. They can be almost any grade.

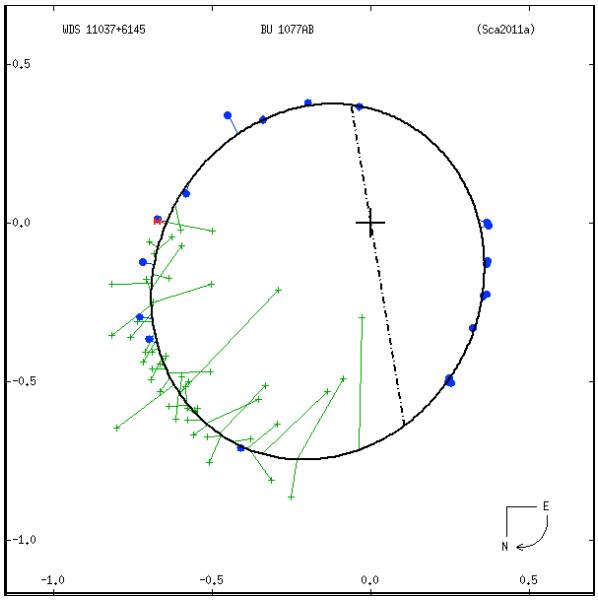

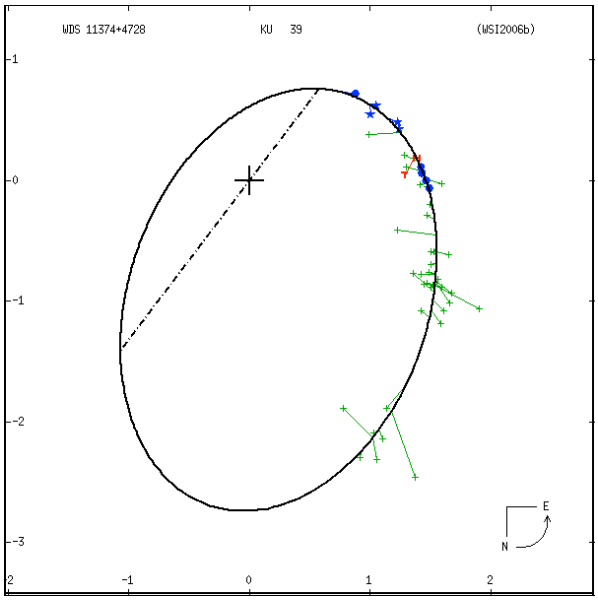

On the left is a short period, 44 year, Grade 3 binary. A few additional speckle observations could move it up to Grade 2. On the right, the period is a much longer 278 years, and it is only a Grade 5. Observations over the next several decades might move it up to a Grade 4 or even 3, perhaps, but generally adding observations to shorter period systems may be more useful.

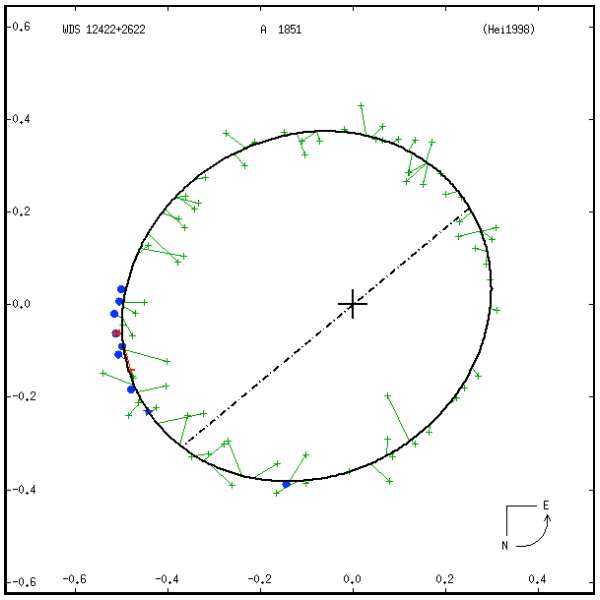

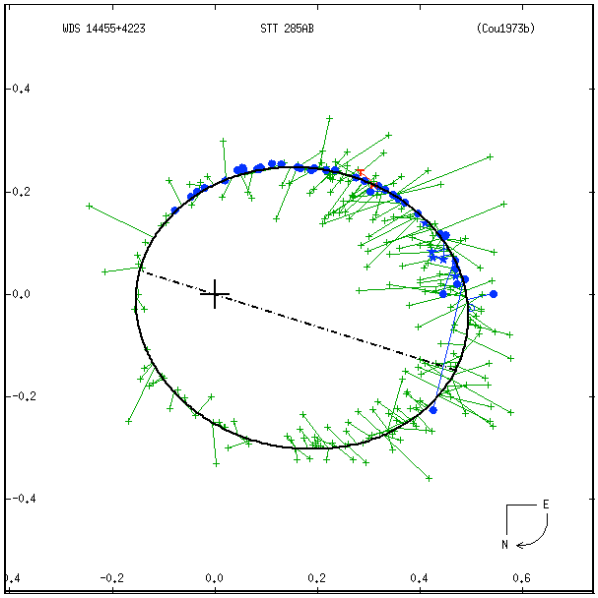

On the left (above) is a 61 year Grade 2 orbit with a rather large gap between many speckle observations and one lone speckle observation. Another Grade 2 orbit is on the right with an 88 year period and many more speckle observations.

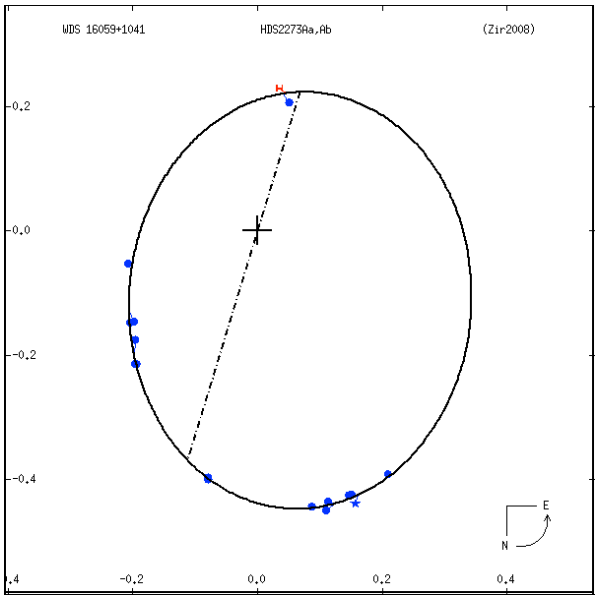

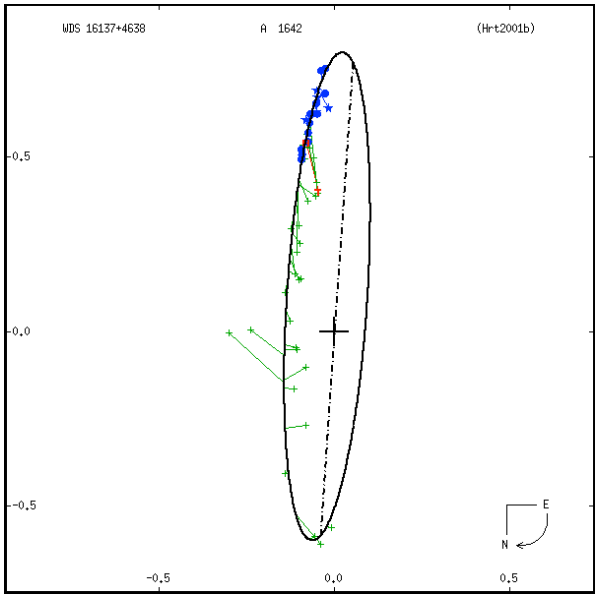

The orbit on the left is only a Grade 4 (although it looks very nice). The period is just 33 years and it has no visual observations. On the left is a much longer period, 188 years, a system with a Grade 4 rating.

Late Component – LC

Binaries with a late spectral-type component are especially valuable to observe, as masses on that end of the HR diagram are not as well known.

Special Request – SR
When we go on an observation run at a large telescope we ask our collaborators in the double star community if there are any special systems they want observed. This designation is added to those systems in our target list to ensure we fulfill our friendly duty.

Conclusion

The classification method that the authors have developed, while in its early stages, has proven to be a useful tool. More categories may be added as our interests broaden and our knowledge deepens. We look forward to creating a streamlined process which is more standardized and time efficient, thus enabling us to create more diverse target lists in a shorter time.

Acknowledgments

Genet thanks California Polytechnic State University Office of Research and Economic Development for support through their Extramural Funding Initiative, and the Keck Foundation for support through the Concordia University Undergraduate Education Program. Both Genet and Weise thank David Rowe for observing time on the 0.5-meter telescope at the Pinto Valley Observatory, and Kitt Peak National Observatory for two weeks of observing time on their 2.1-meter telescope. We also thank the United States Naval Observatory for the use of their *Sixth Catalog of Orbits of Visual Binary Stars*.

Portable Speckle Interferometry Camera Checkout at Kitt Peak

Russell M. Genet[1], Thomas C. Smith[2], R. Kent Clark[3], Paul Wren[4], Hillary Mathis[5], Dave Summers[5], and Brent Hansey[5]

1. California Polytechnic State University, San Luis Obispo
2. Dark Ridge Observatory, Weed, New Mexico
3. University of South Alabama, Mobile
4. University of North Dakota, Grand Forks
5. National Optical Astronomy Observatory, Tucson, Arizona

The National Optical Astronomy Observatory (NOAO) Time Allocation Committee (TAC) awarded eight nights on the 2.1m telescope at Kitt Peak National Observatory for double star speckle interferometry using a portable camera. As described in the proposal, binary orbits, when combined with parallaxes, yield dynamical masses, while photometry of the components restrains astrophysical models. Both are vital to understanding stellar evolution. Speckle interferometry, which is telescope resolution limited as opposed to seeing limited, allows observation of close, short-period binaries. A portable, low cost, EMCCD-based speckle camera will be used to observe several hundred binaries. The run will confirm Hipparcos/Tycho double star discoveries as candidates for new binaries, classify new pairs by determining if their motion is curved (gravitationally-bound binary) or linear (mere optical double), add high-accuracy speckle observations that will allow the first determination of orbits, refine existing orbits by extending orbital coverage with speckle observations, and obtain precise photometry of binary components to link photometric with dynamical masses.

The run was set for 15th-23rd October 2013. Tuesday the 15th was set aside for test and engineering, while the remaining nights were dedicated to observations. To fully utilize this large block of time and accommodate the largest number of students, the observing was split into two four-night sessions, with separate teams for each session. Team A used the 16th-19th (Wednesday-Saturday), while the 20th-23rd (Sunday-Wednesday) was used by Team B. Speckle observations require intense, fast-paced coordination between a telescope operator, a speckle camera operator, and a session director that selects targets, logs data, etc. An additional observer to reduce data on the fly is also helpful. The run will feature a number of undergraduate and graduate student observers as full team members.

Figure 1. Russ in front of the dome of the 2.1-meter telescope.

The 2.1-m / 84-inch telescope is on the south end of the Kitt Peak summit complex, conveniently close to the dining room. Construction began in 1959, with first light in 1964. In Figure 1, Russ stands by the "Beware of Snakes" sign. Hillary Mathis opened the dome slit slightly (pointing north) to let in light for camera installation.

Figure 2. Looking north from the porch of the 2.1-m is a view of the 4-m Mayall and several other telescopes.

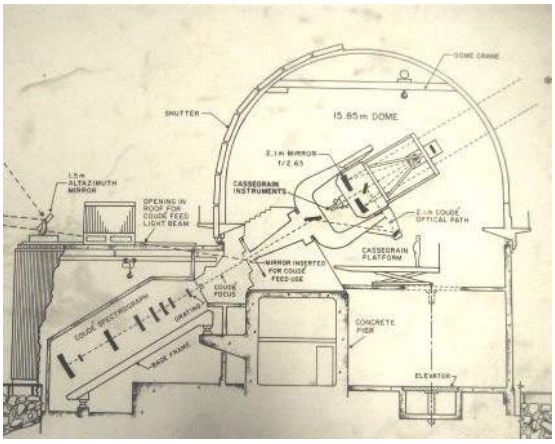

Figure 3. Cutaway of the 2.1-m telescope.

The Coude feed from the auxiliary 0.9-meter telescope is still operational (Figure 3). The Cassegrain platform is very useful for removing and installing instruments, although instrument operation is conducted from the warm room.

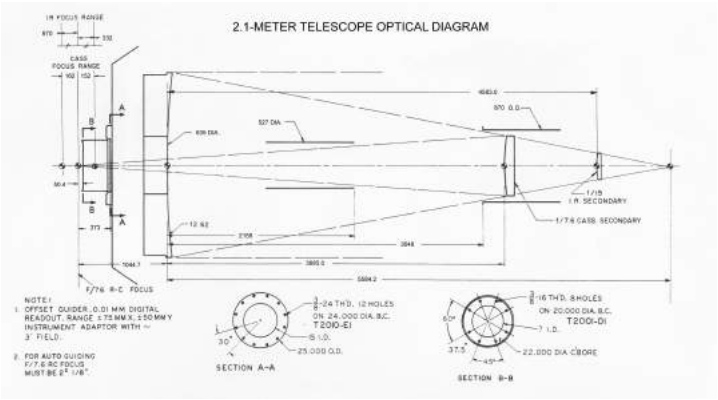

Figure 4. Optical layout of the 2.1 m telescope.

With the F/7.6 secondary in place, the effective focal length of the telescope is 16,200 mm. Our speckle camera has a magnification of about 8x, providing an overall effective focal length of about 129,600 mm and F/ratio of 61.7. This gives a plate scale of about 1.6 arc seconds/mm or 0.016 arc seconds/pixel (10 micron pixels in our Andor Luca-S EMCCD camera). With the Acquisition/Guider unit installed there is only 2 inches of back focus. Our camera is really lightweight, so Hillary Mathis installed lead counterweights to balance the telescope (Figure 5).

Figure 5. Hillary Mathis installing counterweights on the telescope.

Figure 6. Thomas Smith attaching speckle camera to the Kitt Peak-provided plate.

Tom Smith fastened our camera with its 12x12-inch, ¼-inch thick aluminum plate to a larger, round, ½-inch thick aluminum Kitt Peak plate (Figure 6) that had been used to interface an earlier visitor instrument. This "used" plate saved us from making and transporting a large, heavy plate to Kitt Peak. Hillary and Brent then installed the Kitt Peak plate with our speckle camera fastened to it (Figures 7, 8).

Figure 7. Installing the camera assembly on the telescope.

Figure 8. Hillary and Russ check the speckle camera connections.

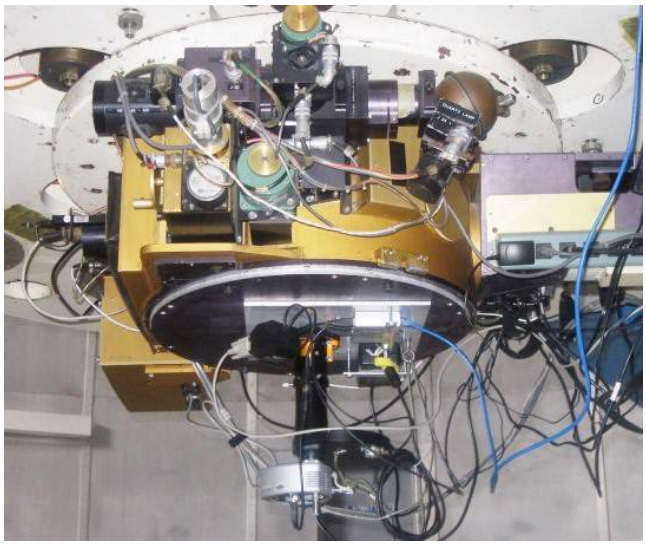

Figure 9. Speckle camera installed.

Figure 9 shows our camera mounted onto the acquisition/guider unit which has three 45° mirrors in the system. Two face toward the guide camera, while the other faces toward the wide-field camera. The guide camera and wide field camera are mounted 180-degrees apart (although the power switches for the two cameras are actually next to each other). The thru position is between the two mirrors that face the guide camera. The "idt" position centers one of the guide mirrors. The "widefield" position moves the slide further along its travel to put that last mirror into position.

A Moonlite motorized focuser allowed us to be parfocal with the 2.1-m telescope's acquisition camera. As there was only 2-inches of back focus (and ¾ inch was used up by their ½ inch thick plate and our ¼ inch thick plate), we placed a negative lens (taken from an OPT 2-inch Barlow) that extended from our focuser up into their Acquisition/Guider to extend the back focus. This lens also provided some of our required magnification. Moonlite Telescope Accessories added set screws on the bottom of our focuser's draw tube to fasten the negative lens. The lens conveniently unscrewed from the 2-inch OD, 2X OPT Barlow. Also mounted on our plate were an Icron Ranger USB extender and the power supply for our Andor Luca-S EMCCD camera. Inserted into the Moonlite focuser were a 4X Tele Vue Powermate, an Orion seven-position filter wheel (Johnson Cousins BVRI, Sloan r'i', and H-alpha filters), and the Andor Luca-S EMCCD camera. A 50-foot Category-5 cable connected the speckle camera to the camera-control laptop in the warm room.

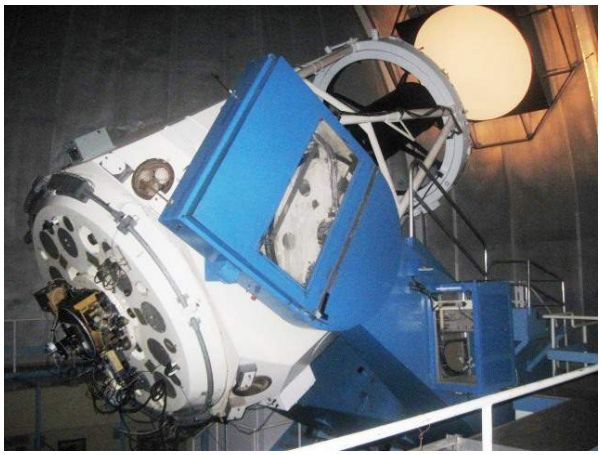

Figure 10. 2.1-meter telescope with speckle camera.

Our speckle camera was dwarfed by the 2.1-m telescope. Figure 10 shows the telescope pointed at the dome flat position. We turned on the flat lights distributed around the top ring of the telescope.

Figure 11. Russ at the telescope operator's station.

Although NOAO has provided 2.1-m telescope operators in the past, users now operate the telescope themselves after reading the instruction manual *(http://www-kpno.kpno.noao.edu/2m-manual/)* and receiving instruction (Figure 11). Two panels (A behind Russ and B with the two round position readouts) are used in conjunction with two computer monitors with GUIs to control the telescope. An additional monitor displays the telescope's position and other key information, while video monitors display the output from the acquisition and guide camera.

Figure 12. The control room. From left to right: Dave Summers, Kent Clark, Tom Smith, and Paul Wren.

Dave Summers taught us how to run the 2.1-m telescope. We took turns operating the three positions: telescope control, camera control, and session director. In Figure 12, Kent Clark is operating the telescope, Tom Smith is operating the speckle camera, while Paul Wren is the session director selecting the next target and keeping the detailed log. Although our checkout was in the middle of the monsoon season and, not unexpectedly, it was cloudy, we still pointed the telescope at the stars and went through all the procedures. These included loading our targets (supplied by Eric Weise) into the telescope's cache, acquiring our targets, fine-positioning the telescope and camera's Region of Interest (RoI), etc.

Besides learning how to open and close the observatory and operate the telescope, we developed and checked procedures for preloading our targets into the telescope's cache and for transferring data from the telescope control system to our data log. We also developed a written procedure for coordinating the operation of the three operating positions, and made notes for improving the master spreadsheet the session director uses to select the next target to observe.

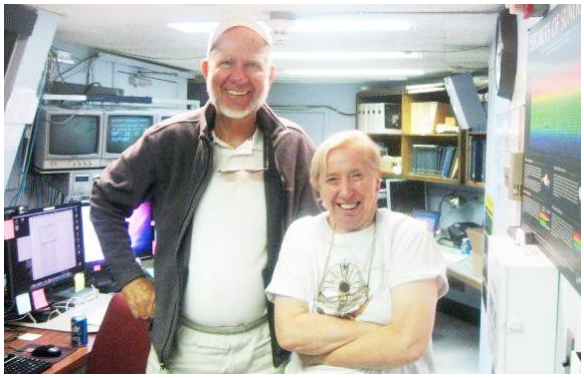

Figure 13. Russ and Di Harmer.

Di Harmer paid us a visit during our checkout (Figure 13). Di is a good friend of Bob Argyle, the double star expert at Cambridge University.

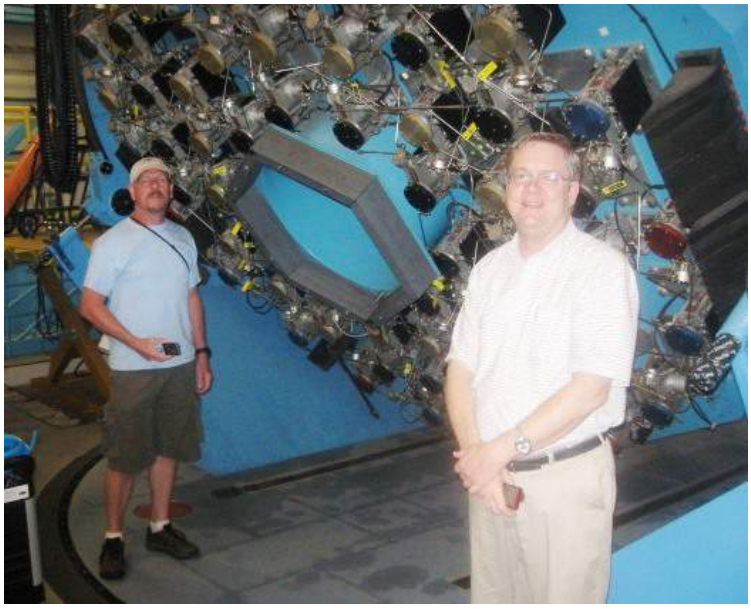

Figure 14. Tom and Kent at the WIYN telescope.

After our engineering checkout, Dave Summers kindly gave us a tour of the 3.5-m WIYN telescope. Tom and Kent stand by the back of the WIYN's primary mirror (Figure 14) which has many active supports controlled by an algorithm. The active supports can also be manually fine-tuned by the telescope operator.

Figure 15. Russ at the 4-meter telescope.

Dave also showed us around the 4-meter telescope. Russ poses in front of the large RA disc (Figure 15). The optical tube assembly (OTA) was tipped over for maintenance, although the Cassegrain cage is visible on the left.

Acknowledgments

We thank NOAO instrument scientists Richard Joyce and Di Harmer for their assistance in the design of the speckle camera/2.1-m telescope interface, David Mills for providing a telescope parameter extraction program, and Bellina Cancio for her help with quarters and other logistical matters. We also thank Vera Wallen for reviewing this manuscript. The Andor Luca-S EMCCD camera was funded through an American Astronomical Society Small Research Grant, while Andor made the camera available at a reduced price. We are grateful to both organizations. Moonlite Telescope Accessories modified their motorized focuser to accommodate the inward facing negative lens.

Kitt Peak Speckle Interferometry of Close Visual Binary Stars

Russell Genet[1,2,3], David Rowe[4], Thomas C. Smith[5], Alex Teiche[1], Richard Harshaw[6], Daniel Wallace[3], Eric Weise[7], Edward Wiley[8], Grady Boyce[9], Patrick Boyce[9], Detrick Branston[10], Kayla Chaney[11], R. Kent Clark[12], Chris Estrada[13], Thomas Frey[1], Reed Estrada[14], Wayne Green[15], Nathalie Haurberg[16], John Kenney[11], Greg Jones[17], Sheri Loftin[18], Izak McGieson[16], Rikita Patel[11], Josh Plummer[12], John Ridgely[1], Mark Trueblood[19], Donald Westergren[20], and Paul Wren[3]

1. California Polytechnic State University, San Luis Obispo
2. Cuesta College, San Luis Obispo, California
3. University of North Dakota, Grand Forks
4. PlaneWave Instruments, Rancho Dominguez, California
5. Dark Ridge Observatory, Weed, New Mexico
6. Brilliant Sky Observatory, Cave Creek, Arizona
7. University of California, San Diego
8. Yankee Tank Creek Observatory, Lawrence, Kansas
9. Boyce Research Initiatives and Educational Foundation, San Diego, California
10. National Solar Observatory, Sunspot, New Mexico
11. Concordia University, Irvine, California
12. University of South Alabama, Mobile
13. California State University, Los Angeles
14. Northrop Aviation, Hawthorne, California
15. Boulder Astronomy and Space Society, Boulder, Colorado
16. Knox College, Galesburg, Illinois
17. Eclipse Technologies, Brookfield, Wisconsin
18. Kitt Peak National Observatory, Tucson, Arizona
19. Winer Observatory, Sonoita, Arizona
20. Morris Ranch Observatory, San Diego, California

Abstract Speckle interferometry can be used to overcome normal seeing limitations by taking many very short exposures at high magnification and analyzing the resulting speckles to obtain the position angles and separations of close binary stars. A typical speckle observation of a close binary consists of 1000 images, each 20 milliseconds in duration. The images are stored as a multi-plane FITS cube. A portable speckle interferometry system that features an electron-multiplying CCD camera was used by the authors during two week-long observing runs on the 2.1-meter telescope at Kitt Peak National Observatory to obtain some 1000 data cubes of close binaries selected from a dozen different research programs. Many hundreds of single reference stars were also observed and used in deconvolution to remove undesirable atmospheric and telescope optical effects. The data base of well over one million images was reduced with the Speckle Interferometry Tool of PlateSolve 3. A few sample results are provided. During the second Kitt Peak run, the McMath-Pierce 1.6- and 0.8-meter solar telescopes were evaluated for nighttime speckle interferometry, while the 0.8-meter Coude feed was used to obtain differential radial velocities of short arc binaries.

Introduction

Binaries is a term that William Herschel coined when he discovered that some of the double stars he had been observing were revolving around each other and hence were gravitationally bound pairs (Herschel 1803; Hoskin 2011). The term *visual* was later added to distinguish the more widely separated astrometric binaries from the generally much closer spectroscopic and photometric (eclipsing) binaries.

The resolutions of conventional visual binary observations were seeing limited until Labeyrie (1970) devised speckle interferometry as a way to circumvent seeing limitations and realize the full diffraction-limited resolution of a telescope. The light from a close binary passing through small cells in the atmosphere produces multiple binary star images which, if observed at high enough magnification with short exposures (typically 10 to 30 milliseconds), will "freeze" out the atmospheric turbulence and thus overcome seeing-limitations. Although the multiple double star images are randomly scattered throughout the image (often superimposed), their separation and position angle remain constant, allowing these two parameters to be extracted via Fourier analysis (autocorrelation).

For images larger than a few arc seconds across, however, the rapid jitter of the binary speckle images is no longer correlated. Speckle interferometry is not effective beyond isoplanatic patch, but close binary stars are always well within the isoplanatic patch. The Fourier transforms of hundreds or thousands of short exposures are averaged to greatly improve the signal-to-noise ratio.

Harold McAlister (1977) used high-speed Tri-X film cameras on the 2.1- and 4.0-meter telescopes on Kitt Peak to observe close binaries. Obtaining Fourier transforms of thousands of film images was a labor-intensive process. His film camera was soon replaced with an intensified CCD (ICCD) camera and Osborne portable computer (McAlister et al. 1982). The speckle observations by McAlister, William Hartkopf, and others at Georgia State University were an order of magnitude more precise than visual observations, making speckle the preferred observational technique for close binaries (McAlister, 1985). The status of speckle imaging in binary star research is reviewed by Horch (2006).

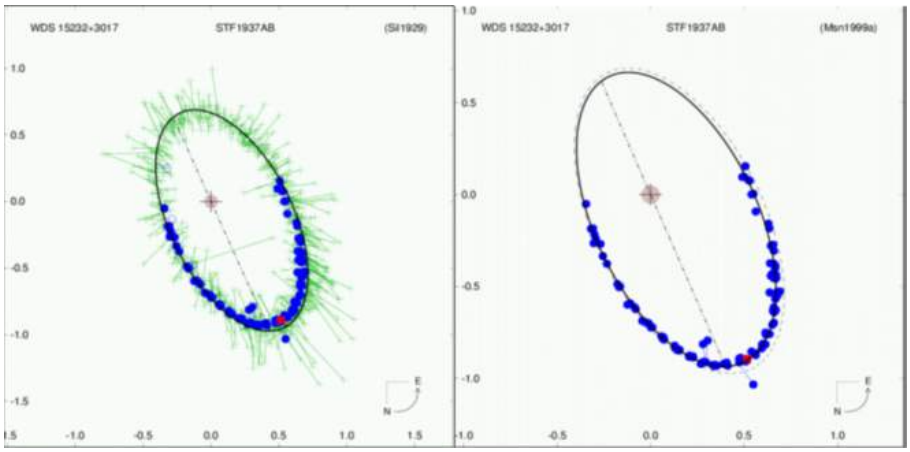

Figure 1. Close binary orbit of η CorBor with and without visual micrometer (green X) observations. Speckle observations are blue dots.

The power of speckle interferometry can be seen from orbital plots and solutions. An orbit of a close binary based primarily on visual observations is not nearly as precise as one based solely on speckle observations. In the example of η CorBor provided by William Hartkopf (Figure 1), the new orbital solution based on the speckle observations alone (right solid line), compared to the earlier solution that included visual micrometer measurements (right dashed line) changed the estimated mass by 14%, astrophysically a very significant improvement! The consistency of the 20 different speckle telescope/detector combinations is remarkable.

Since speckle interferometry observational limits are set by telescope resolution (aperture diameter) rather than seeing, it is natural for smaller telescopes to concentrate on wider binaries, while larger telescopes observe binaries between their seeing and resolution limits. Although a number of smaller telescopes are permanently equipped for speckle observations, larger telescopes are not, so observers must bring their own "visitor" instruments.

An ICCD speckle camera, similar to Georgia State University's camera, was built and installed on the 0.66-meter refractor at the U.S. Naval Observatory (USNO) in Washington. A second, identical camera was then built and used in the USNO's "off campus" observational program. The USNO's highly successful speckle observations of close binary stars with a portable ICCD speckle camera on larger telescopes inspired us to develop an even more portable system based on the Andor Luca electron-multiplying CCD cameras (Genet 2013).

Figure 2. The 2.1-m f/7.6 telescope at Kitt Peak National Observatory dwarfs our portable speckle camera.

Our speckle camera is the primary instrument on the 0.25-meter SCT telescope at the Orion Observatory. Our first "off campus" visitor speckle runs were made with our camera on the 0.5-meter PlaneWave Instruments CDK telescope at Pinto Valley Observatory, providing us with twice the resolution. Double stars with a separation of 0.5 arc seconds were observed. The 2.1-meter telescope at Kitt Peak National Observatory was chosen to continue our quest for observing ever closer binaries, allowing us to observe binaries with separations of 0.1 arc second and periods of well under one decade (Figure 2).

Two bright-time, week-long observing sessions on the 2.1-meter telescope at Kitt Peak spread six months apart provided good coverage of close binary stars in the sky visible from Arizona. On the first run, October 15 to 23, 2013, the first eight nights were totally clear nights, while the last night was partially cloudy. On the second run, April 10 to 16, 2014, although the first two nights were primarily cloudy, the last five nights were completely clear. This gave us a total of 13 completely clear nights for our observations.

Although the Principal Investigator (Genet) stayed full time for both runs, most of the observers participated for just half a week; thus not too much school- or work-time was missed. The 27 observers (the coauthors of this paper) were an eclectic mix of undergraduate and graduate students, and advanced-amateur and professional astronomers (Figures 3, 4).

Figure 3. Seven of the 12 observers on the October 2013 run: Genet, Plummer, Patel, Teiche, Trueblood, Wallace, and Chaney.

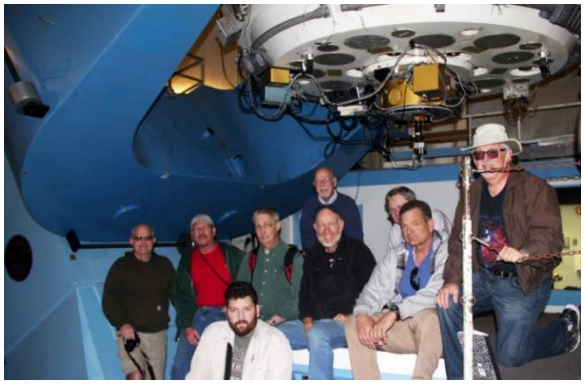

Figure 4. Nine of the 20 observers on the April 2014 run: Jones, Smith, C. Estrada (front), Green, Genet, Wiley (rear), Clark, R. Estrada, and Harshaw.

Research Programs

Our research has concentrated on five classes of double stars: (1) known binaries with published orbits; (2) candidate "binaries" without published orbits that exhibit indications of binarity; (3) unclassified double stars that could be either chance-alignment optical doubles, common proper motion pairs, or binaries; (4) unconfirmed double star candidates (not known if they are even double stars); and (5) special requests by other astronomers. The *Washington Double Star Catalog*, the *Sixth Catalog of Orbits of Visual Binary Stars* (including the accompanying plots of past observations), and the *Fourth Catalog of Inteferometric Measurements of Binary Stars* were all formatted as Excel spreadsheets and used to search for candidates for our various target lists. Each class is described below.

Known binaries with published orbits

(1) Long-period, slow-moving binaries with many past speckle observations. Extensive observations of some of these binaries were used as calibration binaries in the first run and also to establish within- and between-night variances.

(2) Short-period Grade 1 and 2 binaries used as calibration binaries in the second run, to establish within- and between-night variances, and to contribute further speckle observations to these well-observed binaries (Malkov *et al*. 2012).

(3) Both long and short period binaries where recent speckle observations suggested that the orbital parameters could use refinement, as it appeared from the plots that the recent observations were heading "off the track."

(4) Both long and short period binaries with plots that suggested that the current published orbits were woefully inadequate. We termed these "bad orbit binaries."

(5) Both long and short period binaries that had few or no past speckle observations and it was clear that additional speckle observations would significantly contribute to refining their orbits.

Candidate "binaries" without published orbits

(6) Short-arc, long-period binary candidates with extensive past visual observations but, in some cases, with few or no speckle observations. When plotted, short-arc binaries have enough previous observations that an arc is evident. These arcs are likely to be segments of an elliptical orbit. In more developed cases, where a significant portion of an ellipse is available, traditional orbital solutions can be derived. When the arc is too short to accurately build a solution, the apparent motion parameters (AMP) method, an approach developed by A. Kiselev et al. (2003, 2009), can be applied. AMP estimates the sum of the component masses from their relative radial velocities, known parallax, and projected separation. Other papers by Kiyaeva et al. (2008, 2012), Harshaw (2014), and Genet et al.

(in preparation) also speak to this important indicator of binary systems. AMP utilizes the known position angle and separation, as well as measures of the apparent relative velocity in micro-arcseconds per year, the position angle of the relative motion, and the radius of curvature (Kiselev et al. 2003). Parallaxes are derived from Hipparcos, a mass estimate of the system from spectral classes, and relative radial velocities from one-time spectrographic radial velocity measurements of each component of the system. Additional important work in this area has been done by F. Rica of Spain (2011, 2012).

(7) Short-arc, short-period binary candidates found by searching through the *Fourth Catalog of Inteferometric Measurements of Binary Stars.* Typically these close binary candidates do not have any past visual observations, and only have Hipparcos and a few speckle observations. They are placed on our target list if the past observations show a significant change in position angle within the few decades speckle observations have been made.

Unclassified double stars

(8) Few past visual observations.

(9) Few past speckle observations (*Fourth Catalog of Inteferometric Measurements of Binary Stars*).

Unconfirmed double star candidates

(10) Hipparcos unconfirmed doubles, now some 1874 in number (Figure 5). Many approach 0.1 arc seconds in separation (the limit for Hipparcos). These are potential double stars discovered by Hipparcos that have not yet been confirmed by follow-up observations. While many of these may have been false detections, others may end up being binaries of special interest. See Perryman (2012) for details on Hipparcos binaries.

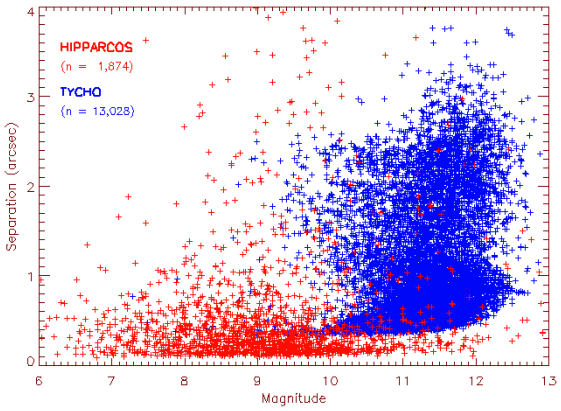

Figure 5. Plot of unconfirmed Hipparcos and Tyco doubles.

(11) Tycho unconfirmed doubles, currently some 13,028 in number, most greater than 0.5 arc seconds in separation (nearly the limit for Tycho, as only 1192 have a separation less than 0.5 arc seconds). We prepared this list but did not observe any on our Kitt Peak runs as they appeared to be more appropriate targets for smaller telescopes (they should be good candidates for the 17.5-inch automatic speckle interferometry system we are building).

(12) Hubble guide stars that were rejected because they did not provide a solid lock-on. This rejection could have been due to binarity.

Special requests

(13) A number of doubles were observed for Oleg Malkov (Russia), Olga Kiyaeva (Russia), Francisco Rica (Spain), Henry Zirm (Germany), and Todd Henry (US).

Portable Speckle Camera

Small-format, regular CCD cameras take about a second to read out a single image that has been accumulated over many seconds or minutes. The readout noise is typically 10 electrons RMS—very small compared to the accumulated light levels. While such cameras can be used to make speckle observations if they are capable of making 10 millisecond exposures, their readout time would be very long in comparison to their exposure time. A typical binary speckle observation consists of 1000 images. Each image typically has an exposure of 20 milliseconds for a total data cube exposure time of 20 seconds. If each image (frame) took 1 second to read out, 1000 frames would take almost 20 minutes, resulting in a very poor duty cycle (about 2%).

A number of small-format, high-speed, frame-transfer CCDs are available for about $500 that can read out one frame at high speed while another frame is being exposed. Continuous readout-while-exposing at speeds of 50 frames/second are not uncommon, allowing these cameras to have a duty cycle approaching 100%. While these cameras are quite useful for obtaining speckle observations of many brighter close binaries, their high-speed charge-to-voltage converters induce significant noise compared to the low signal levels inherent in 20 millisecond, highly magnified speckle images. An image intensifier can be used to boost the signal level, allowing these low-cost cameras to reach fainter binaries. When the image intensifier is integral to the CCD camera (often coupled with short optical fibers), then one has an intensified CCD (an ICCD).

Another way the signal can be amplified before it reaches the charge-to-voltage converter (which is inherently noisy at high speed) is to clock the output charge (electrons) from the pixel array through a final gain register. A high voltage is applied in an avalanche region in the semiconductor (the pixels in the gain register), and as the charge is transferred from one pixel to the next, extra electrons are knocked out of the lattice, causing amplification similar to a photomultiplier. This electron multiplication (EM) boosts the signal to a level where the high speed read noise is insignificant, making EMCCD cameras very attractive for speckle interferometry. The amplification process does introduce some noise, however, so electron multiplication is not advantageous at normal readout rates (Smith et al. 2008).

Similar to other CCD cameras, EMCCD cameras are available in both front- and back-illuminated versions. Andor Technologies, for instance, makes the very compact, front-illuminated, Luca-R camera (which costs about $14K). It has a quantum efficiency of about 50% and can be accessed via USB. The Andor Luca-R camera we used for observations on the 2.1-meter telescope at Kitt Peak cooled to -20° C within seconds, had a dark noise of only 0.05 electrons/pixel/second, and a read noise well under 1 electron RMS. Andor also makes a much larger, back-illuminated, iXon camera which costs about $40K. It has a quantum efficiency of 90%, but must connect to a PCI card with a fairly short cable (5 meters) on a nearby computer. This can require either mounting a PC on the telescope or running a special fiber-optic link which Andor can supply. It might be noted that Andor recently started manufacturing high-speed sCMOS cameras with USB-3 outputs that cost less than $12K. We hope to evaluate one of these cameras for use in close visual binary speckle interferometry in the near future.

Although the Luca-R EMCCD camera was the heart of our overall speckle camera system, it also included magnification with a 2-inch x2 OPT Barlow in front of a Moonlite focuser and a 2-inch x4 TeleVue PowerMate after the focuser (Genet 2013). An Orion 5-position filter wheel immediately preceded the Luca-R camera. All observations were made through a Sloan i’ filter (Astrodon second generation Sloan filter in Figure 6).

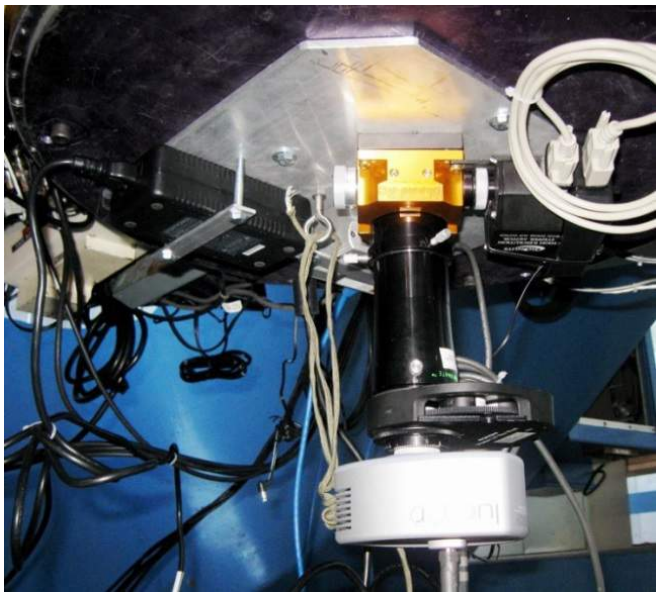

Figure 6. Our speckle interferometry system installed at the Cassegrain focus of the 2.1-meter telescope.

Observations

Preparing for and making observations at a large telescope with sizeable teams is a major technical, organizational, and logistical undertaking (see Figure 7). Preparations for the Kitt Peak observing runs began over a year prior to the first run when the Principal Investigator (Genet) visited Richard Joyce and Di Harmer, experienced experts on the 2.1-m telescope, at the Kitt Peak National Observatory headquarters in Tucson. Drawings of the telescope were examined, and a discussion on interfacing a guest instrument to the telescope was initiated.

One interface problem was that the guest instruments needed a 22-inch diameter plate to fasten to the large opening on the telescope's acquisition-guider unit. A sturdy 22-inch diameter plate, even if made from aluminum, would be difficult to transport to Kitt Peak on an airplane. This problem was solved when Hillary Mathis located a ½-inch thick aluminum plate that had been made by an early observer for a somewhat different guest instrument. This plate already had the holes that exactly matched the acquisition-guider's bolt circle, a somewhat large hole near the center, and three instrument fastening holes spaced 120 degrees apart. Our visitor speckle camera was assembled on a 12 x 12-inch x ¼-inch thick aluminum plate with three holes spaced to match those on the "used" Kit Peak interface plate.

Another interface problem was connecting the USB camera on the back of the telescope to a laptop in the warm room. This problem was solved by connecting an Icron Ranger USB-to-Ethernet unit at the telescope to its mating Ethernet-to-USB unit in the warm room with a 50-foot Cat-5 cable we brought with us to run between the two units.

Our original plan for our visitor system used a very compact and sturdy Hyperion eyepiece projection system for magnification. However, we ended up using two Barlow lenses instead because we wanted to be certain that we had sufficient back focus. A 2-inch diameter x2-power Barlow lens in front of our focuser (actually extending up slightly into the back of the telescope's acquisition-guider unit) extended the focal plane, while a 2-inch x4 TeleVue Power mate completed the magnification. A local area network (LAN) connected equipment in the warm room. This LAN had to be hard wired because Wi-Fi routers are not allowed on the mountain because they could interfere with a radio telescope. Our original plan for a hardwire connection to the telescope control system proved to be impractical.

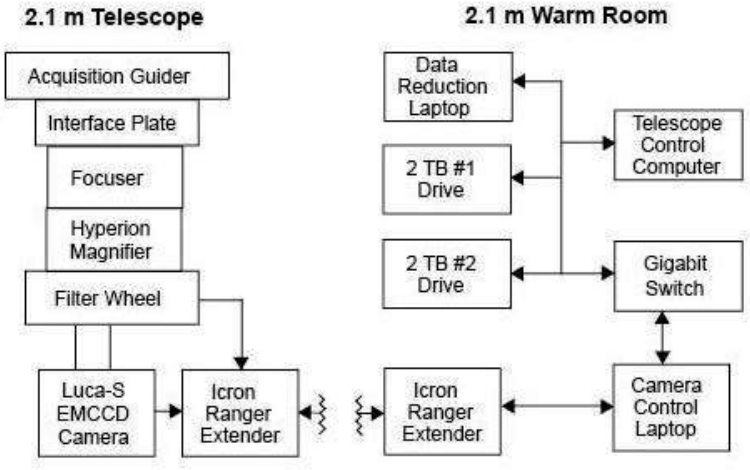

Figure 7. The original speckle system block diagram.

With many specifics of the science research programs and equipment engineering details worked out, our proposal for the second semester of the 2013-14 academic year was submitted in March of 2014. Although obtaining time on Kitt Peak telescopes is highly competitive (they are oversubscribed), the Telescope Allocation Committee awarded us nine nights in October.

Knowing that there is many a slip between the cup and the lip, arrangements were made to bring our visitor speckle camera to Kitt Peak during the monsoon engineering down-time at the end of July (2013) for a form, fit, and function check. Four of us (Genet, Smith, Clark, and Wren) attended the engineering checkout. Genet brought the disassembled camera on the plane with him. Smith assembled the camera and fastened it to the large interface plate. Two Kitt Peak telescope specialists, Mathis and Hensey, then mounted the assembly to the back of the acquisition guider (Figure 9, 10).

Once we were awarded time on the 2.1-meter telescope, we began forming the two observational teams, one for the first half of the run and the other for the second half. This way most of the observers just had to come for four or five nights, although Genet and Smith stayed for the entire run.

Detailed target lists had to be developed. Single reference stars also had to be selected. For our second run in April, Smith developed a semi-automated reference star selection routine. These various lists were then merged into the final target list spreadsheet that was divided into two-hour RA segments. By observing targets in two-hour segments, we were able to make most of our observations within an hour of the meridian at minimal air mass. Finally, Smith developed a target cache for the 2.1-m telescope control computer that allowed us to efficiently move to target coordinates without having to key them in.

Each observing run began with the mid-morning installation of our camera on the back of the telescope. Cables were connected, computers powered up, and the operation of the system confirmed. The first half of the first night on each run was devoted to focusing the telescope and co-aligning the telescope's acquisition camera with the speckle camera.

This was surprisingly difficult on both runs as the field-of-view of the science camera is only a few arc seconds, making both focus and co-alignment difficult. Dave Summers, a highly experienced Kitt Peak telescope operator, not only gave us instructions on operation of the telescope, but helped us achieve focus and co-alignment.

Regular observations then began from the warm room and continued all night, every night, until well past astronomical twilight (Figure 8, 9). One does not lose observing time at Kitt Peak by shutting down early!

Figure 8. Four undergraduate and one graduate student make the observations in the first run: Plummer, Wallace, Patel, Teiche, and Chaney.

Figure 9. First team in the warm room during the second run: (standing) R. Estrada, Ridgely, Genet, (sitting) Clarke, Frey, and C. Estrada.

There were three primary observing positions: the telescope operator (TO), camera operator (CO), and run master (RM). After initialization (and a bit of practice), the three team members were able to work closely together in a highly coordinated fashion to observe a target every four or five minutes.

In a very simplified version of what transpired, the RM chose the next object to observe from the target list and called out the telescope cache ID. The TO located the target in the cache and made it in the "next to observe" target; then, as soon as the CO finished the integration on the previous target, the TO initiated telescope slewing. On arriving at the target, the TO used the telescope's fine motions to move the star displayed on the acquisition camera's video to the location marked for the science camera (Figure 10).

The TO then moved the slider mirror to the position that allowed light to fall through to the science camera, and passed control to the CO (who also had a control paddle). The CO fine-tuned the centering of the target, adjusted the gain and integration time of the EMCCD camera, initiated the exposure, and called out the camera sequence number, which was entered by the RM into the run log.

Figure 10. The telescope operator has four screens, several programs, and numerous switches and analog displays to contend with. C. Estrada quickly became one of the top telescope operators.

Besides the TO, CO, and RM, who were totally occupied in the "production-line," fast-paced observational procedure, sample observations were reduced as an on-going check on the quality of the observations. At any given moment, one or two operators would be in training, or relief observers would be standing by, ready to take up an operating station while several folks headed for the dining room for a coffee break.

Conclusion

Our portable speckle system with its EMCCD camera as the sensor reliably observed close binaries on a 2.1-m telescope with separations down to 0.1 arc seconds. We found that using nearby, fairly bright single stars for deconvolution usually provided much better results than reductions without a reference star. Efficient operation required a telescope operator, camera operator, and run master, although additional observers were useful for quick-look reduction, relief operation, etc. Preprocessing the data with PlateSove 3 and using its semi-automatic feature greatly speeded up the data reduction.

Acknowledgments

Although they were unable to attend the Kitt Peak runs in person, William Hartkopf and Brian Mason at the U.S. Naval Observatory were instrumental in shaping the observing programs and preparing both proposals. Extensive use was made of the *Washington Double Star Catalog*, the *Sixth Catalog of Orbits of Visual Binary Stars*, and the *Fourth Catalog of Inteferometric Measurements of Binary Stars*, catalogs maintained by Brian Mason and William Hartkopf at the U.S. Naval Observatory.

Richard Joyce and Di Harmer provided extensive technical advice on the use of the 2.1-meter telescope. Hillary Mathis and Brent Hansey installed our camera during a one-evening mid-summer pre-run engineering checkout, as well as installing our camera on both the October and April runs. Dave Summers assisted with telescope operation on all of the runs. Daryl Willmarth set up the 0.8-m Coude feed spectrograph for us and provided instruction on its use. Ballina Cancio cheerfully handled dorm rooms, payment, and many logistical details for our unusually large number of participants.

Lori Allen, Kitt Peak's Director, visited us during our October run and was encouraging with respect to our many student observers. Education and outreach are important to Kitt Peak. NASA, through the American Astronomical Society's Small Research Grant Program, funded the Orion Observatory's Luca-S camera, which was the backup camera for both runs. Andor Technologies loaned us a larger-format Luca-R camera for both runs. Concordia University funded time on the Coude spectrograph in conjunction with a W. M. Keck Foundation astronomical grant.

Olga Kiyaeva at the Pulkovo Astronomical Observatory, as well as Francisco Rica in Spain, kindly supplied short-arc binary candidates. Olga Malkov at Moscow State University suggested targets that needed orbital refinement.

Joseph Carro assisted in formulating the target list for the known binaries. The *Journal of Astronomical Instrumentation* supplied our equipment block diagram. The Society for Astronomical Sciences provided an initial forum at their annual symposium for many of the ideas fleshed out in this paper (Genet et al. 2013). We thank Vera Wallen for reviewing this paper prior to submission, and Robert Buchheim for formatting the paper.

References

Genet, R. M. 2013. Portable speckle interferometry camera system. *Journal of Astronomical Instrumentation,* 2, 134008.

Genet, R. M., Hardersen, P., Buchheim, R., Mohanan, K., Church, R., Weise, E., Ricahrds, J., Rowe, D., & Johnson, J. 2013. Close double star speckle interferometry program. *Proceedings of Society for Astronomical Sciences,* 59.

Genet, R. M., Kiyaeva, O., Harshaw, W., & Wren, P. 2014. Short-arc binaries. In preparation.

Green, W., Kenney, J., Harshaw, R., & Genet, R. M. In preparation.

Harshaw, R., 2014. Another statistical tool for evaluating binary stars. *Journal of Double Star Observations,* 10, 39.

Herschel, W. 1803. Account of the changes that have happened, during the last twenty-five years, in the relative situation of double stars. *Philosophical Transactions of the Royal Society*, 93, 339.

Horch, E. 2006. The status of speckle imaging in binary star research. *RevMexAA*, 25, 79-82.

Hoskin, M. 2011. *Discoverers of the Universe: William and Caroline Herschel.* Princeton, NJ: Princeton University Press.

Kisselev, A. & Kiyaeva, O. 2003. Determining the minimum sum of the component masses for a binary with a known parallax from observations of a short arc of its apparent motion. *Astronomy Letters*, 29-1, 37-40.

Kisselev, A., Romanenko, L., & Kalinichenko, O. 2009. A dynamical study of 12 wide visual binaries. *Astronomy Reports*, 53, 126.

Kiyaeva, O., Kiselev, A., & Izmailov, I. 2008. Dynamical study of wide pairs of stars based on data from the WDS Catalog. *Astronomy Letters*, 34, 405.

Kiyaeva, O., Kiselev, A., Romanenko, O., Kalinichenko, O., & Vasil'eva, T. 2012. Accurate relative positions and motions of poorly studied binary stars. *Astronomy Reports*, 56, 952.

Labeyrie, A. 1970. Attainment of diffraction limited resolution in large telescopes by Fourier analyzing speckle patterns in star images. *A&A*, 6, 85.

Malkov, O., Tamazian, V., Docobo, J., & Chulkov, D. 2012. Dynamical masses of a selected sample of orbital binaries. *A&A*, 546, A69.

McAlister, H. 1977. *AJ*, 215, 159.

McAlister, H. 1985. High angular resolution measurements of stellar properties. *ARA&A,* 23, 59.

McAlister, H., Robinson, W., & Marcus, S. 1982. *Proc. SPIE*, 331, 113.

Perryman, M. 2012. *Astronomical Applications of Astrometry: Ten Years of Exploitation of the Hipparcos Satellite Data.* Cambridge, MA: Cambridge Univ. Press.

Rica, F. 2011. Determining the nature of a double star: the law of conservation of energy and the orbital velocity. *Journal of Double Star Observations,* 7-4, 254-259.

Rica, F. 2012. Orbital elements for BU 741 AB, STF 333 AB, BU 920 and R 207. *Journal of Double Star Observations*, 8-2, 127-139.

Smith, N. et al. 2008. EMCCD technology in high precision photometry on short timescales. In *High Time Resolution Astrophysics*. (Eds. Phelan, D., Ryan, O., & Shearer, A.). New York: Springer.

First Speckle Interferometry Observation of Binary BU 1292

Meryl Adam[1], Stephanie Roberts[2], Miriam Schenk[3], Carmen VanRonk[3], Tara Loayza[3], Russell Genet[2,4,5], Bobby Johnson[3], Thomas C. Smith[6], and Paul Wren[5]

1. Saint Joseph High School, Santa Maria, California
2. Cuesta College, San Luis Obispo, California
3. Arroyo Grande High School, Arroyo Grande, California
4. California Polytechnic State University, San Luis Obispo
5. University of North Dakota, Grand Rapids
6. Dark Ridge Observatory, Weed, New Mexico

Abstract The star BU1292 was observed on October 21, 2013 on the 2.1-meter telescope at Kitt Peak National Observatory. A new position angle of 227.90° and separation of 0.225" was determined. This new data point was found to be slightly divergent from the previously calculated orbit. A new orbital period is calculated that is 3.221 years shorter than the previously calculated orbit.

Introduction

On the night of October 21, 2013 BU 1292 (WDS 01078+0425) was observed on the 2.1 meter telescope with a speckle interferometry camera at Kitt Peak National Observatory as part of an eight day run. Subsequent to the observations, a group of students from Arroyo Grande High School, Saint Joseph High School, and Cuesta College worked together in a research seminar class to calculate the position angle and separation of the binary. The group chose binary BU 1292 because this star had no previous speckle interferometry observations. BU 1292 has a published orbital period of 285.3 years and a semi-major axis of 139.2 AU.

Figure 1. Team of high school authors.

Using data collected on BU 1292 during the observing run at Kitt Peak National Observatory in Arizona, the research seminar class determined the separation and position angle of this gravitationally bound double star and compared these results to past observations. This was the first observation of this binary using speckle interferometry. The discovery and first visual observation of the binary was in 1901 by S. W. Burnham, followed by thirteen more visual observations and one Hipparchus observation, not in that order.

Calibration

Although full reduction of the Kitt Peak data had not been made yet, REDUC, a speckle autocorrelation program written by Florent Losse (2012), was used to estimate the camera angle, Δ, and pixel scale, E, for the run at Kitt Peak National Observatory. Five fairly wide binaries were observed during the run. For this paper, REDUC, in its "calibration" mode, was used to reduce a single observation of each of the five binaries on the night we observed BU 1292.

Inputs to REDUC were: (1) the interpolated values of position angle, θ, and separation, ρ, based on the January 2013 and 2014 predictions in the Sixth Catalog of Orbits of Visual Binary Stars (Hartkopf and Mason 2013), and (2) the five FITS data cubes, one from each of the five wide binaries. The values used in the calibration, as well as the calibration results and supplemental information on visual magnitudes reported in the Washington Double Star Catalog (Mason et al. 2012), are given in Table 1.

WDS	V1	V2	θ2013	θ2014	θ Obs	ρ2013	ρ2014	ρ Obs	Seq #	Δ	E
01532+1526	8.75		260.5	260.6	260.580	1.093	1.092	1.0922	942	-11.66	0.01136
03122+3713	8.02	8.29	125.9	125.8	125.820	2.845	2.852	2.8506	964	-11.53	0.01177
03362+4220	8.84	9.54	342.7	343.5	343.342	0.724	0.722	0.7224	983	-11.02	0.01216
04041+3931	7.38	9.35	54.6	54.2	54.279	1.502	1.52	1.5165	1002	-11.36	0.01119
23595+3234	6.47	6.72	338.2	338.9	338.762	2.324	2.347	2.3425	923	-11.15	0.01176

Table 1. Calibration data.

The camera angles, Δ, and pixel scales, E, were averaged, and their standard errors of the mean calculated on a spreadsheet. The results were: Δ = -11.3° ±0.1 and E = 0.0116"/pixel ± 0.0002.

Figure 2. Paul Wren and Russ Genet stand in front of the top portion of the telescope.

Observations

BU1292 was observed on October 21, 2013, on the 2.1-meter telescope at Kitt Peak National Observatory. The observations were made by Genet, Smith, and Wren. The telescope (Figure 2) is f/7.6 with an effective focal length of about 16 meters. The times-eight magnification increased the effective focal length to about 128 meters (420 feet). Frames were taken with an Andor Luca-R electron-multiplying CCD camera.

A portable speckle interferometry camera (Genet 2013) was attached to the acquisition-guider unit at the Cassegrain focus of the 2.1-meter telescope (Figure 3). A magnification of times-eight was used to bring out the speckles. Observations were made using a Sloan i' filter so as to minimize atmospheric dispersion. The observation yielded a FITS data cube 512x512 pixels x1000 frames. Each of the 1000 exposures was 10 milli-seconds.

Figure 3. The Cassegrain focus of the 2.1-meter telescope. To the right of Genet is the gold-colored acquisition-guider unit. Below the acquisition-guider is the black-colored Barlow lens, filter wheel, and silver-colored Andor EMCCD camera of our portable speckle interferometry system.

The telescope was controlled from a nearby warm room (Figure 4). The USB Andor EMCCD camera was connected to the warm room via an Icron Ranger USB-to-Ethernet link and a 50-foot Category 5 cable.

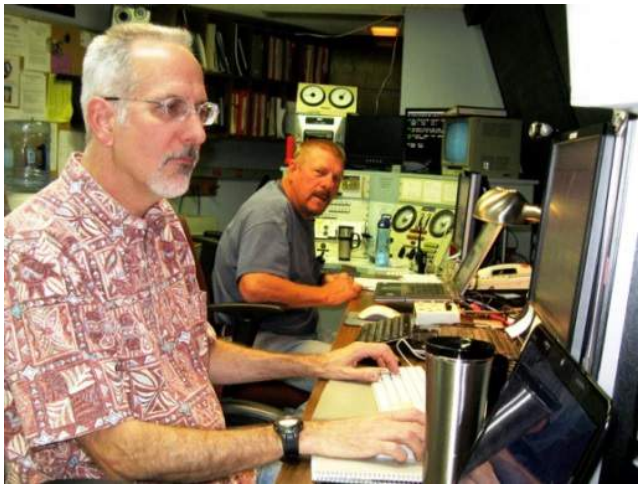

Figure 4. In the warm room, Paul Wren selected the next double to observe while Tom Smith operated the telescope. Russ Genet operated the speckle camera station between them but got up to take this picture.

The FITS data cube for BU 1292 was loaded into REDUC. The first of 1000 frames is shown on the left of Figure 5. After the data cube was loaded, REDUC's "Autocorrelation" option was chosen. The autocorrelogram, shown on the right of Figure 5, was the result when "S4" was chosen as the kernel mask and the gain and bias adjustments were made to enhance the visual image. The calibration values determined for Δ and E were entered after placing REDUC in its "measure" mode. The resulting binary position angle, Θ, was 227.90°, while the separation, ρ, was 0.255''.

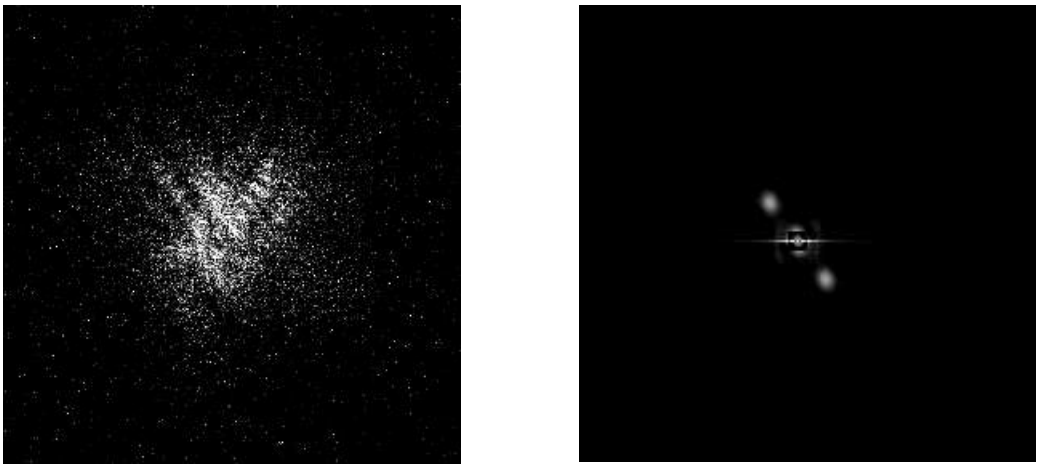

Figure 5. One image taken with the portable speckle interferometry camera system (left). Autocorellelogram (right).

Comparison with Past Observation

Past observations were provided by Brian Mason at the U.S. Naval Observatory. These past observations can be seen in Table 2 along with the observation from October 21, 2013. The position angles were not precessed to a current epoch. When compared with past observations, the new data seems to agree with the motion predicted by past observations.

In Table 2, the first column is the Julian date of observation. Column two is the reported position angle, θ, in degrees from north while column three is the separation, ρ, in arc seconds. Column four is the telescope aperture in meters. Finally, column five is the published reference to the observation cited in the Washington Double Star Catalogue.

Year	ρ	θ	Ap.	References
1901.39	0.30	384.2	1.0	Bu_1903
1936.57	0.30	346.3	0.6	Vou1947b
1945.576	0.25	346.2	0.6	Vou9999
1948.19	0.21	337.3	2.1	VBs1954
1958.3	0.20	310.5	2.1	VBs1960
1961.7	0.21	317.6	0.9	B_1962d
1965.637	0.26	317.7	0.7	Worl1971
1965.97	0.20	314	0.4	Cou1967b
1981.86	0.16	259.2	0.6	Heil1983a
1989.001	0.24	280.4	0.7	Cou1989b
1989.05	0.18	293.0	0.5	LBu1989
1989.91	0.22	287.2	0.5	LBu1990
1991.25	0.248	266	0.3	HIP1997a
1992.04	0.23	266.0	0.5	LBul1992
2013	0.255	227.90	2.1	Adam et al.

Table 2. All published astrometric observations of BU 1292 (Mason et al. 2012).

In Figure 6 the position angle was plotted against the date of observation. The initial discovery observation (Bu_1903) was reported as 24.2 degrees but was plotted on the graph as 384.2 degrees to preserve the trend. Similarly, the separation was plotted against date of observation in Figure 7.

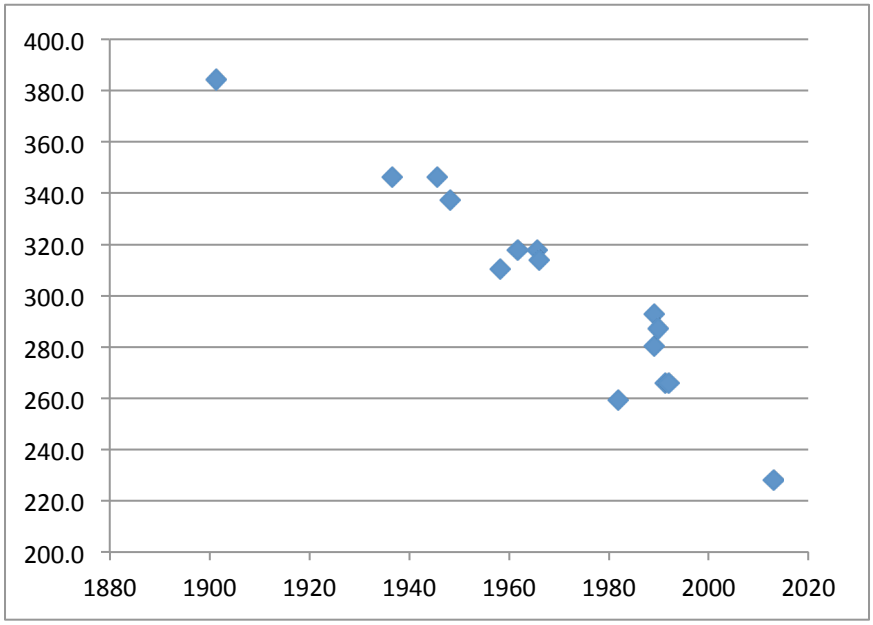

Figure 6. Plot of position angle v. time.

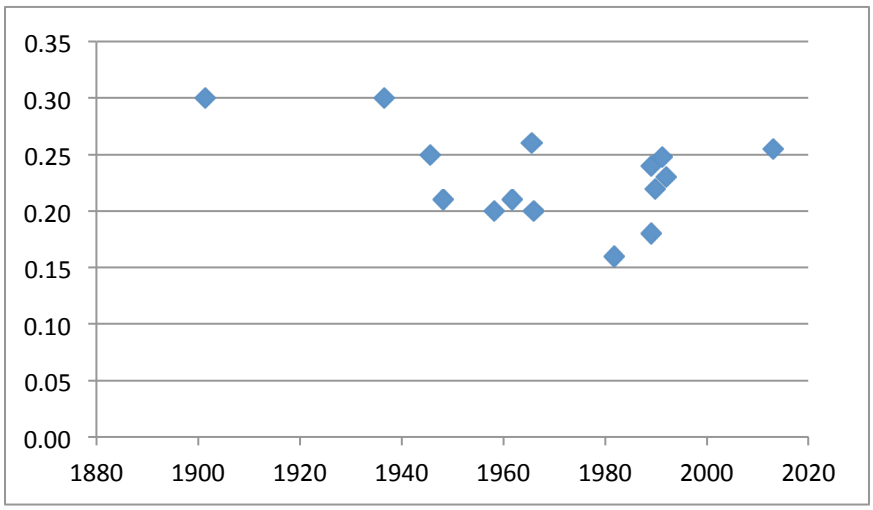

Figure 7. Plot of separation v. time.

Using the Microsoft Paint program and the data from the Kitt Peak observation, the new observational point and the predicted point were plotted on an image from the Naval Observatory (Hartkoph & Mason 2012) of the previously calculated orbit and past observations (Figure 8). Using the scale on the image of the previously calculated orbit, it was calculated that the ratio between pixels on Paint and separation in arc seconds was 700:1. The center coordinates of the binary in paint pixels was (272.5, 264.5). Using the position angle and known separation, simple trigonometry was used to find the distance in arc seconds in the x and y distances of the star from the center, (.189", .171"). These were then converted into pixels using the previously determined 700:1 ratio, (140.2, 144.8). Using these new coordinates, a new data point was added to the orbit plot from the Washington Double Star Catalog. A predicted point for the same date and time, predicted by ephemerides from the Sixth Orbit Catalog, was calculated in the same manner and also added to the graph of the orbit plot.

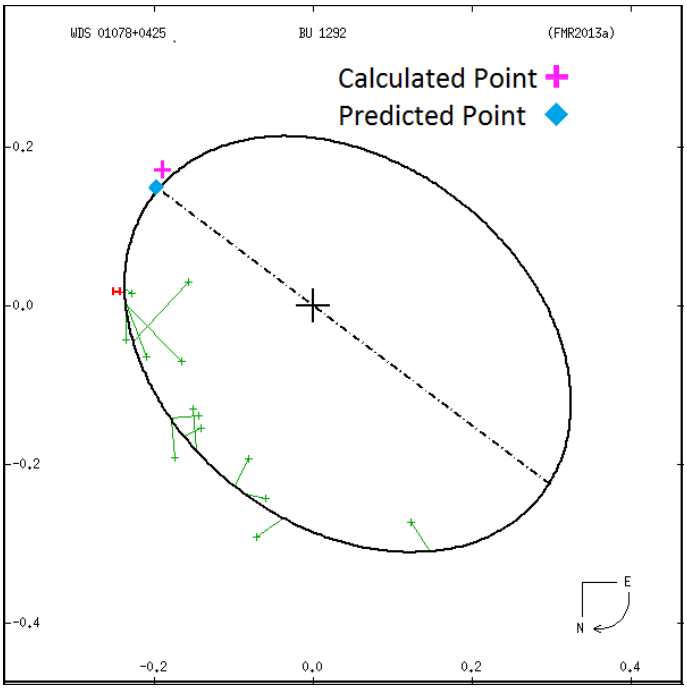

Figure 8. Plot of all Observations

The speckle interferometry and Hipparchus observations are more accurate than the visual observations. Taking this into account, the newly calculated point is not directly aligned with the predicted point. The difference in position angle between the predicted point and the calculated point for the speckle interferometry observations was 4.2°. Comparing this to previous points, it can be roughly estimated that the orbit is off by 3.2 years. Subtracting this from the previously calculated orbit of 285.3 years, it can be estimated that the orbit should be about 282.1 years. The semi-major axis of the orbital ellipse also needs to be adjusted. The difference between the new and the old axes is .011".

Conclusion

The most recently calculated position angle of BU 1292 is 227.90° and separation is 0.255". It has been determined that the published orbital of this star was and is most likely about 3.221 years too long.

Acknowledgments

For their contributions to the paper, we would like to express much gratitude to the NOAO National Optical Astronomy Observatory and Kitt Peak National Observatory for the time on their 2.1m telescope. A special thanks to Andor Technologies for loaning us the camera used for the observations. Finally, the team would like to express much gratitude to Brian Mason for providing data from the US Naval Observatory. To all who helped with the composition of this paper and to the external reviewers, thank you.

References

van den Bos, W. H. 1962. Micrometer measures of double stars II. *The Astronomical Journal*, 67, 141.

Couteau, P. 1967. Measures d'etoiles doubles faites AU refracteur de 38cm de l'Observatoire de Nice. *Journal des Observateurs*, 50, 41.

ESA. 1997. The Hipparcos and Tycho catalogues. VizieR On-Lline Data Catalog: I/239. 1997yCat.1239....0E.

Genet, R. M. 2013. Portable speckle interferometry camera system. *Journal of Astronomical Instrumentation*, 2, 2, 1340008.

Hartkopf, W. I. & Mason, B. D. 2012. *Sixth Catalog of Orbits of Visual Binary Stars*. Washington: US Naval Observatory.

Heintz, W. D. 1983. Micrometer observations of double stars and new pairs. XI, *Astrophysical Journal Supplement Series*, 51, 249-268.
Le Beau, J. 1989. Measures d'etolies doubles visuelles. *Observations et Travaux*, 17, 24.
Le Beau, J. 1990. Binary measurements made at Nice with the 50-cm telescope. *Astronomy and Astrophysics Supplement Series*, 85, 889.
Le Beau, J. 1992. Measures d'etoiles doubles visuelles. *Observations et Travaux*, 30, 30-34.
Losse, F. 2012. REDUC V4.7. http://www.astrosurf.com/hfosaf/Reduc/Tutorial.htm.
Mason, B. D., Wycoff, G. L., & Hartkopf, W. I. 2012. *The Washington Double Star Catalog*, Washington: U.S. Naval Observatory.
Voûte, J. 1947. Measures of double stars, 5th series. *Annalen v.d. Bosscha-Sterrenwacht*, 6, 3.
Worley, C. E. 1971. Micrometer measures of 1,343 double stars. *Publications of the U.S. Naval Observatory,* 22, 136.

Speckle Interferometry Observation of Binary WDS 01528-0447

Meryl Adam[1], Eric Weise[2], Bobby Johnson[3], Barron Lutes[4], Katie Huck[4], Ankur Patel[4], and Russell Genet[3, 5, 6]

1. Saint Joseph High School, Santa Maria, California
2. University of California, San Diego
3. Cuesta Community College, San Luis Obispo, California
4. Arroyo Grande High School, Arroyo Grande, California
5. California Polytechnic State University, San Luis Obispo
6. University of North Dakota, Grand Rapids

Abstract On October 21, 2013 the binary star WDS 01528-0447 was observed on the 2.1-meter telescope at Kitt Peak National Observatory. The current position angle and separation was determined to be 39.32° and 0.373″ respectively. This position continued the trends of recent speckle observations, which appear to be diverging from the predicted path of the previously calculated orbit.

Introduction

As part of an eight-night run, the binary WDS 01528-0447 was observed on the 2.1 meter telescope at Kitt Peak National Observatory on October 21, 2013. A portable speckle interferometry camera was used to make the observation (Genet et al. 2013). Students from Saint Joseph High School, Cuesta Community College, and Arroyo Grande High School made the calculations in a Cuesta College research seminar. WDS 01528-0447 was chosen from the many binaries observed during the Kitt Peak run due to three recent speckle observations that sharply deviated from the predicted orbit. Would this deviation continue, or were these three observations just coincidental outliers?

The current position of the star was graphed against a plot of 22 past observations. The initial observation of this binary was in 1955 by Richard Alfred Rossiter.

Observations

Observations of WDS 01528-0447 were made as part of an eight night run at the Kitt Peak National Observatory (KPNO) in Tucson, AZ. This run was organized to look exclusively at close double stars using speckle interferometry. Observations were made by a team of astronomers led by Genet using a specially developed speckle interferometry system (Genet et al. 2013). The electron-multiplying CCD camera used on this run was an Andor Luca-R, which features a 1004x1002 pixel front illuminated CCD chip with 8 micrometer square pixels.

The 2.1 meter telescope has a focal ratio of f/7.6, which gives a focal length of 16 meters (52 feet). An eight times magnification Barlow was used to give us an effective focal length of 128 meters (416 feet). With this magnification, the speckles were clearly visible with our EMCCD camera.

WDS 01528-0447 was observed on Oct 21, 2013 (Besselian 2013.81). We used a Sloan i' filter to reduce atmospheric dispersion compared to shorter wavelengths. A total of 1000 images, each with an exposure time of 15 milliseconds, were taken of the system.

Methods

An Andor Luca-R electron-multiplying CCD camera was used to capture data for analysis. For WDS01528-0447, 1000 observations were made of 10 millisecond duration.

These frames were used to create a FITS data cube, a culmination of the 1000 frame observation. The FITS cube was loaded into the program REDUC in order to interpret the data. To create an autocorrelogram, the software's "Autocorrelation" option was used. Once in "Measure" mode, values for Δ and E (Adam et al. 2014) were entered so that we could determine measurements for the double (Figure 1).

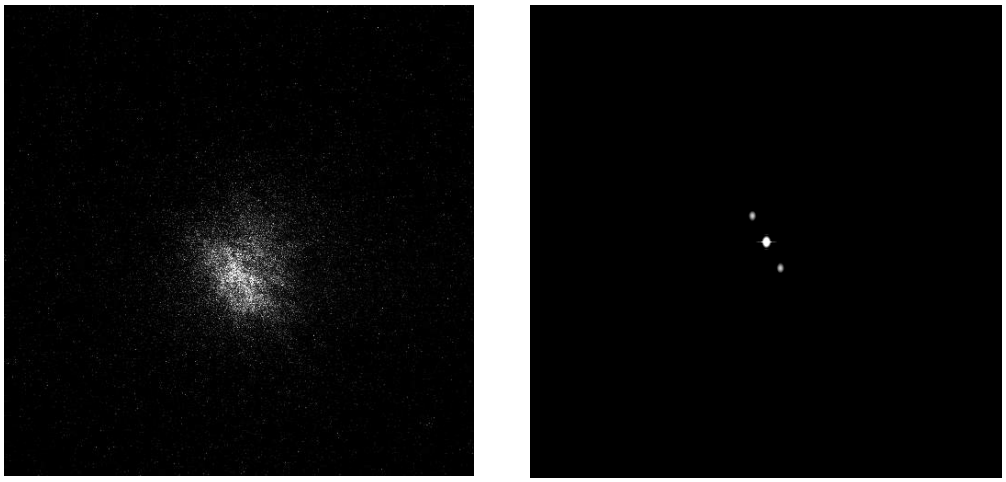

Figure 1. One image taken with the portable speckle interferometry camera system (left) and Autocorellelogram (right).

Data Analysis

After entering the calibration camera angle and pixel scale values, we were able to determine the astrometric measurements of the binary (Table 1). The resulting separation, ρ, of the pair was found to be 0.373", with a position angle, θ, of 39.32°. This new point fits the trend seen in the orbital plot of the motion, moving away from the predicted orbit.

Year	ρ	θ	Ap.	References
1939.45	0.24	301.8	0.7	Rst1955
1944.03	0.28	310.6	0.7	Rst1955
1949.02	0.23	327.6	0.7	Rst1955
1951.47	0.28	330.5	0.7	Rst1955
1961.70	0.34	353.6	0.9	B_1962d
1963.98	0.33	1.5	0.7	Hln1965
1964.00	0.30	355.8	0.4	Cou1964
1965.66	0.33	0.3	0.7	B_1967
1975.84	0.45	4.5	0.6	Hei1978b
1977.920	0.22	8.5	1	Hei1978a
1978.75	0.40	8.3	0.6	Hei1980a
1978.784	0.37	9.9	0.9	wor1989
1984.72	0.47	13.4	0.6	Hei1985a
1989.9410	0.462	18.9	4	Hrt1996b
1990.9185	0.492	17.5	4	Hrt1996b
1991.49	0.44	22.0	0.3	TYC2002
1994.99	0.46	22.8	0.6	Hei1996a
1995.9182	0.468	21.8	2.5	Hrt1997
2001.8680	0.44	26.1	0.7	WSI2002
2007.5994	0.419	31.3	3.8	Msn2011d
2008.5462	0.4226	33.1	4	ToK2010
2013	0.373	39.32	2.1	Adam et al.

Table 1. All observations of WDS 01528-0447.

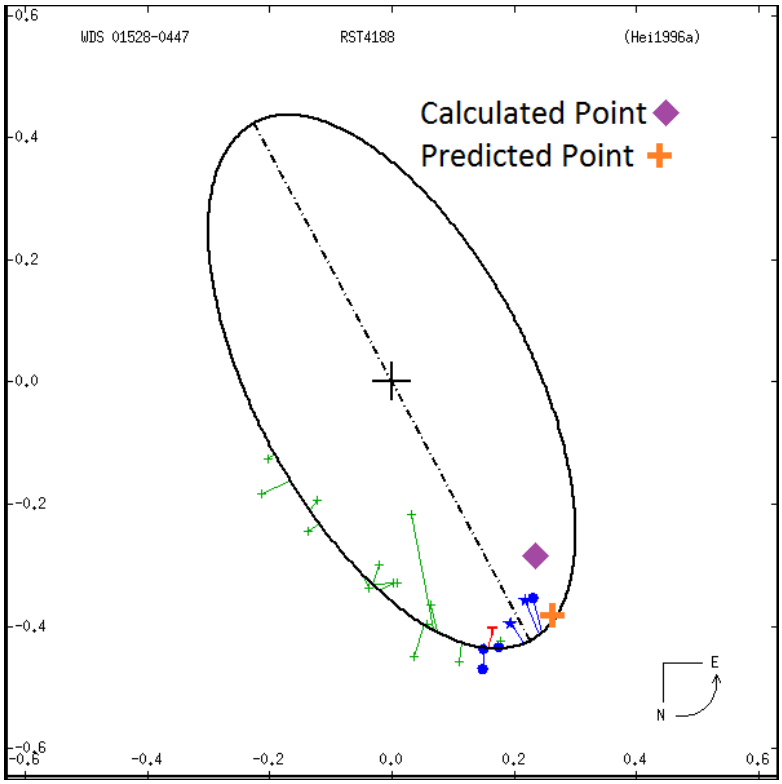

Figure 2. Orbital plot of all observations.

Conclusion

Our group of students successfully reduced data on one binary star from an eight night run at the Kitt Peak National Observatory. We found the position angle and separation of WDS 01528-0447 to be, respectively, 39.32° and 0.373". We graphically compared our data point to the past observations reported in the WDS (Figure 2). It is clear that the orbit was calculated with insufficient data, although, even with the current data set, it does not seem like a satisfactory orbit can be computed. This system should be observed more in the future so that a more satisfactory orbit can be computed.

Acknowledgments

We would like to thank the NOAO (National Optical Astronomy Observatory) and Kitt Peak National Observatory for the use of their 2.1m telescope. We also thank Andor Technologies for allowing us to use their Luca-R camera for the observations. Lastly, we would like to thank Brian Mason for supplying data from the US Naval Observatory, as well as everyone who helped us to compose this paper and the external reviewers.

References

Adam, M., Roberts, S., Schenk, M., VanRonk, C., Loayza, C., Genet, R. M., Johnson, B., Smith, C., & Wren, P. 2015. First speckle interferometry observations of binary BU 1292. *Journal of Double Star Observations*, 1S, 67.

Couteau, P. 1964. Mesures d'étoiles doubles faites au réfracteur de 38 cm de l'Observatoire de Nice. *Journal des Observateurs*, 47, 229.

Fabricius et al. 2002. The Tycho double star catalogue. *Astronomy and Astrophysics*, 384, 180.

Genet, R. et al. 2013. Close double star speckle interferometry program. *Proceedings for the 32nd Annual Conference of the Society for Astronomical Sciences*. Eds. Warner, B., Buccheim, B., Foote, J., & Mais, D.

Heintz, W.D. 1978. Micrometer observations of double stars. IX, *Astrophysical Journal Supplement*, 37, 343.

Heintz, W. D. 1980. Micrometer observations of double Stars and new pairs. Part Ten, *Astrophysical Journal Supplement*, 44, 111.

Heintz, W. D. 1985. Micrometer observations of double stars and new pairs. XII, *Astrophysical Journal Supplement Series*, 58, 439.

Heintz, W. D. 1996. Observations of double stars and new pairs. XVII, *Astrophysical Journal Supplement*, 105, 475.

Holden, F. 1965. First list of stars observed at the Lamont-Hussey Observatory of the University of Michigan. *Publications of the Observatory of the University of Michigan*, 9, 181.

Holden, F. 1978. Visual double stars measured at Las Campanas Observatory, Chile. *Publications of the Astronomical Society of the Pacific*, 90, 463.

Hartkopf et al. 1996. ICCD speckle observations of binary stars. XIII, measurements during 1989-1994 from the Cerro Tololo 4m telescope. *Astronomical Journal*, 111, 936.

Mason et al. 2011. Speckle interferometry of exoplanet host stars. *Astronomical Journal*, 142, 176.

Mason et al. 2002. Speckle interferometry at the US Naval Observatory. VIII, *The Astronomical Journal*, 124, 2254.

Rossiter, R.A. 1955. Catalogue of southern double stars. *Publications of the Observatory of the University of Michigan*, 11, 1.

Tokovinin et al. 2010. Speckle interferometry at the Blanco and SOAR telescopes in 2008 and 2009. *The Astronomical Journal*, 139, 743.

van den Bos, W. H. 1962. Micrometer measures of double stars II. *The Astronomical Journal*, 67, 555.

van den Bos, W. H. 1967. Micrometer measures of double stars. *Republic Observatory Johannesburg Circular*, 126, 127.

Worley, C.E. 1989. Micrometer measures of 2589 double stars. *Publications of the United States Naval Observatory*, 25, 1.

International Speckle Interferometry Collaboration

Eric Weise[1], Yuan-Yuan Ding[2], Chaoyan Wang[2], and Russell M. Genet[3,4,5,6]

1. University of California, San Diego
2. Shanghai Astronomical Observatory
3. California Polytechnic State University, San Luis Obispo
4. Concordia University, Irvine, California
5. Cuesta College, San Luis Obispo, California
6. University of North Dakota, Grand Forks

Abstract Part of a binational cooperation, astronomers from China and the United States observed ten double stars using speckle interferometry. These doubles are STF2021B, STF2140AB, STF2161AB, STF2245AB, STF2264, STF2280AB, STF2486AB, STF2578AB, STF2588A,BC, and STF2789AB. Of these doubles, there are two, STF2616AB and STF2245AB, whose past observations appear to make a short arc, but do not have an orbit published in the sixth Catalog of Orbits of Visual Binary Stars.

Introduction

In the summer of 2013 Yuan-Yuan Ding and Chaoyan Wang, astronomers at the Chinsese state run Shanghai Astronomical Observatory, came to California. In between visits to the California Institute of Technology and the Center for Adaptive Optics at the University of California, Santa Cruz, Ding and Wang spent several days in San Luis Obispo as the guests of Russell Genet and Eric Weise. Seizing the opportunity to form an international collaboration, the group decided to make speckle observations at the Orion Observatory in Santa Margarita, CA (Figure 1).

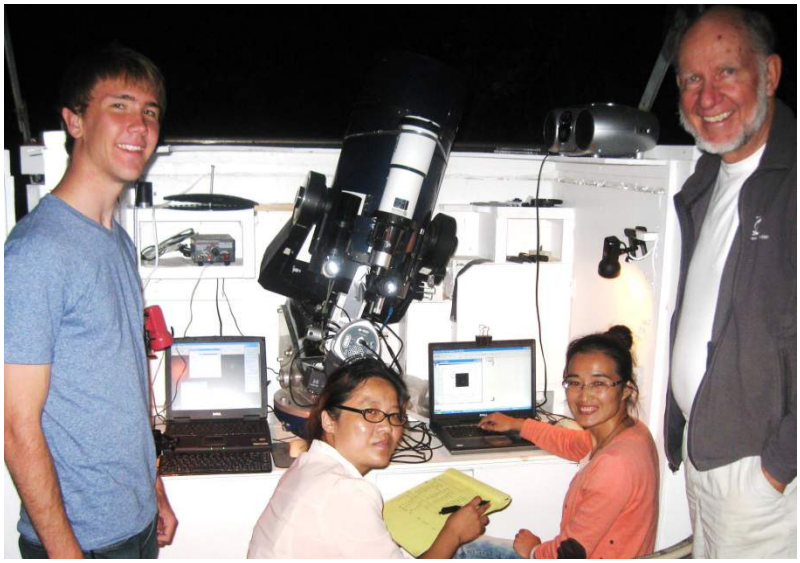

Figure 1. The observers pose in front of their instrument. From left to right: Eric Weise, Chaohan Wang, Yuan-Yuan Ding, and Russell Genet.

Ding and Wang had originally planned on attending the Maui International Double Star Conference, which was held in February 2013 at the University of Hawaii, Institute for Astronomy (Genet 2013b). Unfortunately, their visas were not approved until after the conference. Despite not making it in person, their poster was presented at the conference and Ding's paper was accepted for the proceedings of the conference (Ding 2015).

Equipment and Methods

The Orion Observatory is run by Genet near his home in Santa Margarita, CA. Observations were made using the 10 inch, f/10, equatorial mounted, internally baffled Meade telescope driven by a Sidereal Technology control system. Observations of the double stars were made using Genet's custom speckle camera (Genet 2013a). This system uses an Andor Luca-S camera capable of taking the short exposures and seeing the speckles at low light. A x2 Barlow lense was used to increase the magnification. The speckle images were saved in a .FITS cube which were analyzed using Reduc, a double star reduction program developed by Florent Losse. More details on the camera and the aspirations of Genet's speckle program can be found in his paper (Genet et al. 2013c).

Calibration Methods

The pixel scale (E) and the camera angle (Δ) were found using two different methods (see Table 1). In Method 1, E and Δ were found separately. Δ was found using the drift method on a single star: the telecope tracking was turned off and the star was allowed to drift through the field of view as the camera took a series of images. This series of images was saved into a FITS cube and analyzed using the "Synthetic Drift Analysis" option in Reduc. E was determined using a slit mask. The slit mask had a spacing of d=0.673 inches or 1.71×10^7 nanometers. An Hα filter was used, giving a wavelength of λ=656nm. The angular separation of the diffraction peaks at the focus of the telescope was found using equation 1 (Maurer 2012):

$$\frac{206{,}265\lambda}{d} \qquad \textit{Eq. 1}$$

A single star was observed through the slit mask using speckle imaging; 2,000 images, each exposed for 15 milliseconds, were taken per observation, and an autocorrelogram made and analyzed using Reduc. The slit mask was rotated by an arbitrary angle after each observation in order to reduce any systematic bias in the camera orientation.

In Method 2 a sufficiently static double star was observed through a Sloan R' filter. Each observation yielded a FITS cube comprised of 2,000 images taken with an exposure time of 15 milliseconds. Then, E and Δ were found using the calibration mode of Reduc. The values of θ and ρ entered into Reduc were the averages of the observations from the ten most recent entries in the Washington Double Star Catalog.

				Δ (˚)			E (a.s./pixel)		
Star	Method	Epoch	#obs	Δ	Std Dev	Std Err	E	Std Dev	Std Err
STF2486 AB	2	B2013.629	6	-2.8742	0.3558	0.1453	0.2568	0.0009	0.0004
Deneb	1	B2013.629	6	-2.9933	0.1816	0.0741	0.2543	0.0010	0.0003
Vega	1	B2013.634	6	-3.0417	0.3026	0.1235	0.2548	0.0008	0.0002

Table 1. Calibration results. The final values used for Δ and E were found by averaging the results above: Δ = -2.9697˚, E = 0.2553 a.s./pixel.

Observational Methods

Each of the target double star systems was observed six times in the same manner that the calibration double was measured: each observation involved taking 2,000 images of the system, each image having an exposure time of 15 milliseconds. A Sloan R' filter was used to decrease the effects of atmospheric dispersion and isolate the speckle pattern in each image. Reduc was used to create an autocorrelogram from each FITS cube. This autocorellogram was analyzed in Reduc to find θ and ρ.

Results

Observations were made on two nights, the 19th and 20th of August, B2013.634 and B2013.637, respectively. Results are shown in Table 2. The values of θ and ρ reported for each double star are the averages of the six observations described in Observatonal Methods.

			Position Angle (˚)			Separation (arc. sec.)		
WDS #	Disc Code	Epoch	θ	Std Dev	Std Err	ρ	Std Dev	Std Err
16133 +1332	STF2021AB	2013.637	357.17	0.25	0.10	4.127	0.013	0.006
17146 +1423	STF2140AB	2013.637	102.89	0.52	0.21	4.976	0.086	0.035
17237 +3709	STF2161AB	2013.637	320.70	0.27	0.10	4.165	0.045	0.019
17564 +1820	STF2245AB	2013.637	290.55	0.63	0.26	2.636	0.032	0.013
18015 +2136	STF2264	2013.634	256.60	0.26	0.10	6.510	0.014	0.006
18078 +2606	STF2280AB	2013.634	183.08	0.08	0.03	14.383	0.056	0.023
19121 +4951	STF2486AB	2013.637	204.76	0.07	0.03	7.260	0.016	0.006
19457 +3605	STF2578AB	2013.637	124.38	0.05	0.02	15.023	0.033	0.013
19490 +4423	STF2588A,BC	2013.637	159.10	0.09	0.03	9.769	0.031	0.013
21200 +5259	STF2789AB	2013.637	113.90	0.04	0.02	7.057	0.035	0.014

Table 2. Results from observations of ten double star systems. Each system was observed six times, each observation yielding a fits cube of 2,000 images, each taken with an exposure time of 15 ms.

Figures 1-3 show our data points graphed along with the historical data kept by the United States Naval Observatory in the Washington Double Star Catalog (Mason & Hartkopf 2013). The Position Angles of the past observations were precessed using the procedure given by Greaney (2012). Of the ten systems observed, four have orbital solutions published in the Sixth Catalog of Orbits of Visual Binary Stars. Those systems are: STF2021AB, STF2140AB, STF2486AB, and STF2789AB. The past observations of two systems appear to curve; it is possible that these systems are gravitationally bound. Those systems are STF2161AB and STF2245AB.

In all graphs, the primary star is shown by the black 'plus', past observations are shown as blue stars, and our observation is shown as the magenta diamonds. North is at the bottom of the graph and west is the left side of the graph.

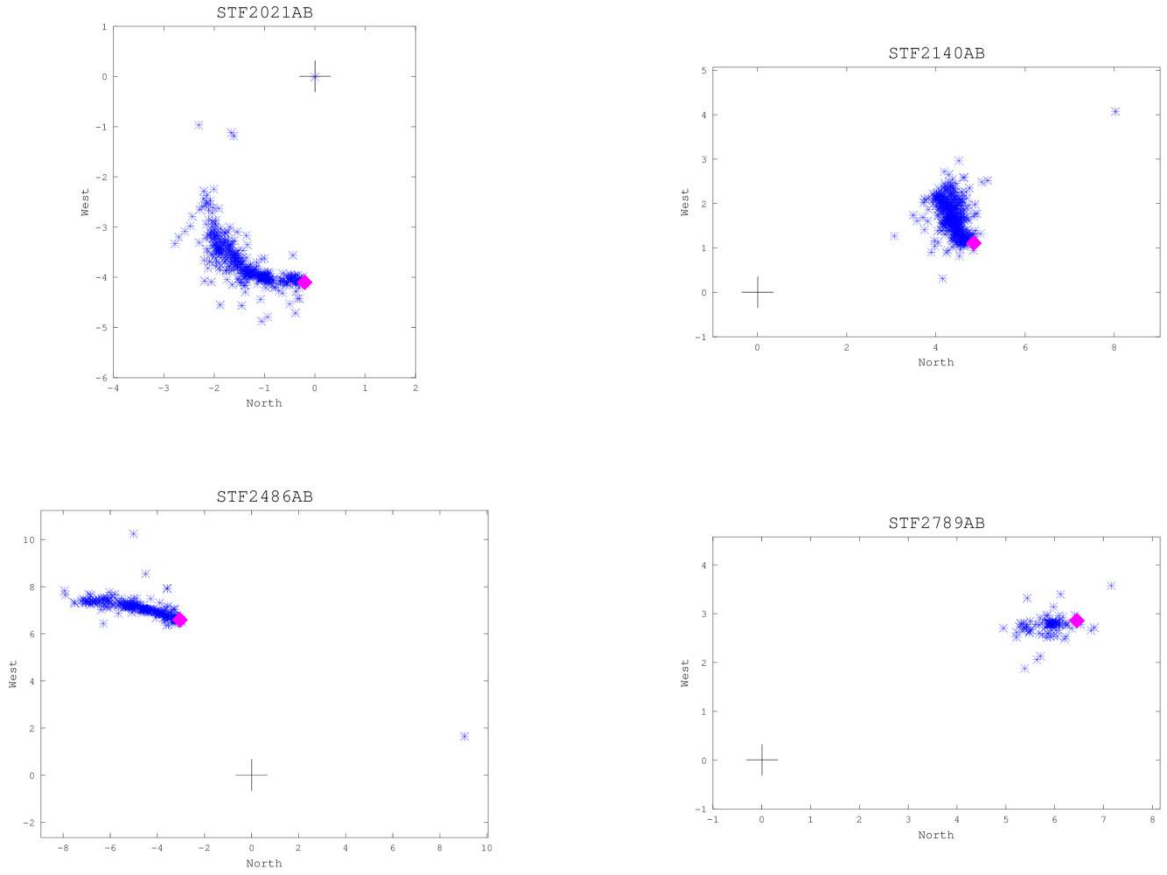

Figure 2. Observed double star systems which have orbits published in the Sixth Catalog of Orbital Elements. Past observations are shown by blue stars, while our observations are marked by the magenta diamonds.

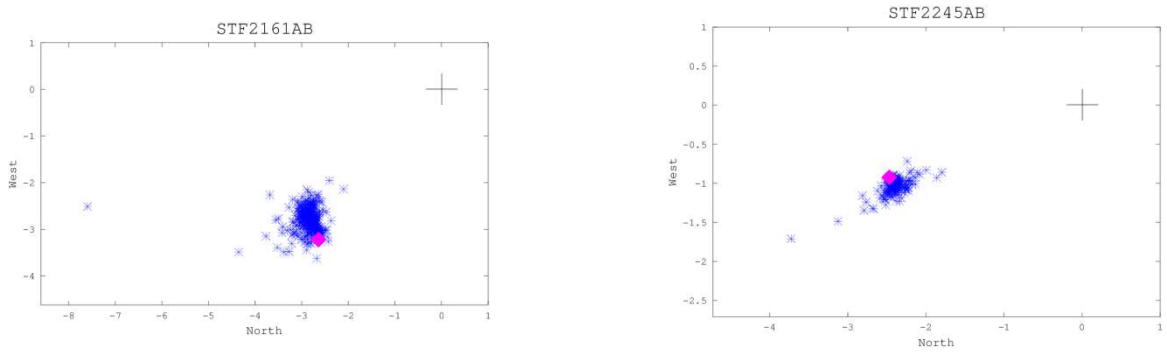

Figure 3. Two observed systems, STF 2161AB and STF2245AB, show interesting trends, perhaps indicating the systems are gravitationally bound. STF2161AB appears to be orbitting in a counter-clockwise direction, while STF2245 appears to be traveling clockwise.

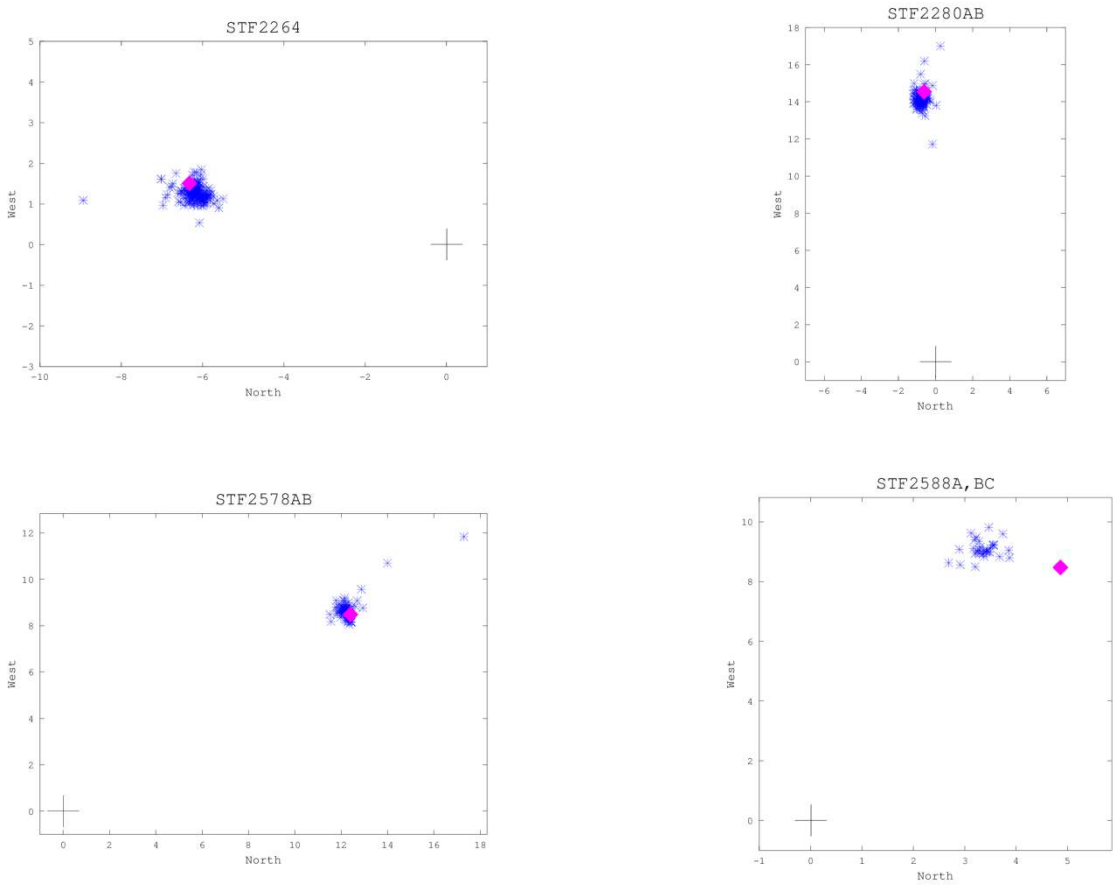

Figure 4. Graphs of the remaining four observed double stars. Past observations are shown with blue stars while our observations are marked by a magenta diamond.

Conclusion

Of the four systems with published orbits, STF2021AB is a grade 4 and has a period of 1354 years (Baize & Petit 1989), STF2140AB is a grade 4 and has a period of 3600 years (Baize 1978), STF2486AB is a grade 4 and has a period of 3100 years (Hale 1994), and STF2789AB is a grade 5 and has a period of 180 years (Kiselev et al. 2009). It seems unlikely that any of these orbits will soon be upgraded; in the case of the first three, the period is too long, and the last one was calculated very recently. The doubles STF2161AB and STF2245AB could possibly have orbits calculated after a few more observations are made.

Acknowledgments

The authors would like to thank Florent Losse for generously allowing us to use Reduc and for his help in understanding how to use the program. This research also made use of the past data kept by the United States Naval Observatory. Thanks are due to William Hartkopf and Brian Mason for their diligence and expedience in providing data from the Washington Double Star Catalog.

References

Baize, P. 1978. *Inf. Circ.*, 76.

Baize, P. & Petit, M. 1989. *A&AS*, 77, 497.

Ding, Yuan-Yuan. 2015. Speckle imaging experiment with the 1.56 meter telescope at the Shanghai Astronomical Observatory. *The Journal of Double Star Observations*. In preparation.

Genet, R. M. 2013a. Portable speckle interferometry camera system. *Journal of Astronomical Instrumentation*, 2. 1340008-14.

Genet, R. M. 2013b. The Maui International Double Star Conference. *The Journal of Double Star Observations*, 9, 2, 158.

Genet, R. M., Hardersen, P., Buchheim, R., Mohanan, K., Church, R., Weise, E., Richards, J., Rowe, D., & Johnson, J. 2013c. Close double star speckle interferometry program. *Proceedings for the 32nd Annual Conference of the Society for Astronomical Sciences*, 61. http://www.socastrosci.org/images/SAS_2013_Proceedings.pdf

Greaney, M. 2012. Some useful formulae; precessing the position angle. In *Observing and Measuring Visual Double Stars*, 2. Ed. Argyle, R. W. New York: Springer, 355.

Hale, A. 1994. *AJ*, 107, 306.

Kiselev, A. A., Romanenko, J. G., & Kalinichenko, O. A. 2009. *Astr. Reports*, 53, 126. (SvAL 86, 148, 2009).

Mason, B. & Hartkopf, W. I. 2013. *The Washington Double Star Catalog*: Personal Correspondence.

Maurer, Andreas. 2012. The diffraction grating micrometer. In *Observing and Measuring Visual Double Stars*, 2. Ed. Argyle, R. W. New York: Springer, 184.

Kitt Peak Speckle Interferometry Program Database Generation

Alex S. Teiche
California Polytechnic State University, San Luis Obispo

Abstract During our fall 2013 run on the Kitt Peak 2.1-meter telescope, we gathered over 1000 speckle measurements of double stars. These observations occupy roughly 1.3 terabytes of disk space. This paper describes the current format of the database, the process used to produce it, and makes format and database recommendations for future speckle interferometry programs of this scale.

Introduction

At Kitt Peak in October of 2013, we made over 1000 observations of double stars, resulting in roughly 1.3 terabytes of FITS cubes. Separately, we logged the TCS (Telescope Control System) information in a text file along with the catalog number of the object observed.

This information was merged into the headers of the FITS cubes to make it easier to access, particularly during automated data processing and reduction. An Excel spreadsheet was then generated with one entry per observation, containing all relevant information from the FITS header and TCS log.

Database Layout

The database is separated into 4 folders, "*Cubes*", "*Merge_Logs*", "*Other*", and "*Pictures*". The "Cubes" folder contains all FITS data collected. This is further divided into "*Calib*" and "*Observations*". "*Calib*" contains all camera calibration data taken, including flat fields, dark frames, and drifts. "*Observations*" contains all observations, including both double stars and single stars. The FITS cubes in the "*Observations*" folder have been renamed to place the sequence number first (Andor SOLIS places it last by default). Also, the TCS data has been merged into their FITS headers.

The "Merge_Logs" folder contains notes from merging TCS logs into FITS headers. There is a list of all the FITS cubes for which a matching TCS log could not be found (*cubes_without_tcs.txt*), a list of all incomplete TCS log instances(*incomplete_tcs.txt*), a list of FITS cubes renamed (*cubes_renamed.txt*), and a list of all changes made to the TCS logs (*tcs_log_changes.txt*). The list of FITS cubes renamed is in the format of a UNIX shell script, and could be run on a folder containing untouched FITS cubes to reproduce the filename changes. These changes were due to a variety of causes, most frequently a misspelled HIP or WDS identifier.

The "*Other*" folder contains strut temperature logs (copied from Kitt Peak's rose system each morning), an untouched copy of the TCS logs, and files from a CCD sensor linearity test conducted during the run.

The "*Pictures*" folder contains pictures taken by several people on the run. Also present in the root folder is an Excel spreadsheet (*KPNO_DB.xls*), and this document. The Excel index contains one line per FITS cube, and has all the relevant information from the FITS headers, as well as all the information about the target contained in the Washington Double Star Catalog**.**

Spreadsheet

The spreadsheet has 43 pieces of information for each FITS cube, in addition to the FITS cube file name. The first seven columns contain the information necessary for automated data reduction. A description of each follows:

DS – Double or single star. The only valid values are D for double star and S for single star.
DSFN – Double star file name.
RSFN – Reference(single) star file name. They were selected using the algorithm described below.
Lstθ, Lstρ – Most recent measurements of theta and rho.
CA – Camera angle, in degrees.
PS – Plate scale, in arc-seconds per pixel.
Target **–** The target identifier number, with a preceding catalog identifier for all cubes except WDS cubes.
Type – The type of object observed. Possible options for this particular run were WDS, HIP, GH, and LH (all abbreviations for catalogs), and NOTCS (no telescope control system data).
TCS RA, TCS Dec, RO, DO – Precision pointing information with RA and Dec offsets from the telescope control system. RO and DO are measured in arc seconds.
TCS Time – Mountain Standard Time as reported by the TCS.
Focus – Primary focuser position as reported by the TCS, measured in microns. This value is likely not meaningful, as the visiting instrument had its own focuser (Moonlite Crayford-type) that was set twice during the run.
ZD – Zenith distance, as reported by the TCS in degrees.
I – Integration time specified in the Andor SOLIS FITS header, reported in seconds.
Gain – Electron-multiplier gain specified in the Andor SOLIS FITS header. It is a unitless value between 0 and 1000.
FITS Cube Time – GMT of the acquisition of the first frame in the FITS cube, specified in the Andor SOLIS FITS header.
DC – Discoverer code and number.
Comp – Components, when more than two are present.
First, Last – Year of first and last observation.
No – Number of observations.
Fstθ, Fstρ – First measurement of theta and rho.
Mag1, Mag2 – Magnitude of primary and secondary star, respectively.
Spectral 1, 2 – Spectral class of primary and secondary, respectively.
PRA, Pdec – Primary proper motion in RA and Dec.
SRA, Sdec – Secondary proper motion in RA and Dec.
DM, N, B, C, – Durchmusterun number, notes, differential magnitudes, orbital or linear solution.
Decimal RA + Dec – Precision RA and Dec in decimal format (J2000).
RA, Dec – Precision RA and Dec in traditional format (J2000)**.**
ROI – The four ROI columns contain the region of interest information found in the Andor SOLIS FITS header. The format of this information is currently unknown.

Merging TCS Data

The TCS data includes local time, telescope RA and Dec, RA and Dec offsets, epoch, focus, zenith distance, equinox, and the name of the telescope. This data along with the target (manually entered by the person recording TCS logs) was added to the FITS header for each cube. Comments as they appear in the TCS system were copied to corresponding FITS header comment fields. TCS data was added to the FITS header in a field using its TCS name prefixed by "TCS_". In situations where this resulted in a field name over 8 characters, a HIERARCH card was added to permit the longer name.

On the 2.1-meter telescope this data is exposed through a network socket on a machine named "rose." We accessed this data using the Windows telnet program, and manually copy/pasted it into Notepad (along with the object name) for each observation.

Each time the telescope was slewed to a new target, the telescope operator would call out the name of the target. The camera operator and TCS logger would each record this information, and the camera operator would alert the TCS logger as soon as the exposure was started. No data to correlate individual FITS cubes to TCS logs was recorded other than timestamps.

As the Andor SOLIS software used to record FITS cubes does not have support for adding arbitrary FITS header fields, the TCS logs had to be added to FITS headers after the fact. The author wrote a Python script to match FITS cubes to TCS log instances, and merged the data. The STSI PyFITS library was used to modify the FITS files.

First, the data was separated into groups by night and processed individually. The script then iterated through each FITS cube, generating a list of all TCS logs from the same target.

This was determined by searching for the target name (manually entered by the TCS logger during the run) in the filename of the FITS cube. In most cases this was a 1:1 correlation, and TCS data could be written to the FITS cube.

In cases where a target was observed more than once on a given night, the TCS log instance with the closest time stamp was used. Unfortunately, as the FITS and TCS time stamps were generated by two different computers (Kitt Peak's rose and the laptop running Andor SOLIS), there was significant deviation even for cube/log pairs that were known to be correct. A cube/log pair with a time difference of less than one hour was considered a “good match”, and the TCS log instance was flagged to prevent multiple cubes from being matched to it. All matches with a time difference greater than one hour were skipped at this stage and handled later.

After all “good matches” were found, the program iterated through the remaining cubes and found the closest match (among both matched and unmatched TCS instances). The script recorded these in the FITS header with a note explaining that the TCS log merged was from a different cube, and named that cube.

After the first run through, there were 126 unmatched FITS cubes. A variety of factors caused this, the most common being two numbers switched in the target name (either in the FITS cube file name or TCS log), prefixing a double star with WD instead of WDS, or a number missing from the target name. Most of these were manually corrected by searching for other cubes with the same RA/Dec, and in the end only 22 cubes were left unmatched. All changes made to TCS logs or filenames were logged in the “*Merge_Logs*” folder.

Assigning Single Deconvolution Stars to Doubles

The suitability of a reference star to a double star for deconvolution depends on many factors, related to both the object itself and the observations. Important properties of the two observations include their relative difference in air mass, parallactic angle, atmospheric dispersion, and time of measurement. Important properties related to the objects are spectral class and relative position. As the observations were roughly 90% double stars and 10% single stars, an algorithm to select single stars based on all these criteria would have been impractical.

Instead, the best single star for each double star was selected solely based on time between observations and difference in declination. It was assumed that if two objects are physically close and observed at similar times, their relative air mass, zenith distance, and parallactic angle would all be within reasonable limits. The parameter for selection for a given double star was the closest single star (compared in Dec only), observed within three hours of the double.

Conclusions and Recommendations

While some human errors were expected, almost 10% of the data we collected had a naming error. This drastically complicated the merging process, and required significant human intervention to fix. Uncorrected, these errors could have resulted in a significant amount of unusable data.

There are a number of ways this could be prevented in the future. One easy way is decreasing the number of steps it takes to save FITS cubes. On this run, we saved data into folders by night, then by sections of the sky (two hours in RA and 20 degrees in Dec). In the future, we could save all cubes to one folder, and automate the process of separating by night or sky-region.

Acknowledgments

A special thanks to Russ Genet for inviting me to observe at Kitt Peak, to everyone present on the run for a wonderful experience, and to Kitt Peak National Observatory for providing time on their telescope. This research has made use of the Washington Double Star Catalog maintained at the U.S. Naval Observatory. PyFITS is a product of the Space Telescope Science Institute, which is operated by AURA for NASA.

User's Guide to PS3 Speckle Interferometry Reduction Program

David Rowe[1] and Russell Genet[2,3,4]

1. PlaneWave Instruments, Rancho Dominguez, California
2. California Polytechnic State University, San Luis Obispo
3. Concordia University, Irvine, California
4. Cuesta College, San Luis Obispo, California

Abstract The PS3 Speckle Interferometry Reduction Program, which runs on Windows PCs, reduces FITS cubes of close double star images taken at high speed. Single comparison star image cubes can optionally be used for deconvolution to help remove unwanted atmospheric and optical distortions. Data cubes can be automatically preprocessed to speed up the reduction process. Preprocessing can reduce the data volume by a factor of 1000, facilitating Internet transfers. Gaussian high- and low-pass filters can be employed to improve the signal-to-noise ratios. The Program can be run in either a manual or semi-automatic mode. Results are placed on a spreadsheet, and autocorrelograms are placed in a file.

Introduction

PlateSolve 3 (PS3) is a general purpose program developed for stellar astrometry by one of us (Rowe). Given an image with a sufficient number of stars—but without any information as to plate scale, camera angle, RA, or Dec—PS3, using a patented process, quickly determines the plate scale, camera angle, and the RA and Dec of the image center. The main screen is shown in Figure 1.

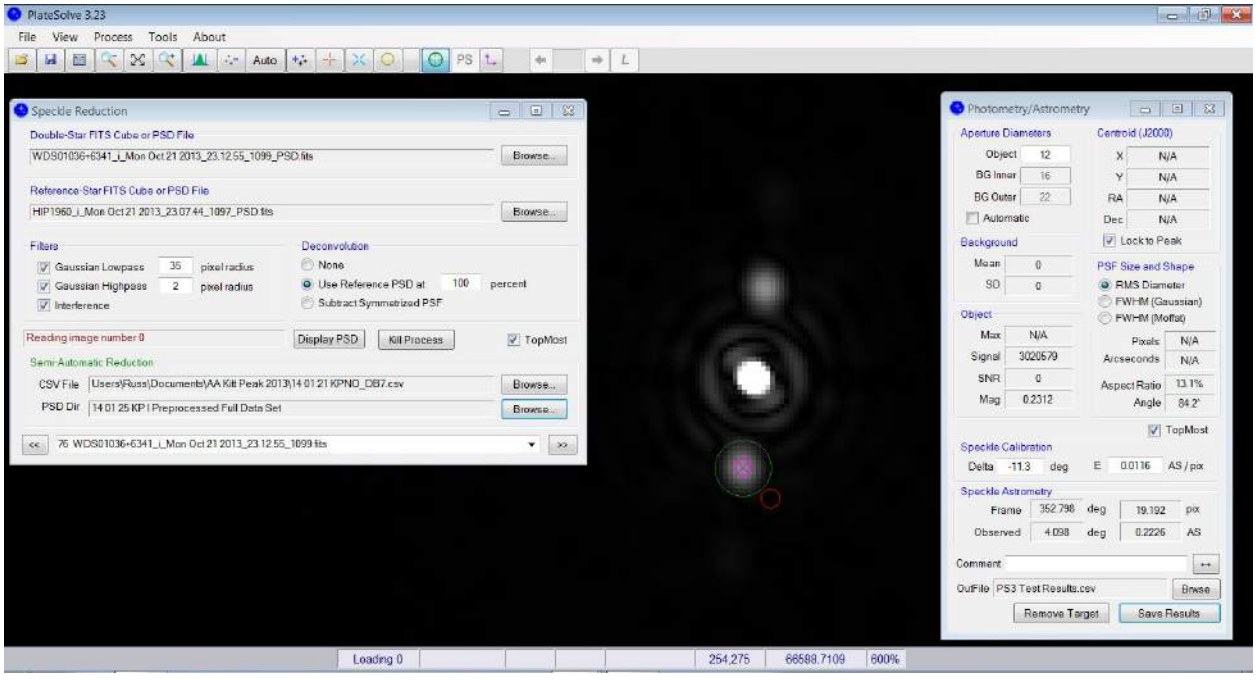

Figure 1. The two major GUIs for PS3 speckle reduction are *Speckle Reduction* (left) and *Photometry/Astrometry* (right). In between the two is a typical double star image.

Besides this unique plate solving capability, PS3 also has many other capabilities such as viewing FITS headers, subtracting darks and flat fielding, aligning and combining images, lucky imaging analysis, and the double star speckle interferometry reduction process described in this paper.

This description of speckle reduction covers: *Preprocessing* of the data, which greatly speeds up the reduction process; *Speckle Reduction*, which sets the reduction parameters and modes and selects the input; *CSV Input File*, which, with PS3 running in a semi-automatic reduction mode, reads a CSV file with the list of object values used in subsequent double star reduction, facilitating much faster reduction of large data sets; *Photometry/Astrometry Tool*, which readies a reduction for final output (including insertion of comments); and the output file, *OutFile*, which records the results (including an image of the final reduction).

Preprocess FITS Cubes Folder

Preprocessing allows an entire folder of raw FITS data cubes to be preprocessed automatically. For each image in the original FITS cube, the modulus squared of the Fourier transform is computed. This is called the power spectrum. The average of all the power spectra is computed and then saved as the pre-processed FITS image. These preprocessed data cubes are megabytes instead of gigabytes in size, greatly reducing the overall file size. For example, the raw FITS data cubes data file from a run on a 2.1-meter telescope at Kitt Peak National Observatory in October 2013 was 1.4 terabytes. After preprocessing, it was a manageable 1.2 gigabytes, allowing downloading via the Internet. Not only does preprocessing produce manageable file sizes, but after preprocessing, the computer time required for each reduction is just seconds instead of minutes.

To preprocess a file of raw FITS data cubes, go to *Tools* and select *Process FITS Cube(s)*. Click *Select FITS Cubes*, navigate to the appropriate folder, and, using the multifile selection feature of Windows, select the file to be preprocessed. Under Target Folder, check Save Images in New Folder and click Browse to select the destination folder. Finally, click Process and the FITS cubes will be preprocessed. This can take many hours, but it only needs to be done once and it runs unattended. *Cancel* can be used at any time to stop the preprocessing. It is important to allow the suffix _PSD to be added to the file name to differentiate the preprocessed FITS cubes from the "raw" FITS cubes. This suffix is required when using the semi-automated features of PS3.

On a Windows-7 machine with a 2 GHz processor, it takes approximately 2 minutes to preprocess a FITS cube with 1000 512x512 images. For a long, multi-night run, there can be upwards of 1000 data cubes, so preprocessing can take more than 24 hours.

Speckle Reduction (Used to set the reduction parameters and modes)

Once the FITS cubes have been preprocessed (although the preprocessing step can be skipped, we do not recommend it), go to *Tools* and select *Speckle Reduction*. Figure 2 shows the overall GUI.

For a run on a specific telescope, the *Filters* can often be set once (perhaps after some experimentation) and then left alone for the reduction of an entire run. Proper setting of the two Gaussian filters should optimize the detection and measurement of the double. The *Gaussian Lowpass, Gaussian Highpass, and Interference* filters are each described below.

Gaussian Lowpass Filter

A telescope's optical system is a spatial low pass filter where the low pass cutoff frequency (in pixels) is a function of the wavelength, the f/ratio of the telescope, and the size of the pixels. Recall that the Airy disk radius, R, is given by

$$R = 1.22 * \text{Lambda} * F/D$$

where Lambda is the wavelength and F/D is the focal ratio of optical system. In pixels, this is given by

$$R(\text{pixels}) = 1.22 * \text{Lambda} * (F/D)/ h$$

where h is the pixel dimension.

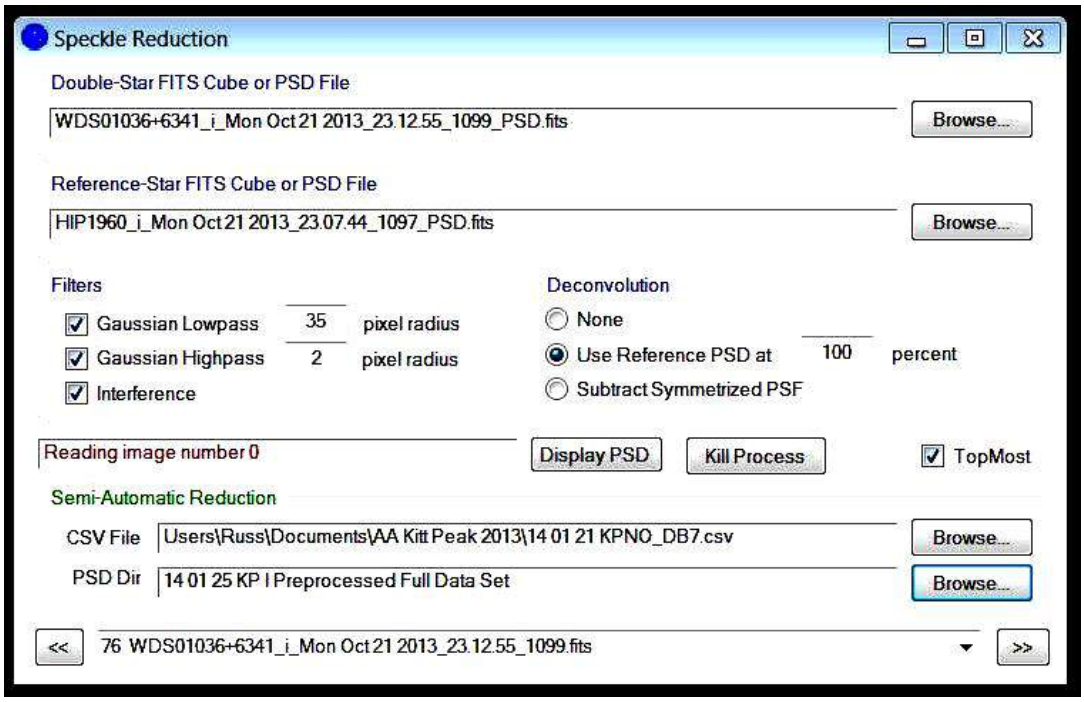

Figure 2. The *Speckle Reduction* GUI.

As an example, take the pixel dimension to be 10 microns, the wavelength to be 0.8 microns, and the focal ratio to be 50. The Airy disk radius will be approximately 5 pixels. The Fourier transform of the Airy disk will have most of its energy within a spatial frequency, fc, given by:

fc = N/(2*R)

where N is the size of the image and R is the radius of the Airy disk, all values being in pixels.

In the spatial frequency domain, there is very little signal higher than this frequency. However, beyond this frequency there is considerable noise from the electronics, from the sky background, and from photon shot noise from the object. Therefore, to improve the signal-to-noise ratio and to reduce unwanted interference from the electronics, it is wise to apply a low pass filter with a cutoff proportional to this spatial frequency. Thus, the cutoff frequency, fc (pixel radius), should be approximately:

fc = (h * N) / (2.44 * Lambda * F/D)

Taking an example from the second speckle interferometry run at Pinto Valley Observatory (PVO II), Lambda = 0.8 microns, h = 10 microns, F/D = 50, N = 256, yields fc = 26 pixels. In practice, it is a good idea to make the low pass filter somewhat wider than this so that most of the signal information is allowed through the filter.

This only provides a good starting point. In fact, the auto-correlation has noise and signal statistics that are more complicated than the above simplified argument would suggest. For PVO II, experimentation suggested that an fc of about 50 pixel radius worked best, although the solutions were not overly sensitive to this setting. For the Kitt Peak run mentioned above, experimentation suggested a setting of about 35 pixels worked best.

Clicking *Display PSD* will toggle from the normal autocorrelogram solution image to the *PSD* (Power Spectral Density) fringe pattern display. If, as shown in Figure 3, the *Gaussian Lowpass* is set too wide, noise beyond the telescope cutoff will be seen, suggesting that the setting should be reduced to a smaller *pixel radius.* On the other hand, if there is no signal at all beyond the telescope cutoff, then the filter is set too narrow and should be widened.

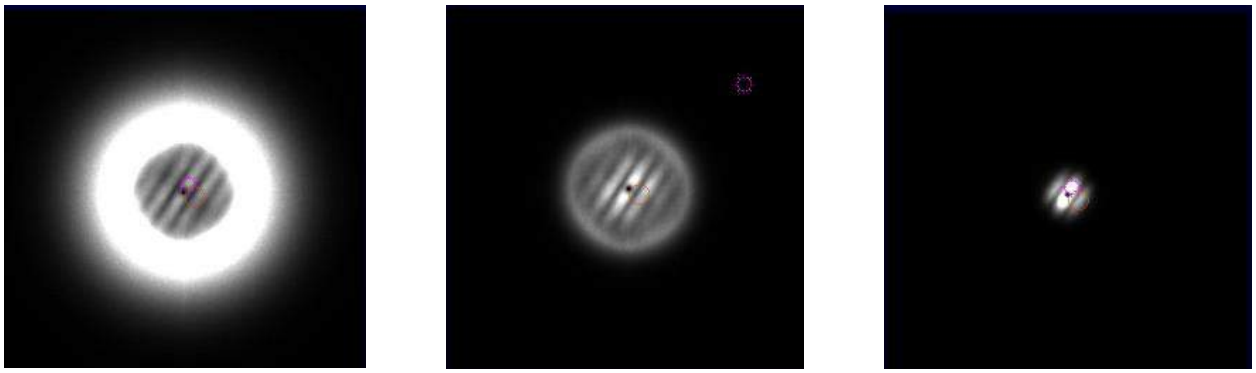

Figure 3. On the left, the *Gaussian Lowpass* filter was set too wide (70 pixels), allowing high frequency noise to be included. On the right, it was set too narrow, cutting off useful information. In the middle it was set just slightly larger than the spatial cutoff frequency imposed by the telescope's aperture.

Gaussian Highpass Filter

The Power spectral density (PSD) is the Fourier transform of the image. The purpose of the Gaussian Highpass Filter is to remove, as much as possible with a simple filter, the broad tail of the point spread function (PSF) that is due to seeing and optics. This filter removes the lowest-frequency information in the image and is typically set between a 2 to 5 pixel radius. It is set empirically to give the best auto-correlation.

A useful way to set the filter is to look at the PSD, which can be done by toggling Display PSD to bring up the fringe pattern. As shown in Figure 4, set the pixel radius to remove the bright spot in the zero-order PSD fringe pattern without hurting the rest of the fringe pattern. The Gaussian high pass is usually not needed when single star reference deconvolution is used.

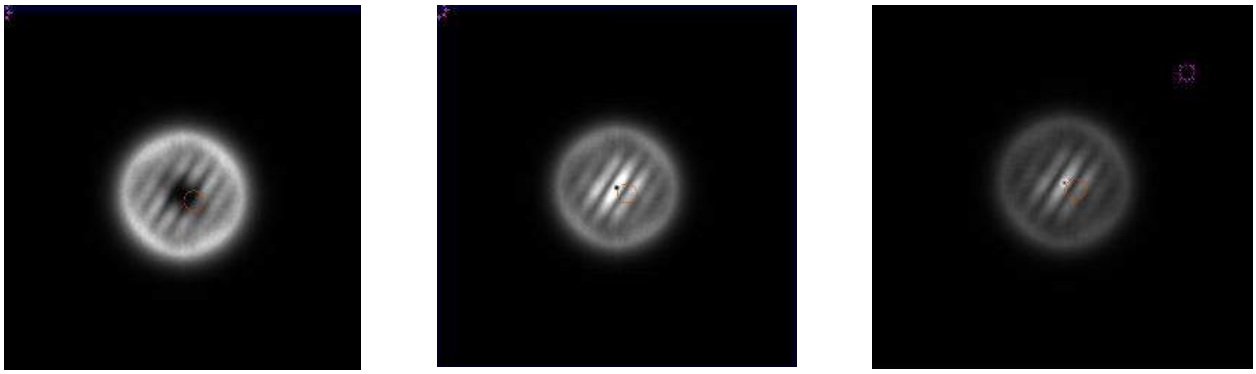

Figure 4. On the left, the *Gaussian Highpass* filter was set too wide, not only cutting out the bright central peak, but also much of the fringe pattern. On the right the filter was set too narrow, allowing the bright central peak to shine through. The center is set correctly.

Interference Filter

In certain situations we have encountered significant interference, possibly due to the interaction of the camera with the main 120V AC power source at remote locations. Much of the unwanted interference was found to lie along the lines fx = 0 and fy = 0 in the spatial frequency domain. If the Interference filter is checked, the values along the fx = 0 and fy = 0 axes in Fourier space are replaced by the average values of their neighboring pixels. This filter is quite specific to the type of interference produced by the camera.

Deconvolution

There are three *Deconvolution* options: None, Use Reference PSD, and Subtract Symmetrized PSF. Each is discussed below.

None Although not recommended, speckle interferometry reduction can be accomplished without the use of single reference stars for deconvolution. For this option, simply select *None* under *Deconvolution.* It can be quite helpful to apply a Gaussian high pass filter when not using deconvolution.

Use Reference PSD The use of deconvolution reference stars is highly recommended. Not only will it sharpen the double star image, it will also remove much of the telescope's optical aberrations, including the effect of the central obstruction. In addition, if the reference star was taken close in time and located near the double star, deconvolution will remove much of the atmospheric dispersion and broad tail due to the effects of seeing. Deconvolution will help in almost all instances. If the reference star is a poor match for the double star, there are cases where a false detection can occur for doubles with dim, close companions.

Deconvolution is based on the following mathematical properties: (1) the recorded image of a very short exposure is the convolution of the "perfect" image of the object with the PSF of the telescope plus the instantaneous atmosphere, and (2) the convolution operation can be implemented by taking the inverse Fourier transform of the product of the Fourier transforms of the "perfect" image and the point spread function (PSF) of the telescope plus instantaneous atmosphere. Symbolically:

$$F(I) = F(O) * F(T)$$

where F( ) denotes the Fourier transform, I is the actual image recorded, O is the "perfect" image of the object, and T is the PSF of the telescope plus instantaneous atmosphere. Speckle interferometry is based on averaging a large number of very short exposures which "freeze" the atmospheric seeing, allowing us to take the average of the above equation in transform space. If we let $\langle I \rangle$, $\langle O \rangle$, and $\langle T \rangle$ denote the averages of the Fourier transforms of I, O, and T, as defined above, then we can calculate an approximation for the Fourier transform of the object's power spectral density (PSD) as:

$$\langle O \rangle = \langle I \rangle / \langle T \rangle.$$

Taking the inverse Fourier transform of $\langle O \rangle$ yields an approximation to the object's autocorrelation, with the telescope and atmosphere removed. This process is called deconvolution.

To perform this operation, we need an estimate of $\langle T \rangle$, the autocorrelation of the telescope plus atmosphere. A convenient way to find this estimate is to obtain a speckle cube of a nearby single star. The most effective deconvolution will be based on single star speckle observations that are very near the object from the point of view of the atmospheric conditions and telescope pointing. We feel that it is good practice to observe a single reference star that is as near as possible to the double star in both time and space. The reference star must, of course, be bright enough to show excellent SNR after speckle preprocessing.

To use a reference star for deconvolution, check *Use Reference PSD* and set it to 100 *percent.* The percentage option was included so one can experiment with the strength of the deconvolution when using non-ideal reference PSDs.

Subtract Symmetrized PSF This option was developed for close, dim double stars without good reference stars. A symmetrized PSF is made from the image and is subtracted from it, yielding only the non-symmetrical part. This can highlight an otherwise difficult-to-detect companion. This technique should be used with caution, since non-rotationally symmetric telescope aberrations can mimic a close, dim double.

Display PSD

Toggling *Display PSD* will move back and forth between the autocorrelogram solution and the power spectral density fringe pattern.

Kill Process

Kill Process simply stops the FITS cube speckle preprocessing.

Manual Speckle Reduction (Selecting data cubes)

There are two ways to manually select data for reduction. Each is described below:

(1) If, under *Deconvolution, None* has been selected, a *Double-Star FITS Cube or PSD File* can be navigated to by clicking the *Browse* button at the top of the *Speckle Reduction* box. If a file, you will be asked to click on the desired FITS cube. The file name will appear in the window, and if it is a PSD (preprocessed), a solution will appear in seconds. Otherwise, it may take a couple of minutes for the raw data cube to be processed.

(2) In addition to (1) above, if, under *Deconvolution, Use Reference PSD* has been selected, a *Double-Star FITS Cube or PSD File* can be navigated to by clicking the corresponding *Browse* button. If a file, you will be asked to click on the desired FITS cube. The file name will appear in the window. The solution image (autocorrelogram) will change as the single reference star is included in the solution. The improvement in the solution can be dramatic.

Semiautomatic Speckle Reduction (Selecting an entire file)

Although the speckle interferometry tool in PlateSolve 3 can be operated entirely by way of user GUI inputs, there is a *Semi-Automatic Reduction* option for using a comma-delimited input file (*CSV File*) that speeds up the reduction process. The *CVS File* allows PS3 to automatically load each double star file as well as the corresponding single star file. With hundreds of targets and corresponding reference stars to process, looking up individual files can be tedious. An added benefit of this mode of reduction is that, based on information on the "expected" position angle and separation of the two stars (from last observed catalog values or calculated values) provided in the *CVS File*, PSD places a red circle at the "expected" solution location. This allows the 180° ambiguity inherent in autocorrelograms to be avoided. It also gives immediate visual feedback on how close the automated PS3 solution is to the "predicted" position. If the automated PS3 solution is not the best solution, one can intervene and pick a more appropriate solution.

Image Navigation and Brightness

The main image displayed by PS3 can be manipulated for better viewing and interpretation of the target.

Image Size

These three buttons are used to control the displayed image size. From left to right, they make the image smaller (zoom out), fit the image to the screen, and make the image larger (zoom in). One can also zoom in and zoom out by right clicking on the main screen and selecting from the various Zoom options.

Image Position

Right-click on the image and select Center to center it. The image can be dragged by left-clicking and holding down the mouse button.

Image Brightness and Contrast

These three buttons are used to control the brightness of the image. From left to right, they reduce the image brightness, autoscale the image brightness, and increase the image brightness.

Photometry/Astrometry Tool

With an autocorellogram now displayed (with either manual or semiautomatic inputs), click on the green "target" icon on the toolbar to bring up the *Photometry Tool* shown in Figure 5. Under *Centroid (J2000)*, click on *Lock to Peak* to activate centroid detection.

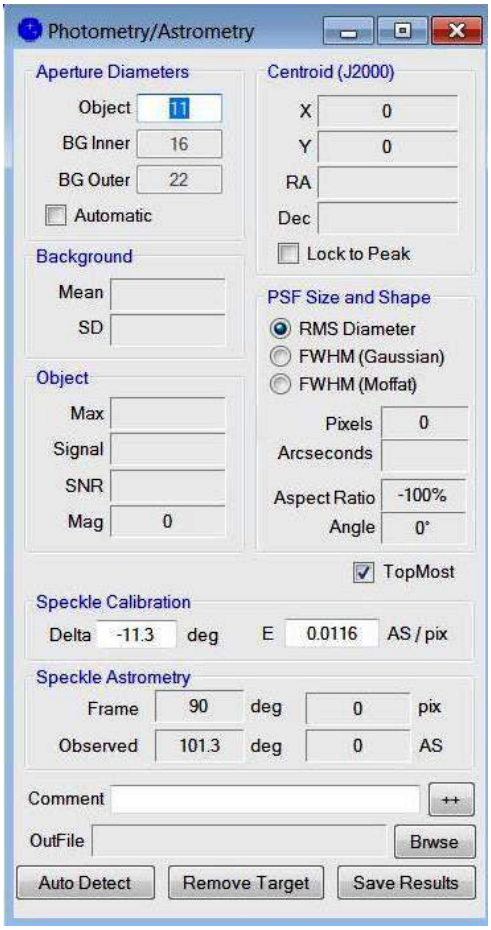

Figure 5. The Photometry/Astrometry GUI.

Under *Aperture Diameters*, set *Object* to a pixel radius that will fully encompass the image of the secondary star but not the primary star or any noise. For widely spaced doubles, setting the *Object* aperture diameter (in pixels) is straightforward. For very close doubles, however, setting the *Object* pixel diameter can be more difficult. It might be noted that in many cases the dark circle around the companion is the first null in the Airy function. Often the *Object* pixel diameter can be set so that the "green circle" falls in this first null.

Under *Speckle Calibration*, enter, if known, the values of the camera angle, *Delta*, (in degrees), and the plate scale, *E* (in arc seconds per pixel). These values, *Delta* and *E*, are used to transform the *Frame* separation and position angle, *ThetaF* and *RhoF* respectively, to *Observed* separation and position angle, *ThetaO* and *RhoO* respectively. If *Delta* and *E* are not known, as may be the case during initial calibration, the values of *ThetaO* and *RhoO* will not have any meaning.

To arrive at a final *Observed* position angle, *ThetaO*, the camera angle, *Delta*, determined by calibration, is subtracted by PS3 from the frame camera angle, *ThetaF*. To arrive at a final *Observed* separation, *RhoO*, the frame separation in pixels, *RhoF*, is multiplied by PS3 by the plate scale constant, *E* (in arc seconds/pixel), that has been previously determined through a calibration process.

Manual Solution

With the *Object* diameter set appropriately, center the green aperture over the appropriate one of the two secondary star images. It is good practice to check the "solidness" of the solution results by moving the cursor around a small amount near the center of the secondary. Do the *Observed* values of position angle and separation, *ThetaO* and *RhoO,* change as the cursor is moved? If so, try increasing or decreasing the *Object* pixel diameter until a solid *Lock to Peak* is achieved in spite of small cursor position variations. If this is not possible, then the quality of the solution may be in question and should be noted in the *Comment* or written down if the *OutFile* is not being used.

With an appropriate *Aperture Diameter* set for the *Object,* and with the green circle centered on the secondary and a satisfactory *Lock to Peak* achieved, right click the mouse to display the drop-down menu shown in Figure 6. Select *Set Target Location* and a red circle with eight short radials will appear centered over the secondary. This completes the solution.

At this point the answers can simply be written down. However, it is usually more convenient to record them in the *OutFile,* along with an automatically-recorded image of the final solution. If recording is desired, *Browse* to and select the desired *OutFile* using the Multifile selection feature of Windows.

An optional *Comment* can be typed in. The comment can be of any size and can include commas, even though the *Comment* will be placed in a comma delimited file. For long comments, clicking ++ will bring up a larger *Add Comment* text entry box. A corner of this box can be dragged to increase its size. Multi-line comments are supported and will appear in the CSV file with the pipe symbol "|" as the delimiter between lines.

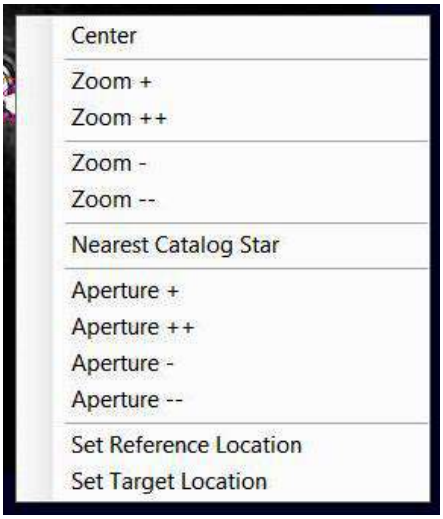

Figure 6. The drop-down menu that appears for the final solution.

Automatic Solution

In its semi-automatic mode, PS3 provides an automatic solution that, under normal circumstances, will be correct. However, it may not be the best solution if the signal-to-noise ratio (S/N) is poor, the secondary is not the brightest object in the autocorellogram (other than the central peak), or the separation is very small and Airy rings are prominent.

The first step in obtaining an automatic solution is detecting all the brightest peaks in the image. Typically there are several thousand. The centroid location of each peak is found by activating *Lock to Peak.* Typically, the centroid location (to a fraction of a pixel) will be different than the brightest pixel location. The centroid location is noted and a new *Lock to Peak* initiated. This is repeated twice more. If after four tries the *Lock to Peak* still results in a shifting centroid location (greater than two pixels), the solution is deemed unsatisfactory. Also, if the elongation of the secondary image is too great, the solution is considered unsatisfactory.

At this point, from all possible remaining solutions, PS3 simply selects the brightest one. As there typically will be two equally bright secondary solutions 180° apart, PSE simply selects the one closest to the predicted position (the red circle) as the final solution. PS3's automatic solution can be accepted simply by clicking *Save Results.* One can then increment to the next target by simply clicking >> in the bottom right corner of the *Speckle Reduction* box.

It is not unusual to have many correct automatic solutions in a row, especially if good single reference deconvolution stars have been carefully chosen and the observations are not pushed too close (or beyond) their limits. With a plethora of correct solutions, one simply presses >>, the automatic solution appears in a couple of seconds, one checks to see that the solution is correct, and, if so, presses *Save Results.* This can be accomplished in about 5 seconds, allowing a dozen targets to be processed per minute, as long as correct solutions continue unabated.

Reduction Autocorellogram

The reduction autocorellogram is the "picture worth a thousand words." As shown in Figure 7, the primary star is always at the exact center. The secondary star is displayed as two fainter images exactly 180° apart. If semi-automatic reduction is employed, as it was for the double shown in the figure below, then a "predicted" position will be indicated with a **red** circle (in this case offset from the lower secondary at the 5 o'clock position). The large **green** circle around the lower secondary is the *Object Aperture*. It should encompass all or most of the secondary's image. Once satisfied with the solution, *Set Target Location* is clicked if manual, and the bright **pink** circle with the X and eight short radials will appear. If this is an automatic solution, the bright **pink** circle will automatically appear.

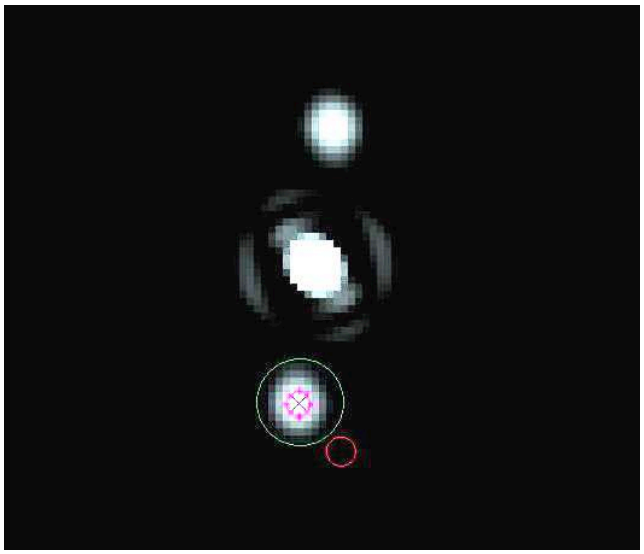

Figure 7. Autocorellogram of a typical "easy" solution.

If, in a semi-automatic mode, the automated solution (**pink** circle) is not in the center of the secondary star, then one can revert to a manual solution mode by clicking *Remove Target* in the bottom-center of the *Photometry/Astrometry* box. Conversely, if one is in a manual solution mode and desires an automatic solution, simply click *Auto Detect* in the lower left-hand corner of the *Photometry/Astrometry* box.

OutFile Columns and Abbreviations

As shown in Table 1, the output file is coma delimited; one row per output. The top row provides column content abbreviations. These abbreviations are provided below, followed by a short description.

Num	Target	ThetaO	ThetaC	ThetaO-C	RhoO	RhoC	RhoO-C	ThetaF	RhoF	ApD	RelInt	DMag	Comm
24	00283+6344	111.831	91	20.831	0.3857	0.4	-0.0143	100.531	33.251	12	0.2216		
76	01036+6341	4.098	19	-14.902	0.2226	0.3	-0.0774	352.798	19.192	12	0.2312		
1	00022+2705	228.354	273	-44.646	0.166	0.8	-0.634	217.054	14.312	12	0.0571		Close one!
2	00024+1047	69.213	73	-3.787	0.2468	0.2	0.0468	57.913	21.273	12	0.0535		Prediction close.
3	00029+4715	294.729	295	-0.271	1.5947	1.6	-0.0053	283.429	137.47	12	0.155		Wide and easy. Prediction right on.
4	00046+4206	105.922	95	10.922	0.1304	0.1	0.0304	94.622	11.244	5	0.0486		Very close but good solution.
5	00055+3406	307.239	304	3.239	0.15	0.2	-0.05	295.939	12.933	5	0.0675		Also close. Prediction off a bit.
6	00073+0742	321.309	323	-1.691	0.3515	0.4	-0.0485	310.009	30.3	11	0.2919		Easy. 2nd & 3rd order images.
7	00085+3456	52.817	79	-26.183	0.1383	0.1	0.0383	41.517	11.922	5	0.1508		Close. Solution not stable.
13	00118+2825	67.367	69	-1.633	0.4474	0.5	-0.0526	56.067	38.571	11	0.1454		Easy. Prediction close.
14	00121+5337	317.605	313	4.605	0.3344	0.3	0.0344	306.305	28.827	11	0.1709		Very easy.
18	00174+0853	305.499	307	-1.501	0.1556	0.2	-0.0444	294.199	13.417	5	0.0411		Difficult. Not quite stable.
19	00174+0853	303.657	307	-3.343	0.1553	0.2	-0.0447	292.357	13.386	11	0.1254		Easy and stable.
20	00205+4531	96.724	102	-5.276	0.656	0.7	-0.044	85.424	56.553	11	0.0896		Verey easy. Clean!
21	00209+1059	118.746	117	1.746	0.7557	0.7	0.0557	107.446	65.145	11	0.1286		Very easy. Clean.
23	00251+4803	273.507	242	31.507	0.3186	0.3	0.0186	262.207	27.464	11	0.0335		Prediction off, but not too far.

Table 1. The first 14 columns of output. The .cvs file was saved as .xlsx and lightly formatted. *Differential Magnitude, DMag,* is being worked on.

Num — This is the object sequence number from the input CSV file directory, when used. If an input CSV file is not used, this entry will be blank.

Target — This is the target (double star) identification. Usually it is the Washington Double Star (WDS) catalog name, such as 09345+0723, but it can be some other identifier, such as GJ3579.

ThetaC — This is the last catalog or predicted (input) double star position angle (PA, θ, and Theta are all abbreviations for position angles). This calculated (prediction) may be the last reported position angle, but could be an interpolated value from an orbit ephemeris, or even a maximum likelihood prediction. *ThetaC* is used by PS3 to place a small red circle on the autocorrelogram, where the secondary is expected.

ThetaO — The observed position angle. This only has meaning when the user provides the camera angle, *Delta,* from some calibration external to the reduction. If not available, the user can enter any number and ignore the results, or enter a camera angle of "0" and the output would be the "uncorrected" camera angle.

ThetaO-C — PS3 simply calculates this as *ThetaO* minus *ThetaC.* This is the difference between the observed position and the calculated (i.e. predicted or expected) position angle; the classic O-C.

RhoC — This is the last catalog or predicted (input) double star separation (Sep, ρ, and Rho are all abbreviations for separation). This calculated (predicted) separation may be the last reported separation, but could be an interpolated value from an orbit ephemeris, or even a maximum likelihood prediction. *RhoC* is also used by PS3 to place the small red circle on the autocorrelogram where the secondary is expected.

RhoO — The observed separation angle. This only has meaning when the user provides the plate scale (arc seconds per pixel), *E,* from some calibration external to the reduction. If not available, the user can enter any number and ignore the results, or enter a plate scale of "1" and the output will be the "uncorrected" frame pixel separation.

RhoO-C — PS3 simply calculates this as *RhoO* minus *RhoC.* This is the difference between the observed position and the calculated (i.e. predicted or expected) separation; the classic O-C.

ThetaF — Position Angle in the Frame. *ThetaF* is calculated by PS3, using simple trigonometry, from the centroid pixel locations.

RhoF — Separation in the Frame. *RhoF* is calculated, using simple trigonometry, by PS3 from the centroid pixel locations.

ApD — Aperture Diameter (radius in pixels).

RelInt — This is the total (integrated) intensity of the companion divided by the integrated intensity of the primary. This will be used to form an estimate of the differential magnitude of the double star.

DMag — This will be calculated in a future version of the program. At this time the entry is blank.

Comm — User comment added during reduction.
DSFN — Double star (FITS cube) file name.
RSFN — Reference star (FITS) cube file name.
AR — Elongation Aspect Ratio (degrees).
AA — Elongation Angle (degrees). The angle that corresponds to the elongation aspect ratio.
Delta — Camera Angle (degrees). Camera orientation angle with respect to the sky.
E — Plate scale (arc seconds/pixel).
GLP — Lowpass Radius (pixels). Settings for Gaussian lowpass filter.
GLPen — Lowpass used (True/False).
GHP — Highpass Radius (pixels). Setting for Gaussian highpass filter.
GHPen — Highpass used (True/False).
IFen — Interference Filter used (True/False).
DCon Deconvolution — Type: *None*=0, *Use Reference PSD*=1, *Subtract Symmetrized PSF=2*.
DConP — Deconvolution percent, usually set at 100%.
LTPen — Lock to Peak (True/False).
JPEGFN — Filename of the solution image.
DaT — Date and time output created.

Optional Input File (CSV File)

The seven items, below, must appear in the input file, *CSV File*, in the order shown. They must be the first seven columns, although there may be any number of other columns to the right. All columns past seven are simply ignored by PS3. Please note that changing *Delta* and *E* in the *Photometry/Astrometry* box during semi-automatic reduction will not actually change their values as they are read from the input *CVS File*The *Delta* and *E* values need to be changed in the file itself.

TID — Target ID. If the Target ID is a "D", then PS3 will process this file, otherwise it will be ignored. This allows a master database to contain, for instance, single stars used for deconvolution, slit mask or drift calibrations, etc.
DSFN — Double star (FITS cube) file name.
RSFN — Reference star (FITS) cube file name.
ThetaC — Calculated (input) estimated, predicted, or last catalog reported double star position angle.
RhoC — Calculated (input) estimated, predicted, or last catalog reported double star separation.
Delta — Camera Angle (degrees). Camera orientation angle with respect to the sky.
E — Plate scale (arc seconds / pixel).

Acknowledgments

Genet thanks California Polytechnic State University Office of Research and Economic Development for support through their Extramural Funding Initiative and the Keck Foundation for support through the Concordia University Undergraduate Education Program. We thank Vera Wallen for editorial suggestions.

The Double Star Speckle Interferometry Observation and Reduction Process

Russell M. Genet[1,2,3]

1. California Polytechnic State University, San Luis Obispo
2. Concordia University, Irvine, California
3. Cuesta College, San Luis Obispo, California

Abstract The process of planning for, obtaining, and reducing speckle interferometry observations can be broken down into three major phases: pre-run, during-the-run, and post-run. Establishing formats for a target list, run log, and reduction program facilitates a smooth flow of data that minimizes human work and errors.

Introduction

Lists of double star observational candidates are maintained by various astronomers in formats they have devised that work for them. They may maintain a single master list, or perhaps more than one list—a different list for each observational program. Astronomers often make their observations on the same telescope year after year. For any specific run, their master list or lists may be pared down to match the run constraints in terms of RA, Dec, etc., thus providing them with a run list. If there are multiple master lists, they may be combined prior to trimming, to yield a single run list. Some but not all of the candidates on the pared-down run list will then be observed during the run. After the run, the data is reduced, often with a custom program written by the astronomer.

The situation being considered here is a somewhat different (and specialized) situation than the normal situation for single astronomers. The observational process discussed below would typically involve multiple astronomers, multiple at-the-telescope observers, and observations on different telescopes at different times. The observational results are widely shared and relatively easy-to-use and well-documented "public" reduction and analysis techniques are vital. Due to the variety of observational programs and participants (including beginning students), a somewhat standardized, well documented observational process that specifies file formats and provides well-documented software should aid efficiency and accessibility.

What is presented below is a work in progress. A seven-night run at Kitt Peak National Observatory required that a standardized format be generated on rather short notice. That said, it should form a starting point for more refined processes for similar runs and perhaps help with the formulation of a fully automated speckle interferometry observation and reduction process.

A computerized Scheduler is a requirement for automated observations. The input to a Scheduler is the Run List of potential targets. The Scheduler decides, based on a set of decision rules, what specific target is to be observed next by an automated telescope. This set of decision rules can be somewhat complex as it has to consider closeness to the meridian to minimize air mass, spatial nearness to other targets to minimize slew times, azimuthal location if observed at a domed observatory to minimize long dome rotations, scientific priority of the target, past observations of the target, any special observational needs such as repeated observations for calibration, changes in the overall observing program in case of major weather or equipment problems, etc.

In the process described below, the Run Master is the human Scheduler, and the decision on what to observe next during a run is made by the Run Master based on the sorted contents of the Target List. The advantage of a *Run List* is that, if properly generated, it can reduce the scope of the decisions the Run

Master needs to make, although some human assessment would still be required as decisions would have to be made on what should and should not be observed as one fell behind in the "meridian window." The Run Master would also need to note on the *Run List* what had been observed so it would not be needlessly re-observed on following nights unless that was what was desired.

The binary star speckle interferometry observational process can be broken down into three major phases: Pre-Run, During-the-Run, and Post-Run. Each phase is described briefly below. Two separate documents provide suggested file formats and describe a speckle interferometry reduction program, PlateSolve3 (PS3), written by David Rowe.

Four principles have guided the development of the speckle interferometry observation and reduction process. They are: (1) minimizing human entries, (2) separate flows for target information and image data (FITS cubes), (3) minimizing data carry through in the reduction program, and (4) aiming for eventual full automation. Each principle is described briefly below:

(1) In organizing the data flow and specifying file formats, attention has been paid to minimizing human entries, especially in terms of copying information from one format to another. Such minimization reduces human-induced errors. This minimization required working backwards from the required inputs for the reduction program, PS3, to the Run Log, and finally to the Target List. This is not to suggest that humans (or computers) do not need to add data as they go through the process from beginning to end (they do), just that inputs should not have to be repeated and formats should be specified such that they can directly feed into the reduction program.
(2) While the Andor EMCCD cameras used in some of our runs automatically place considerable camera-related information into the FITS headers, we have chosen not to add any outside human- or machine-entered data into the FITS headers, relying instead on a separate flow of information via spreadsheets.
(3) The third organizing principle was minimizing data "carry through" in the reduction program. The reduction program, PS3, is intended for general use, both manual one-FITS-cube-at-a-time operation as well as semi-automatic operation on an entire file of FITS cubes. By only acting on the minimum required inputs, placing these at the beginning of each row in the input, and ignoring everything beyond these columns, the reduction program minimizes constraints on users. This does require, however, that the PS3 output needs to be merged with other data to provide the final results.
(4) Besides serving human-operated telescopes and cameras, it is the aim of this speckle interferometry observation and reduction process to achieve total automation, given the appropriate telescopes and cameras.

There are six files with specified formats. Movement from one file to another is made easier to the extent possible by insisting that the parameters in the files have the same names and definitions, are in the same column order on spreadsheets, and are grouped together in intelligent ways. The six files are: (1) Target List, (2) Run Log, (3) FITS Cubes, (4) PS3 Out File, (5) Final Results, and (6) Reference Stars.

The Run Log and Target List files are identical in format. However, there are two distinct differences between these files. One difference is that more run-specific values have been entered by the Run Master into the Run Log during the run than are contained in the Target List. For instance, the Run Master enters FITS Cube numbers (the camera sequence number) of both double star targets and single reference stars and the filter ID.

The other difference is that while the Target List contains all possible targets that could potentially be observed, one per row, the Run Log contains what was actually observed, both Targets and single reference stars, one FITS Cube per row. The double star rows are in exactly the same format as the rows in the Target List, and in fact the rows are simply copied out as they are observed. The Run Master fills in the empty cells in the row with the camera sequence numbers, etc. The single star rows, however, only contain the single star ID, camera sequence number, and the filter ID.

If a target is observed several times in a row on one night, or on several different nights, it will appear multiple times in the Run Log at different places in the log, while it will only appear once in the Target List.

The FITS Cubes file is simply the raw observational data file of FITS cubes. It can be transformed to a preprocessed file where the Fourier transforms have been taken of all the frames (typically a thousand or so) and averaged. Preprocessing reduces the file size by roughly the number of frames in a FITS cube, or roughly a thousand. Once preprocessed, this much smaller file is easy to handle and distribute. It is vital, however, to maintain the raw data, as one never knows what reduction techniques might be applied to the raw observational data in the future.

The PS3 Out File is the reduced observations (with position angle, separation, and delta magnitude), along with reduction parameter settings and any comments by the reducer. The Final Results file merges data from the Run Log and the PS3 Out File to provide final results.

Pre-Run

The objective of the pre-run phase is to develop a Target List for a specific observational run. The pre-run process is shown in Fig. 1. Candidate target lists are developed by searching catalogs such as the Washington Double Star Catalog, the Sixth Orbit Catalog, the Fourth Interferometric Catalog, etc., for suitable targets for a specific scientific research program. Past papers in a given research area often provides target suggestions.

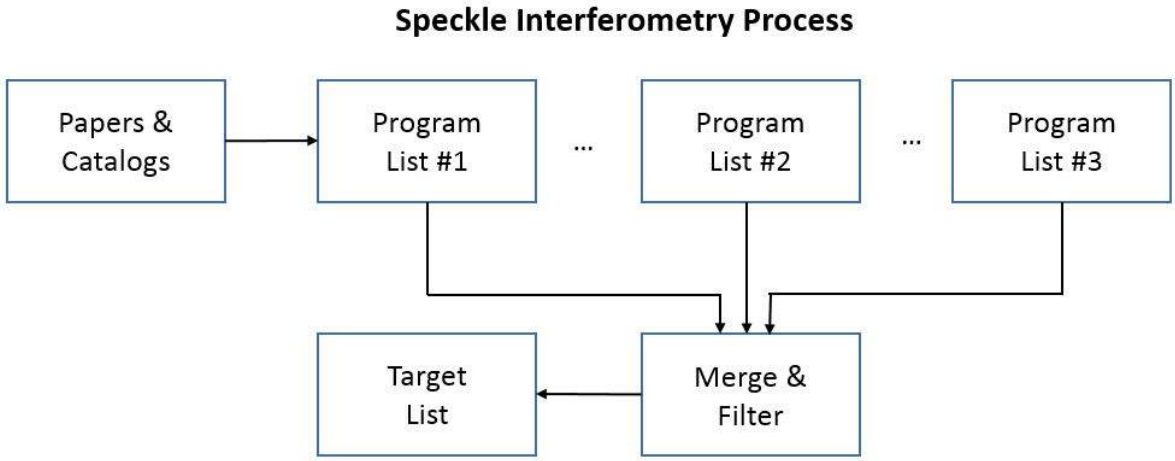

Figure 1. Pre-run major functions.

The various program lists are then merged in preparation for a run on a specific telescope. If the Program Lists are in different formats, merging may require manual intervention. Thus there is merit in employing a uniform format across various Program Lists. On the other hand, some research programs may have important parameters unique to an observational program (such as the period and other orbital parameters for known binaries). One approach to maintaining uniformity with diversity is to standardize a limited number of columns on the "left" of the spreadsheet lists, thus allowing uniform filtering and sorting, while leaving the remaining columns to be free form and thus vary from one program to the next.

Once the program lists are merged, then the observational constraints for the specific run can be applied to filter out unsuitable candidates. Such constraints typically include a range of RA and Dec coordinates, as well as upper and lower limits for separation, delta magnitude, and brightness. Typically, target lists should contain somewhat more targets than could possibly be observed even if the weather was clear for the entire run and the equipment operated perfectly.

Single reference stars need to be assigned to each target double. One way of doing this is to develop an all-sky "catalog" of single reference stars within an appropriate magnitude range. For any given double star target, a selection "aid" could then display the possible single reference stars within some specified radius, and an appropriate star selected. Alternatively, this selection process could be fully automated. For targets that have small separations, are observed at high air mass, or are otherwise "difficult" targets (large delta magnitude, faint, etc.), it will be important to select a nearby reference star and observe it

immediately before or after the double star. On the other hand, for "easy" targets, the reference star will not need to be so close in space and time. Thus one reference star might be observed just once and provide the reference for a number of sufficiently close double stars. This would increase observational efficiency by reducing the number of unnecessary reference star observations.

Target lists should include instructions on how many times a target is to be observed within a single night, and for how many nights. For instance, a few well-known binaries might be observed several times a night on each night of a run to help establish within- and between-night observational precision.

We have found it useful, prior to the run, to sort the Target List into RA bands where the width of each band is two hours in RA. Within each band, the targets are then sorted in Dec, with high Dec targets at the top and low or negative Dec targets at the bottom. These RA bands can all be on the same overall spreadsheet as individual pages, with the western-most RA band at the first page in the spreadsheet and the eastern-most as the last page in the spreadsheet. Over a time period of a couple of hours, one observes targets within one RA band, knowing that targets will rarely be more than one hour away from the meridian and thus have minimal air mass. Roughly every two hours, one moves on to the next RA band. This procedure can be modified somewhat if one wants to extend RA coverage by picking up somewhat high air-mass targets in the west in the early evening and similar targets in the east in the early morning.

Target lists can also be supplemented with information extracted from catalogs as well as graphical plots of past observations, calculated orbits, etc. For instance, for lists containing known binaries, the plots of the binaries can be placed in the same folder that also contains the Target List spreadsheet with the plots linked to the Target List spreadsheet. This way, while considering the Target List during a run, one can view a plot with a click of the mouse and the visual display can help determine whether the target should be observed or not. If the target is observed, then the plot will help determine if quick-look results match what was expected.

As mentioned in the Introduction, to minimize human entries and allow direct reduction without reformatting, it is necessary that the required reduction entries be placed in the left-most columns of every target row. Work can be minimized if this requirement is also applied (working backwards) to the individual program lists, although this is not an absolute requirement.

During-the-Run

Telescopes at major observatories are not usually equipped for speckle interferometry, so observers bring and operate their own systems. Some telescopes have staff operators, while others are operated by the using astronomers themselves. Speckle interferometry is fast-paced, and while it is possible for a single person to operate the telescope, speckle camera, and select targets and maintain an observing log, a team of three observers is ideal. Having relief replacements, especially for long, multi-night winter runs, is highly desirable. It is helpful to have enough observers on hand so data can be reduced during the observations and their quality assessed. Suggested team assignments/titles are: Run Master, Camera Operator, Telescope Operator, and Quick-Look Analyst (see Figure 2).

As targets are observed, the information from the Target List is carried through and combined with additional information to form the Run Log. The Run Log is a chronological record of what actually happened during the run. Although the Run Log carries through the information from the Target List, it differs from the Target List in four ways:

(1) Not all targets on the Target List will be observed, so those not observed are not carried through to the Run Log. Poor weather and many other factors can affect how many targets are actually observed.
(2) Some targets are observed more than once on a given night, and may be observed more than one night, weather and other circumstances permitting. Thus what starts out as a single row on the Target List, with instructions on the desired number of repeated observations/night and number of nights, can end up as many rows on the Run Log, each associated with a specific double star FITS cube.
(3) While each target on the Target List includes information (in its row) on the single reference star that should be observed, it would not make sense to make this a separate row on the Target List and, in any event, several double star targets may share the same single reference star.

On the other hand, each row in the Run Log needs to correspond to an observation, i.e. a FITS Cube. So, as reference stars are observed, they need to become rows in the Run Log, along with the corresponding camera sequence # that ties a Run Log row to a specific FITS Cube. The rows for a given target star may not be contiguous, depending on the sequence of its observations.

(4) Additional information is obtained during the run that was not available prior to the run on the Target List but needs to be incorporated in the Run Log. Specifically, the camera sequence # (FITS Cube) associated with each target observation, and, if multiple filters are being employed, the filter(s) used in the observation need to be included.

The Target List itself can be modified during the run to show which targets have been observed on which nights (and how many times they were observed during the night—almost always observations taken one right after the other). We have found that a handy way to do this is to have narrow columns in the Target List, one for each night of observations. As targets are observed, the Run Master simply enters the number of times the target was observed (most often, just a "1") for that night. As the run progresses, it is easy for the Run Master to glance at these columns and determine if the target has been observed sufficiently or not. If the weather turns bad during a run, the Run Master may elect to only observe very high priority targets. Knowing at a glance what has already been observed can aid this decision process.

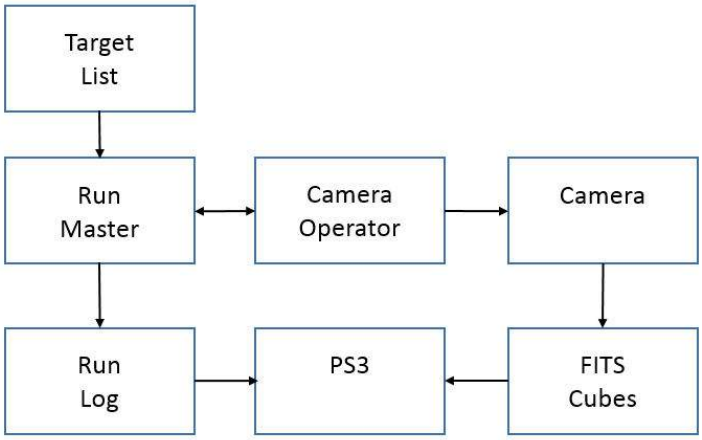

Figure 2. During-the-run major functions.

After selecting the next target to be observed from the Target List, the Run Master informs the Telescope Operator of the target, with precise coordinates often stored in advance in the telescope's queue. The target is then acquired and passed on to the Camera Operator, who may fine-center the telescope pointing, adjust the camera settings (integration time, gain setting, number of frames, and filter), and start the integrations.

At this point, the Camera Operator informs the Run Master of the FITS cube sequence # so the Run Master can enter the FITS cube sequence # in the Run Log. If more than one filter is used, the Run Master enters the filter ID in the Run Log. Great care must be taken to assure that each and every FITS Cube has a unique sequence number that is entered in the Run Log for the observed target. Finally, the Run Master checks off the appropriate row on the Target List that an observation was made on this night. The Run Master than selects the next target.

During the run, it is prudent to reduce some of the observations as a check on quality. Although at this point, calibration constants may not be well known, "quick look" reductions can still assess the quality of the observations. To make quick looks truly "quick," it is helpful if the Run Log and FITS Cubes can be directly fed into the reduction program, PS3, without any modification.

Finally, it might be noted that during the run it may be convenient to use PS3 to preprocess the FITS Cubes, as this reduces the file size by a factor of roughly 1000 and also reduces reduction time.

Although the original unprocessed FITS Cubes should be retained, preprocessed FITS Cubes can be easily replicated and dispersed among the observers or even placed on line, thereby assuring that the data from the run will not be accidentally lost.

Post-Run

After the run, the data is reduced. The Run Log contains critical information on each target, and has the FITS Cube sequence numbers that tie the appropriate FITS Cubes to the targets and reference stars. The post-run major functions are shown in Figure 3.

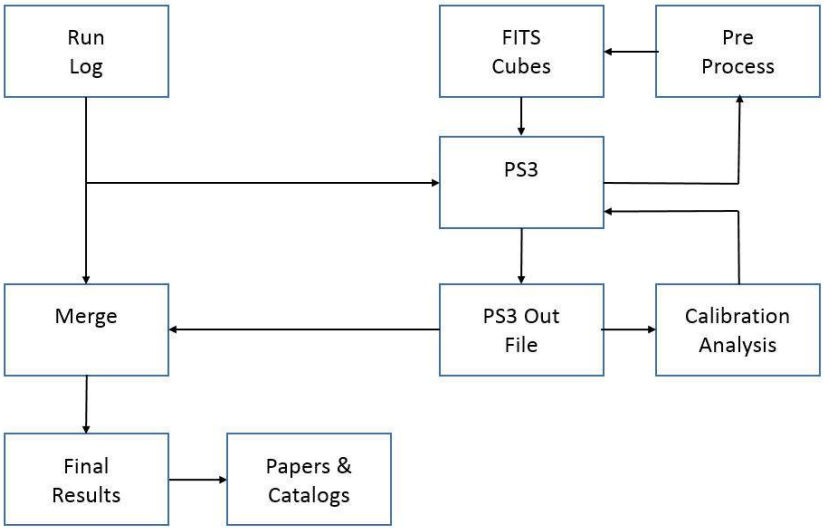

Figure 3. Post-run major functions.

The FITS Cubes file can be quite sizeable. On longer runs it can exceed a terabyte. PlateSolve3 (PS3) has a Pre Process feature that obtains a Fourier transform of each image in a FITS Cube and averages the results. This not only greatly increases the S/N, but reduces the file size by a factor of 1000 or more. While preprocessing can be time consuming, it is an entirely automatic process and can be completed before data reduction proper begins.

The PS3 In File actually only requires and utilizes eight parameters for each target in the Run Log. These parameters must be contained in the first eight columns of the Run Log PS3 In File. Any other columns are ignored, thus the requirement to merge these ignored columns in the Run Log with the PS3 Out File to obtain the Final Results.

The PS3 Reduction is typically done in two iterations. In the first iteration, only observations intended to calibrate the camera angle and pixel scale are reduced. These observations may be of calibration binaries, clusters, drifts, slit masks, or known telescope movements. Analyses of these observations yield the camera angle, Δ, and the pixel scale, E. These calibration values are then used in the subsequent reduction of the entire data set.

The PS3 Out File contains the information provided in the first eight columns of the Run log, the PS3 “solutions” in terms of camera angles, separations, and delta magnitudes, as well as supporting information on the settings of various solution parameters. The PS3 Out File may also contain comments from the Reducer such as “triple star noted” or “suspect reduction” etc.

The final PS3 Out File is then Merged with data from the Run Log to generate the Final Results file. The Results File can then be placed on line and various users can access their portion of the results. After further analysis, the observations appear in published papers or IAU Commission 27 circulars, and eventually in the various catalogs, thus completing the overall process.

Content of the Spreadsheets

Introduction

The formats for the spreadsheets (or their .csv file equivalents) in the double star speckle interferometry observation and reduction process were established by starting with the essentially "firm requirement" for specific spreadsheet (.csv) inputs to the PlateSolve3 (PS3) reduction program and working backwards to the Run Log spreadsheet and then to the Target List spreadsheet. Once this was done in terms of required information on these spreadsheets, then further "propagation" backwards to the Program Lists could be made. Similarly, one can start with the information in the Run Log and PS3 Out File and merge and select and/or arrange so as to form the Final Results.

While the above was how the contents were established, the contents and order of the individual parameters in the columns in the Target List and Run Log are identical, the only difference in the two spreadsheets being that some of the cells in the Run Log, such as camera sequence numbers, have to be filled in during the run. Given below is the content in column order.

Required PS3 InFile First Column's Content

For double stars, the required Run Log .csv file content is established in a forthright manner. The first seven columns of each row in the Run Log must contain the following information:

T – If the Target is a "D" (for double), then PS3 will process this file, otherwise it will be ignored. This allows the Run Log spreadsheet to have rows, for instance, for single stars used for deconvolution, slit mask, or drift calibrations, etc., with codes assigned to these other cases. Single reference stars have been assigned an "S".

DSFN – Double star (FITS cube) file name. This required information will be provided by the Camera Operator when starting a FITS Cube observation and will be entered into the Run Log by the Run Master. Our plan at this point is to have the FITS Cube filename be the camera sequence number.

RSFN – Reference star (FITS) cube file name. As above, this required information will also be provided by the Camera Operator when starting a FITS Cube observation and entered into the Run Log by the Run Master. Our plan at this point is to also have the single star FITS Cube filename just be the camera sequence number.

ThetaC – Calculated (input) estimated, predicted, or last catalog reported double star position angle. This information is used by PS3 to place a "predicted position" of the double star on the autocorellogram. This prediction can then be compared with the automatic solution provided by PS3. If the two are close, one simply accepts the automatic solution and moves on to the next double star. If the predicted position is close to an obvious solution that the automatic solution process somehow missed, then one overrides the automatic solution and readily provides the correct solution. There are other cases where the correct solution is not obvious and this would normally be noted in the "comments" section of the PS3 Out File. The point is that ThetaC is helpful but not critical to the process. Thus it does not have to be a highly accurate value nor, in fact, does it even have to be entered, although a blank cell must be included in the .csv file.

RhoC – Calculated (input), estimated, predicted, or last catalog reported double star separation.

Delta – Camera Angle (degrees). Delta is the camera orientation angle with respect to the sky. Until the calibration data is reduced and analyzed, Delta (and E, below) will not be known with precision. However they can be estimated beforehand and the Delta and E values entered in all the cells in these two columns in the Run Log in advance. When the camera is installed on the telescope, the goal is to have a camera angle of 0° so 0 can be the initially assigned camera angle.

E – Pixel scale (arc seconds / pixel). E can be estimated based on the telescope's focal length and camera chip's pixel size. Alternatively, if the same camera has been previously used on the same telescope, then the earlier pixel scale can be used.

Filter – A single letter code identifying the filter. For the Johnson-Cousins system, the filter code is B, V, R, or I (and possibly Y), while for Sloan it is b, g, r, I, or z. If other filters are used, an identifier can be devised (such as H for H-alpha).

In addition to the "mandatory" information in the Run Log required as an input by PS3, additional information for double stars may be supplied.

Comment – Any comment the Run Master deems appropriate to enter that might help in subsequent analysis and interpretation of the observational results. At a minimum, the date and time when observations began and ended for each night during the run should be recorded. Recording weather comments would be appropriate, as well as any equipment problems, etc.

Date and Time – Also, while the date and time each FITS Cube is initiated is contained in the FITS headers, and can also (optionally) be automatically included in the FITS Cube file name, it is important to also enter this information into the Run Log to help assure that a firm tie exists between the targets and FITS cubes. To enter the date in a cell in the Run Log, click on the date cell and hit *control*; and then click on the time cell and hit *control shift*. The clocks on the PCs that will record or handle data should be set to correct date/time (check time zone!).

For single stars, only *T* (an S), *RSFN*, and *Filter* from above are required. The other columns may be left blank except for:

Single star identifier – SSID This will normally be the Hipparcos (HIP) number or SAO number of the single star, and will identify what specific single star observation is to be assigned during reduction to each double star. Several double stars can share the same single star, although the converse is not allowed.

Target List/Run Log Content

For the KP2 run, candidates for the run will be submitted as Program Lists (Excel spreadsheets) where each row is a double star or single reference star to be observed. There will be mandatory entries and optional entries as described below. Missing or unknown information can be signified with an XXX.

Research Program – Three character identifier of the overall science research program. There may be several researchers from different institutions participating in the same overall research program. Examples include short arc binaries (SAB), large delta mag (LDM) binaries, common proper motion (CPM) pairs, etc.

Requestor Code – Three character identifier of the researcher who is requesting the observation. If a code has already been assigned for first author references in the WDS, please use this code (such as Hor for Elliot Horch, Los for Florent Losse, etc.). If this is more of an institutional request, a three letter (all CAPs) code (similar to those in the WDS) could be used instead.

Target Classification Code – A three character classification code which can be unique to a given research program, that provides information on the object. For instance, "known" binaries have been given codes such as KBO (known bad orbit), KSP (known string of pearls), KNS (known no previous speckle observations), etc. There is a beginning of a classification system for short arc binary candidates. The *Target Classification Code* allows the KPI results to be partitioned according to characteristics of the target. Known binaries have been classified based on a visual inspection of the orbital plots of their past observations provided by the US Naval Observatory in their *Sixth Catalog of Orbits of Visual Binary Stars.* This classification scheme was originally developed by R. Genet and E. Weise and has been further refined. "K" was for "Known" to be a binary.

KBO Bad Orbit
KCB Calibration Binary
KFO Fair Orbit
KFS Few Speckles
KFM Fast Moving
KNP No Points (on plot)
KNS No Speckles
KSP String of Pearls
KVC Very Close
KVF Very Fast

Many of the targets are not known to be binaries but, based on their short arcs, are binary candidates. We have not yet developed a classification scheme for short arc targets but may adopt or modify one developed by Richard Harshaw: SAX Short Arc X (binary candidate with X to be defined in the future).

Individual Double Star Information 1 – In the case of known binaries, this is the Grade. Other information could be displayed in the case of short arc binaries or common motion pairs, etc.

Individual Double Star Information 2 – In the case of known binaries, this is the Period. Other information could be displayed in the case of short arc binaries or common motion pairs, etc.

Within night repetitions M – Number of times to observe per night (assumed in a row). Often more than one data cube if a calibration binary or a difficult (faint, large delta mag, high air mass) target.

Number of nights N – How many nights should object be observed? Calibration binaries, for instance, might want to be observed on several nights. Also, in general, there can be some merit in observing on two different nights. For instance, a triple star "discovery" may actually just be a transient asteroid or satellite.

Night of Observation – Columns, one for each night of the run, where the number of observations actually made on that night are entered by the Run Master. This can be compared with the number of requested observations to assess whether or not additional observations are warranted.

The remaining columns are an exact copy of the target double star from the WDS catalog. It is expected that this will be a straight cut and paste without any alteration. Almost all targets will have WDS entries. For those that do not, similar information should be supplied.

2000 Coordinates (WDS number)
Discoverer & Number
Components
Date (first)
Date (last)
Number of Observations
Position Angle (first)
Position Angle (last)
Separation (first)
Separation (last)
Magnitude of First Component
Magnitude of Second Component
Spectral Type (Primary/Secondary)
Primary Proper Motion (RA)
Primary Proper Motion (Dec)
Secondary Proper Motion (RA)
Secondary Proper Motion (Dec)
Durchmusterung Number
Notes 1
Notes 2
Notes 3
Notes 4
2000 arc second coordinates

Target List and Run Log Spreadsheet Examples

Shown below is a Target List example in two parts. The first part (on the left of the spreadsheet) is the "custom" columns that require inputs either when the Target List is created or entry by the Run Master during the run. In the example below, the blank columns in the Target List are filled in later by the Run Master after a row in the Target List is pasted into the Run Log. Note the **green x's** checked off on the right. These are the nights that these double stars were observed. The Run Master made these entries in the Target List as they were observed. Thus on Wednesday night, the last night of this run, the Run Master will know on which nights the double star has already been observed (as an aid to deciding what to observe next).

T	DSFN	SSFN	TheC	RhoC	Delta	E	F	Com	Date	Time	SAO#	RPg	RqC	TCC	G	Per	WN	BN	T	F	S	S	M	T	W
D			116.6	0.209	-11.0492	0.01166	i				12345	KBS	Gen	KVS	1	1.7	1	2			x	x	x		
D			356.6	0.201	-11.0492	0.01166	i				54321	KBS	Gen	KVS	2	2.5	1	2						x	

Shown below is the second part (on the right of the spreadsheet). It is a straight paste in from the Washington Double Star Catalog (or more exactly, an Excel copy of the WDS Catalog).

WDS	Dis	Comp	First	Last	Nob	PAF	PAL	SF	SL	MagF	MagL	Spec	PPMRA	PPMDec	SPMRA	SPMDec	DM	N	2	3	4	Coord
16555-0820	KUI 75	AB	1934	2009	370	135	81	0.2	0.2	9.73	9.81	M3Ve	-829	-879			-08 4352	N	O			165529.24-082003.1
19121+0254	AST 1		1982	2007	30	224	297	0	0	11.3	13.1	M3.5V	179	-52				N	O	D	P	191213.55+025315.6

Finally, below is an example of the left side of a Run Log spreadsheet (the right side is identical to the Target List as it is the same straight extract from the WDS Catalog, just copied over along with the rest of the row from the Target List to the Run Log). The cells in **blue** were entered by the Run Master. As can be seen for any given observation (row) the Run Master actually does not have to enter much, just the **camera sequence numbers** on the left, and the **date and time** on the right which is a nearly automatic click entry on the spreadsheet as described above.

T	DSFN	SSFN	TheC	RhoC	Delta	E	F	Com	Date	Time	SSID	RPg	RqC	TCC	I1	I2	WN	BN	T	F	S	S	M	T	W
S		234					i		3/31/2014	10:38:45 PM	12345														
D	235	234	116.6	0.209	-11.0492	0.01166	i		3/31/2014	10:43:22 PM	12345	KBS	Gen	KVS	1	1.7	2	1							
D	236	234	116.6	0.209	-11.0492	0.01166	i		3/31/2014	10:47:17 PM	12345	KBS	Gen	KVS	1	1.7	2	1							
S		237					i		3/31/2014	10:53:23 PM	54321														
D	238	237	356.6	0.201	-11.0492	0.01166	i		3/31/2014	10:57:13 PM	54321	KBS	Gen	KVS	2	2.5	1	2							

DSFN and/or SSFN are filled in by the Run Master when informed by the Camera Operator what the camera sequence number is for the double star or the sequence number for the "matching" single star observation. It might be appropriate to always observe the single star first so multiple observations of the double star would fall below the single star observation in the Run Log and the SSFN (camera sequence number for the single star) could just be copied. Every double star observation must have a DSFN and a matching SSFN, while single star observations will only have a SSFN.

F (filter) can be filled in in advance on the Target List if all the observations will be made in the same color band. If not, the Run Master will need to enter the filter values. In the example above, the Run Master did not have any comments (Com).

The first four observations were made on the 14th close to midnight, while the last observation was made on the 15th just after midnight. Finally, all the observations were made on Monday, M, except the last observation which was made on Tuesday, T.

PlateSolve 3 Out File Contents and Column Order

The PS3 Out File contents are comma-delimited, one row per output. The column order is always the same, so any "missing" data is filled with a place holder missing data designator, *9999*. Conventional order in double star astrometry is angle and then separation (θ, ρ). Keeping outputs in this order makes transcriptions, etc., easier. Also a convention in much of astronomy is to call the result "observed" and any pre-observation estimates "calculated." These calculated values may just be the last reported position in a catalog, or may be calculations from an ephemerides table or orbital formulae, etc.

The classical "observed minus calculated" provides the disagreement between what was measured and what was "expected." By placing "observed" and "calculated" values side by side, the user can immediately spot deviant results. All observed and "raw" angles are given as values between 0 and 360 degrees. The traditional double star convention is followed with 0° straight down, 90° to the right, 180° at the top, and 270° to the left. In other words, 0° = North, 90° = East, 180° = South, and 270° = West. The only exception to this rule is that *CA*, the camera orientation angle (which is expected to be near but not exactly 0°) is given as a (normally) small + or – angle. This helps make the math come out properly.

DSFN – Double star (FITS cube) file name. Please see above for the standard for file names.
RSFN – Reference star (FITS) cube file name. Similar to above.
F – Filter standard AAVSO abbreviation: *U, B, V, Rc, Ic, Y, SG, SR, SI,* and *SZ* for the Johnson-Cousins and Sloan filters. Similar abbreviations may be formed for Stromgren or other filter systems Entered by observer. For Tycho, *T435* and *T505* are abbreviations for its filters, although obviously not used by any Earth-bound observers!
θc – Alternative symbol is *PAC* for Position Angle Calculated. This is the last catalog or predicted (input) double star position angle (PA, θ, are abbreviations). This may not always be provided in the input spreadsheet, so we either need to instruct users to include some "no data" code, or need to sense a blank. This estimate would often be the last reported PA, but could be an interpolated value from an orbit ephemeris. This would be up to the spreadsheet user, of course. The main use of this would be to place the cursor in an initial location. This is not a useful input for pure manual operation.
θo – Alternative symbol is *PAO* for Position Angle Observed (output from PS3) double star position angle. This would only have meaning when the user provides the camera angle from some calibration external to the reduction. If not available, the user could enter any number and ignore the results, or enter a camera angle of "0" and the output would be the "uncorrected" camera angle. It should be easy to see if they are off by about 180 or 360. A possible refinement at some point would be to automatically add or subtract 180 or 360 degrees to get closest match between input and output sky position angles. Sky position angle is calculated as frame position angle (always between 0 and 359.999) minus camera orientation angle. We expect the camera orientation to be near 0 (unless like me one places the camera 180 out!), so I think we should ask users to input their camera angle (from their calibration) as a plus or minus value (from north). This should make the math come out right.
θf – Alternative symbol *PAF,* Position Angle Frame. Position angle calculated by PS3 from the centroid pixel locations. Although there are two values (ambiguity), I suggest we only report one. When running automatically, it would be the solution closest to the input sky angle solution. When running manually, it would be the one (of two possibilities) the user selects.
ρc – Alternative symbol *SepC,* Separation Calculated (input). The estimated, predicted, or last catalog reported separation. Similar to above for position angle.
ρo – Alternative symbol *SepO* Separation Observed (output). Separation calculated by PS3 using plate scale. Also similar to above except the input scale factor, instead of input camera orientation angle, is used for the calculation (a multiplication instead of a subtraction).
ρf – Alternative symbol *SepF,* Separation Frame calculation separation in pixels. Similar to above but only one value is available, so do not have to make any decisions, just output.
CA – Camera Angle (degrees). Camera orientation angle with respect to the sky.
PS – Plate scale (″/pixel).
AD – Aperture Diameter (radius in pixels).
LTP – Lock to Peak (True/False).
DCT – DeConvolution Type: *None* 0, *Use Reference PSD* 1, *Subtract Symmetrized PSF* 3.
DCS – DeConvolution Strength, usually set at 100%.
GPR – Lowpass Radius (pixels). Settings for Gaussian lowpass filter.
LPU – Lowpass used (True/False).
HPR – Highpass Radius (pixels). Setting for Gaussian highpass filter.
HPU – Highpass used (True/False).
IF – Interference Filter used (True/False).
EAR – Elongation Aspect Ratio (degrees).
EA – Elongation Angle (degrees). Angle (that matches elongation aspect ratio).
RI – Relative Intensity.
DMag – Magnitude Difference. Delta (differential) magnitude calculated by PS3.

Comm – User comment. A GUI insert based on user assessment of the solution. We might work (with users) on developing some sort of "standard" assessment language, abbreviations, or rating scales. This might help us move toward automation. If humans can provide quantitative ratings, then perhaps we can correlate the human decisions with calculated parameters to allow the reduction program to make similar ratings.

DaT – Date and time output created.

Note on Optional Autocorellogram Assessment Code

The autocorellogram provides a useful visual display of the solution that is automatically saved by PS3 along with each row of the csv output file. PS3, running in the semi-automatic mode used to reduce the KPI data, shows on the autocorellogram both the predicted position angle and separation (ρ and θ) as well as the automated solution (which can be overridden to provide a manual solution). As an aid to identifying problems with the input data, interpreting results, and refining the automatic solution algorithm in the future, a two-digit *Autocorrelation Assessment Code* has been assigned to each reduced target based on a visual inspection of the autocorellogram.

Prediction

1. Dead on
2. Close
3. Same general area
4. Uncertain
5. Not on screen
6. Way off

Automatic Solution

1. Excellent (dead on)
2. Good
3. Poor
4. Missed, but an easy manual solution
5. Solution does not look possible
6. No solution provided, but easy manual solution
7. No solution provided, but possible manual solution

Final Results

The Final Results file could, in its simplest form, simply be a merging of the PS3 Out File and the Run Log. Each PS3 Out File row would have the corresponding row from the Run Log appended to it. A more sophisticated Final Results file might only include selected data and might rearrange its order. A "standardized" Final Results file content and format has not yet been devised.

Acknowledgments

Genet thanks California Polytechnic State University Office of Research and Economic Development for support through their Extramural Funding Initiative, and the W. M. Keck Foundation for support through the Concordia University Undergraduate Education Program. Grady Boyce kindly supplied the final flow diagrams, while Vera Wallen reviewed the manuscript.

Potential of the McMath-Pierce 1.6-Meter Solar Telescope for Speckle Interferometry

Richard Harshaw[1], Gregory Jones[2], Edward Wiley[3], Patrick Boyce[4], Detrick Branston[5], David Rowe[6], and Russell Genet[7]

1. Brilliant Sky Observatory, Cave Creek, Arizona
2. Eclipse Technologies, Lake Oswego, Washington
3. Yankee Tank Creek Observatory, Lawrence, Kansas
4. Boyce Research, San Diego, California
5. National Solar Observatory, Tucson, Arizona
6. PlaneWave Instruments, Rancho Dominguez, California
7. California Polytechnic State University, San Luis Obispo

Abstract We explored the aiming and tracking accuracy of the McMath-Pierce 1.6 m solar telescope at Kitt Peak National Observatory as part of an investigation of using this telescope for speckle interferometry of close visual double stars. Several slews of various lengths looked for hysteresis in the positioning system (we found none of significance) and concluded that the 1.6 m telescope would make a useful telescope for speckle interferometry.

Introduction

Atmospheric conditions play a vital role in resolving binary stars. On some nights, the sky is so turbulent that it is impossible even at mountain top locations to obtain good resolution of stars closer than an arcsecond or so using conventional imaging technology. Variations in the local temperature of the atmosphere cause changes in the index of refraction, which in turn cause differences in the starlight's wave front phase. The temperature variations are random and have the spectrum of Kolmogorov turbulence. One often characterizes the effect of turbulence with a single parameter, the Fried cell diameter, which is a measure of the coherence length of the wave front passing through the atmosphere. Wind causes these "Fried cells" to pass across the aperture of the telescope, causing scintillation and distortion of the point spread function (PSF). The effect is known as atmospheric seeing distortion (ASD).

If short integrations are taken, typically less than 30 milliseconds, the averaging effect of the wind is greatly reduced, and the captured image is then composed of "speckles." Even though distorted, the image still contains a high degree of correlated information at the resolution limit of the optics. Labeyrie (1970) first proposed the method of speckle interferometry to recover the high-resolution information in the image. In this technique, many images are taken at high speed.

The power spectrum of each image is computed by forming the modulus squared of the Fourier transform. The ensemble average of all the power spectra is then calculated, and from this averaged power spectrum, the autocorrelation is found by Fourier inversion. Since the image phase is lost in this process, the autocorrelation has inversion symmetry about its center, causing the companion star of a double to appear in two places, 180 degrees apart. This ambiguity must be resolved by other methods. In the case of close double stars, the position angle is usually approximately known in advance based on previous observations; this knowledge resolves the ambiguity. Speckle interferometry has been highly successful for imaging and measuring double stars with separations close to the theoretical resolution limit of a telescope's optics. All one needs is a high-speed camera, a telescope operating at an appropriately long focal length, and a program to perform the fast-Fourier transformation. Programs such as PlateSolve 3 (Rowe 2014) and REDUC (Losse 2015) perform this function.

Obtaining time on large-aperture telescopes (i.e. telescopes with high resolution) is problematic; most large telescopes are oversubscribed due to the needs of other observers. This motivated Genet to investigate the use of solar telescopes, such as the McMath-Pierce Solar Telescope, in hopes that while daytime use might be fully subscribed, nighttime use might be available. Thus was born the experiment described in this paper.

The McMath-Pierce as a Stellar Telescope

The McMath-Pierce Telescope was not built to serve as a stellar telescope but rather as a solar telescope for imaging and spectroscopy (see Fig. 1). During its long career it has done (and is still doing) outstanding work in this capacity. More recently, it has also been employed in stellar spectroscopy (Washuettl et al. 2009), suggesting the possibility of using this telescope for other stellar work.

The slewing and tracking requirements of this telescope for solar imaging and long exposure spectroscopy are rigorous. However, the acquisition requirements for finding the sun are not nearly as constraining as those for finding faint stars. Acquisition is especially difficult when the star's image must fall on the small CCD sensor of a high-speed camera used for speckle interferometry.

For instance, Andor Technology's Luca-R EMCCD camera's chip is just 8mm by 8mm, which, at the focal length of the 1.6 meter McMath-Pierce telescope, is 20 X 20 arcseconds. The Andor Luca-S, another EMCCD camera, would only have a field-of-view of 12 arcseconds. Our research question was: Can the 1.6 m telescope slew to targets with enough accuracy (and repeatability) to be useful as a speckle interferometry instrument?

Figure 1. The 1.6 meter heliostat.

Method

Our experimental protocol and equipment were simple and straight-forward. The crew (consisting of Richard Harshaw, Ed Wiley, Pat Boyce, and Detrick Branston) used a round white target marked with crosshairs placed at the focus of the 1.6 meter telescope north port, utilizing an experimental setup (Figure 2) already in place in the observing room. (This setup is used by Ron Oliversen of the NASA Goddard Space Flight Center, and it was used with his kind permission.) Projection of the light beam onto the reticule allowed us to visually detect stars to about 5th magnitude in a totally darkened room.

Their displacement from center was marked and measured. Knowing the image scale of the telescope (approximately 2.36 arcseconds/mm), we were able to measure the angular pointing error of bright target stars.

In each of two experiments, a bright star was taken as the reference, centered on the crosshairs via paddle control, and the telescope was initialized (encoders reset to the star's coordinates). From this reference location, we slewed the telescope to another bright star (e.g. Sirius to Procyon, Table 1) and recorded where on the target plate the star was located. This was taken as the slewing error (Table 1, Acquisition). This displacement was measured from the crosshairs using a metric straightedge and was also photographed (Figure 3). The star was then centered using the hand paddle and the telescope encoders zeroed to the star's position. Slewing north and then returning to the original coordinates yielded the North Displacement; slewing south and returning to the original coordinates yielded the South Displacement (Table 1). The second star was then returned to the center via the hand paddle controls, the telescope was reinitialized, and the telescope was slewed to the coordinates of the third star (see Tables 1 and 2). Four slews were made using Sirius as the starting point and three with Spica as the starting point. The Spica experiment was designed to see if there was an indication that a slew of two degrees yielded smaller pointing errors than the ten degree slew used for the Sirius experiment.

Figure 2. D. Branston (McMath-Pierce T.O) adjusts the target reticle for the slewing tests while P. Boyce, R. Harshaw, and E. Wiley look on.

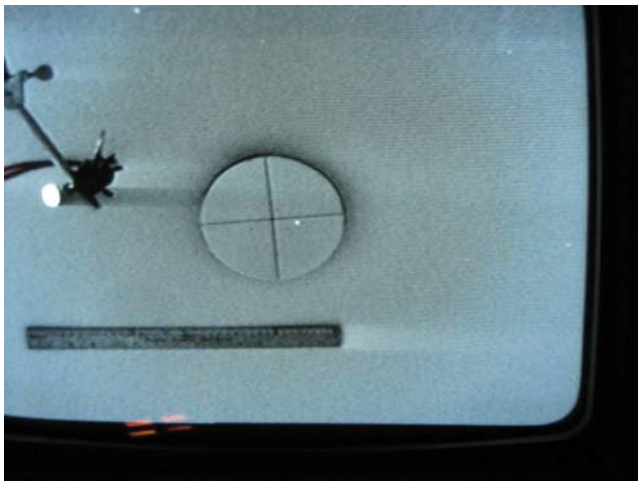

Figure 3. Sirius near the crosshair of the foam core target board.

Slew Test of the 1.6m McMath-Pierce Telescope Run 4/15/14 3:15-5:15 UT			
		10 deg drift	
Star	**Acquisition Error**	**Slew from North**	**Slew from South**
Sirius	n/a	not applicable; starting point reference star	
Procyon	30mm	12mm E	8mm E
Pollux	35mm	4mm E	0mm
Arcturus	60mm	2 mm *(?)*	2mm *(SE)*
Spica	22mm	2mm NW	13mm WNW
started 2 deg tests at Spica		**2 deg drift**	
Star	**Acquisition Error**	**Slew from North**	**Slew from South**
Spica	n/a	4mm SE	3mm SE
Sirius	*350mm (E)*	not applicable; returned to reference star	
Pollux	*56mm (NW)*	2mm NW	3mm W
Arcturus	*45mm (SE)*	4mm S	11 mm W

Table 1. Results of experiments as a function of displacement in millimeters and slew angle.

					10 Degree Offset				
Star	**Acquisition**	***photo***	**Acquisition Aiming Error**	**Distance to North**	**Slew from North**	**Slew Aiming Error**	**Distance to South**	**Slew from South**	**Slew Aiming Error**
Sirius	n/a		n/a	n/a	n/a	n/a	n/a	n/a	n/a
Procyon	30mm (70.8")	*1*	70.8"/92,525"	11° 00' 00"	28.3" E	28.3"/39,600"	11° 00' 00"	18.9" E	18.9"/39,600"
Pollux	35mm (82.6")	*4*	82.6"/82,245"	11° 47' 00"	9.4" E	9.4"/42,420"	10° 00' 00"	0"	0"/36,000"
Arcturus	60mm (141.6")	*7*	141.6"/206,855"	10° 31' 50"	*4.7" ??*	4.7"/5,510"	10° 05' 24"	4.7" SE	4.7"/3,924"
Spica	22mm (51.9")	*10*	51.9"/118,054"	10° 51' 43"	4.7" NW	4.7"/6,703"	10° 44' 33"	30.7" WNW	30.7"/ 6,273"
started 2 deg tests at Spica					**2 Degree Offset**				
Star	**Acquisition**		**Acquisition Aiming Error**	**Distance to North**	**Slew from North**	**Slew Aiming Error**	**Distance to South**	**Slew from South**	**Slew Aiming Error**
Spica	n/a		n/a	2° 04' 42"	4mm SE (9.4")	9.4"/7,482"	2° 13' 23"	7.1" SE	7.1"/8,003"
Sirius	*350mm E*	*A*	826"/346,251"	n/a	n/a	n/a	n/a	n/a	n/a
Pollux	*56mm NW*	*15*	132.2"/169,391"	2° 13' 00"	4.7" NW	4.7"/7,980"	2° 18' 22"	7.1" W	7.1"/8,302"
Arcturus	*45mm SE*	*18*	106.2"/304,055"	1° 58' 35"	9.4" S	9.4"/7,115"	1° 55' 35"	26.0" W	26"/6,535"

Table 2. Errors in acquisition. (Interpretation of Acquisition Aiming Error: 70.8″/92,525″ signifies that the acquisition error was 70.8″ out of a total slew of 95,525″.)

Plate 1. Graphical Representation of the Data

(+ HA from meridian means the star was west of the meridian; - HA means the star was east of the meridian. The data clearly show a systemic error with the telescope's aim. However, it appears the error is proportional to the distance from the meridian, so adjustments in pointing should be possible.)

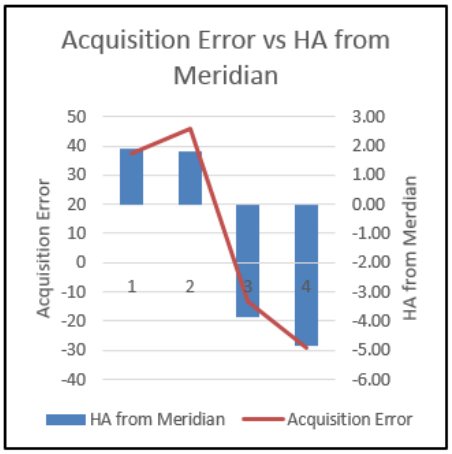

Graph 1. Acquisition Errors (arc seconds).

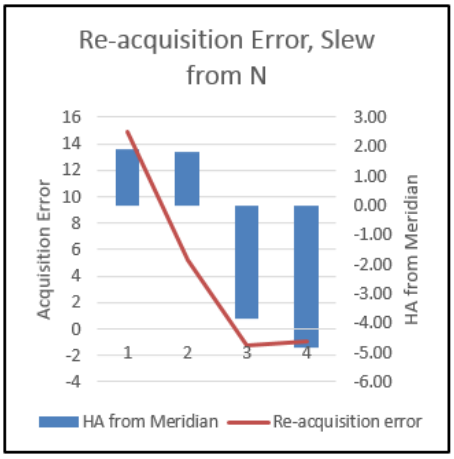

Graph 2. 10^{o} Slewing errors, approach from the north.

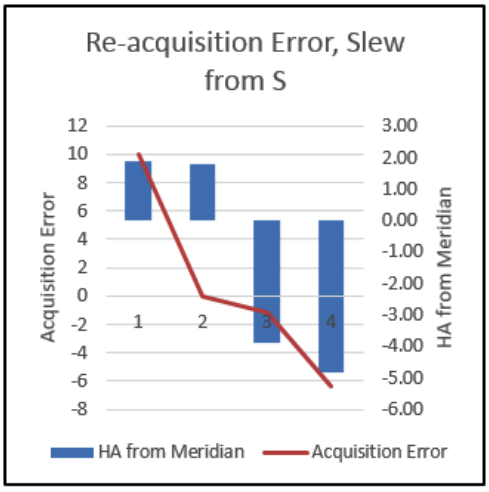

Graph 3. 10^{o} Slewing errors, approach from the south.

Discussion

The primary function of the 1.6 m telescope is for solar observations, which does not require exceptional pointing accuracy. Nevertheless, we were encouraged to find that the largest pointing error was approximately 30″ after a slew of 1.74°, while the smallest error was close to zero. Additionally, our slew tests, although too small for statistical analysis, suggests that there is not much difference in accuracy between a 10° slew and a 2° slew. Slews longer than 10 degrees were not attempted at this time.

Subsequent to our experiment, we learned that a T-Point telescope pointing model had not been updated for a number of years (and is not really required for solar research). With a new model it may be possible that much of the residual pointing errors reported here could be reduced. In addition, there is a suggestion in the data (see Plate 1) that the error vector of the star is consistent with the side of the meridian on which it was observed. For acquisitions west of the meridian, in three cases the star was to the east of the crosshair and once it was to the west. For acquisitions east of the meridian, there was one case where the star was to the southeast of the crosshair and three cases of it being to the west or northwest. It is clear that these acquisition errors are virtually mirror images of each other and suggest that the error is in the pointing model of the telescope. Thus a new model may allow quick and accurate acquisition of double stars.

We are currently designing several methods to improve telescope pointing in case a new pointing model proves insufficient, or if significant hysteresis is found in the positioning system of the heliostat. A leading candidate is to place a small acquisition telescope with a CCD camera in the main tunnel, pointed at the heliostat but out of the light beam of the main telescope. A USB cable from the camera to the observation room would be used to control the camera and download images. An all-sky plate solving program, such as PlateSolve 3, would be used to find the exact pointing direction of the main telescope after appropriate initialization. From this, either an open-loop or closed loop pointing algorithm would be implemented. A second candidate would utilize a wide-angle acquisition system at the focal plane of the telescope. The location of the target star would be determined from an image of the wider field, and the telescope would be slewed to center the target in the science camera. The choice of an acquisition method would depend on the outcome of a new pointing model.

Recommendations for Future Work

A two or three night experimental observing run could accomplish several things. A new pointing model could be made, and the model tested by slewing to bright stars over a substantial portion of the sky. The vector offsets from the center of the target plate would be recorded and analyzed. (This would involve acquisition of many stellar targets and the updating of the T-Point database.)

If the RMS pointing error of the new model was less than 15 arcseconds for target stars within one hour of the meridian and appropriate declination, no further acquisition work would be necessary. If the pointing error was larger than this, but less than 30 arcseconds RMS, a square-spiral search algorithm could be implemented. If the pointing error was greater than 30 arcseconds RMS then we could install the auxiliary telescope in the main tunnel and develop a pointing model. The pointing offset between the main telescope and the auxiliary telescope would be determined by slewing a bright star to the center of the field and plate solving. We would then use open- and closed- loop algorithms to point the telescope to bright stars, recording the location of the star at the focal plane.

If this still does not yield accurate acquisition, then we could install, at the focal plane, a wide-field image acquisition camera and test the ability to move the image of a bright star to the center of the science camera using very short offset slews. After the acquisition system was set up and working, we would make a number of observations using the science camera on known, close double stars to prove the feasibility of the overall system.

In the future, to semi-automate the acquisition and imaging of double stars, it would be useful to input telescope coordinates directly without the intervention of an operator. This could be accomplished if an interface was developed between our control computer and the telescope positioning system as currently pointing commands must be manually entered via keyboard.

Conclusion

Based on the initial experiments documented in this paper, it is likely that the 1.6 meter McMath-Pierce telescope could be useful for semi-automated double star observations using high-speed, low read-noise cameras. At R-band, the resolution of this telescope should allow measurements of double stars down to approximately 0.1 arcsecond separation, opening the possibility for discovery and measurement of thousands of new and existing targets.

Acknowledgments

This work was made possible by a grant of observing time on the McMath-Pierce telescope at Kitt Peak from the National Solar Observatory. We thank Ron Olivierson (Planetary Magnetospheres Laboratory, NASA Goddard Space Flight Center) for generously sharing his telescope time and observing table for our slew tests, and Mathew Penn (McMath-Pierce Director for the NSO) for assistance with scheduling our observing run. We also wish to thank Mark Giampapa, National Solar Observatory, for his overall guidance. Special thanks to Vera Wallen for her editorial review of the manuscript. Genet thanks NASA through the American Astronomical Society for funding to acquire an Andor Luca R camera for our speckle tests, and California Polytechnic State University for providing the travel funds.

References

Couteau, P. 1981. *Observing Visual Double* Stars. Cambridge, MA: The MIT Press.

Pierce, K. 1964. The McMath solar telescope at Kitt Peak National Observatory. *Applied Optics*, 3(12):1337-1345.

Labeyrie, A. 1970. Attainment of diffraction limited resolution in large telescopes by Fourier analysing speckle patterns in star images. *Astronomy and Astrophysics*, 6, 85-87.

Losse, F. 2015. website material at http://www.astrosurf.com/hfosaf/Reduc/Tutorial.htm and http://www.astrosurf.com/hfosaf/uk/tdownload.htm.

Rowe, D. & Genet, R. M. 2015. User's guide to PS3 speckle interferometry reduction. *Journal of Double Star Observations*, 1S, 89.

Washuettl, K., Strassmeier, G., & Weber, M. 2009. The chromospherically active binary star EI Eridani: II. Long-term Doppler imaging, Astronomische Nachrichten - ASTRON NACHR , 330(4): 366-376.

Testing of the McMath-Pierce 0.8-Meter East Auxiliary Telescope's Acquisition and Slewing Accuracy

Richard Harshaw[1], Jimmy Ray[2], Lori Prause[3], David Douglass[4], Detrick Branston[5], Russell M. Genet[6]

1. Brilliant Sky Observatory, Cave Creek, Arizona
2. ASDOG Observatory, Glendale, Arizona
3. Master's in Astronomy Candidate, Swinburne University, Melbourne, Australia
4. AZ-DaHut Observatory, Tempe, Arizona
5. National Solar Observatory, Kitt Peak, Arizona
6. California Polytechnic State University, San Luis Obispo

Abstract Following mediocre results with pointing tests of the McMath-Pierce 0.8-meter East Auxiliary Telescope in April 2014, a team of astronomers/engineers met again in May 2014 to test other pointing models and assess the telescope's ability to point with enough accuracy to permit the efficient use of speckle interferometry. Results show that accurate collimation is a pre-requisite for such accuracy. Once attained, the telescope performs extremely well.

Definition of the Problem

Speckle interferometry requires large aperture at very high focal ratios. The 0.8-meter East Auxiliary telescope at the McMath-Pierce Solar Observatory on Kitt Peak in Arizona certainly qualifies as a suitable aperture, given its objective and focal length (f50). The question is, does this telescope have the ability to acquire stars with enough accuracy to make placing the light of a double star on the small chip of an EMCCD camera?

To test this question, a team of six astronomers convened at the McMath-Pierce 0.8-meter telescope in late May 2014 to run engineering tests and one speckle test of the instrument for possible uses as a speckle imaging system. The team is shown in Figure 1.

Past Experiences With the 0.8-Meter

One of the team members (Harshaw) was a member of a team that investigated this telescope in April 2014 (Wiley et al. 2014). During that engineering and observing run, the investigating team (Wiley, Harshaw, Boyce, Branston, Green, Genet, and Rowe) found consistent but minor pointing problems with the telescope, most acquisitions being slightly off center when the telescope was instructed to slew to a particular target.

Since the placement of the target star tended to be consistently off by the same general quadrant and angular distance, the possibility existed that the April 2014 setup was slightly off-center of the telescope's optical axis—that is, slightly off collimation. Therefore, collimation of the observation optical bench with the telescope's optical axis was the first priority for this run of tests.

Figure 1. Engineering Test Team (Ray, Prause, Douglass, Harshaw; not pictured: Branston, Genet).

Figure 2. Douglass and Prause put the final touches on the collimation rig.

Constructing the Pointing Accuracy System

The team set about building a test rig for the pointing accuracy tests. This rig consisted of a sheet of foam core with quadrille graph paper (5 squares to the inch) affixed with Mastic. A small crosshair was drawn on the graph paper at the center of the collimated light path from the telescope and a small low-lux camera (a ZWO ASI120MC) was affixed to a magnetic mount on a steel pole near the telescope's ceiling port. This would allow us to view a target star's proximity to the crosshair from the nearby observing control room, letting us keep the observing room (Figure 2) totally dark.

Figure 3. Douglass, Green, Prause, Ray at the Dining Hall.

The Pointing Accuracy Tests

Once the pointing test rig was completed, we waited for dark, having dinner in the Kitt Peak Lodge Dining Hall in the meantime (Figure 3). (Wayne Green, a spectroscopist from our April observing run, joined us as he was doing differential radial velocity measurements of double stars at the Coude Feed housed in the 2.1 meter telescope building.)

We began our pointing tests by aiming the telescope at Arcturus. (The East Auxiliary telescope, while controlled directly by a DFM computer system, is aimed using Software Bisque's TheSky (version 4) as the user interface. This makes issuing pointing commands as easy as finding the target in TheSky and issuing a slew command.)

Once centered on Arcturus, we issued a "Sync" command through TheSky (this command tells the DFM computer that we were precisely on Arcturus, allowing the DFM computer to reset the encoder readings). From Arcturus we then issued commands to slew the telescope 2° north of Arcturus, then return, noting the aiming error by measuring the offset of the star from the crosshair on our rig. We then slewed 2° south and repeated the return to Arcturus. We then did slews 6° north and south, and finally 15° north and south.

We then directed the telescope to Spica to repeat the tests, but as soon as we acquired Spica, we realized that we had a similar problem to what we encountered in April—the stars were always close to the crosshair, but never exactly on it. This suggested that our problem may have more to do with collimation than telescope control.

The results of our aiming tests are summarized in Table 1, where the offsets from the crosshair are measured in grid squares north, south, east, and west of the crosshair. (At the image scale of the East Auxiliary telescope, 0.2 inches—the size of the quadrille squares—is approximately 36.6″ of angular displacement.) Once the primary star (Arcturus or Spica) was acquired, a Sync command was issued to align the DFM computer with the sky, but no syncs were issued during the slews from the north or south.

Star	Direction of Slew	Acquisition Error	True Error
Arcturus	2° from the north	9N, 4W	71" @ 336°
	2° from the south	11N, 3 W	82" @ 345°
	6° from the north	12N, 4 W	91" @ 342°
	6° from the south	14N, 4W	105" @ 344°
	15° from the north	15N, 5W	114" @ 342°
	15° from the south	19N, 5 W	141" @ 345°
Spica			
	2° from the north	2N, 1W	16" @ 333°

Table 1. Preliminary Pointing Test Results for the East Auxiliary Telescope.

As can be seen, without syncing between slews, the system errors seem to accumulate. However, it is of some comfort to see that the errors always lie on the same side of the crosshair, suggesting that a good pointing model can be built that would compensate for the errors.

Collimation of the 0.8 Meter Telescope

A group discussion the next morning led to the possibility that we were not precisely aligned with the East Auxiliary's true optical axis—in other words, we were not precisely collimated. With the assistance of Detrick Branston, chief operator of the McMath-Pierce complex, we were able to set up as accurate a collimation as was possible the next afternoon. Figure 4 shows Prause, Ray, and Branston checking collimation using skylight in a darkened observing room.

The collimation process involved reflecting the light coming down through the ceiling view port of the telescope off a 5-inch diameter optical flat to a vertical sheet of foam core board located approximately 150 cm away. A pinhole was placed in the foam core and the telescope's collimating motors operated until the heliostat was perfectly centered in the tertiary mirror as seen through the pinhole. This setup took a little over an hour to complete. Once collimation was completed, we had to wait until dark to start testing the telescope's acquisition accuracy using stars.

Figure 4. Prause, Ray (kneeling), and Branston during collimation.

Combining Pointing Tests With Speckle

As the afternoon progressed, the weather forecast for the following night—the night we had planned to devote 100% to speckle acquisition—deteriorated, so we had to move our speckle tests up one night. This meant we would have to combine slewing accuracy tests with speckle acquisition in one long run.

That being the case, our afternoon was a hectic one in which our chief optician, Jimmy Ray, worked on building an optical bench that would allow for both fast target acquisition and facilitation of speckle image capture.

After experimenting with a few setups that were not successful, Ray ended up around midnight with a good setup. Figure 5 shows Ray and Prause building our optical bench.

The optical bench we settled on used a 5-inch optical flat to reflect light from the ceiling port of the East Auxiliary to a flip mirror on which was mounted a 20mm eyepiece (giving us an estimated field of view of about 3 arcminutes). With the flip mirror raised, light could then be routed to the science camera's CCD chip, which consisted of the ZWO camera for initial testing.

Due to the less than perfect pointing experienced in earlier tests, we elected to use a procedure where we pointed to a bright star as near as possible to the our target star. The telescope was then aligned with the bright star (after we centered the star on the camera) and synced with TheSky. Then the telescope was moved to the target star (be it a reference star for deconvolution or the actual double we wanted to study).

In all cases, the bright star, as well as the deconvolution star, were acquired using catalog numbers (SAO or HIP). However, when slewing to the final target double, J2000 coordinates were used.

As mentioned previously, pointing is done using Software Bisque's TheSky 4. Using TheSky to point to known names or object ID's generated good pointing results. However, pointing to coordinates proved problematic. General observation of TheSky screens, along with digitized sky survey images of the immediate area of the target and visual confirmation from the eyepiece observer (Ray), provided adjustments necessary to find the targets.

The problem was later identified. TheSky V4 was released by Software Bisque in 1996. Correspondence between Douglass and the Bisque team confirmed that TheSky 4 used B1950 coordinates. The coordinates we were using were J2000. Thus, the problem.

A quick test of acquisition ability using Mars, then Saturn, then Spica, and Arcturus showed that the East Auxiliary consistently put the target in the eyepiece field of view, allowing Ray, the acquisition operator, to center the star for the science camera. A turn of the flip mirror put the star (or planet) on the camera's chip! We had solved our aiming problem, and it turned out to be a combination of collimation and final coordinates.

Beginning about 1:00 AM on Wednesday morning, May 28, we switched out the ZWO camera for the Andor Luca R EMCCD camera and began doing speckle (at least until the seeing deteriorated so badly, around 3:30 am local time, that we had to stop). The results of our speckle run are reported in a separate paper.

Figure 5. Ray and Prause building the optical bench.

A Solution for the Coordinate Problem

The following day, Douglass did an extensive search for utilities to convert J2000 data to B1950. Although many utilities exist and are available for converting from B1950 to J2000, the opposite was not true. Several educational papers exist on the web for how to do the calculations, but only one working utility was found, and it was available for on-line use. Several sets of coordinates have been tested with this utility, and the conversions all appear to be good.

The author of the utility, Robert Martin Ayers, a former member of the Lowell Observatory Advisory Board, has given his permission for us to co-host his utility, and provided the code for the conversion utility. (See *www.robertmartinayers.org/tools/coordinates.html* for Ayers' original posting, or *www.az-dahut.net/ACCTool.html,* where Ayers has graciously allowed us to set up this backup page.) Thus, we will be able to continue using the existing software at the McMath, along with our existing J2000 coordinate information, and resolve the final accurate pointing issue. With good coordinate information, the final pointing to the target should be very accurate, thus eliminating the final search for the actual target. It is also possible that giving TheSky 4 the HIP or SAO number of the primary of the pair we wish to study will result in better acquisition too. Both approaches will be tested on our next observing run on the McMath-Pierce 0.8 meter East Auxiliary.

Conclusion

When properly collimated, the McMath-Pierce 0.8 meter East Auxiliary Telescope can render adequate pointing performance, a vital requirement for efficient speckle interferometry image acquisition.

Recently, the East Auxiliary DFM interface was made accessible on-line so operators could access the East Auxiliary using the internet from any location in the world. This opens the doors to new possibilities, provided the telescope has been properly collimated and a standardized optical bench set in place by a telescope engineer prior to the observing run (a mode sometimes known as remote control/operator assisted). If a protocol can be worked out for using the East Auxiliary in this manner, a whole new universe of possiblities opens for its use as an instrument for stellar astronomy.

Acknowledgments

The authors wish to thank the National Solar Observatory and Kitt Peak National Observatory for use of the East Auxiliary telescope for these tests.

References

Pierce, K. 1964. The McMath solar telescope at Kitt Peak National Observatory. *Applied Optics*, 3(12):1337-1345.

Wiley, E., Harshaw, R., Jones, G., Branston, D., Boyce, P., Rowe, D., Ridgely, J., Estrada, R., & Genet, R. M. 2015. Close binary star speckle interferometry on the McMath-Pierce 0.8-meter solar telescope. *The Journal of Double Star Observations*, 1S, 127.

Close Binary Star Speckle Interferometry on the McMath-Pierce 0.8-Meter Solar Telescope

Edward Wiley[1], Richard Harshaw[2], Gregory Jones[3], Detrick Branston[4], Patrick Boyce[5], David Rowe[6], John Ridgely[7], Reed Estrada[8], and Russell Genet[7]

1. Yankee Tank Creek Observatory, Lawrence, Kansas
2. Brilliant Sky Observatory, Cave Creek, Arizona
3. Eclipse Technologies, Lake Oswego, Washington
4. National Solar Observatory, Tucson, Arizona
5. Boyce Research BRIEF, San Diego, California
6. PlaneWave Instruments, Rancho Dominguez, California
7. California Polytechnic State University, San Luis Obispo
8. Northrop Aviation, Palmdale, California

Abstract Observations were made in April 2014 to assess the utility of the 0.8-meter solar telescope at the McMath-Pierce Solar Observatory at Kitt Peak National Observatory for performing speckle interferometry observations of close binary stars. Several configurations using science cameras, acquisition cameras, eyepieces, and flip mirrors were evaluated. Speckle images were obtained and recommendations for further improvement of the acquisition system are presented.

Introduction

From 10-16 April 2014, a group of observers met at Kitt Peak National Observatory to collect measurements on double stars with an emphasis on short arc binaries. Part of the observing plan was to evaluate the use of the National Solar Observatory McMath-Pierce Telescope facility (Figure 1) for speckle imaging. Herein we report on initial results using the 0.8 meter East Auxiliary telescope.

Figure 1. The McMath-Pierce Solar Telescope at Moon rise.

The National Solar Observatory at Kitt Peak consists of three telescopes: a main 1.6-meter telescope and two 0.8-meter auxiliaries. Each telescope consists of a heliostat (M1) that reflects light to a spherical primary mirror (M2), and then to a tertiary flat (M3) that projects the light path down into the observing room (Figure 2).

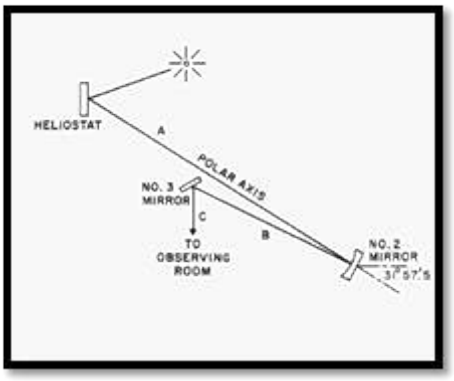

Figure 2. Optical configuration of the McMath-Pierce Solar Telescope.
(Source: *www.nsokp.nso.edu/mcmp-inst*)

The East Auxiliary telescope consists of a 0.91-meter heliostat, a 1.07-meter spherical primary and a 0.61-meter secondary, the overall system having an effective aperture of 0.81-meters. The focal length is 40.4 meters with a focal ratio of f/50. A spherical mirror of this size and f-ratio is limited by diffraction and not spherical aberration. Light from the telescope's tertiary mirror is directed to an optical bench equipped with a flat (M4) that projects the light horizontally along an optical bench on which image acquisition and capture apparatus can be mounted (Figure 3).

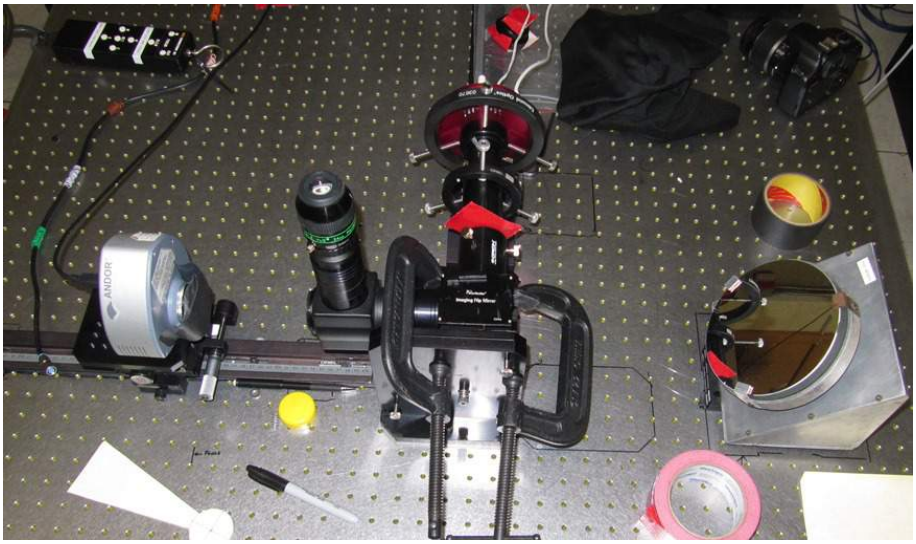

Figure 3. The optical bench "open" set-up and Andor Luca S camera.

The 0.8m East auxiliary telescope has an off-axis optical design (very slight) and has two main constraints: (1) it is alt-azimuth with no correction for field rotation, and (2) pointing is limited to mid-declination (<+40°) due to foreshortening of images by the heliostat. Nevertheless, there are a great number of doubles that can be imaged within these constraints. It is controlled by TheSky® IV software.

Methods and Materials

Several image acquisition configurations were tested on the optical bench. Each consisted of three components: the science camera for imaging the double, an eyepiece to provide a wide-field image, and an acquisition camera with an intermediate field-of-view (FOV) to center the target before switching to the small-format chip of the science camera.

As the FOV of each science camera was approximately 12 arc seconds by 12 arc seconds, acquisition was a major consideration in configuration of the apparatus. Three different science cameras were tested: a Flea3 (Point Grey), a DMK618AU (Image Source), and a Luca S (Andor). Several different optical table configurations were tested, consisting of two basic types:

(1) An "open system" consisting of two flip mirrors mounted on a rigid stand directing light to a science camera and an acquisition camera. One flip mirror was used to direct light to the eyepiece, the other to the acquisition camera. Both cameras could be moved in X, Y, and Z axes. This setup (Fig. 3) was necessary for mounting the Andor Luca S camera, which was too heavy to mount directly to a flip mirror. This arrangement was also used with the Flea3 as the science camera.

(2) A "closed system" consisting of a smaller science camera (IS DMK21) coupled directly to the flip mirror, with the entire assembly mounted on an X/Y platform to facilitate collimation and centering the star on the science camera CCD (Figure 4).

Figure 4. The "closed" set-up with Pat Boyce and Richard Harshaw.

Acquisition

We found that the 0.8 meter telescope had a fast slew rate and good pointing, placing the target with sufficient accuracy that a bright pair could be seen using a white card above the diagonal. However, placing the target into the acquisition camera was difficult due to two factors. 1) The acquisition optics and camera were not precisely aligned with the optical axis of the telescope. 2) The FOV of the acquisition camera was not large enough to acquire the target after a slew. As a temporary solution, we "walked" the target image to a point where it could be visualized by the acquisition camera (open set-up) or eyepiece (closed set-up) and then positioned the image on the science camera chip.

Speckle Results

Using manual acquisition, speckle images were successfully obtained on two nights with both the "open" and "closed" configurations. Figure 5 shows a typical image and the autocorrelation of WDS 12417-0127STF1670AB (Porrima), demonstrating that the 0.8-meter auxiliary telescope is quite capable of being used to image binary star systems. Furthermore, this particular pair was imaged with the inexpensive Image Source DMK21618 camera. The autocorrelation resulted from 1,000 frames taken with 15 ms exposure. The plate scale is 0.028 pixels/arcsecond based on a separation of 2.161 arc seconds, calculated using ephemeris data from the Sixth Catalog of Orbits of Visual Binary Stars (Hartkopf et al. 2001).

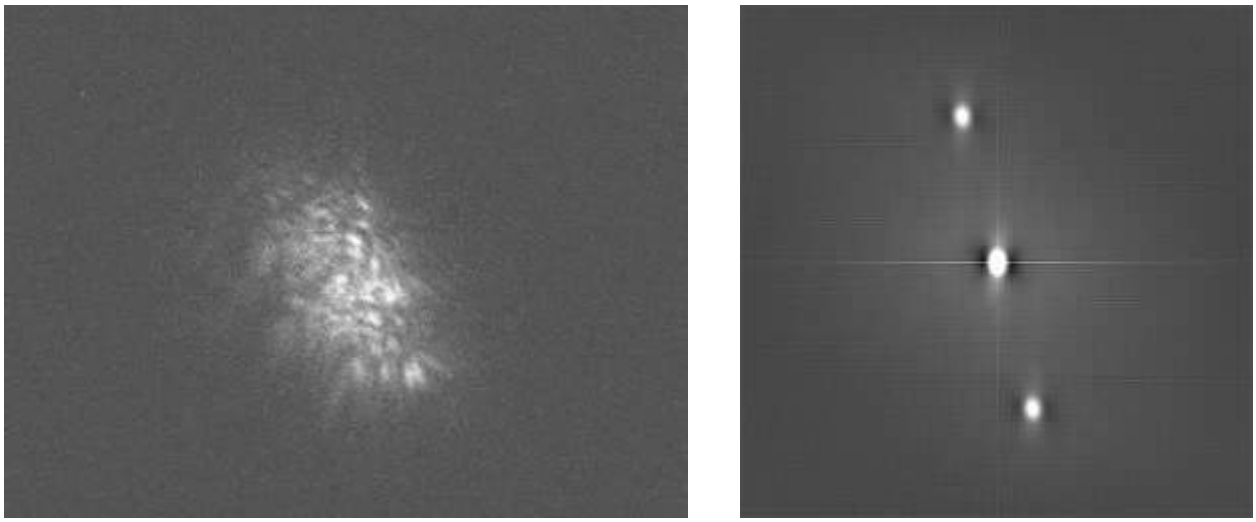

Figure 5. Speckle image (left) and autocorrelation (right) of STF1670AB (Porrima) from the IS DMK21618 camera and "closed" set-up.

Future Directions

We have successfully demonstrated that the 0.8-meter McMath-Pierce auxiliary telescope can be used to perform speckle imaging of bright binaries. Further work is needed to develop a more robust acquisition system and to achieve better collimation between the telescope optical path and the capture apparatus, permitting us to quickly acquire and image faint doubles.

The improvements are:

(1) Use a focal reducer in front of the acquisition camera to increase its FOV. This will allow the acquisition of faint doubles in the presence of large telescope pointing errors.
(2) Provide for collimation mechanics between the acquisition system and the science camera. This will allow quick in-situ alignment of the apparatus.
(3) Initialize the pointing model to the optical axis of the apparatus.

If these improvements are insufficient to reliably acquire faint doubles, a small telescope with camera (possibly a DSLR) could be placed in the McMath-Pierce telescope shaft near M3, directly above the observing room ceiling. The small telescope's camera would be positioned just outside the optical path of the McMath-Pierce telescope, not obscuring the light path. This acquisition camera would capture light directly from the heliostat, thus forming a wide field of view that would be used with a plate-solver to determine the pointing angle of the heliostat with sub-arcsecond accuracy. The pointing direction of the telescope would then be determined through simple vector geometry, allowing accurate closed-loop pointing in order to position target stars in the field of view of the science camera.

Conclusion

The 0.8-meter McMath-Pierce East auxiliary telescope has the potential to be a very capable speckle interferometry instrument. Once acquisition problems are resolved, the telescope should allow an experienced team to efficiently capture speckle interferometry data on double stars.

Acknowledgments

We are thankful for the generous and comprehensive support provided by the staff of the National Solar Observatory; Mathew Penn assisted in all phases of our run, while Mark Giampapa provided overall guidance. Ronald Oliversen, NASA Goddard Space Flight Center, generously shared some of his time on the McMath-Pierce 1.6-meter telescope with us and provided considerable help.

NASA, through the American Astronomical Society's Small Research Grant Program (to R. Genet), funded the Luca-S EMCCD camera. This research made use of the Sixth Catalog of Orbits of Visual Binary Stars maintained by the U. S. Naval Observatory. REDUC was used to reduce the Porrima data (Florent Losse: *www.astrosurf.com/hfosaf/)*.

References

Hartkopf, W.I., Mason, B.D., & Worley, C.E. 2001. *Sixth Catalog of Orbits of Visual Binary Stars*. http://www.ad.usno.navy.mil/wds/orb6/orb6.html.

Speckle Interferometry with the McMath-Pierce East Auxiliary Telescope

Richard Harshaw[1], Jimmy Ray[2], David Douglass[3], Lori Prause[4], and Russell Genet[5,6,7]

1. Brilliant Sky Observatory, Cave Creek, Arizona
2. ASDOG Observatory, Glendale, Arizona
3. AZ-DaHut Observatory, Tempe, Arizona
4. Swinburne University Astronomy Program, Melbourne, Australia
5. California Polytechnic State University, San Luis Obispo
6. Concordia University, Irvine, California
7. Cuesta College, San Luis Obispo, California

Abstract Engineering runs and tests on the McMath-Pierce 0.8 meter East Auxiliary telescope successfully configured the telescope for speckle interferometry observations of close visual double stars. This paper reports the procedure and results of the speckle analysis of four double stars.

Observing Stars With a Solar Telescope

The McMath-Pierce Solar Telescope at Kitt Peak National Observatory is, at this writing, the largest solar telescope in the world. For over 50 years, it has performed outstanding service and helped astronomers gain deep insights into our own star, the Sun. Controlled by a 1960's era PDP-11 computer and run by winches and other equipment that would be viewed by many as not exactly state of the art in 2015, the telescope is a marvel of engineering and still delivers excellent performance.

Of particular interest to our team was the prospect of using the McMath-Pierce for speckle interferometry of double stars. Since time on large telescopes is difficult to secure, we believed it might be easier to obtain time on a telescope that was used primarily in the daytime. As it turned out, we were correct. The staff at the National Solar Observatory in Tucson was more than happy to let us observe at night on the McMath-Pierce. While most people would not think that stellar astronomy could be done with a solar telescope, that is not the case. For example, see LCROSS impact events (Killen et al. 2010) and Doppler imaging of binary stars (Washuettl et al. 2009).

Setting Up the Solar Telescope for Stellar Astronomy

Observing stars with a solar telescope presents challenges of its own, as we learned in an engineering run in April of 2014 (Wiley et al. 2014). Acquisition of the target is achieved by moving a heliostat. The design of the McMath-Pierce telescope dictates that three mirrors must be well-collimated (the heliostat, the main spherical mirror inside the optical tube assembly, and the tertiary mirror that deflects the light into the observing room (Figure 1)).

Not only that, but once the mirrors are in collimation, focusing adjustments must be made, as there are multiple observation ports for each of the solar telescopes in the McMath-Pierce complex, which actually consists of *three* solar telescopes—the 1.6 meter main telescope, and two 0.8 meter East and West Auxiliary telescopes.

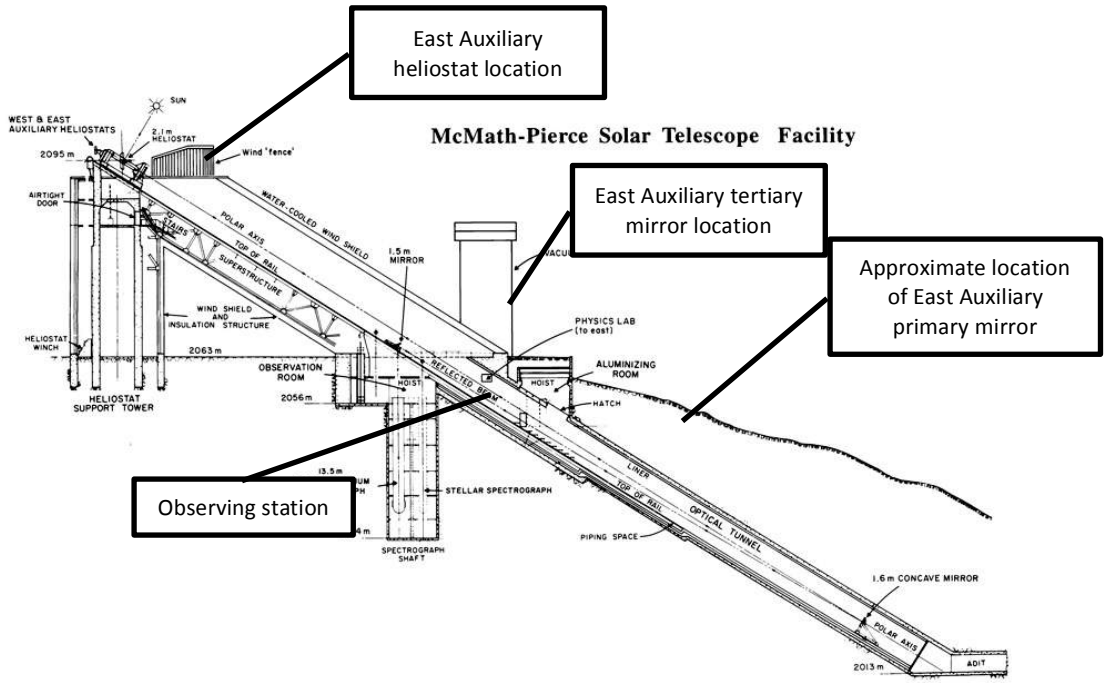

Figure 1. Layout of the McMath-Pierce Solar Telescope.

The McMath-Pierce telescopes all enjoy exceptionally long focal lengths. The main telescope is an f/54 instrument with a total focal length of 87 meters; the west auxiliary is an f/39 instrument with a focal length of 35.6 meters; and the east auxiliary (the telescope we used for our speckle work) is an f/50 instrument of 40.37m focal length. As mentioned by Wiley et al. (2014), we opted not to use the main telescope for speckle interferometry as it lacked the acquisition accuracy required by our acquisition system. However, the east auxiliary is a much more accurate telescope in terms of control (Harshaw et al. 2014) and so was chosen for our speckle observing run in May of 2014. Use of the East Auxiliary Telescope introduced a new set of problems. Since the East Auxiliary's tertiary mirror drops its light into the observing room through a port in the ceiling onto an optical table (Figure 2), we had to set up a fourth mirror, a flat diagonal, to divert the light into our optical bench, acquisition, and science cameras (Figure 3).

Figure 2 also shows the 4-inch diameter optical flat diagonal we used to divert the vertical light beam from the tertiary into our optical bench, under construction in the photo. Prior to building our optical bench, we had a great deal of other work to do. For solar observing, the target is bright enough and large enough to find easily, so determining the exact center of the light path as it impinges on the optical table is not critical. Unfortunately, this is not the case when working with starlight.

We had to first determine the exact center of the light path coming down into the observation room from the tertiary mirror. To do that, we tried centering the Sun in the telescope, but the East Auxiliary's field-of-view is approximately 45 minutes of arc, meaning the Sun had a ring of sky around it. Trying to determine the exact center of the Sun in that arrangement proved to be nearly impossible. So we decided to darken the room and point the heliostat at a clear patch of sky near the Sun but not on the Sun. With the observation room darkened, the round disc of light was easy to observe, and using foam core board and some simple geometry, we were able to pinpoint the center of the light path. Once that point was determined, we drew a small circle in permanent marker on the steel optical table.

Next, we had to collimate the telescope. At first, this posed some challenges, but Jimmy Ray, our chief optician for the observing run, proposed we make a simple pinhole camera and use it to align the four mirrors of our telescope. Figure 4 shows the team collimating with the pinhole in the darkened observation room.

Figure 2. The East Auxiliary light feed port in the observation room ceiling

We ended up with the optical shown in Figure 3.

Figure 3. Jimmy Ray and Lori Prause work on the optical bench.

Figure 4. Prause and Ray collimate with the pinhole while telescope engineer Detrik Branston looks on.

After collimation, we brought the east auxiliary to focus, a process that only took about five minutes with the help of telescope engineer Detrik Branston. We were now collimated, focused, and ready for observing that night.

With collimation and focus accomplished, Jimmy Ray built the optical bench. We had a few hours until sunset. To build a suitable optical bench for our use, Jimmy used an assortment of lenses and a finder scope he brought along, as well as various optical bench assembly parts on hand in the vast storerooms of the McMath-Pierce, to build a suitable optical bench for our use.

Lessons Learned from Slewing Errors

After completing our collimation, focus, and construction of our optical bench, we spent our second night on the mountain obtaining images with the ZWO camera. The device worked quite well, but does produce a fair amount of background noise.

During that run, Lori Prause selected a star to observe and gave that information to David Douglass, who was our telescope operator. The east auxiliary is controlled by a desktop computer (that runs TheSky Version 4), which in turn operates the old mainframe computer that actually controls the telescope.

This became apparent when we tried to find our next target—and could not. After searching for nearly half an hour, we had to concede defeat when we realized what had happened. Unfortunately, it was impossible to find *any* star or planet we could re-sync on, so we had to shut the telescope down for the night.

It took Detrik Branston about 2 hours the next morning to recalibrate the encoders for the heliostat and reset it to its normal "park" position so it would be ready to go with accuracy the next night.

Another issue that came up on the second night of our engineering run was that TheSky speaks "J Now" positions while the control computer for the East Auxiliary telescopes speaks epoch B1950.0! This issue, as well as its solution by David Douglass, is covered in Harshaw et al. (2014).

Speckle Interferometry with an Andor Luca R Camera

Our third and final night on the mountain was a test to determine if we could obtain good speckle interferometry results using the Andor Luca R camera. This camera is an EMCCD instrument with an extremely fast shutter and very low noise.

For our observing run, we had about ten stars we wanted to observe, but encroaching weather limited us to just five. As it turned out, one of these was apparently the wrong star, as after the image was processed, it turned out to be a single star on the autocorellogram.

A set of 1,000 FITS images were obtained with the Andor camera for each star, these images being compiled into a FITS cube. As we imaged each double star, we also imaged a single star that was nearby for purposes of deconvolution. Thus we created ten FITS cubes, 9 of which were usable.

We then used Plate Solve 3.33 by David Rowe to process the FITS cubes and do the speckle analysis. Shown in Figure 5 is a typical raw image at f50 showing a classic speckle pattern (left) and the processed autocorellelogram (right).

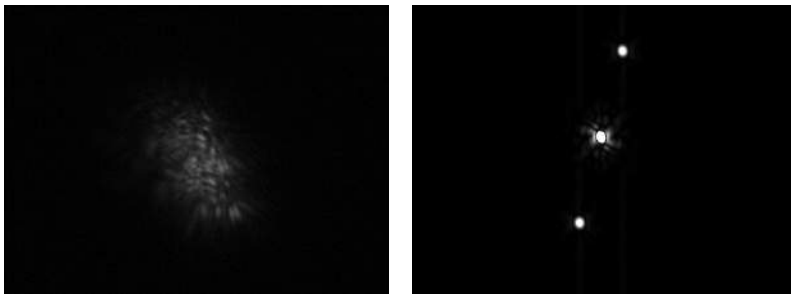

Figure 5. Raw speckle image of a double star (Wiley 2014) and the processed autocorellelogram using Plate Solve 3.

The Speckle Reduction

In doing reduction using Plate Solve 3.33, one needs to give the program the camera angle (the angle between true north and the camera's main axis) and the pixel scale. In mounting the camera on our optical bench, we took careful steps to be sure it was as close to vertical as possible, with the intention of having the camera angle at the meridian be zero.

However, the McMath-Pierce, being a stationery telescope that tracks stars by a heliostat, experiences field rotation. The amount of field rotation can be calculated by taking the local zenith meridian hour angle and subtracting the star's right ascension. The result must then be converted to decimal hours and divided by 24 to get what percentage of a full rotation (360°) has occurred since the star was on the zenith, then multiplying that result by 360° to get the rotation in terms of degrees.

For example, we observed WDS 13381+3910 when the zenith meridian hour angle was 16315 (16 hours, 31 minutes, 0.5 minutes, or 30 seconds). The difference between the zenith and the star's RA is 2.644167 hours. Dividing 2.644167 by 24 yields 0.1101736, which is multiplied by 360° to give the amount of rotation as 39.6625°.

For the pixel scale, we used the known focal length of the east auxiliary telescope (40.37m or 40,370mm) and the pixel scale formula: Arcseconds per pixel = (pixel size in microns / telescope focal length in mm) x 206.5 In this case, the pixel size in the Andor Luca camera is 8 microns, so we end up with 0.04087 arcseconds per pixel.

Shown below (Figure 6) are the autocorellograms Plate Solve 3.33 generated for each of our four stars. These are not the actual images of the double stars; rather they are the power spectrum distribution in a graphical format. Since a power spectrum solution is symmetric around its mean, there are companion stars on both sides of the central star (the primary).

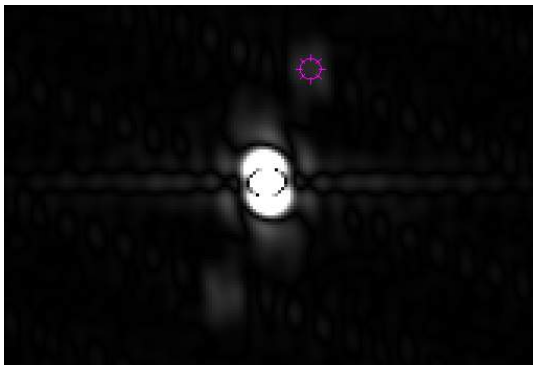

WDS 13381+3910

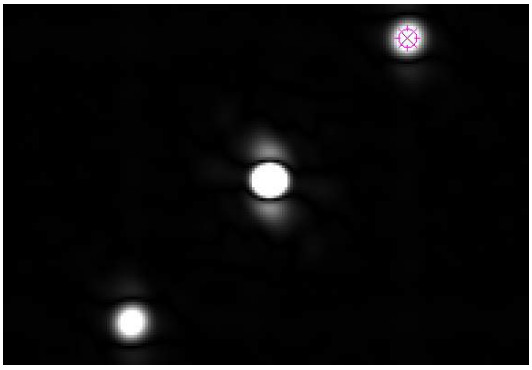

WDS 13491+2659

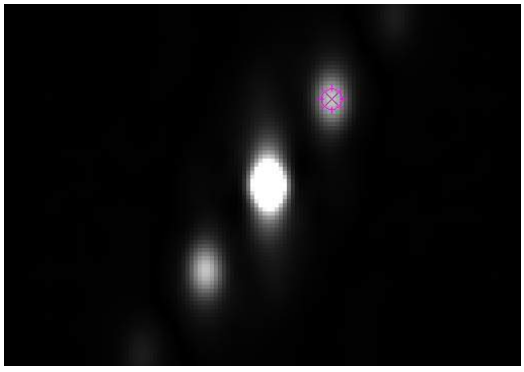

WDS 13544+2955

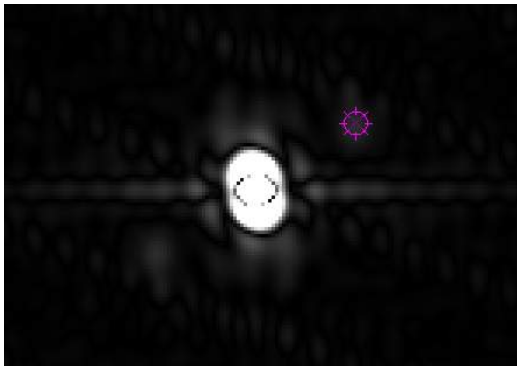

WDS 16044-1222

Figure 6. Autocorellelograms for the four pairs we studied.

When we used the angle of field rotation in Plate Solve 3.33, the measured values for theta were all off by a large amount, and there was no consistency to the discrepancies. Table 1 presents the data from the first round of analysis:

Star	Rotation	Theta 1[a]	Rho 1[b]	Theta M[c]	Rho M[d]	Res Theta[e]	Res Rho[f]
13381+3910	43.3458°	158.902°	1.6239”	115.365°	1.5946”	+43.255°	+0.0293”
13491+2659	41.4125°	135.628°	2.9516”	94.399°	2.961”	+41.299°	-0.0094”
13544+2955	46.675°	121.928°	1.3735”	77.042°	1.4102”	+44.866°	-0.0367”
16044-1122	39.6625°	143.921°	1.0772”	104.275°	1.0737”	+39.646°	-0.017”

Table 1. Analysis using the field rotation values for the camera angle.

Notes:
[a]The value for theta based on recent observations and the Sixth Orbit Catalog (when available).
[b]The value for rho based on recent observations and the Sixth Orbit Catalog (when available).
[c]The measured value for theta.
[d]The measured value for rho.
[e]The residual between theta and observed theta.
[f]The residual between rho and observed rho.

The average residual for Theta M was +42.3245°. The mean residual for Rho M was -0.0033”. The standard deviations (based on four data points) was 16.2574° for Theta M and 0.0275 for Rho M.

In trying to find a reason for the high residuals between Theta 1 and Theta M, we tried several combinations and permutations—we tried using the rotation angle as a negative number (minus 43.3458° for instance), subtracting the rotation angle from 90°, adding it to 90°, and likewise for 180° and 270°. Nothing we tried produced Theta M that was even close to Theta 1 nor in any way consistent.

At this point, we decided to set all values of the camera angle at 0 in Plate Solve. Here are the results:

Star	Rotation	Theta 1[a]	Rho 1[b]	Theta M[c]	Rho M[d]	Res Theta[e]	Res Rho[f]
13381+3910	43.3458°	158.902°	1.6239”	158.711°	1.5946”	+0.191°	+0.0293”
13491+2659	41.4125°	135.628°	2.9516”	135.812°	2.961”	-0.184°	-0.0094”
13544+2955	46.675°	121.928°	1.3735”	123.717°	1.4102”	-1.789°	-0.0367”
16044-1122	39.6625°	143.921°	1.0772”	143.938°	1.0737”	-0.017°	-0.017”

Table 2. Analysis using a camera angle of 0°.

Notes:
[a]The value for theta based on recent observations and the Sixth Orbit Catalog (when available).
[b]The value for rho based on recent observations and the Sixth Orbit Catalog (when available).
[c]The measured value for theta.
[d]The measured value for rho.
[e]The residual between theta and observed theta.
[f]The residual between rho and observed rho.

The mean residual for Theta M was now -0.4965° and for Rho M it was -0.0033”. The standard deviations are -0.4965 for Theta M and 0.0275 for Rho M. It is as if there was no field rotation in this experiment, for when we assumed a camera angle of 0° *no matter when the FITS cube was generated*, the observed value for theta is in almost perfect agreement with the predicted value.

As an astronomy mentor of Harshaw once said, “We cannot always give the reason for everything!” Harshaw fully expected the field rotation angles to act as inputs for Plate Solve 3’s camera angle function, but as you can see, doing that gives wildly discordant values for Theta M.

Overall the values for rho look very good.

Conclusion

We concluded that the McMath-Pierce 0.8m east auxiliary telescope can—with the proper preparation, collimation, focus, and coordinate inputs—do high quality speckle interferometry. As far as we know, we may be the first team to ever successfully obtain speckle interferometry data using a solar telescope. Hopefully our success will inspire others to try similar experiments with solar telescopes that do not see much night use.

Acknowledgments

The authors thank the United States Naval Observatory for use of the Washington Double Star Catalog and the Sixth Orbit Catalog; the National Solar Observatory at Kitt Peak National Observatory for their support, specifically Mark Giampapa, Matt Penn, and Detrik Branston. We thank David Rowe for his many helpful suggestions. Genet thanks California Polytechnic State University Office of Research and Economic Development for support through their Extramural Funding Initiative, and the Keck Foundation for support through the Concordia University Undergraduate Education Program.

References

Harshaw, R., Ray, J., Prause, L., Douglass, D., Branston, D., & Genet, R. M. December 2014. Testing of the McMath-Pierce 0.8 meter east auxiliary telescope's acquisition and slewing accuracy. *Journal of Double Star Observations*, 10, 4a, 366-371.

Hartkopf, W. I., Mason, B. D., & Worley, C.E. 2001. *Sixth Catalog of Orbits of Visual Binary Stars*. http://www.ad.usno.navy.mil/wds/orb6/orb6.html.

Killen, R. M., Potter, A. E., Hurley, D. M., Plymate, C., & Naidu, S. 2010. Observations of the Lcross impact event from the McMath-Pierce solar telescope: sodium and dust. *41st Lunar and Planetary Science Conference*.

Washuettl, A., Strassmeier, K. G., & Weber, M. 2009. *The chromospherically active binary star EI Eridani: II. Long-term Doppler imaging.* Astron. Nachr. / AN 330, No. 4, 366 – 376 (2009) / DOI 10.1002/asna.200811136.

Wiley, E. O., Harshaw, R., Jones, G., Branston, D., Boyce, P., Rowe, D., Ridgely, J., Estrada, R., & Genet, R. M. December 2014. Close binary star speckle interferometry on the McMath-Pierce 0.8-meter solar telescope. *Journal of Double Star Observations*, 10, 4a, 372-375.

Calibrating a CCD Camera for Speckle Interferometry

Richard Harshaw
Brilliant Sky Observatory, Cave Creek, Arizona

Abstract Due to advances in high speed CCD cameras, speckle interferometry has now become an area of research for amateur astronomers. This paper describes several approaches to calibrating the pixel scale of a camera and suggests that using a transmission diffraction grating with a monochromatic light source is the best method.

Introduction

Since discovered by Antoine Labeyrie, speckle interferometry has held great potential as an analytical tool for the observation of close binary stars (Labeyrie, 1970). While Labeyrie's approach was labor-intensive and relied upon photographic film, new electronic cameras transfer the data analysis from the domain of hard work and manual computation to the domain of computerized analysis, thereby saving the researcher valuable time and yielding higher accuracy than was possible by manual methods. Since the introduction of intensified CCDs in the late 1980's, astronomy has undergone a revolution in the astrometry of close binary star systems.

These star systems are of immense interest to astronomers because a close pair is likely to be a gravitationally bound pair with a relatively short period. It is the determination of binary star orbits that is the Holy Grail of modern stellar astronomy as the determination of an orbit allows us, with appropriate additional information, to determine the masses of the two stars. With the masses determined and the distance to the pair known, we can determine each star's absolute luminosity and thereby fill in the mass-luminosity diagram with more data points. In a house-that-Jack-built chain of reasoning, the mass-luminosity relationship is the driving force of stellar evolution and dynamics.

Until the last 15 years or so, speckle interferometry has been the domain of large research-grade telescopes and high-end CCD cameras. But recent advances in camera technology have brought the price point of good cameras down to a level where amateurs with sufficient aperture can now do speckle interferometry. See Teiche et al. (2014), Genet (2013), and Wiley (2013). This was the development that led to the speckle interferometry with an 11-inch SCT reported in this paper.

The Equipment

In late 2014, a Skyris 618C color CCD camera was procured. The Skyris is manufactured by The Imaging Source (Germany) under license to Celestron. The Skyris 618 uses a Sony 618 color chip of 640 x 480 pixels, each pixel being 5.6 microns in size, but is run in black and white mode for speckle and CCD imaging of stars (Y800 using FireCapture software). The Skyris was chosen because its integration times run a wide range, from 1 millisecond to 30 seconds. Since speckle is best done in the 10-40 millisecond range (and the lower end of that range is better), the Skyris is a good choice for amateur speckle. The Skyris was mounted to a Celestron C-11 SCT.

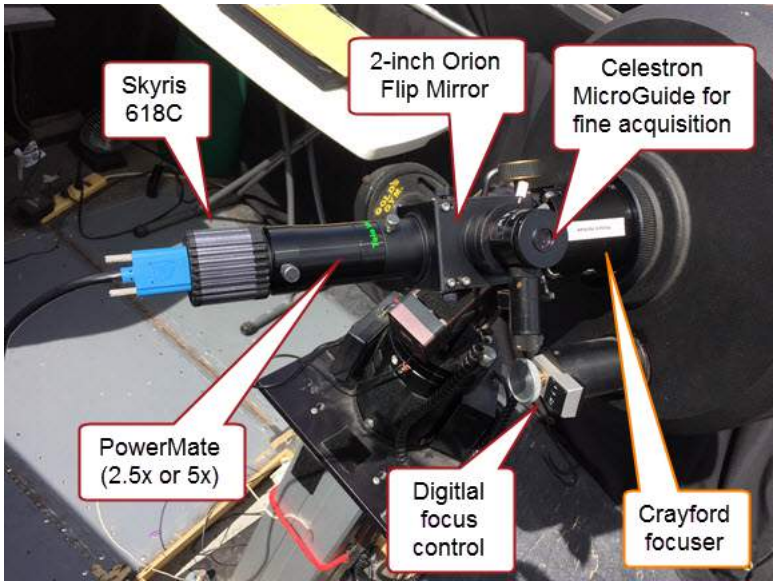

Figure 1. The setup of the C-11 for speckle.

Target acquisition was made by using a 32mm Plössl eyepiece on the flip mirror's acquisition leg. Once the target was centered in this eyepiece, it was replaced with a Celestron MicroGuide for final centering. Once the target was at the center of the MicroGuide, the mirror was flipped and the starlight sent to the camera.

Measures at f/10 were obtained without a PowerMate in the optical train. Measures at f/25 were taken with a 2.5x PowerMate in the position shown in Figure 1, and f/50 measures were obtained with a 5x PowerMate.

FireCapture (by Thoren Edelmann, available as a freeware / shareware program from his website, *http://firecapture.wonderplanets.de/*) was used for camera control.

REDUC by Florent Losse (available as freeware by contacting the author at florent_losse@yahoo.fr) was used to determine camera angle. The target star is centered on the camera chip. A momentary switch to disable power to the RA drive motor of the telescope was depressed, allowing the star to drift to the west. It was noted which direction this is on the computer screen, and the drive motor repowered. The star is then moved to just off the east side of the chip, FireCapture started, and the drive motor disabled, letting the star drift across the camera field of view. When the star exits the field, the drive motor is repowered.

REDUC allows one to easily determine camera angles much the same way that using an astrometric eyepiece on a Dobsonian telescope works—the rotation of the earth takes the star from exactly east to exactly west, independent of any polar alignment errors in the mount. See Figure 2 for a sample camera angle determination.

For data reduction and final measurements, Plate Solve Version 3.33 by David Rowe (PlainWave Instruments) was used.

In addition to the equipment described thus far, three transmission diffraction gratings were used of different slit/bar widths ("pitch"). Figure 3 shows the three gratings used.

The 6mm and 12mm gratings were made from 0.032" aluminum sheet and precision cut with a water jet (CSC process) at a local machine shop. The 18.8mm grating was made by gluing two Bahtinov masks together (discarding the slanted slits).

Image files were copied to a 2 TB external hard drive connected to a Lenovo W950 laptop computer.

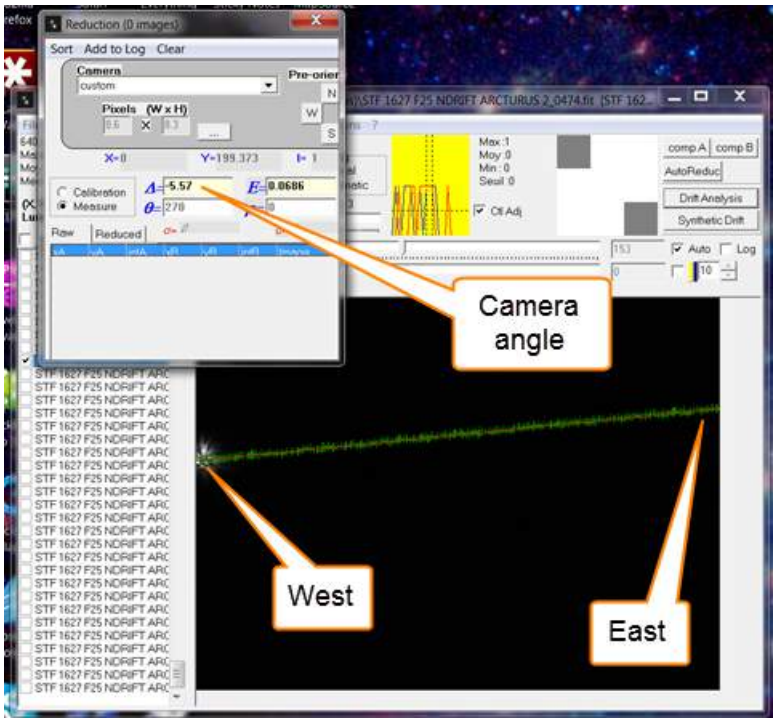

Figure 2. A typical drift analysis by REDUC.

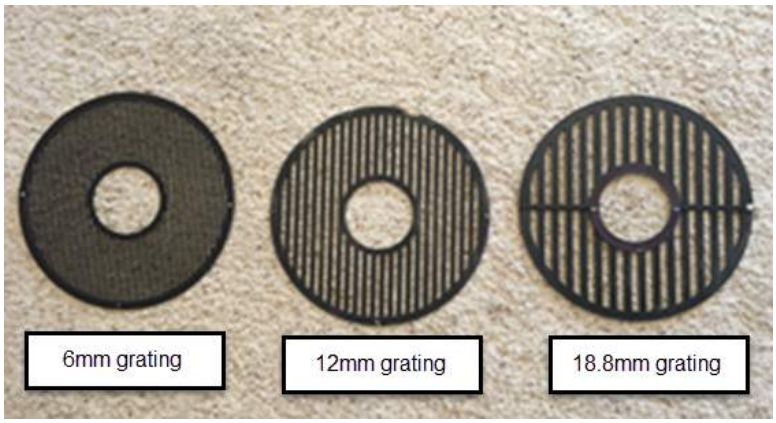

Figure 3. The three gratings used for calibration.

First Test: Drift Calibrations

A well-known expression exists for correlating the camera's pixel scale (defined as the number of arcseconds each pixel of the camera measures) to the telescope's focal length and is given by

$$E = \frac{P_{um}\ x\ f}{206.5}$$

where E is the pixel scale, P_{um} is size of the camera pixels in microns, f is the telescope's focal length, and 206.5 is a constant that converts radians to degrees. For telescopes with well-known focal lengths (such as those custom built for observatories), this approach is satisfactory.

But for an SCT, which achieves focus by moving the primary mirror, the f-ratio is not constant. The published value given by a manufacturer is the mean the engineers design for, but any one factory-produced telescope may have actual focal ratios that can vary by several millimeters from the published value.

For wide-field imaging, this poses no problem. But for speckle interferometry, where even a calibration error of 0.1 seconds of arc can lead to unreliable results, this approach is simply not usable. The first attempt at calibration was with a series of star drifts across the eyepiece, a similar approach being used for the Skyris after Iverson and Nugent (2015). The test consists of placing a star off the east edge of the camera field of view and letting it drift across the total field. A count of the number of frames between the entrance and departure of the star is made. FireCapture writes a text file for each exposure detailing the exact length of the exposure, so knowing the exposure length and number of frames exposed, one can easily compute the milliseconds per frame. Knowing this, and the number of frames between entrance and egress, and the pixels between the entry and egress points, one can calculate the field diameter using this expression:

$$FOV = \frac{T_t \, x \cos(\Delta) * 1.0027379}{4}$$

FOV is the field of view diameter in arc seconds. T_t is the transit time in seconds, Δ is the star's declination, and 1.0027379 is a constant that converts sidereal time to solar time. The result is then divided by the number of pixels along the transit path to determine the pixel scale.

Eighty transits of bright stars were made (Rigel, Betelgeuse, Sirius, and Arcturus) and results averaged. Standard deviations were computed for each focal ratio and standard errors calculated. Any measurement that was more than three standard deviations from the mean was discarded (five such measures had to be deleted). The pixel scale derived from these tests is shown in Table 1.

F ratio	Mean "E"	St. Dev.	St. Error	Data points
25	0.162"	0.004"	0.0008"	28
50	0.076"	0.005"	0.0001"	47

Table 1. Pixel scale from drift tests.

These results were then tested with two "calibration pairs." (Calibration pairs are stars that are members of the U. S. Naval Observatory's "Calibration Candidates" as given at this web page: *ad.usno.navy.mil/wds/orb6/orb6c.html.* However, please note the disclaimer by the U. S. Navy: "Caveat emptor!") While calibration binaries may produce adequate results for traditional astrometric methods such as micrometers and CCDs, they may produce misleading results for such high precision systems as speckle.

Data was taken on Gamma Leonis and Gamma Virginis, both members of the Calibration Binaries list. The results of the measures are shown in Table 2.

		Predicted Values		Measured		Residuals	
Star	Date	Theta	Rho	Theta	Rho	Theta	Rho
γ Leo f/25	2015.241	126.2°	4.627"	128.1°	4.873"	+1.8°	+0.246"
γ Vir f/50	2015.241	6.6°	2.230"	9.8°	2.456"	+3.2°	+0.226"

Table 2. Results of measuring Rho with the drift pixel scale.

The residuals are out of line for such small values of rho, so it was decided that the drift method was not satisfactory. The reason for the discrepancies will be covered in the Discussion section.

Second Test: Series of CPM Stars

For the next test, it was decided to select 14 common proper motion stars (CPM stars) that met these criteria: 7 of them must be good f/25 candidates and 7 of them good f/50 candidates. In all cases, stars were chosen that had shown no significant motion in almost 200 years of observation (especially in the last 100 years). Each star chosen was selected based on a graphical plot of its measurement data (obtained from the U. S. Naval Observatory), using a spreadsheet written in Excel.

This spreadsheet allows the user to enter the measurement histories of double stars in the text format in which the data is sent from the Naval Observatory. The spreadsheet adjusts values of theta for precession, and plots the measurements on an X-Y coordinate plane. Figure 4 shows a typical case.

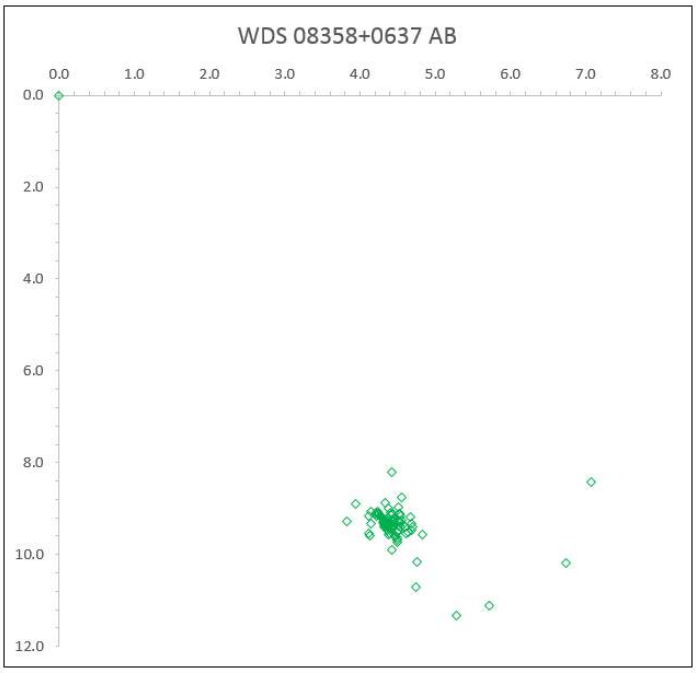

Figure 4. Typical CPM pair measurement plot of stars chosen for tests. The scale is in arc seconds.

None of the pairs chosen were speckle candidates as they were all too wide in separation to qualify. (Speckle stars should be 5" or closer to each other.) However, by using the Skyris as a CCD and carefully analyzing the results with Plate Solve, it was possible to establish a value for the camera pixel scale. The results of these 14 tests are shown in Table 3. These results are significantly different than the drift tests and confirmed suspicions about the drift tests.

Focal ratio	f/25	f/50
	0.156"	0.069"
(Drifts)	*0.162”*	*0.076”*
(Deltas)	*+0.006”*	*+0.007”*

Table 3. Results of CPM Star Tests.

Transmission Diffraction Grating Tests

The transmission diffraction gratings shown in Figure 3 were designed to fit over the secondary mirror mount of the C-11 and rest on top of the retainer ring for the corrector plate. The slit spacing (or “pitch”) was determined for each grating by counting 20 pairs of bars and slits (10 for the Bahtinov grating) and measuring that distance with a high-precision machinist’s rule marked in mm. The results were divided by 20 (or 10 for the Bahtinov).

The grating is based on Thomas Young’s famous double slit experiments of 1803. Stars viewed through such a grating produce a bright central image flanked by “ghost” images of 1st, 2nd, 3rd order (etc). See Figure 5. A slit experiment works best with monochromatic light, and since no star emits light of one wavelength, the trick is to get a broad-spectrum light source to behave as a monochromatic source. The solution, of course, is narrow-band filters.

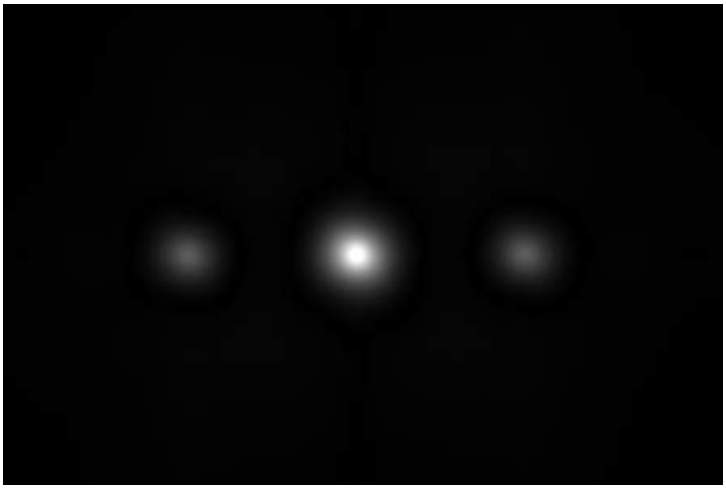

Figure 5. Typical Main and n-order images through a grating.

When the grating tests were begun, an O-III filter was used, as it was the narrowest band-pass filter available at that time. But the results were so far off from what the CPM tests had shown, they were rejected outright.

An H-Alpha filter was then obtained from a local fellow astronomer (David Douglass) and used to produce acceptable light for the tests. In this way, 60 images of Arcturus were made allowing for a high confidence / low standard error result. Two tests were run using the 12mm grating, and one test each with the 6mm and Bahtinov gratings. The results are shown in Table 4.

Test	Value of "E"	Std. Dev.	Std. Error	Measures
f/25, 6mm	0.154"	0.014"	0.004"	40
f/25, 12mm (1)	0.156"	0.230"	0.059"	40
f/25, 12mm (2)	0.156"	0.082"	0.026"	10
f/25, Bahtinov	0.155"	0.053"	0.012"	20
f/50, 6mm	0.069"	0.146"	0.038"	40
f/50, 12mm (1)	0.069"	0.092"	0.024"	40
f/50, 12mm (2)	0.069"	0.043"	0.010"	20
f/50, Bahtinov	0.068"	0.057"	0.018"	10

Table 4. Results of diffraction grating star tests.

Green Laser Field Test

One final test remained to be done to solidify the calibration results. This test consisted of using a green laser reflected off a convex mirror to generate an artificial star of 532nm wavelength and was inspired by a copy of a personal note from Andrei Tokovinin of the Cerro-Tololo Inter-American Observatory to Russell Genet (2013) regarding use of a laser to calibrate a camera.

This test involved the fabrication of a convex mirror affixed to a piece of plywood painted flat black and mounted on a steel pole that could be pounded into the ground, letting the telescope be set up some distance away (Figure 6).

Figure 6. The convex mirror target for the laser tests.

This mirror, along with the C-11 and field mount, was taken to a flat desert location and set up 0.72 miles (1,159 m) from the telescope. With the help of two local astronomy students, a green laser was placed on a stand about 3 meters from the mirror and turned on. The images at the telescope were recorded. The results are shown in Table 5.

Test	Value of "E"	Std. Dev.	Std. Error	Measures
f/25, 12mm laser	0.156"	0.161"	0.042"	20
f/50, 12mm laser	0.069"	0.019"	0.005"	20

Table 5. Results of the Green Laser Test.

Summary of All the Calibration Methods

Table 6 presents the results of all the calibration tests. In the table, the weight refers to the confidence placed in the method as a determinant of the final calibration.

Discussion

You will note from Table 6 that no weight was given to any of the drift tests or the O-III filter tests.

The drift tests were initially done to replicate the work of Iverson and Nugent (2015). But it was discovered that even a tool as useful as REDUC can be in determining pixel scale, the method itself has drawbacks. First, when one works at f/25 or f/50, star images dance around on the camera chip. On some nights, this dance could describe an area nearly 5" in diameter! At high magnifications, a sudden jump could mean dozens of pixels. Trying to determine when a star actually enters the camera's field of view (and not merely choosing an early "jumper" as the starting point), or egress frame, is difficult at best. Even though the frame selection was varied within the same AVI file to help eliminate these errors, it was simply not possible to get consistent results (as evidenced by the large standard error). No doubt it works well for CCD calibration, but speckle is a whole order of magnitude more demanding.

It is not necessary to get the camera precisely oriented along the east-west axis of the sky, since REDUC provides an X-Y readout of each star's position for each frame. Knowing the X-Y positions of the starting and ending stars allows one to easily calculate the total traverse by finding the hypotenuse of the subtended triangle.

F Ratio	Method	Value of "E"	Weight	Wtd Total	Wtd Mean
10	12mm H-Alpha	0.375	4	1.5	**0.375**
	18.8mm H-Alpha	0.372	4	1.488	
25	Star drift	0.162	0	0	**0.154**
	γ Leo	0.141	2	0.282	
	6mm H-Alpha	0.154	4	0.616	
	12mm H-Alpha	0.156	4	0.624	
	18.8mm H-Alpha	0.155	4	0.620	
	7 CPM Pairs	0.156	3	0.468	
	12mm O-III	0.092	0	0	
	12mm Laser	0.156	4	0.624	
50	Star drift	0.076	0	0	**0.069**
	γ Vir	0.069	2	0.138	
	6mm H-Alpha	0.069	4	0.276	
	12mm H-Alpha	0.069	4	0.276	
	18.8mm H-Alpha	0.068	4	0.272	
	7 CPM Pairs	0.069	3	0.207	
	12mm O-III	0.041	0	0	
	12mm Laser	0.069	4	0.069	

Table 6. Summary of all the calibration methods.

The O-III filter tests were discarded because the 100nm or so wide band pass of the filter made the images of the star and its n-order offspring too spread out for Plate Solve to do an accurate job of determining the centers of each point spread function. It also appears that the O-III filter "leaked" light at other bandwidths as there were ghost images scattered between the 0, 1, 2… n order (bright) images. The calibration pairs tests were given moderate weight in keeping with the Naval Observatory's "Caveat emptor!" warning.

A much higher trust level was placed with the CPM pairs in this study, knowing that if a pair has not significantly moved in over 100 years (and especially the last 50), it would likely remain relatively fixed in the year or so since last measurements.

The H-Alpha and green laser tests yielded the highest level of confidence due to their extremely small standard deviations and standard errors and led to the conclusion that the best method to calibrate a CCD for astrometry is to use a transmission diffraction grating and a narrow band-pass filter (such as an H-Alpha) or green laser (532nm). Due to the inconsistent output of most red lasers, it was decided to avoid a red laser test for the same reason the O-III filter was rejected.

Acknowledgments

This research has made use of the Washington Double Star Catalog maintained at the U.S. Naval Observatory. The author wishes to thank Russell Genet, David Rowe, and Vera Wallen for editorial assistance and review of the manuscript; Mike Collins of Phoenix, Arizona for procurement of the aluminum gratings; David Douglass of Tempe, Arizona for use of his H-Alpha filter; Ethan and Randall Wuthrich, Kyle Dolbear, and Gary Mason for their assistance with the green laser tests in the desert; Jack Drummond for his Orbit Prediction spreadsheet; and Bob Buchheim for his assistance in preparing an Excel spreadsheet for the analysis of the data generated by the transmission grating tests.

References

Genet, R. M. 2013. High speed astrometry of STF 2848 with a Luminera camera and REDUC software. *Journal of Double Star Observations*, 9, 2, 124-129.

Iverson, E. & Nugent, R. 2015. Reaching magnitude +16 with the modified video drift method. *Journal of Double Star Observations*, 11, 2, 128-134.

Laberyie, A. 1970. Attainment of diffraction limited resolution in large telescopes by Fourier analysing speckle patterns in star images. *Astronomy and Astrophysics*, 6, 85-87.

Losse, F. April 2015. REDUC data reduction software. Downloaded via http://www.astrosurf.com/hfosaf/uk/tdownload.htm.

Rowe, D. Plate Solve 3.33 speckle analysis software. Downloaded from author.

Teiche, A., Genet, R. M., Rowe, D., Hovey, K., & Gardner, M. 2014. Automated speckle interferometry of double stars. *Journal of Double Star Observations*, 10, 4, 342-245.

Tokovinin, A. April 2013. Speckle calibration with laser. Private correspondence.

Wiley, E. O. 2013. A pixel correlation technique for smaller telescopes to measure doubles. *Journal of Double Star Observations*, 9, 2, 142-152.

Speckle Interferometry of Short-Period Binary Stars

Russell M. Genet[1], John Ridgely[1], Alex Teiche[1], Edward Foley[1], Corey Christiansen[1], David Rowe[2], Neil Zimmerman[3], Keith Knox[4], Keith Hege[5], John Kenney[6], R. Kent Clark[7], Bruce Holenstein[8], Kakkala Mohanan[9], and James Armstrong[10]

1. California Polytechnic State University, San Luis Obispo
2. PlaneWave Instruments, Rancho Dominguez, California
3. Princeton University, Princeton, New Jersey
4. Air Force Research Laboratory, Maui, Hawaii
5. University of Arizona, Tucson
6. Concordia University, Irvine, California
7. University of South Alabama, Mobile
8. Gravic Inc. Malvern, Pennsylvania
9. Leeward Community College, Pearl City, Hawaii
10. University of Hawaii, Institute for Astronomy, Maui

Abstract A research and development program for advancing speckle interferometry of short-period binary stars has seven major components. These are to: (1) create discovery target lists that are rich with potential binaries with under-observed components; (2) observe the binary targets with components with very small separations as guests at larger telescopes; (3) develop an atmospheric dispersion corrector to observe targets at high air masses from telescopes based in Hawaii; (4) continue the automation of speckle interferometry to survey thousands of binary candidates; (5) develop shaped-aperture masks to disperse the bright primary star light away from faint secondary star discovery zones; (6) refine the speckle data reduction procedures and develop bispectrum analysis to reduce multi-band differential photometric measurements; and (7) develop a simplified multi-frame blind deconvolution reduction technique for use with binary stars.

Introduction

Accurate determinations of stellar masses are critically needed to advance models of stellar evolution. Orbits determined by astrometric measurements of binary stars are the only assumption-free, model-independent way of directly measuring stellar masses. Binary orbits are established by observing the changing orientation of their two components, and then Kepler's Third Law is applied to yield dynamical masses.

The masses of stars in the middle of the main sequence are accurately known. This, however, is not the case for evolved stars, or for stars on either end of the Main Sequence. The masses of many of these types of stars are only known to 5%, while we need to achieve an accuracy of 1%. In the case of late-M stars, masses were recently found to be off by a factor of two, and these are the most numerous stars in the Universe! Few short-period binaries containing one of these stars as components are known because the brightness difference between the two components is large, making them difficult to observe.

The program described in this paper will employ automated speckle interferometry on telescopes equipped with masks developed by the exoplanet imaging community to discover many short-period, large differential magnitude visual binaries that have, as one of their components, a star of a spectral type or luminosity class with poorly known mass. This program's automation of speckle interferometry should make it feasible to observe the tens of thousands of double stars required to find a few hundred binaries with an under-observed component. Aperture masking-techniques should enable the discovery of heretofore invisible faint secondary components.

Automated differential photometric measurements should suggest spectral classifications, while multi-frame blind deconvolution reduction could improve precision. The program's target lists will be placed online so other observers can join the discovery process. Information on binaries discovered with under-observed components will also be placed online so observations can be initiated to establish their orbits and hence dynamical masses. Although well over 95% of the observations are not expected to discover the sought-after binaries, the astrometric and multi-band photometric information obtained should be of considerable value to the astronomical community.

Gaia, the Large Synoptic Survey Telescope, and other survey telescopes will suggest millions of close double stars that could benefit from observations made with systems employing the techniques developed by this program.

This program may lead to the development of four-meter class sparse aperture, speckle interferometry telescopes that should cost a full two-orders-of magnitude less than filled-aperture telescopes. Such automated telescopes would be highly productive binary-star-discovery and follow-up instruments.

Overall Program Objective

Improving our understanding of the basic evolution of isolated stars, *i.e.* stars that do not exchange mass, is a vital aspect of stellar research. The most influential parameter, by far, affecting single-star evolution is stellar mass. Advances in stellar evolutionary models are limited by the accuracy of known stellar mass (Malkov et al. 2012).

The objective of this program is to discover many short-period visual binaries that have, as one of their two components, a star of a spectral type or luminosity class with poorly known mass. Observations will be made using speckle interferometry because of its proven ability to economically observe binaries with separations below the seeing limit—usually the case for short-period binaries.

As will be detailed below, the closest binaries will be observed manually with student help as guest observers on larger telescopes, while the bulk of the observations will be automated. Borrowing technology from the exoplanet imaging community, masks will be used to preferentially diffract the light away from the bright primary star to provide a dark faint secondary star discovery zone. Automated, multi-band, differential speckle photometry will provide the estimates of spectral types needed to determine whether one of the components is of an under-observed type and hence worthy of follow-up observations. Finally, a very computationally-advanced reduction technique borrowed from the space surveillance community, multi-frame blind deconvolution, will be applied to the much simpler case of binary stars. This will allow reductions on fast PCs as opposed to supercomputers.

Measurements of binary stars are the primary, assumption-free, model-independent way of directly measuring (as opposed to inferring) stellar mass. As first suggested by Herschel in 1803, the two stars in a binary system act as mutual gravitational probes, and the first binary orbit was determined by Savary in 1830. For accurate single-star mass determinations, the two stars in the binary system cannot be too close, or mass exchange between the two components would affect their evolution. On the other hand, if they are too far apart, they will take hundreds or thousands of years to complete a significant portion of their orbit; a nearly complete orbit is a prerequisite for accurate mass determination. Thus short-period visual binary stars are well-suited for determining isolated-star stellar masses. Short periods, almost by definition, infer small separations—usually below the atmospheric seeing limit for ground-based telescopes. Thus special observational techniques are required, as discussed below in the Methods section.

The masses of stars in the middle of the Main Sequence are known with good accuracy from eclipsing binaries (Anderson 1991). Stellar types with the least well known mass are M stars, early stars (both white dwarfs and Main Sequence), and evolved giants and supergiants. The masses of Late M stars were recently shown by Trent Dupuy to be off by an amazing factor of two! (Dupuy et al. 2012; Dupuy et al. 2013). The program targets binary star systems with these types of under-observed stars.

How can the stellar masses of close visual binaries be directly determined? There are three complementary observational techniques:

(1) Light curves from the photometry of eclipsing binaries—also known as photometric binaries.

(2) Radial velocity curves via high resolution spectroscopy of binary pairs—i.e. spectroscopic binaries. Double-lined spectroscopic binaries also provide a parallax that is usually more accurate than trigonometric parallax (Farrington et al. 2014).
(3) Orbital determination via visual binary astrometry.

Typically it takes two of these techniques, working together, to obtain the individual stellar masses in a binary system (Mason et al. 1996). While all three techniques are vital and complementary, visual binary astrometry is our area of concentration.

How does visual binary astrometry lead to the determination of stellar masses? When viewed with the naked eye, close visual binaries appear as a single star. Viewed through a telescope at high magnification, they can appear as two separate or partially-blended stars. Repeated observations of the position angles and separations of a close binary over time can yield an apparent orbit—the programming of the binary's true orbit in three-dimensional space on the two-dimensional plane of the sky (Argyle 2012).

We know from Kepler's First Law that the orbits of two bodies trace out an ellipse. We also know from solid geometry that an ellipse tilted at any angle with respect to the line-of-sight is still an ellipse. Thus the apparent orbits of binary stars are ellipses. The measured position angles and separations of a binary can be fitted to an ellipse, providing an estimate of the apparent orbit.

Kepler's Second Law states that two objects in orbit around one another sweep out equal areas in equal periods of time. From all the possible orientations of an orbit with respect to the line-of-sight from Earth, Kepler's Second Law (given a sufficient number of observations) can be used to determine the specific orientation of a binary's orbit.

Kepler's Third Law states that for two bodies, the square of the rotational period is proportional to the cube of the semi-major axis of the true orbital ellipse. Newton extended Kepler's Third Law:

$$P^2 = a^3 / M_d$$

where P is the period in years, a is the semi-major axis in astronomical units, and M_d is the dynamical mass of the two stars in units of solar mass. The dynamical mass is simply the sum of the primary and secondary stellar masses, i.e., $M_d = M_p + M_s$.

It should be noted that the units of the semi-major axis in Newton's formulae are astronomical units, not arc seconds. Thus, we need to know the actual physical separation, not just the apparent angular separation. This is readily determined if we know the distance of the binary pair from Earth. Distances have been determined through the measurement of parallaxes—the displacement of nearby stars against distant stars as the Earth orbits the Sun. Parallaxes of over 100,000 stars were measured by the European Space Agency's telescope, Hipparcos (Perryman 2010). Gaia, launched by ESA in December of 2013, will, within a few years, provide many more highly accurate parallaxes (Eyer et al. 2013).

The overall research goal of this program is to improve our understanding of the evolution of stars by directly measuring, via visual binary astrometry, the dynamical masses of short-period binaries. Since the masses of stars in the middle of the Main Sequence are known with good accuracy, we will concentrate on binaries with a late M component, a very early component, or an evolved giant or supergiant component. As detailed below, there simply are not a sufficient number of these binaries with an under-observed star as a component to allow accurate determinations of stellar masses of these types of stars. Thus new binaries with these under-observed components need to be discovered. The overall objective of this program is to make the discoveries required to advance our knowledge of stellar evolution.

Specific Research Objective

Close binary astrometry concentrates on obtaining two values from true orbits: the orbital period in years, and the semi-major axis in arc seconds. These two values are derived from orbital solutions based on many measurements of the position angles and angular separations of binaries. The challenge is obtaining accurate position angles and separations over nearly complete orbits. When this can be done, and the parallaxes are known, the dynamical masses of binaries can be directly determined (Malkov et al. 2012).

Our program will concentrate on visual binaries with orbits between 100 days and 100 years. Binaries with periods less than 100 days typically have separations below the resolution limit of a 4-meter telescope. On the other hand, while observations of binaries with periods greater than 100 years are useful for other research objectives, the scope of the program requires that accurate, nearly complete orbits be obtained in a reasonable amount of time.

The *Sixth Catalog of Orbits of Visual Binary Stars* (Hartkopf et al. 2001) (VB6) includes published orbits of 795 binaries with periods less than 100 years but greater than 100 days. Of these, the binary with the widest angular separation is α Cen at 17.5″. Only 20 binaries have separations greater than 1.0 arc second. The remaining 775 pairs have separations of 0.03″ to 1.0″. This exemplifies the need for sub-arcsecond observations that will be made as part of this proposed effort.

Since the masses of stars in the middle of the Main Sequence are well known, we are concentrating on binaries with either early or late Main Sequence components or evolved components. If we define the "middle of the Main Sequence" (Class V dwarfs) as running from spectral classes A5 to K5, these comprise about 80% of the stars bright enough for our observing program. It is the other 20% at the two ends of the Main Sequence or those that have evolved off the Main Sequence for which observations are particularly valuable.

Of the 795 binaries within the limits noted above, only about two hundred pairs have a component of special interest, *i.e.* a component that is not in the middle of the Main Sequence. This number of stars is not nearly enough to accurately determine dynamical masses across this wide range of different stellar types. The specific research objective of our program is to discover many new short-period binaries with late M or very early Main Sequence stars, and evolved giants and supergiants as a component.

Method

There are four challenges that will work against the achievement of the program's primary objective. The first challenge is that short-period visual binaries have small separations—almost always below the seeing limit caused by atmospheric turbulence. Thus, an observational method that overcomes the limitations imposed by the seeing limit is required.

The second challenge is one of observational quantity. To discover new binaries with an under-observed component will require that we observe many thousands of double star candidates to find a few hundred short-period binaries with the needed components.

The third challenge is that, in most cases, the difference in magnitude between the primary (bright) and secondary (faint) components will be large. Typically, an M dwarf will be a very faint secondary, with a large differential magnitude difference between the two components, making the secondary difficult to detect. Much the same could be said for white dwarfs—also targets for the observational program. A similar large differential magnitude problem exists with evolved stars. Here the evolved, primary star in the binary is likely to be very bright compared to the lower-mass companion star.

The fourth challenge is to obtain differential photometric magnitudes in multiple color bands and then use these measurements to estimate the spectral types and luminosity classes of the two components.

Six basic methods are used to measure the position angles and separations of visual binaries. This list of methods is not exhaustive but covers the most common techniques:

(1) Visual micrometers have two illuminated crosshairs which are rotated to the binary's position angle; a micrometer screw then moves a crosshair to measure the separation (Couteau 1981).
(2) Images of visual binaries are obtained with a CCD camera. The position angles and separations can be determined with considerable accuracy, as long as the separations between the two components are significantly greater than the seeing limit (Tokovinin & Shatskii 1995).
(3) Lucky imaging overcomes seeing limitations by taking many hundreds or thousands of short exposures, each typically 10 to 30 milliseconds long, depending on the seeing (Law et al. 2006). Such short exposures "freeze out" the rapidly changing atmospheric effects. While most of the images are still badly distorted by "cells" of air of differing density passing over the telescope at high altitude and diverting the binary images in multiple directions, the air cells occasionally "line up" such that a

few “lucky” images are relatively undistorted. These lucky images can be automatically selected and stacked to produce images with a resolution that is only limited by the optical diffraction limit of the telescope. For a 0.2-meter telescope, the diffraction limit is about 1 arc second, while for a 2-meter telescope the limit is about 0.1 arc seconds (i.e. 100 milli arc seconds). Because a large number of frames have to be obtained, lucky imaging is not observationally efficient for simple objects such as binary stars.

(4) Speckle interferometry is similar to lucky imaging in that it also takes hundreds or thousands of short-exposure images. It differs from lucky imaging by utilizing all of the images. While the vast majority of the images are hopelessly scrambled in image space, the images are unscrambled in Fourier space to produce fringe patterns (Laberyrie 1970; McAlister 1985; Horch 2006). These patterns can then be converted to an “image” of sorts, called an autocorellogram, by taking the inverse Fourier transform. Alternatively, a real image can be obtained through bispectrum analysis, a computationally-intensive, four-dimensional technique using complex numbers to maintain the phase information of the observations via phase closure (Knox & Thompson 1973).

(5) Adaptive optics (AO) overcomes seeing limitations by sensing the phase distortion of the incoming light in real time (typically at a rate of several hundred Hz) and using this information to “warp” a small mirror in the optical train in a manner that will cancel out the atmospheric phase distortion. To sense the phase distortion, a high-power laser is often used to create an artificial star in the sodium layer of the atmosphere at about 40,000 feet elevation. The “Robo-AO” program has both automated and significantly reduced the cost of AO systems, although it still is about a million dollars (Baranec et al. 2014).

(6) Amplitude interferometry combines the light from two or more telescopes to produce interference fringes (ten Brummelaar et al. 2005). The baseline between the telescopes can be hundreds of meters, thus the resolution of these interferometers can be very high—just a few milli-arc seconds (McAlister, 1999). Binaries with very short orbital periods (months to days) can be observed. There are, however, very few of these expensive interferometers, and their ability to observe faint binary stars is limited.

Of these six methods, we have chosen speckle interferometry as the program’s observational method. Due to the emphasis on short-period binaries, most of the observations must be of systems with separations below the seeing limit. Compared with lucky imaging, speckle interferometry utilizes all of the observations, providing higher signal-to-noise ratio solutions. While adaptive optics and amplitude interferometry each have their advantages, their complexity and cost place them well beyond the capabilities and scope of this program. The low cost of speckle interferometry—a robust technique which has been used for several decades of efficient observing of double and multiple stars—allows this method to be efficiently applied to discovering new binaries and following them after discovery.

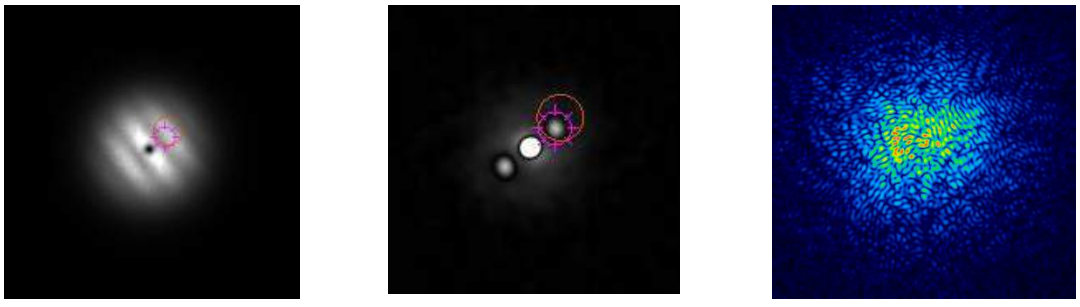

Figure 1. One of a thousand frames shows the speckles from a close binary. (Middle) The fringe pattern (from 1000 frames) in Fourier space of a binary with a separation of 0.22″ (left). The autocorellogram with the predicted position (brown circle) and measured solution (circle with spokes). Observations made with a student team on the 2.1-meter telescope at Kitt Peak National Observatory (right).

While speckle interferometry has, as described above, discovered a few hundred binaries with the requisite under-observed components, it hasn't discovered very many for two reasons: (1) a very large number of carefully selected targets have to be observed and there simply has not been the observational capability to do this, and (2) many of the desired components were secondaries simply too faint compared to the primaries to be detected without additional techniques such as specially shaped masks.

In addition to repeatedly measuring the position angles and separations of binaries over time, speckle interferometry can be used to obtain differential photometric magnitudes in multiple color bands. Not only is such photometry useful for theorists in the development of stellar evolutionary models, but it can be used to estimate spectral types, allowing us to determine whether or not the components of a binary star are under-observed and thus especially worthy of follow-up observations. However, reduction techniques such as bispectrum analysis are required to obtain accurate differential magnitudes (Baranec et al. 2014).

Short exposures suffer from a small amount of signal photons, and camera analog-to-digital converters operating at high speed are inherently noisy. However, the signal can be amplified within the camera itself prior to readout, reducing the read noise to an insignificant level. As the electron packets are being clocked out, a high voltage is applied between a cascade of output gain registers. Even at very high speeds, electron-multiplying (EMCCD) cameras have negligible readout noise.

This program's observational method of choice for discovering binaries with under-observed components will be speckle interferometry with EMCCD cameras. This method will allow us to circumvent the seeing limit, obtain the position angles and separations of close binaries, and also obtain differential magnitudes in multiple color bands.

Program Activities

While economical and robust, the observational method we have chosen, speckle interferometry with EMCCD cameras, is not without its challenges. To discover hundreds of binaries with under-observed components, determine their spectral types with multi-band differential photometry, and initiate observations to establish their orbits, it will be necessary to:

(1) Create discovery target lists that are rich with potential binaries with under-observed components.
(2) Observe the binary targets with components with very small separations as guests at larger telescopes. As few observatories are equipped for speckle interferometry, we will provide our own portable EMCCD-based speckle camera system, which we currently have.
(3) Develop and implement an Atmospheric Dispersion Corrector (ADC) to observe high airmass, far southern binaries from telescopes based in Hawaii.
(4) Automate speckle interferometry to survey thousands of binary candidates.
(5) Develop shaped-aperture masks to disperse the bright primary star light away from faint secondary star discovery zones. This large-differential-magnitude observing technology is borrowed from exoplanet imaging where the contrast ratios are typically five orders of magnitude more severe.
(6) Refine the speckle data reduction procedures and develop bispectrum analysis to reduce multi-band differential photometric measurements. Use these measurements to estimate the spectral types of the individual components.
(7) Develop a simplified multi-frame blind deconvolution reduction technique for use with binary stars.

Over the past two years we have created our first target lists, developed a portable EMCCD-based speckle camera and used it to make observations with students on several large telescopes, computerized an atmospheric dispersion corrector, and achieved initial automation of speckle interferometry on a small (0.25-meter) telescope. We have begun to develop shaped-aperture masks and bispectrum analysis. The seven program activities described below should, over the next few years, bring these efforts to fruition and produce a substantial body of data.

1. Create Discovery Target Lists Rich in Binaries with Under-Observed Components

This program requires that target lists of candidate objects be generated and maintained. As the overall intent of this program is to facilitate the discovery of new binary stars with under-observed components for the community, the program plan is not only to develop lists for our own use, but to publish these lists so they will be available to others in the astronomy community. This program will develop, publish, and maintain five lists contained in a database that is readily accessible to all, somewhat similar to the WDS "neglected doubles" list (see *adsabs.harvard.edu/abs/2001)*. The lists will be: (1) rapidly moving doubles, (2) unconfirmed Hipparcos pairs, (3) unconfirmed Tycho pairs, (4) Hipparcos "problem" stars, and (5) Gaia new discoveries and "problem" stars. These lists should be a valuable resource to the double-star research community.

Rapidly Moving Doubles

The first list will be comprised of double stars that have shown a rapid change in position angle (or separation) as reported in the *Fourth Catalog of Interferometric Measurements of Binary Stars* (INT4) (Hartkopf et al. 2001b), but to date do not have published orbits and are good candidates. Many of these rapidly-moving doubles are Hipparcos or Tycho discoveries that, since their discovery in 1991, have been observed only a few times—typically via speckle interferometry. A number of astronomers (Horch et al. 2012; Mason et al. 1999; Mason et al. 2000; Mason et al. 2001; Toknovinin et al. 2014) have been observing these potential binaries, but there are far more candidates than today's observers, using the currently available techniques, can handle.

Unconfirmed Hipparcos Pairs

Hipparcos discovered 3,383 potential doubles (Perryman et al. 1997). To date, 1,810 have not been confirmed, are in the magnitude range of 7-11, and have separations 0.1″ or wider (see Figure 2). Because these unconfirmed pairs are so close, it is expected that follow-up observations will confirm many of these as binaries, and some of these, in turn, will have under-observed components of special interest (i.e., stars not in the middle of the Main Sequence).

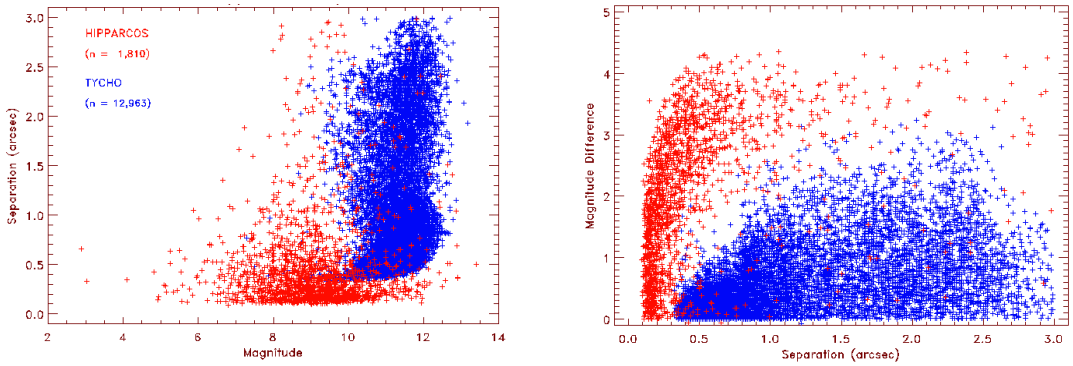

Figure 2. Unconfirmed Hipparcos and Tycho doubles: separation versus magnitude (left) and magnitude difference versus separation (right).

Unconfirmed Tycho Doubles

Another discovery source is the Tycho doubles (Høg et al. 2000). Tycho discovered 14,188 pairs. Approximately 91% of the Tycho doubles remain unconfirmed—no published follow-ups have yet been made. Of these, 2816 are targets with separations so small that only 4-meter class telescopes can handle them, 8701 are targets with separations that only 2-meter class telescopes (or 4-meter class telescopes) can handle, while 12,963 are potentially capable of being observed with 0.5-meter class telescopes (and larger telescopes).

Hipparcos Problem Stars

Another discovery source is the Hipparcos non-component (C) double star solutions, the so-called "problem" stars. There were 11,692 stars observed by Hipparcos which were unresolved but showed some indication of being double stars. Of these, only 754 have subsequently been resolved. The remaining 10,838 remain unconfirmed (no published observations since their 1991 anomalous solution). While some are not doubles, many will be doubles, and some of these doubles will be short-period binaries with an under-observed, non-middle-of-the-main-sequence component.

These Hipparcos problem stars fall into several classes. Two of these classes, G and O, are of special interest. G-code stars, of which there are 2,474, are apparently single stars that showed significant non-linear astrometric motion, *i.e.* acceleration or deceleration; thus there is an indication of orbital motion. If they were indeed binaries too close for Hipparcos to resolve, they could have opened up since 1991, or may be resolvable by telescopes with resolution limits beyond the 0.1″ limit of Hipparcos. The G-code systems are certainly of special interest—especially those with large parallaxes (*i.e.,* close to Earth). With our large differential-magnitude capability, it should be possible to resolve many of these G-Code doubles and, with follow up, some will turn out to be short-period binaries. The secondaries in large differential-magnitude binaries may often be faint because they are late-M stars, making such discoveries especially valuable.

O Code stars, of which there are 172, are orbital (astrometric) pairs that show photocentric motion. Thus their apparent angular semimajor axis is a photocentric orbit, and thus is just a minimum value. They are almost certainly binaries. There must be some magnitude difference between the two stars or they would not be photocentric, but not a large difference or the secondary would not have enough mass to cause a discernible photocentric motion (unless the faint component is a white dwarf or neutron star).

Unconfirmed Lunar and Asteroid Occultations

Lunar and asteroid occultations occur when the limb of the moon or asteroid temporarily blocks the flux from a distant star. The International Occultation Timing Association (IOTA) is a prominent volunteer organization which predicts occultations and organizes groups of members and others in the amateur astronomy community to observe these events. Quite frequently, occultation light curves generated show a step possibly indicating that the occulted star is a double (Herald et al. 2010; Loader et al. 2014). Most IOTA data is collected with video recorded at 25 to 30 frames per second. Since the lunar limb advances about half an arc second per second with respect to the background stars, the vector separations of components may be resolved with a precision of around 30 milli-arc seconds. If only one or two observations happen to record a step event and the step is only one or two frames in duration, there is a lack of confirmation that a double has in fact been detected, since scintillation is often pronounced at high frame rates. As a result, follow-up speckle observations could be crucial for ascertaining the true double state of a star, since an occultation of the star may not repeat for many years.

Gaia New Discoveries and Problem Stars

The Gaia advanced astrometric space telescope was launched in December 2013 by the European Space Agency (Perryman 2008). The first set of results is expected in late 2016. Gaia will uncover a bonanza of newly discovered binaries that will benefit from ground confirmation and follow up. Gaia will also generate a large number of "problem" stars with solutions similar to the Hipparcos G- and O-code solutions. These stars, a problem for Gaia, will be a windfall for this proposed effort. Follow-up observations should reveal many binaries with under-observed components. Since Gaia's resolution is about 0.5 arc seconds, many of their solutions may be resolvable via speckle interferometry with telescopes of only modest aperture.

2. Make Observing Runs as Guests at Larger Telescopes with a Portable Speckle Camera

We have developed and used a portable EMCCD-based speckle interferometry camera for our observations as guest observers (Genet 2013b), including three runs on the 0.5-meter telescope at Pinto Valley Observatory in the Mojave Desert Preserve (Genet et al. 2014a), runs during two winter seasons on the 0.5-meter telescope at Leeward Community College in Oahu, HI (Church et al. 2014), and two week-long runs on the 2.1-meter telescope at Kitt Peak National Observatory (Adam et al. 2014a; Adam et al. 2014b; Wallace 2014) (Figure 3).

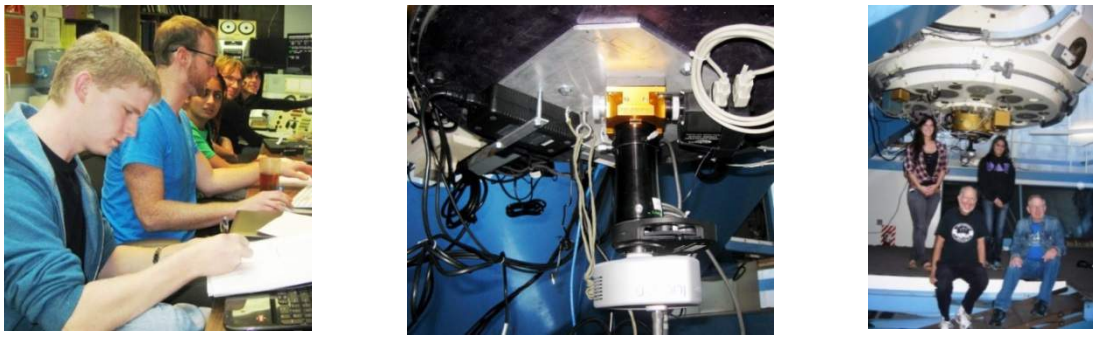

Figure 3. Five students (left) control the 2.1-m telescope at Kitt Peak National Observatory, operate our portable speckle interferometry camera, and keep up the log. The speckle camera (center) is the small silver-colored item directly under the Cassegrain focus (right), and is dwarfed by the telescope (Genet et al. 2014b).

We have concentrated our observations on refining the orbits of known, relatively short-period binaries, and obtaining additional data points on fast-changing doubles discovered by Hipparcos that could, potentially, be short-period binaries. This program will continue with students as guest observers at larger telescopes. Observing time on the 0.6- and 1.2-m telescopes at the Tierra Astronomical Institute (east of San Diego, CA), the 0.5-m telescope at the Pinto Valley Observatory (Mojave Desert, CA), and the 0.5-m telescope at Leeward Community College (Oahu, HI) have been confirmed. We are discussing observing possibilities with the Steward Observatory (1.5-m), and the Vatican Observatory (1.8-m).

3. Atmospheric Dispersion Corrector

Atmospheric dispersion only becomes an issue when observing through the high air masses relatively near the horizon. Atmospheric refraction affects wavelengths differently, acting like a prism. Blue light is bent more than red light. This skews the shape of an observed star. By using altitude data from a star catalog, a computer-controlled atmospheric dispersion corrector (ADC) can greatly mitigate the problem of atmospheric refraction by using a pair of counter-rotating Risley prisms. With an ADC, it will be possible to observe many southern binaries from Hawaii down to declinations of -50 degrees.

For his Master's thesis at California Polytechnic State University, Christiansen (2014) is developing a prototype atmospheric dispersion corrector (ADC) that uses two servo-controlled, counter-rotating Risley prisms for the correction. We plan to deploy a version of Christensen's ADC when working as guest observers on larger telescopes in Hawaii.

4. Automate Speckle Interferometry to Survey Thousands of Binary Candidates

Genet, in conjunction with Louis Boyd, developed some of the first practical automated telescopes. Their telescopes began operation in 1983, and have operated continuously since then at the Fairborn Observatory (founded in 1979 by Genet). The Fairborn Observatory was located for 10 years on Mt. Hopkins, and is now located near the Arizona/Mexico border (Boyd & Genet 1984; Hall & Genet 1988; Trueblood & Genet 1985; Genet 2011; see Figure 4).

Full automation of photometry revolutionized the study of variable stars, transforming the field from being data poor to data rich. Many automated observational programs were launched and successfully completed that would never have been attempted using manual observations. These included an automated search for exoplanet transits suggested by Borucki and Genet in 1992; the first successful transit detection with an automatic telescope was made by Henry et al. in 1999; and a simultaneous transit detection on another robotic telescope by Charbonneau et al. (2000). With full automation, a large increase in the quantity of observations can lead to major advances in the quality of scientific research (Genet & Boyd 1987). Full automation can also result in observations of higher precision and accuracy, given the ability to efficiently conduct observations for calibration and quality control (Young et al. 1991; Henry 1999).

Figure 4. Seven automatic telescopes are on the left at the Fairborn Observatory's robotic observatory on Mt. Hopkins in 1989 (left). A quarter century later, Alex Teiche, an undergraduate student at California Polytechnic State University, stands beside the 0.25-meter telescope at the Orion Observatory (right) on the morning after the first speckle automation was achieved in September 2014.

Automation of astronomical observations provides a number of benefits over manual observations, as pointed out by Boyd and Genet (Boyd et al. 1986). These include lower staffing costs because observers are not required, lower maintenance costs because the systems are designed to operate with minimal intervention, observations which are repeatable and can be standardized, and telescopes which can be sited in locations that are difficult, uncomfortable, or expensive for human observers.

Speckle automation was recently achieved by Teiche as part of our feasibility demonstration program (Teiche et al. 2014). Our first automated telescope has an aperture of 0.25 meters, so it can only observe binaries with a separation down to 1 arc second (Figure 4). This small telescope will initially be dedicated primarily to the task of refining hardware, software, and procedures for the automation of speckle interferometry. Peter Heatwole, for his EE Master's thesis at California Polytechnic State University, plans to extend Teiche's pioneering work.

One component of this proposed program will extend automation to a larger, 0.45 meter aperture telescope. The optics, optical tube assembly, and control system will be provided by the Orion Observatory, while the mount will be manufactured by Equatorial Platforms. With this telescope it will be possible to observe binaries with a separation of 0.5 arc seconds. An Andor iXon, back-illuminated EMCCD camera on long-term loan from Gravic Lab will be the principal detector for this automated system. This camera has a peak quantum efficiency of over 90% and is unusually sensitive at longer wavelengths, which will be helpful when observing binaries with late-M components.

Full automation will allow us to undertake the extensive, large-scale discovery programs needed to discover many binaries with under-observed components. The weather at the Orion Observatory is excellent. We can observe about 200 nights a year for an average of about 8 hours per night, and can obtain 15 or more speckle observations per hour per telescope.

This provides roughly 24,000 speckle observations per telescope per year. With this volume of observations, not only can a large-scale discovery program be undertaken, but many calibration and quality-check observations can be included.

For many close double stars, only the color magnitudes of the combined pair are known. Obtaining automated differential magnitude measurements in several color bands is required to determine the spectral types of the components in double star systems. Knowing the component spectral types informs us whether either component is of interest to this effort. Quite precise differential photometry (albeit not automated) has been obtained in two color bands on many stars (Horch et al. 2004).

To discover the hundreds of binaries being sought, many thousands will be observed. Rather than discarding the "rejects," they will be placed online for the benefit of the double-star community.

5. Develop Masks to Create Dark Discovery Zones for Faint Secondaries

As mentioned previously, binaries with under-observed components will usually have large differential magnitudes. The light from the bright primary swamps the light from the faint secondary. Our masks are based on work at Princeton University where they are being developed for imaging exoplanets with space telescopes.

Shaped aperture masks diffract the bright light from the primary star away from "discovery zones," allowing faint secondaries to be discovered. Many shaped masks have limited-angle discovery regions, so one must rotate these masks to fully survey the neighborhood of a star (Kasdin et al. 2003). Other mask species provide full 360-degree visibility around a star, but do so at the expense of throughput or resolving power (Vanderbei et al. 2003). In general, larger discovery zones are associated with poorer contrast.

Other mask varieties have been proposed in the context of high-contrast imaging, including Lyot coronography and apodized masks. Lyot coronagraphs use a series of lenses and masks to isolate and remove centrally-incident light from the image (Sivaramakrishnan et al. 2001). These systems require accurate manufacturing techniques and precise positioning to function properly (Singh et al. 2013). Apodized masks, also called gradated masks, are used much like shaped aperture masks but feature a continuous transmission profile rather than only complete transparency or complete opaqueness. The smooth patterns theoretically can provide results superior to shaped aperture masks, but these results are difficult and expensive to achieve in practice. Single full-aperture shaped masks are expected to provide sufficient contrast to meet the initial goals of our program. However, we expect, in the future, to develop Lyot mask systems, as it seems likely that they will further extend our ability to detect faint, close secondary stars.

Foley, Zimmerman, and Rowe are simulating the potential effectiveness of various aperture mask designs using Rowe's speckle interferometry simulator (Foley et al. 2015). The simulator takes into account atmospheric distortion and camera noise, producing a result that is more realistic than an idealized diffraction pattern. The prolate-spheroidal mask (Figure 5) will be tested alongside "spider web" masks produced by Zimmerman specifically for this program. Masks with promising simulation results are being manufactured using CNC tools and tested with manual rotation on a telescope at the Orion Observatory. The most promising masks will then be incorporated in automated speckle interferometry telescopes at the Orion Observatory as part of Foley's Master's thesis research (Foley 2014).

While a single, full-aperture, shaped pupil mask looks promising, additional masks of various sorts can be placed at the image plane or Lyot stop. Adding such masks increases the degrees-of-freedom in the design space, which should allow a larger contrast ratio to be reached and therefore difference in magnitude. Although these additional masks would be much smaller, with tighter manufacturing and alignment tolerances, the contrast-ratios sufficient for double star research (approximately 10^2 to 10^3) are more modest than those for exoplanet imaging and so may be within reach.

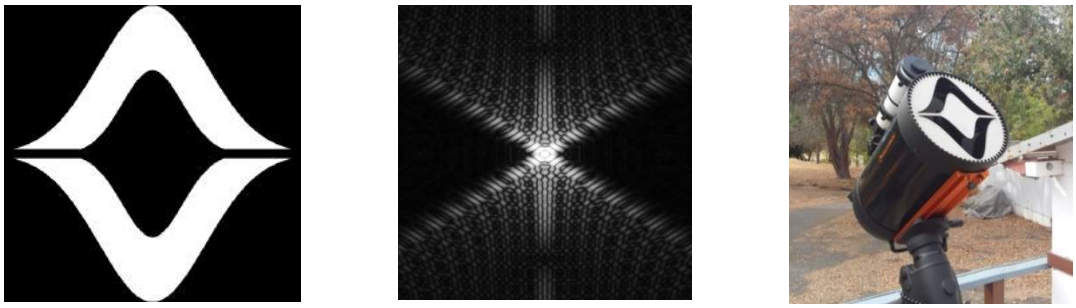

Figure 5. Foley's mask (left) is based on the Spergel–Kasdin prolate-spheroidal mask originally described by Kasdin et al. (2003). It produces the diffraction pattern (middle) plotted on a nonlinear brightness scale. Note the two triangular secondary star "discovery zones" that are relatively free of diffracted light from the primary star. A CNC cut mask (right) is shown on a C-11 Telescope.

There are a number of young giant planets (such as the HR 8799 system, to give the most famous example) that are within reach of 10^5 contrast, and have been imaged from the ground with AO systems at Keck, Palomar, and GPI. A contrast ratio of 10^8 is the design figure being used for space-based science goals.

6. Data Reduction, Bispectrum Analysis, and Spectral Classification

A number of speckle interferometry reduction programs have been written by individual astronomers to reduce data. While these programs work well, they were not intended for widespread use, so they are not extensively documented or "user friendly." Rowe developed software called PlateSolve 3 (PS3) as a general purpose program for stellar astrometry. Given an image with a sufficient number of stars—but without any information as to plate scale, camera angle, RA, or Dec— PS3 quickly determines these parameters [US patent 8,401,307]. Besides this plate-solving capability, PS3 also has many other capabilities such as image calibration, aligning and combining images, etc.

A speckle interferometry reduction capability has been added by Rowe to PS3 (Rowe & Genet 2014). A preprocessing capability calculates and averages the power spectra of all the frames in the FITS data cubes, allowing this time-consuming process to be completed prior to analysis. The program can apply both high- and low-pass Gaussian filters to the data. The science frames can be processed alone or deconvolved with data obtained from a single star located near the double.

PS3 speckle interferometry reduction can be run in one of two modes. In the "manual" mode, individual double-star FITS cubes are selected from a data base, one at a time. Matching deconvolution single-star FITS cubes can also be selected if desired. In the semi-automatic mode, the FITS cubes for both the double star and single deconvolution star are loaded automatically, along with any *a priori* estimates of the position angle and separation of the double—typically the last observation published in the *WDS*. With these inputs, PS3 uses an algorithm to obtain an automatic solution and displays the resulting autocorellogram. The user can accept this solution with a click, or override the automatic solution and provide a manual solution. In either case, both the results and the autocorellogram image are automatically recorded. In the semi-automatic mode, a user can process hundreds of double stars an hour.

An important development, with respect to the high volume of reductions required for use with fully automated telescopes, is a more completely automated reduction process. The automated reduction process will be refined to reduce the number of mistaken solutions it makes (ones that are often patently obvious to a human), and to also develop a metric for the certainty of the automated solutions. If the automated error rates for high certainty solutions can be brought to very low values, then we may be able to avoid human intervention for the vast majority of the observations. However, it is expected that some human intervention may always be required for low certainty automated solutions; otherwise these observations would have to be discarded.

Rowe is working on a speckle imaging addition to PS3, namely bispectrum analysis, also known as triple correlation (Knox & Thompson 1974; Lohmann et al. 1983; Weigelt 1977). Unlike speckle interferometry power spectrum averaging which we have been using, speckle imaging recovers the object phase information via phase closure. Image reconstruction, such as bispectrum analysis, is required to accurately determine differential photometric magnitudes. These magnitudes will be used to estimate spectral types and luminosity classes. A technique such as isochrone matching may also be used to make these estimates (Davison et al. 2009). This technique can also be used to estimate individual stellar masses and, in some cases, ages.

7. Multi-Frame Blind Deconvolution Reduction

Much progress has been made in speckle imaging over the last two decades. Iterative techniques have been developed to reconstruct images from the sequence of short-exposure images. The general name for these algorithms is multi-frame blind deconvolution (MFBD). MFBD is a computer-intensive image reconstruction technique that iteratively utilizes the full set of frames to converge on the best estimate of the set of point spread functions (PSF) and the image of the object (Hirsh et al. 2011).

Although MFBD techniques have been developed and applied to reconstructing images of extended objects such as satellites in orbit around the Earth (space surveillance), they have not been widely applied to the problem of reconstructing binary stars.

A good initial estimate of the PSF can speed up convergence. Similarly, an accurate model of the object can increase the effectiveness and accuracy of the reconstruction. In the case of binary star astrometry, the image can be described very simply by three parameters: position angle, separation, and differential magnitude of two point objects.

The proposed program will develop an MFBD algorithm which will be specifically designed for the reduction of binary star speckle interferometry. For our simple binary or multiple star case, it could be both fast and make optimal use of the information in all the frames in an iterative manner, producing information of both higher accuracy and precision than can be produced by other techniques.

Conclusion

The most influential parameter affecting single-star evolution is stellar mass. The accuracy of evolutionary models is limited by the accuracy of known stellar mass. Binary star orbits are the only way of directly measuring (as opposed to inferring) stellar mass. By discovering and initiating astrometric observations of short-period binaries with evolved components or components on either end of the Main Sequence, this program should significantly increase the accuracy and size of the database of known stellar masses where it is most needed. Any time a new level of accuracy is achieved for a key parameter vital to understanding, such as stellar mass, a transformation of knowledge is possible.

Automation of speckle interferometry should allow the proposed massive observational program to be undertaken at exceptionally low cost. As has been the case in astronomy and elsewhere, an order-of-magnitude increase in the quantity of observations brought about by automation can result in unexpected breakthroughs. Shaped-aperture masks should allow close binary stars with a large differential magnitude difference between the components to be observed. By iteratively using the full set of observations to converge on a solution, multi-frame blind deconvolution (MFBD) reduction more fully utilizes observations to determine binary parameters. Together, these three technologies should produce a potent discovery system with the potential to significantly advance and transform our knowledge of stellar evolution. Taken together, automation, shaped aperture masks, and multi-frame blind deconvolution have the potential of significantly advancing the field of visual binary astrometry for many observers.

In order to find a few hundred binaries with an under-observed component, tens of thousands of double stars will have to be observed. Reporting these observations will, in its own right, be a major contribution to double star astrometry.

Although their spatial resolution is limited, when Gaia, LSST, and other survey telescopes come online, they will suggest thousands, perhaps even millions of close double stars that could benefit from this program's high resolution, large differential magnitude observational capabilities (Terziev et al. 2013). This program will help prepare for the coming flood of targets. Observations with our systems and other similar systems could transform our knowledge of binary and multiple stars in many areas.

We will rely, as we have in the past, on students from a number of different institutions and our well-developed community of supporting astronomers, engineers, and technical experts. Frequent conferences, workshops, and extensive communications will help to keep our diverse binary star research and development community on course (Genet 2013b; van Belle & Genet 2014).

Our student-centered research and development program draws on community college students (some of them first-year college students also finishing up high school), undergraduate university students, and Master's students (Genet et al. 2010). It benefits students by enhancing their educational careers with early, hands-on experiences in research and development. This often results in entry into choice graduate schools with a scholarship and a successful career in science or engineering. As pointed out in the decadal recommendations to the National Academy of Sciences (Henry et al. 2009), "The most important recommendation is to provide the educational foundation required so that a new generation of astrometrists can make best use of the rich data sets that will arrive in the coming decade."

This program naturally brings together the binary-star-astrometry, exoplanet-imaging, and space-surveillance communities in a synergistic manner. Although we are borrowing shaped-aperture mask technology from exoplanet imaging, and multi-frame blind deconvolution from space surveillance, reverse innovation could occur if our modestly-funded program came up with innovations that significantly impact these more generously funded areas. This is sometimes referred to as "trickle-up innovation" (Govindrajan & Trimble 2012).

Acknowledgments

We thank William Hartkopf and Brian Mason for the extensive help in defining the observational program and for editorial suggestions, and both Bob Buchheim and Vera Wallen for their helpful reviews.

References

Adam, M., Roberts, S., Schenk, M., VanRonk, C., Loayza, T., Genet, R. M., Smith, T., & Wren, P. 2014. First speckle interferometry observation of binary BU 1292. *Journal of Double Star Observations,* 1S, 67.

Adam, M., Weise, E., Johnson, B., Lutes, B., Huck, K., Patel, A., & Genet, R. M. 2014. Speckle interferometry observations of binary WDS 01528-0447. *Journal of Double Star Observations,* 1S, 75.

Argyle, R. 2012. *Observing and Measuring Visual Double Stars,* London: Springer-Verlag. http://adsabs.harvard.edu/abs/2012omvd.book.....A.

Anderson, J. 1991. Accurate masses and radii of normal stars. *A&Arv*, 3, 91, http://adsabs.harvard.edu/abs/1991A%26ARv...3...91A.

Baranec, C., Riddle, R., Law, N., Ramaprakash, A., Tendulkar, S., Hogstrom, K., Bui, K., Burse, M., Chordia, P., Das, H., Dekany, R., Kulkarni, S., & Punnadi, S. 2014. High-efficiency autonomous laser adaptive optics. *ApJL*, 790, L8, http://adsabs.harvard.edu/abs/2014ApJ...790L...8B.

Borucki, W. & Genet, R. M. 1992. The use of robotic telescopes for detecting planetary systems. In *Robotic Telescopes in the 1990s.* Ed. Filippenko, A. *ASP Conf. Series*, 34, 153, http://adsabs.harvard.edu/abs/1992ASPC...34..153B.

Boyd, L. & Genet, R. M. 1984. Automatic photoelectric telescopes at the Fairborn Observatory. In *Microcomputers in Astronomy II.* Eds. Genet, R. M. & Genet, K. Fairborn, OH: Fairborn Observatory. http://adsabs.harvard.edu/abs/1984mca2.conf....3B.

Boyd, L., Genet, R. M., & Hall, D. 1986. Automatic telescopes large and small. *PASP*, 98, 618, http://adsabs.harvard.edu/abs/1986PASP...98..618B.

Charbonneau, D., Brown, T., Latham, D., & Mayor, M. 2000. Detection of planetary transits across a sun-like star. *ApJ* 529, L45. http://adsabs.harvard.edu/abs/2000ApJ...529L..45C.

Christiansen, C. 2014. A computerized atmospheric dispersion corrector. Master's thesis, Calif. Polytechnic State Univ. In preparation, 18.

Church, R., Mohanan, K., & Genet, R. M. 2014. Speckle interferometry of Beta 321 in Lepus. *Journal of Double Star Observations.* In preparation.

Couteau, P. 1981. *Observing Visual Double Stars,* Cambridge: MIT Press. http://adsabs.harvard.edu/abs/1981ovds.book.....C.

Davison, J. W., Baptista, B. J., Horch, E. P., Franz, O., & van Altena, W. F. 2009. A photometric analysis of seventeen binary stars using speckle imaging, *AJ,* 138, 1354. http://adsabs.harvard.edu/abs/2009AJ....138.1354D.

Dupuy, T., Allen, P., Kraus, A., Biller, B., Blake, C., Davison, C., Deacon, N., Duchêne, G., Geller, A., King, R., Law, N., Nguyen, D., Reipurth, B., Winters, J., & Zhang, Z. 2013. Multiplicity of cool dwarfs. *AN,* 334, 36. http://adsabs.harvard.edu/abs/2013AN....334...36D.

Dupuy, T., Liu, M., & Ireland, M. 2012. Testing theory with dynamical masses and orbits of ultracool binaries. *ASP Conference Series,* 16. In preparation.

Eyer, L., Holl, B., Pourbaix, D., Mowlavi, N., Siopis, C., Barblan, F., Evans, D., & North, P. 2013. The Gaia mission. *CEAB,* 37, 11. http://adsabs.harvard.edu/abs/2013CEAB...37..115E.

Farrington, C., ten Brummelaar, T., Mason, B., Hartkopf, W., Mourard, D., Moravveji, E., McAlister, H., Turner, N., Sturmann, L. & Sturmann, J. 2014. Separated fringe packet observations with the CHARA array, II Omega Andromeda, HD 178911, and XI Cephei. *AJ,* 148, 48. http://adsabs.harvard.edu/abs/2014AJ....148...48F.

Foley, E. 2014. Shaped aperture masks for speckle interferometry of binaries with large differential magnitudes. Master's thesis, Calif. Polytechnic State Univ. In preparation.

Foley. E., Genet, R. M., Ridgley, J., & Rowe, D. 2015. Observations of large-delta-magnitude close binaries with shaped aperture masks. *Journal of Double Star Observations,* 1S, 173.

Genet, R. M. 2011. Telescopes from afar. *Proceedings of the Society for Astronomical Sciences 2011*. http://adsabs.harvard.edu/abs/2011SASS...30...25G.

Genet, R. M. 2013a. The Maui international double star conference. *Journal of Double Star Observations,* 2, 158. http://www.jdso.org/volume9/number2/Genet_158_169.pdf.

Genet, R. M. 2013b. Portable speckle interferometry camera system. *Journal of Astronomical Instrumentation,* 2, 134008, http://adsabs.harvard.edu/abs/2013JAI.....240008G.

Genet, R. M. & Boyd, L. 1987. The automatic photoelectric telescope service. *PASP,* 99, 660, http://adsabs.harvard.edu/abs/1987PASP...99..660G.

Genet, R. M., Johnson, J., & Wallen, V. 2010. One-semester astronomical research seminars. In *Small Telescopes and Astronomical Research.* Eds. Genet, R. M., Johnson, J., & Wallen, V. Santa Margarita, CA: Collins Foundation Press. http://www.collinsfoundationpress.org.

Genet, R. M., Rowe, D., Smith, T., Teiche, A., Harshaw, R., Wallace, D., Weise, E., Wiley, E., Boyce, G., Boyce, P., Branston, D., Chaney, K., Clark, R. K., Frey, T., Green, W., Haurberg, N., Jones, G., Kenney, J, Loftin, S., McGeison, I., Patel, R., Plummer, J., Ridgely, J., Trueblood, M., Westergren, D., & Wren, P. 2014. Kitt Peak speckle interferometry of close visual binary stars. 2014a. *Proceedings of the Society for Astronomical Sciences*, 77. http://www.socastrosci.org/images/SAS_2014_Proceedings.pdf.

Genet, R. M., Zirm, H., Rica, F., Richards, J., Rowe, D., & Gray, D. 2014b. Two new triple star systems with detectable inner orbital motions and speckle interferometry of 40 other double stars. *Journal of Double Star Observations,* 1S, 19.

Govindarajan, V. & Trimble, C. 2012. *Reverse Innovation.* Boston: Harvard Business Review Press. http://hbr.org/product/reverse-innovation-create-far-from-home-win-everyw/an/12716-HBK-ENG. http://adsabs.harvard.edu/abs/1989AJ.....98.1014H.

Hall, D. & Genet, R. M. 1988. *Photoelectric Photometry of Variable Stars,* 2. Richmond, VA: Willmann-Bell. http://adsabs.harvard.edu/abs/1988ppvs.book.....H.

Hartkopf, W., Mason, B., & Worley, C. 2001a. The 2001 US Naval Observatory double star CD-ROM. II. The Fifth Catalog of Orbits of Visual Binary Stars. *AJ,* 122, 3472. http://adsabs.harvard.edu/abs/2001AJ....122.3472H. Please see the current version at http://ad.usno.navy.mil/wds/orb6.html.

Hartkopf, W., McAlister, H., & Mason, B. 2001b. The 2001 US Naval Observatory double star CD-ROM. III. The Third Catalog of Interferometric Measurements of Binary Stars. *AJ*, 122, 3480, http://adsabs.harvard.edu/abs/2001AJ....122.3480H.

Henry, G. 1999. Techniques for automated high-precision photometry of sun-like stars. *PASP*, 111, 845, http://adsabs.harvard.edu/abs/1999PASP..111..845H.

Henry, G., Marcy, G., Butler, R., & Vogt, S. 2000. A transiting "51 Peg-like" planet. *ApJ,* 529, L41, http://adsabs.harvard.edu/abs/2000ApJ...529L..41H.

Henry, T., Monet, D., Shankland, P., Reid, M., van Altena, W., & Zacharias, N. 2009. Ground-based astrometry 2010-2020. In *Astro2010: The Astronomy and Astrophysics Decadal Survey, Science White Papers*, 120. National Academies of Science, http://adsabs.harvard.edu/abs/2009astro2010P..20H

Herald, D., Boyle, R., Dunham, D., Hirose, T., Maley, P., Timerson, B., Farris, T., Frappa, E., Lecacheux, J., Hayamizu, T., Kozubal, M., Nothenius, R., Roberts, L, & Tholen, D. 2010. New double stars from asteroidal occultations 1971 – 2008. *Journal of Double Star Observations*, 6, 88. http://www.jdso.org/volume6/number1/herald.pdf.

Herschel, W. 1803. Account of the changes that have happened, during the last twenty-five years, in the relative situation of double stars. *Phil. Trans. Royal Soc*., 93, 339. http://adsabs.harvard.edu/abs/1803RSPT...93..339H.

Hirsh, M., Harmeling, S., Sra, S., & Scholkopf, B. 2011. Online multi-frame blind deconvolution with super-resolution and saturation correction. *A&A*, 531, A9. http://adsabs.harvard.edu/abs/2011A%26A...531A...9H.

Høg, E., Fabricius, C., Makarov, V., Urban, S., Corbin, T., Wycoff, G., Bastian, U., Schwekendiek, P., & Wicenec, A. 2000. The Tycho-2 catalogue of the 2.5 million brightest stars. *A&A*, 355, L27. http://adsabs.harvard.edu/abs/2000A%26A...355L..27H.

Horch, E. 2006. The status of speckle imaging in binary star research. *RevMexAA*, 25, 79. http://adsabs.harvard.edu/abs/2006RMxAC..25...79H.

Horch, E., Howell, S., Everett, M., & Ciardi, D. 2012, Observations of binary stars with the differential speckle survey instrument IV: observations of Kepler, CoRoT, and Hipparcos stars from the Gemini North Telescope. *AJ*, 144, 165. http://adsabs.harvard.edu/abs/2012AJ....144..165H 17.

Horch, E., Reed, M., & van Altena, W. 2004. Speckle observations of binary stars with the WIYN telescope IV: differential photometry. *AJ*, 127, 1727. http://adsabs.harvard.edu/abs/2004AJ....127.1727H.

Kasdin, J., Vanderbei, R., Spergel, D., & Littman, M. 2003. Extrasolar planet finding via optimal apodized-pupil and shaped-pupil coronographs. *ApJ*, 582, 1147. http://adsabs.harvard.edu/abs/2003ApJ...582.1147K.

Knox, K. & Thompson, B. 1973. New methods of processing speckle pattern star images. *ApJ*, 182, L133, http://adsabs.harvard.edu/abs/1973ApJ...182L.133K.

Knox, K. & Thompson, B. 1974. Recovery of images from atmospherically-degraded short-exposure photographs. *ApJ*, 193, L45. http://adsabs.harvard.edu/abs/1974ApJ...193L..45K 19.

Labeyrie, A. 1970. Attainment of diffraction limited resolution in large telescopes by Fourier analyzing speckle patterns in star images. *A&A*, 6, 85. http://adsabs.harvard.edu/abs/1970A%26A.....6...85L.

Law, N., Mackav, C., & Baldwin, J. 2006. Lucky imaging: high angular resolution imaging in the visible from the ground. *A&A*, 446, 739. http://adsabs.harvard.edu/abs/2006A%26A...446..739L.

Loader, B., Asada, Y., Breit, D., Bradshaw, J., Gault, D., Hearld, D., Iverson, E., Ishida, M., Karasaki, H., Kashiwagura, M., Miyashita, K., Messner, S., Oono, T., Russell, S., Smith, G., & Talbot, J. 2010. Lunar occultation observations of known double stars - Report #1. *Journal of Double Star Observations*, 6, 176. http://www.jdso.org/volume6/number3/Loader.pdf.

Lohmann, A., Weigelt, G., & Wirnitzer, B. 1983. Speckle masking in astronomy: triple correlation theory and applications. *Applied Optics*, 22, 4028. http://adsabs.harvard.edu/abs/1983ApOpt..22.4028L.

Malkov, O., Tamazian, V., Docobo, J., & Chulkov, D. 2012. Dynamical masses of a selected sample of orbital binaries. *A&A*, 546, A69. http://adsabs.harvard.edu/abs/2012A%26A...546A..69M.

Mason, B., Martin, C., Hartkopf, W., Barry, D., Germain, M., Douglass, G., Worley, C., & ten Brummelaar, T. 1999. Speckle interferometry of new and problem HIPPARCOS binaries. *AJ*, 117, 1890. http://adsabs.harvard.edu/abs/1999AJ....117.1890M.

Mason, B., Hartkopf, W., Holdenried, R., & Rafferty, T. 2001. Speckle interferometry of new and problem Hipparcos binaries. II. Observations obtained in 1998-1999 from McDonald Observatory. *AJ*, 121, 3224. http://adsabs.harvard.edu/abs/2001AJ....121.3224M.

Mason, B., McAlister, H., & Hartkopf, W. 1996. Binary star orbits from speckle interferometry. IX. The nearby solar-type speckle-spectroscopic binary Fin 347 AA. *AJ*, 112, 276. http://adsabs.harvard.edu/abs/1996AJ....112..276M.

Mason, B., Wycoff, G., Urban, S., Hartkopf, W., Holdenried, E., & Makarov, V. 2000. Double stars in the Tycho-2 Catalogue. *AJ*, 120, 3244. http://adsabs.harvard.edu/abs/2000AJ....120.3244M.

McAlister, H. 1985. High angular resolution measurements of stellar properties. *ARA&A*, 23, 59. http://adsabs.harvard.edu/abs/1985ARA%26A..23...59M.

McAlister, H. 1999. The CHARA array on Mt. Wilson: an overview, In *Optical and IR Interferometry from Ground and Space. ASP Conference Series*, 194. http://ad.usno.navy.mil/wds/wdstext.html#neglected.

Perryman, M. 2008. *Astronomical Applications of Astrometry: Ten Years of Exploitation of the Hipparcos Satellite Data*. Cambridge: Cambridge Univ. Press. http://adsabs.harvard.edu/abs/2008aaa..book.....P.

Perryman, M. 2010. *The Making of History's Greatest Star Map*. New York: Springer.
Perryman, M., Lindegren, L., Kovalevsky, J., Hoeg, E., Bastian, U., Bernacca, P., Crézé, M., Donati, F., Grenon, M., & Grewing, M. 1997. The Hipparcos Catalogue. *A&A*, 323, L49, http://adsabs.harvard.edu/abs/1997A%26A...323L..49P.
Rowe, D. & Genet, R. M. 2015. User's guide to PS3 speckle interferometry reduction. *Journal of Double Star Observations*, 1S, 89.
Savary, F. 1830. *Connaissance des Tems pour Pan.* Paris, France: Bachelier.
Singh, G., Martinache, F., Baudoz, P., Guyon, O., Matsuo, T., & Clergeon, C. 2013. Lyot-based ultra-fine pointing control system for phase mask coronagraphs. *Proceedings of AO4ELTs3 Conference*, 12667.
Sivaramakrishnan, A., Koresko, C., Makidon, R., Berkefeld, T., & Kuchner, M. 2001. Ground-based coronography with high-order adaptive optics. *AJ*, 552, 397. http://adsabs.harvard.edu/abs/2001ApJ...552..397S.
Teiche, A., Genet, R. M., Rowe, D., Hovey, K., & Gardner, M. 2014. Automated speckle interferometry of double stars. *Journal of Double Star Observations*, 10, 342. http://www.jdso.org/volume10/number4/Genet140912.pdf.
Terziev, E., Law, N., Arcavi, I., Baranec, C., Bloom, J., Bui, K., Burse, M., Chorida, P., Das, H., Dekany, R., Kraus, A., Kulkarni, S., Nugent, P., Ofek, E., Punnadi, s., Ramaprakash, A., Riddle, R., & Tendulkar, S. 2013. *ApJS*, 206, 11. http://adsabs.harvard.edu/abs/2013ApJS..206...18T.
ten Brummelaar, T., McAlister, H., Ridgway, S., Bagnuolo, W. Jr., Turner, N., Sturmann, L., Sturmann, J., Berger, D., Ogden, C., Cadman, R., Hartkopf, W., Hopper, C., & Shure, M. 2005. First results from the CHARA Array. II, A description of the instrument. *AJ*, 628, 453.
Tokovinin, A., Mason, B., & Hartkopf, W. 2014. Speckle interferometry at SOAR in 2012 and 2013. *AJ*, 147, 123. http://adsabs.harvard.edu/abs/2014AJ....147..123T.
Tokovinin, A. & Shatskii, N. 1995. CCD observations of visual binary stars. *Astr. Ltrs.*, 21, 464.
Trueblood, M. & Genet, R. M. 1985. *Microcomputer Control of Telescopes.* Richmond, VA: Willmann-Bell. http://adsabs.harvard.edu/abs/1985mct..book.....T.
van Belle, G. & Genet, R. M. 2014. Speckle Interferometry Workshop (website), http://www2.lowell.edu/workshops/speckle2014/index.html.
Vanderbei, R., Spergel, D., & Kasdin, J. 2003. Spiderweb masks for high-contrast imaging. *AJ*, 590, 593. http://adsabs.harvard.edu/abs/2003ApJ...590..593V.
Wallace, D. 2014. Speckle interferometry of close binary stars. Master's thesis, Univ. of North Dakota.
Weigelt, G. 1977. Modified astronomical speckle interferometry "speckle masking." *OptCo*, 21, 55. http://adsabs.harvard.edu/abs/1977OptCo..21...55W.
Young, A., Genet, R. M., Boyd, L., Borucki, W., Lockwood, G., Henry, G., Hall, D., Smith, D., Baliunas, S., Donahue, R., & Epand, D. 1991. Precise automatic differential stellar photometry. *PASP*, 103, 221. http://adsabs.harvard.edu/abs/1991PASP..103..221Y.

Automated Speckle Interferometry of Double Stars

Alex Teiche[1], Russell Genet[1], David Rowe[2], Kyle Hovey[3], and Mitchell Gardner[3]

1. California Polytechnic State University, San Luis Obispo
2. PlaneWave Instruments, Rancho Dominguez, California
3. Cuesta College, San Luis Obispo, California

Automation of astronomical observations provides a number of benefits, as pointed out by Boyd and Genet (1986). These include lower operating costs because observers are not required, and lower maintenance costs because the system is rarely disturbed by humans. Although human observers are required to handle unique, one-time observations, automated systems are usually more efficient than manual systems in repetitive, well-understood situations. As humans are rarely needed, telescopes can be sited almost anywhere without much concern for site access or human comfort.

Automation was first implemented on small telescopes making photometric observations of variable stars. In these pre-CCD-camera days, a "one-pixel" photomultiplier tube was used in an aperture photometry mode—with a real, physical aperture to block the light from all but the star under observation. The early days of automated astronomy have been described by Genet (2011, 2012). Full, continuous automation began at the Fairborn Observatory in 1983 (Genet & Boyd, 1984). The early automated telescopes are described in book-length detail in *Microcomputer Control of Telescopes* (Trueblood and Genet, 1985).

Borucki and Genet (1992) proposed using automatic photoelectric telescopes to detect transiting exoplanets. The first transit was detected by Henry (1999) with an automatic photoelectric telescope at the Fairborn Observatory, with a simultaneous detection by Charbonneau et al. (1999). Borucki went on to propose and successfully lead the Kepler space telescope which discovered well over a thousand exoplanets.

Speckle interferometry observation of close double stars is a repetitious, labor intensive, fast paced procedure. As most observatories are not equipped for high-speed speckle interferometry, we developed our own portable speckle camera (Genet 2013). This camera has been used with student operators at a number of observatories, including two week-long runs on the 2.1-meter telescope at Kitt Peak National Observatory.

Gathering and processing a terabyte of data during a speckle interferometry run in an orderly, reasonably error-free manner by human operators was difficult, as explained by Teiche (2014). Our thoughts turned to semi-automation for data processing, and soon thereafter to full automation.

First automated speckle interferometry was achieved on the 0.25-meter telescope at the Orion Observatory on the night of September 12, 2014. Custom software modules written by Teiche consisted of a Run Manager, Scheduler, Database, Andor EMCCD Camera Control, and Monitor/Logger. The custom software also included interfaces to a Sidereal Technology Controller, PlateSolve 3, MaxIm DL 6, and a stepper-based slider control system. Written, but not used on this first night of automatic operation, was software that controls a filter wheel and telescope focus.

The speckle camera, described by Genet (2014), consisted of a Van Slyke instrument slider that switched the optical path between a Canon T3i acquisition camera and an Andor Luca-R EMCCD science camera. For this test run, no Barlow magnification was employed, and the filter was set to clear. The acquisition and science cameras were mechanically configured to be parfocal.

For this initial run, a number of doubles were selected from Haas (2006). Separations were 1.0 arc seconds or greater, secondary magnitudes were brighter than 9.0, and differential magnitudes were less than 3.0. This list of double stars was loaded into the database ahead of time. The scheduler automatically selected targets from this list as it observed, taking into account the distance from the meridian, proximity to the moon, slew time to the next target from the current position, and the location of the local horizon. Single deconvolution stars near the target doubles were automatically selected from a list of 118,219 Hipparcos stars.

The exposure of the Andor camera was automatically set for each target by the custom control software. The exposure algorithm adjusted the integration time and EMCCD gain until the average well fill of the brightest N pixels was within a specified range. To avoid atmospheric smearing, EMCCD gain adjustments up to a gain setting of 300 were preferred over increasing integration times. The integration time was initialized at 10ms, and increased in increments of 10ms if the full EMCCD gain for a given integration time setting was insufficient. At each integration time, all gain settings between 0 and 300 in increments of 50 were attempted. On this first run, N was set to 26214 (10% of the pixels), and the average well fill goal was set to 50%. This algorithm was found to be unreliable at low magnifications. An adaptive algorithm is being developed to address this problem.

Figure 1. System performance can be monitored from the warm room at the Orion Observatory. Alex Teiche made corrections to the software from the warm room until the system finally ran entirely on its own.

The system starts by requesting a target from the scheduler, which returns either a double star or single reference star as appropriate. The sequences of events for the two cases are identical. The system concurrently slews the telescope and moves the slider to the acquisition camera. It then uses the acquisition camera to iteratively plate solve, using PlateSolve 3 developed by Rowe, and adjusts the pointing until the target is centered to within a specified value. The autoexposure routine is run, and a FITS data cube of 512x512 pixels and 1000 frames is collected if the target is detected in the science camera. The system logs this observation to the database, and requests a new target.

The software was written in Python 2.7, with the exception of the Andor EMCCD Camera Controller which was written in Microsoft Visual C++. SQLAlchemy was used to map MySQL database entries to Python objects for the target list, run log, and catalogs. PyEphem was used to calculate the moon and meridian distance. The software ran on an x64 Windows 7 machine.

The observational files and the “run log” that points to them were designed to work smoothly in conjunction with a semi-automated reduction program (Rowe & Genet 2014). Without this link, the reduction task would be overwhelming.

We are currently developing some additional GUI interfaces, working on user documentation, and refining some of the procedures. We are confident that automation of double star speckle interferometry will begin soon at other observatories, and that sizeable, productive research projects will be undertaken that would not have been attempted with manually operated systems.

Acknowledgments

We gratefully acknowledge funding from California Polytechnic State University's Office of Research and Economic Development via its Extramural Funding Initiative for the Andor Luca R EMCCD camera and student summer salary. We also gratefully acknowledge student summer salary provided by the California Polytechnic State University's College of Engineering R-IDC pool. Andor Technologies kindly made their Luca R camera available at a reduced price. Bruce Holenstein (Gravic Inc.) and Rowe kindly helped with student summer salary. Dan Gray (Sidereal Technology) provided the control system for the telescope. Donald Westergern (Morris Ranch Observatory) repeatedly applied his in-depth knowledge of the Sidereal Control System's operation to solve problems as we headed toward full automation. Thomas C. Smith (Dark Ridge Observatory) provided many helpful suggestions on both hardware and software. John Ridgely (California Polytechnic State University) and Izak McGieson (Knox College) helped develop the software flow diagram. Don D'Egido kindly loaned the Orion Observatory the Clement focuser used to support the sizeable instrument payload. We thank the U.S. Naval Observatory for the use of their *Washington Double Star Catalog,* and the European Space Agency for use of their *Hipparcos Catalog.* Finally, we thank Vera Wallen for suggesting improvements to this manuscript.

References

Borucki, W. & Genet, R. M. 1992. The use of robotic telescopes for detecting planetary systems. In *Robotic Telescopes in the 1990's,* ASP Conference Series. Ed. Filippenko, A. 3, 153.

Boyd, L. & Genet, R. M. 1986. Automatic telescopes large and small. *Publications of the Astronomical Society of the Pacific,* 98, 618-621.

Charbonneau, D., Brown, T., Lathan, D., & Mayor, M. 2000. Detection of planetary transits across a sun-like star. *Astrophysics Journal,* 529, L45-L48.

Genet, R. M. 2011. Telescopes from afar. In *Proceedings of the Society for Astronomical Sciences*. Eds. Warner, B., Foote, J., & Buchheim, R., 25-31.

Genet, R. M. March 2012. How robotic telescopes are changing astronomy. *Astronomy Magazine,* 58-60.

Genet, R. M. 2013. Portable speckle interferometry camera system. *Journal of Astronomical Instrumentation,* 2, 1340008-14.

Genet, R. M. & Boyd, L. 1984. Automatic photoelectric telescopes. *Publications of the Astronomical Society of the Pacific,* 96, 789.

Haas, S. 2006. *Double Stars for Smaller Telescopes.* Cambridge, MA: Sky Publishing.

Henry, G., Marcy, G., Butler, P., & Vogt, S. 2000. A transiting "51 peg-like" planet. *Astrophysical Journal,* 529, L41-L44.

Rowe, D. & Genet, R. M. 2015. User's guide to PS3 speckle interferometry reduction. *Journal of Double Star Observations,* 1S, 89.

Teiche, A. 2014. Database generation for the fall 2013 Kitt Peak speckle interferometry program. *Journal of Double Star Observations,* 1S, 85.

Trueblood, M. & Genet, R. M. 1985. *Microcomputer Control of Telescopes.* Richmond: Willmann-Bell.

Observation of Large-Delta-Magnitude Close Binaries with Shaped Aperture Masks

Edward L. Foley[1], Russell M. Genet[2], John R. Ridgely[1], David Rowe[3], and Neil T. Zimmerman[4]

1. California Polytechnic State University, San Luis Obispo
2. Orion Observatory, Santa Margarita, California
3. PlaneWave Instruments, Rancho Dominguez, California
4. Princeton University, Princeton, New Jersey

Abstract In this paper, the motivation, history, mechanism of operation, and practical usage of shaped aperture masks are discussed in the context of binary star observation and discovery.

Introduction

Binary star systems are important subjects for astronomical study. Records of star separations and position angles, taken over a number of years, allow us to establish orbits and calculate the dynamical mass of binary systems via Kepler's Third Law. The dynamical mass, when coupled with other information, yields the mass of each constituent star, the single most sensitive parameter affecting stellar evolution. In close pairs with a large brightness difference, the light from the brighter star often overwhelms the light from the dimmer star. The faint stars are thus difficult to isolate, and so they are relatively under-observed.

Many of these overlooked stars are late-M stars, which are cool, faint, and red (Figure 1). The charge-coupled device (CCD) cameras used to observe these stars has low sensitivities at red wavelengths where late-M stars radiate the most energy, further exacerbating the problem (Figure 2). Recent adaptive optics (AO) observations of late-M stars showed that some mass estimates were off by a whopping factor of two or more (Dupuy et al. 2010). With accurate speckle observations and orbital analyses of a larger number of short-period binaries with late-M secondaries, we can refine our stellar evolutionary models and strengthen the conclusions we draw from them. First, however, we must discover these stars!

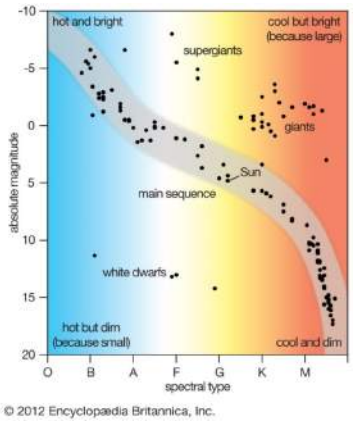

Figure 1. The Hertzsprung–Russell diagram (Encyclopædia Britanica). We are most interested in the late-M secondary stars that appear in the lower-right of the diagram.

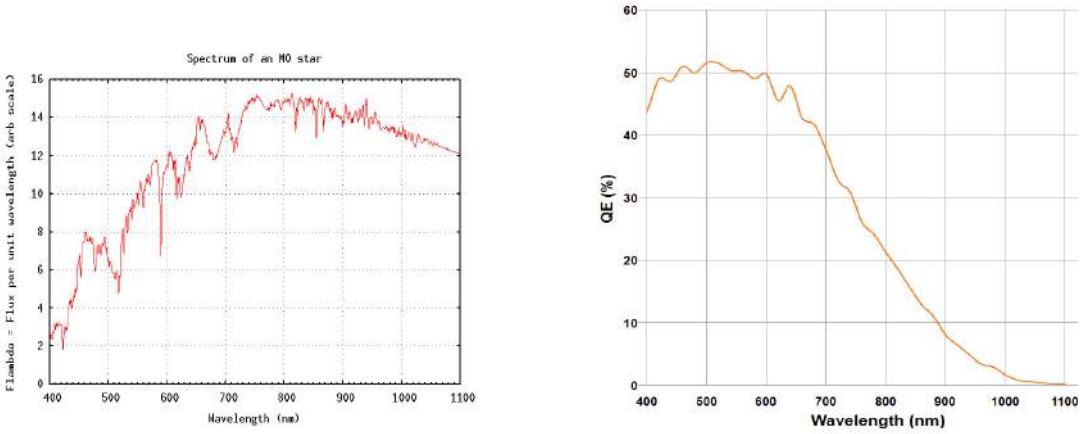

Figure 2. A typical spectrum of an M0 star (left) compared to a typical CCD sensitivity profile (right) ("Andor Luca-S 658M Specifications"; Richmond 2011). This star has significant energy output at wavelengths longer than 800 nm. The camera's sensitivity is low in this range, though the camera can still detect infrared light.

Shaped aperture masks and shaped pupil masks are innovative solutions to the double-star, large-delta-magnitude problem, and have been used successfully in practice (Debes et al. 2002; Debes & Ge 2004, Daley 2014). The masks' strategically-shaped contours diffract light in such a way that the light destructively interferes with itself in prescribed image regions. These regions, known as *discovery zones*, provide exceptional contrast. Astronomers can use this contrast to their advantage: if a telescope is centered on the primary star of a double-star system, the light from the bright primary will disperse about the image, leaving the discovery zones largely unaffected and facilitating the detection of any faint companion stars therein.

Modern pupil masks are proposed for use in exoplanet discovery and observation because of the extremely high contrast requirements of this area of research. Host stars can outshine hot Jupiters by factors exceeding 10^6 and Neptunes by factors around 10^9 (Kasdin 2014). Consequently, aperture masks must be designed with great care and machined precisely to allow such observations to take place. The inherently high contrast ratio requirements surrounding exoplanet study are an expensive barrier to entry. Luckily for smaller observatories, there is a considerable amount of science that can be performed on binary stars at more modest contrast ratios closer to 10^3—ratios that may be possible to attain without specialty equipment. Further, small, ground-based telescopes have easily accessible apertures near which a mask can be placed, as opposed to larger telescopes with available pupils further down the optical path. The terms s*haped aperture mask* and *shaped pupil mask* imply different placements, but the masks' functions are identical.

Speckle interferometry can be used with shaped masks to resolve regions within the atmospheric seeing limit; thus, these masks are theoretically capable of distinguishing stars that simultaneously have large delta magnitudes and small angular separations. There is much to learn from binary stars with magnitude differences between 3.0 and 8.0 and angular separations near the seeing limit (less than a few arc seconds). Shaped masks may enable small observatories to study stars meeting these criteria. For the same distance from Earth, more closely spaced binaries have shorter-period orbits, meaning star motion can be tracked over a shorter timeframe to arrive at meaningful orbits and mass estimates. Adaptive optics systems can be used in large observatories to replace the speckle process, but the system's higher cost is not a realistic investment for some astronomers.

The shaped masks that can be readily manufactured have azimuthally-limited discovery zones. This is not an issue during observation where the approximate position of the secondary star is known, but when it is not—as in the case of binary star discovery—one must repeatedly rotate the mask to survey the primary star's surroundings. For example, if a symmetric mask has 20 degrees of visibility on each side,

it has a 40-degree discovery window and must be positioned in at least nine different orientations to completely scan the 360-degree neighborhood of a primary star. In practice, each new discovery zone should slightly overlap the previous to avoid problems when the secondary happens to fall on a discovery zone border. Manual realignments would be slow and tedious, making the rotation of shaped masks an ideal target for automation.

Other Approaches

While we concentrate in this paper on the use of shaped aperture masks to disperse the light from the bright primary star away from a discovery zone for secondary stars, there are other approaches that have been or could be taken to observe close binary stars with large delta magnitudes. Below we discuss occulting bars, photometric systems, and Lyot stops.

Occulting Bars

One simple method of shielding dimmer stars from brighter companions is to use an occulting bar (or "dot"). Occulting bars are strips of highly-attenuating or opaque material placed at the focal plane. When this strip is aligned with the brighter star in the image, that star's light is diminished or blocked entirely within the region covered by the strip. See Figure 3 for an example.

Figure 3. Aluminum foil occulting bar applied to an eyepiece (Sinnott & Ashford 2005).

The construction of occulting bars needs not be precision science: hobbyists on online forums have used aluminum foil, toothpicks, wire, and other readily-available materials to good effect. The goal is to produce a crisp edge in the image, but this can be difficult to obtain when the occulting material has rough edges or is placed away from the plane of focus (Sinnot and Ashford 2005). Securing these materials without damage to the telescope optics can be a daunting task (Daley 2014).

The simple construction and operational principle of occulting bars are attractive, but the occulting method becomes ineffective when applied to close binaries. Because the strip attenuates only the most direct light but does nothing about halos from bright stars, light from dim secondaries can still be overwhelmed, even when the telescope is perfectly aligned. Worse, the jitter of atmospheric seeing prevents continuous perfect alignment: depending on the arrangement of the visual cell artifacts at any moment, primary light may escape the occulted region or secondary light may enter it.

Shaped masks do not have this problem because they have the power of spatial convolution on their side. As explained further in the "Shaped aperture masks" section, the diffraction patterns caused by telescope apertures will appear *locally* at each point of light. Effectively, shaped masks perform their function without regard to light position. Occulting bars, on the other hand, are highly sensitive to light position.

Photometric Systems

Photometric systems employ filters that transmit light over only a particular range of wavelengths. For example, a filter designed to exclusively transmit infrared light would attenuate or remove shorter-wavelength visible light. The transmission profile of this filter would resemble that of Figure 4. This filter would allow better visibility for secondary stars emitting light at longer wavelengths if they are coupled with primary stars emitting light at shorter wavelengths.

Infrared-pass filters remove a significant portion of the light at the wavelengths that CCD cameras are most sensitive to (see Figure 5); thus, while the filters are effective at emphasizing red stars over blue stars, the amount of usable light is reduced dramatically. The combined effect of the infrared filter of Figure 4 and CCD sensitivity profile of Figure 5 is shown in Figure 6 for two stars: a 10,000-kelvin A-type star and a 3,000-kelvin M-type star.

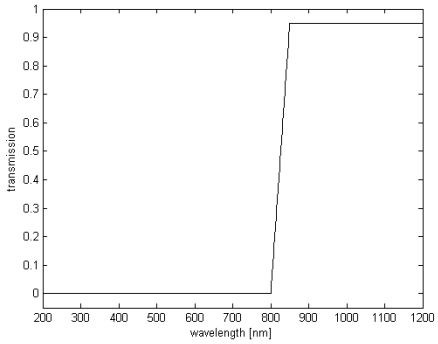

Figure 4. Example transmission profile of a filter designed to transmit infrared light.

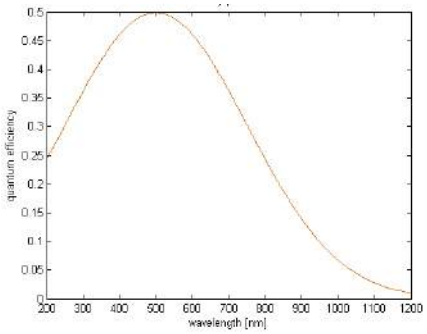

Figure 5. Approximate sensitivity profile of a CCD camera, modeled as a Gaussian distribution. Compare with Figure 2.

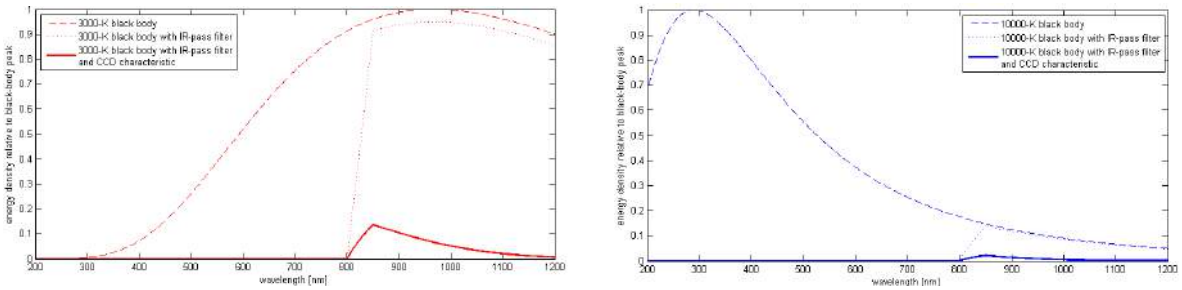

Figure 6. The effects of an infrared filter and CCD transmission profile on a 10,000-kelvin black body (right) and a 3,000-kelvin black body (left). Note how the combination of the IR-pass filter and poor CCD sensitivity removes nearly all of the original energy from the 10,000-kelvin star but not the 3,000-kelvin star.

When applied to binary systems with significantly dissimilar spectral classes, photometric systems can be effective and relatively inexpensive. They also benefit from the ability to be combined in series with other equipment such as occulting bars and shaped masks. Of course, the usefulness of photometric systems is limited when stars have nearly the same color.

Lyot Stops

Lyot stops are masks that are shaped to block unwanted diffracted light caused by some obstruction in the optical train. In the context of coronography, this obstruction is typically a central occulting dot that is intended to block primary light at the center of the field of view. The dot causes a diffraction pattern whereby the central light is effectively relegated to a circular fringe. The Lyot stop then blocks a large portion of this fringe. The net result is highly attenuated primary light and high contrast for off-axis elements such as stars and exoplanets. This process is diagrammed in Figure 7.

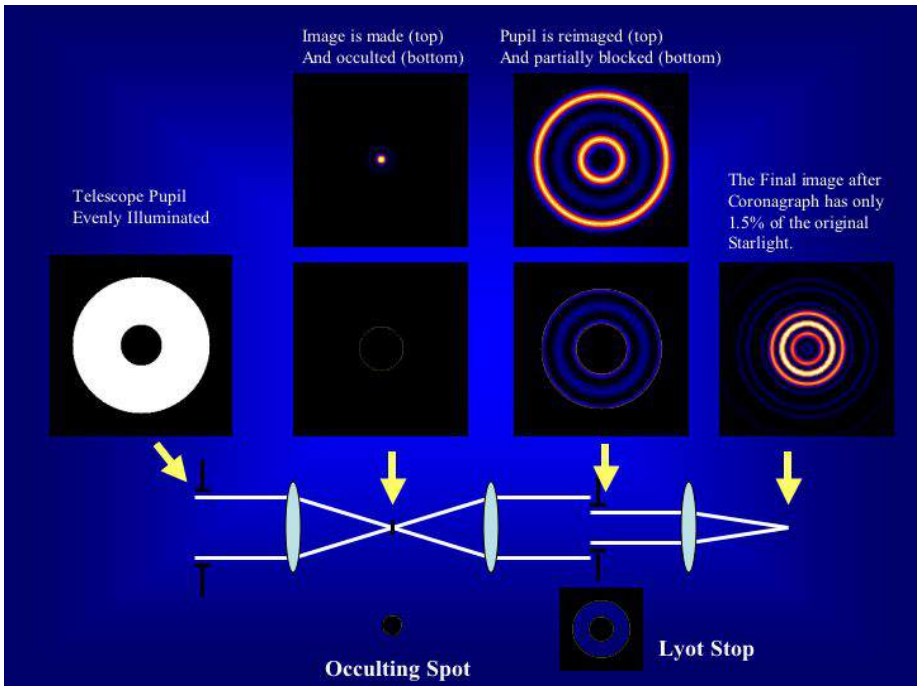

Figure 7. An overview of Lyot stops' mechanism of operation (Oppenheimer 2003, adapted from Sivaramakrishnan et al. 2001).

Lyot stops fall victim to the same problems that occulting bars have: they cannot guard against atmospheric seeing effects themselves. Instead, an expensive adaptive optics system is required to reverse the atmospheric distortion and keep light in the same location in the image plane.

Shaped Aperture Masks

Shaped aperture masks are obstructions placed at telescope apertures that are machined into shapes that strategically diffract light away from discovery zones in the image. Standard circular apertures will produce interference patterns in the shape of Airy rings (Figure 8), but shaped apertures—whose forms are often generated using numerical methods—can yield complicated diffraction patterns that defy concise mathematical representation. Because the discovery zones are spared the vast majority of the light produced by the primary star, secondary stars should be easier to spot in these regions than they would be without a mask.

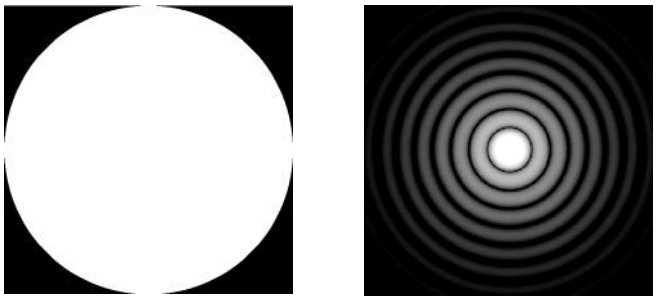

Figure 8. A simple circular aperture (left) and the Airy disc diffraction pattern it creates (right), plotted on a nonlinear brightness scale

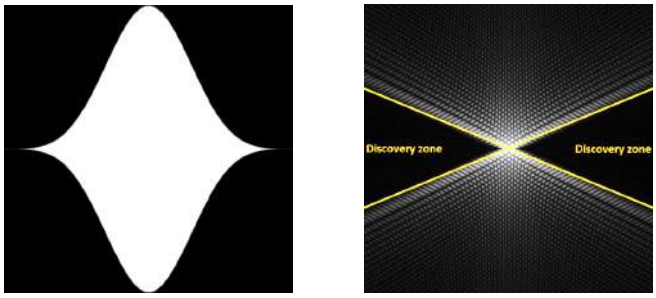

Figure 9. Left: A reproduction of a mask developed by Kasdin et al. (2003) based on the generalized prolate spheroidal wave function proposed as an apodization function by Slepian (1965). Right: The characteristic diffraction pattern, plotted on a nonlinear scale. The discovery zones are marked.

Figure 9 shows an aperture mask in the shape of a Gaussian curve reflected about the horizontal axis. This shape was derived by Kasdin et al. (2003) based on prior work by Slepian (1965).

The power spectrum is the diffraction pattern we would expect for a single, infinitesimally small point of concentrated light. When multiple points of light are imaged, a superposition of these diffraction patterns is visible in spatial agreement with the points of light themselves (see Figure 10). It is important to note that this superposition is not linear with respect to intensity because of the imaginary components of the original Fourier transform.

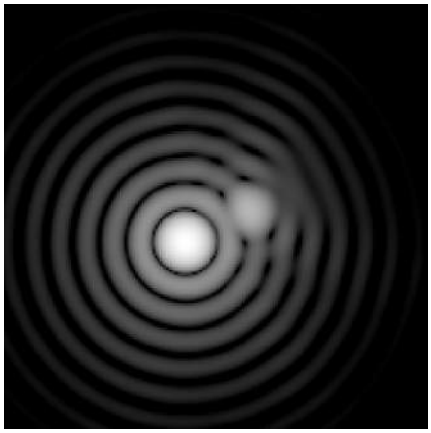

Figure 10. When imaging two points of light, the diffraction patterns superimpose themselves in the complex domain. This is a simulated Airy pattern formed by two nearby points of light at different brightnesses, shown on a nonlinear intensity scale.

In realistic usage conditions, the incoming light is not arranged into neat points but rather into distributed regions caused by atmospheric diffusion and other distortion effects. In this case, the convolution of the distributed regions with the nominal PSF will smear the output pattern. Thus, we cannot expect our mask-aided astronomical images to match the theoretical results perfectly. Only the more prominent features of the nominal pattern, such as the aforementioned discovery zones, will still be visible.

Telescope obstructions will cast their own diffraction patterns, so special care must be taken to avoid compromising a mask's beneficial effects. Consider a Gaussian mask applied to a telescope with a secondary mirror (Figure 11). The intended diffraction pattern of Figure 9 is present, but so too is the Airy pattern of Figure 8. The obstruction eliminates our discovery zones!

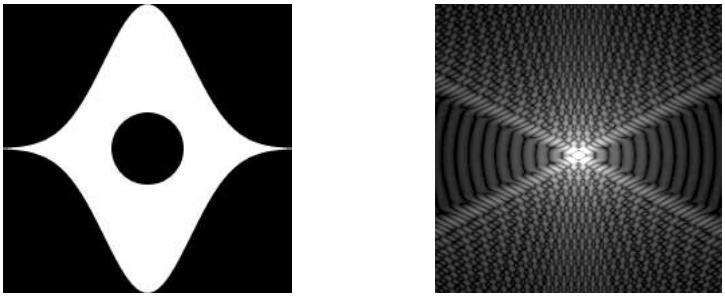

Figure 11. The combination of a Gaussian mask with an unaltered central obstruction (left) leads to an undesirable diffraction pattern (right), plotted on a nonlinear brightness scale.

There are at least two ways to address this problem. One might design a mask with multiple small apertures placed such that they do not overlap the central obstruction. Alternatively, one might reshape the obstruction by covering it with a shaped occulter that casts a similar diffraction pattern as the aperture itself (Figure 12). The throughput will be reduced, but more importantly, the diffraction pattern will retain its discovery zones. As mentioned in "History" below, Carlotti et al. (2011) present an optimal, though perhaps less intuitive, method of handling central obstructions.

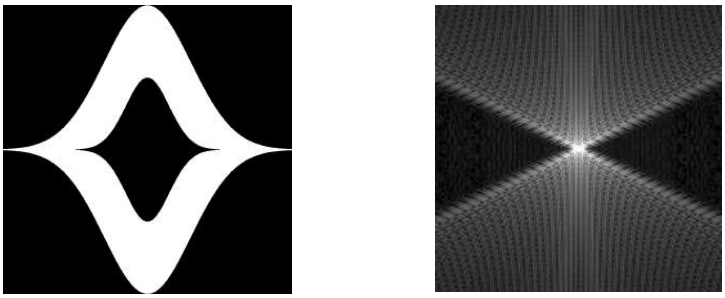

Figure 12. Covering the obstruction with a secondary Gaussian shape (left) restores a usable diffraction pattern (right), plotted on a nonlinear brightness scale.

History

The first aperture masks had simple geometries. In the 1830s, John Herschel used an equilateral triangular opening (Figure 13) to observe double stars while surveying the southern sky at the Cape of Good Hope (Herschel 1847). This shape tends to distribute points of light along six flanges of an image (Smith and Marsh 1974) and allows better visibility of faint companion stars. Edward Emerson Barnard built upon Herschel's work by developing a hexagonal mask (Figure 14) in the early 20th century that yields a similar six-flanged pattern (Sheehan 1995; Smith and Marsh 1974).

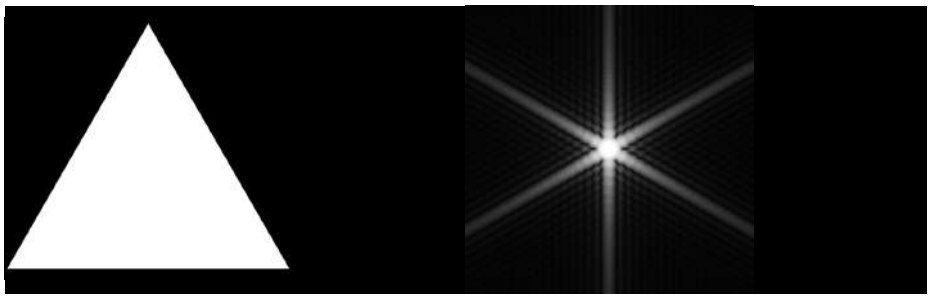

Figure 13. An equilateral triangle aperture (left) and its characteristic diffraction pattern (right), plotted on a nonlinear brightness scale.

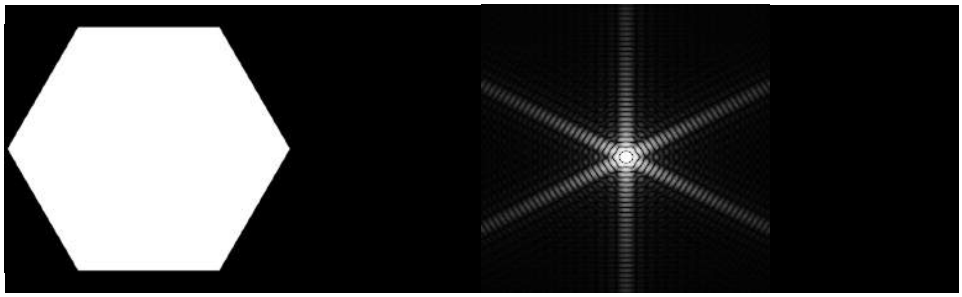

Figure 14. A regular hexagon aperture (left) and its characteristic diffraction pattern (right), plotted on a nonlinear brightness scale.

Mask designs advanced as the mathematics to describe wave interference advanced. David Slepian proposed a prolate spheroidal wave function as an apodization function in the 1960s (Slepian 1965). Unlike a shaped mask that uses a binary transmission profile, Slepian's apodizer had a transparency gradient, with some regions more opaque and others more transparent. Indeed, he never discussed a shaped pupil mask (Kasdin 2014). Only in the early 2000s did David Spergel and Jeremy Kasdin adapt Slepian's work into mask shapes such as the one in Figure 9.

Robert Vanderbei, Jeremy Kasdin, and David Spergel made further mask design advances in the early 2000s by using complex numerical techniques. Their masks, formed at the hands of mathematical theory, take on rather unusual shapes such as those seen in Figure 15 (Kasdin et al. 2003). Other proposed masks comprise concentric ring obstructions (Figure 16) (Vanderbei et al. 2003a) and intricate checkerboard patterns (Figure 17) (Vanderbei et al. 2004). Many of these complex masks would not be possible to manufacture with conventional construction methods due to their lack of full structural connectivity. Vanderbei, Kasdin, and Spergel recognized the construction difficulties (Kasdin et al. 2003) and developed a subset of masks following additional mathematical constraints to ensure their manufacturability (Vanderbei et al. 2003b).

Alexis Carlotti later joined Vanderbei and Kasdin to develop optimal apodization functions for masks to be used in the presence of arbitrary telescope obstructions and aperture shapes (Carlotti et al. 2011). Thus, even if some incoming light is blocked by a secondary mirror or a spider support structure, an optimal mask shape can still be calculated numerically. For example, Carlotti et al. (2011) derived an optimal mask for the unique mirror and support structure of the James Webb Space Telescope (Figure 18). The mask and its diffraction pattern are shown in Figure 19.

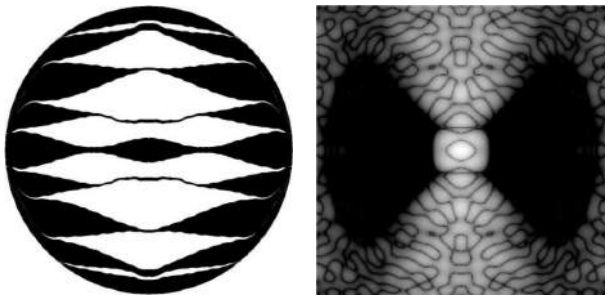

Figure 15. Left: One mask proposed by Kasdin et al. (2003). Some walls are thin, but the mask does have complete structural connectivity. Right: The mask's characteristic diffraction pattern (Kasdin et al. 2003), plotted on a nonlinear brightness scale. Note how the discovery zones are limited both by azimuth angle and radius.

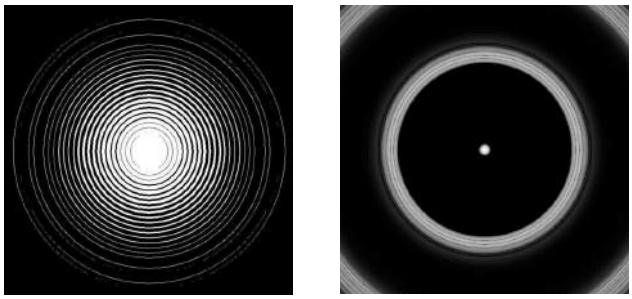

Figure 16. Left: A mask comprised of concentric annular openings (Vanderbei et al. 2003a). Right: The mask's characteristic diffraction pattern (Vanderbei et al. 2003a), plotted on a nonlinear brightness scale.
Note how the pattern is not azimuthally limited.

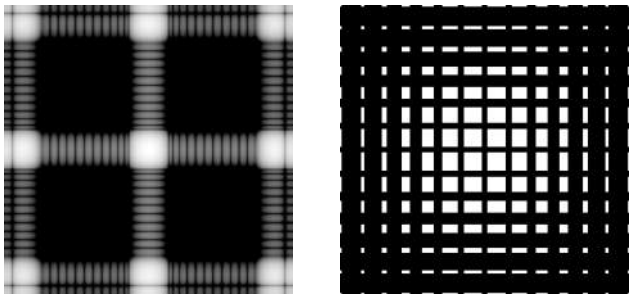

Figure 17. Left: A checkerboard mask (Vanderbei et al. 2004). Right: The mask's characteristic diffraction pattern (Vanderbei et al. 2004), plotted with a nonlinear brightness scale. The bright "struts" of the PSF intersect to form especially bright points, insulating the remaining square regions from light's influence.

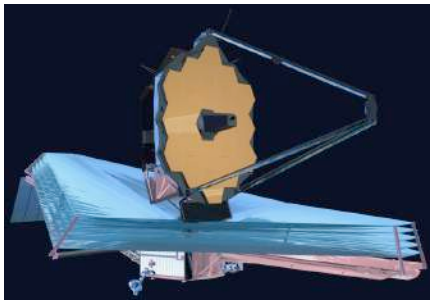

Figure 18. The James Webb Space Telescope (*NASA.gov*).

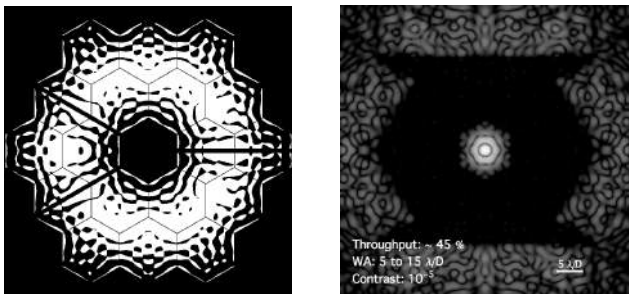

Figure 19. Left: A mask Carlotti et al. (2011) optimized for the James Webb Space Telescope of Figure 18. Note how the mask accounts for the hexagonal shapes in the primary mirror, the central obstruction caused by the secondary mirror, and the structure supporting the secondary. Right: The mask's characteristic diffraction pattern, plotted on a nonlinear intensity scale (Carlotti et al. 2011).

The aforementioned masks operate entirely on the amplitudes of the frequency components. Other scientists, including Rouan et al. (2000) and Haguenauer et al. (2006), have proposed phase masks that shift the phase of the incoming light to achieve a similar effect as the amplitude masks. While these phase-shift masks work very well in simulations, their physical realization presents fabrication challenges, typically involving the formation of a glass plate with a precise thickness profile. These challenges lead to a high cost.

Today, shaped masks are proposed for use in exoplanet discovery and observation, a field concerning delta magnitudes even more extreme than those of large-delta-magnitude close binary systems. The masks described above are designed for high contrast ratios ranging from 10^5 to 10^{10} and are "baselined for an upcoming mission" (Kasdin 2014).

Practical Usage

Masks influenced by Slepian (1965) and the subsequent developments by Vanderbei, Kasdin, and Spergel have already been used by a number of astronomers. Daley (2014) constructed a Gaussian mask (Figure 9) out of a manila folder affixed to plywood and combined it with a highly-attenuating occulting strip. His results for Sirius and its faint double—stars differing by 9.96 stellar magnitudes and separated by 9.66 arcseconds—are seen in Figure 20. Note how the secondary star is clearly seen in the discovery zone (rotated approximately 90 degrees from Figure 9) and how the occulting strip further reduces interference from the bright primary. The angular separation between the stars is larger than the seeing limit. Speckle interferometry techniques would have allowed even closer stars to be identified.

Debes et al. (2002) used a mask with multiple Gaussian apertures (Figure 21) to study binary stars, including μ Her A (Figure 22), with Mt. Wilson's 100-inch telescope. Debes et al. (2002) estimated the star separation of μ Her A as 1.3 ± 0.2 arcseconds. In prior observations, Turner et al. (2001) found the magnitude difference to be 9.29 in R-band and 7.26 in I-band.

These observations at Mt. Wilson were "the first attempt at high-contrast imaging with a [Gaussian aperture pupil mask]" (Debes et al. 2002). The group commented on the "relative ease and speed with which these first masks [were] produced" and described the technology as "promising," but they did acknowledge some difficulties, largely those caused by "imperfect atmospheric correction, scattered light in the telescope, and a diffuse thermal background" (Debes et al. 2002). Their mask's imperfect diffraction pattern is compared with the theoretical diffraction pattern in Figure 23.

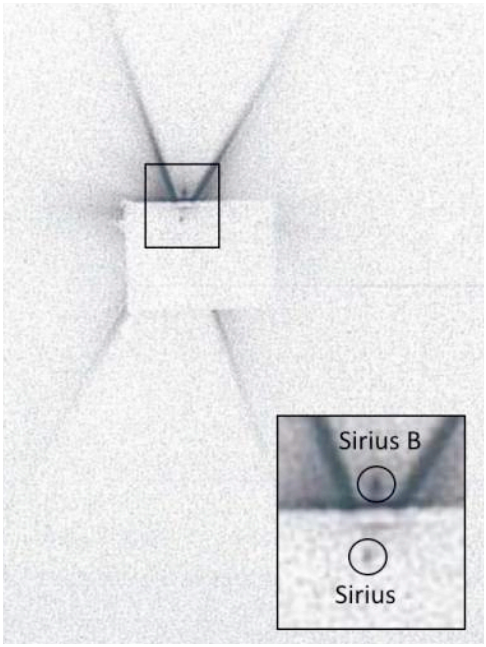

Figure 20. CCD image of AGC 1AB (Sirius) acquired by Daley (2014) using a shaped aperture mask of the design shown in Figure 9, coupled with a thin foil occulting strip. The image is black–white inverted and a portion has been copied and enlarged for clarity. The dot of light contained within the light rectangular region is the attenuated primary star (Sirius); the dot immediately above is the secondary (Sirius B).

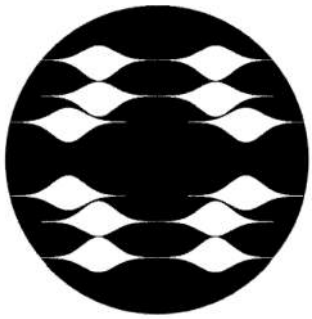

Figure 21. The mask used by Debes et al. (2002) on Mount Wilson's 100-inch telescope.

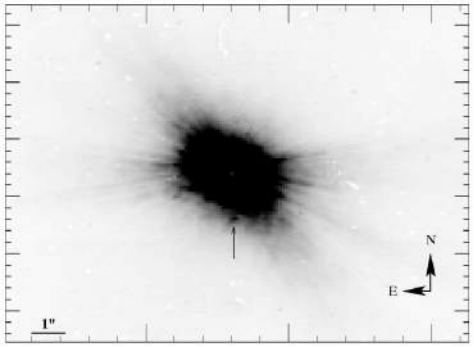

Figure 22. The result obtained by Debes et al. (2002) for μ Her A using the mask of Figure 21 at Mount Wilson's 100-inch telescope. A faint companion is visible at the small arrowhead toward the image's center.

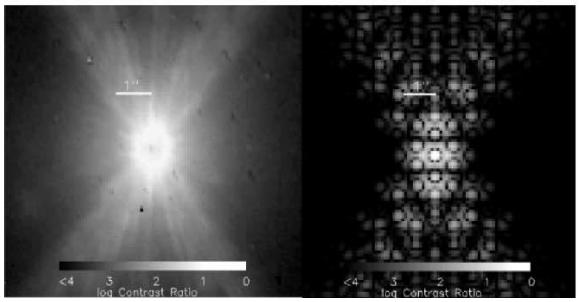

Figure 23. Obtained diffraction pattern (left) compared to theoretical diffraction pattern (right) for the observations performed by Debes et al. (2002) on ε Eridani. Intensity is plotted on a nonlinear scale.

The Mt. Wilson telescope has a secondary mirror and a structure to support it that both obstruct the optical path. Debes et al. (2002) used multiple Gaussian openings placed about the center of the telescope to avoid these obstructions. Debes and Ge demonstrated the merits of this Gaussian array approach over other possible configurations in a subsequent paper (Debes & Ge 2004).

Aperture Masks for a Schmidt–Cassegrain Telescope

Secondary mirrors are not unique to large telescopes. Consider the more modestly sized Celestron C11 Schmidt–Cassegrain telescope of Figure 24 which the authors will use to evaluate mask performance on smaller apertures. The circular obstruction caused by the secondary mirror accounts for over one third of the diameter of the primary mirror. Figure 25 shows the aperture shape and its default diffraction pattern. The PSF somewhat resembles an Airy disc because of the aperture's azimuthal symmetry.

Figure 24. The aperture of the Celestron C11 Schmidt–Cassegrain telescope. Note how the secondary mirror embedded in the corrector plate obstructs the aperture.

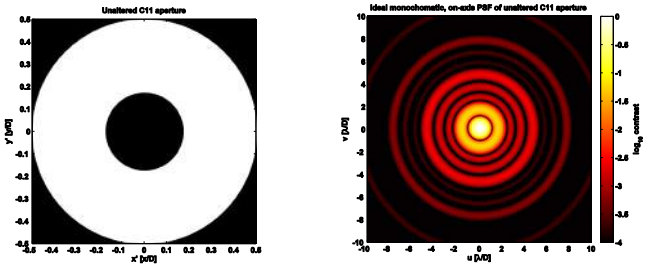

Figure 25. The unaltered C11 aperture (left) and its characteristic diffraction pattern (right), plotted on a nonlinear scale. Black regions have theoretical contrast ratios better than 10–4, equivalent to 10 stellar magnitudes.

Double Gaussian Mask

One simple mask design comprises a Gaussian outline with a Gaussian obstruction in the center akin to Figure 12. The central shape is just large enough to cover the secondary mirror cap. The mask's diffraction pattern, scaled to a small angular window, is seen in Figure 26.

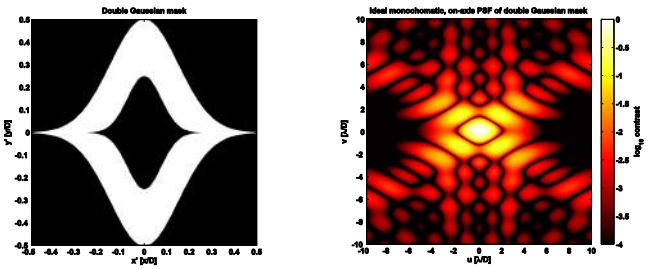

Figure 26. A Gaussian mask with a Gaussian obstruction large enough to cover the secondary mirror cap (left), and the mask's theoretical diffraction pattern (right), plotted on a nonlinear scale. Note the excellent contrast toward the left and right of the pattern.

This design achieves very deep contrast, but it does so at a relatively large angular distance from the center of the diffraction pattern. We would willingly sacrifice some contrast for a smaller inner working angle (IWA). For this, we resort to numerical optimization.

Optimization Overview

Based on the measurements by Foley, we start with an 11-inch circular telescope pupil with a 36% circular obstruction in the center. To be conservative with the alignment tolerance, we slightly oversize this obstruction. (The actual diameter ratio measured by Foley is $\frac{3.811\text{ in}}{11\text{ in}} = 0.346$.)

The project is aiming for contrast ratios between 7 and 6 astronomical magnitudes (equivalently, in base 10 logarithms the range is –2.8 to –2.4, and in terms of linear ratios, 630 to 250), and as small an inner working angle (IWA) as possible. For reference, observing at a wavelength of 550 nm with an 11-inch aperture, the λ/D diffraction width is

$$\frac{\lambda}{D} = \left(\frac{550\times10^{-9}\text{ m}}{11\text{ in}}\right)\left(\frac{1\text{ in}}{2.54\text{ cm}}\right)\left(\frac{100\text{ cm}}{1\text{ m}}\right)\left(\frac{360^\circ}{2\pi\text{ rad}}\right)\left(\frac{3600\text{ as}}{1^\circ}\right)$$

$$\rightarrow \boxed{\frac{\lambda}{D} = 0.406\text{ as}}$$

Also note, from here on out we describe contrast in base-10 logarithms, including the plots. There are two classes of shaped pupil solutions we explored. First, circular solutions that create full annular (360-degree) dark zones around the star (Vanderbei et al. 2003). Second, shaped pupils that create dark zones confined to symmetric bowtie-shaped wedges on opposite sides of the star PSF. The telescope pupil has two-fold symmetry (x and y). Therefore, for efficiency, the shaped pupil can be optimized on one quadrant of the image plane and retain the desired symmetry in the pupil (after Carlotti et al. 2013).

Circular (Concentric Ring) Solutions

Even for the modest contrast we aim for, we hit a wall trying to reach any circular solution with inner working angle below $2.4\,\lambda/D$. When we fix the inner working angle (IWA) to $2.4\,\lambda/D$ and the contrast constraint to 10^{-3} (deeper than the survey spec), we get the shaped pupil mask, PSF, and radial contrast cut shown in Figure 27. Note that in the mask diagram, the bright (yellow) pixels represent the transparent parts, while dark pixels are opaque.

We also plotted the radial contrast curve of the open C-11 aperture (open circle with 36% central obstruction) as a reference. It is evident that at angular separations above about $2.2\,\lambda/D$, the ideal telescope PSF is already meeting and exceeding the contrast spec of the binary star survey.

The circular mask optimization program has no trouble creating deep contrast above angular separation $2.4\,\lambda/D$. However, it remains to be seen whether seeing-limited speckle interferometry observations can take advantage of such large "ideal" wavefront contrast gains. This, combined with difficulty of fabricating two free-standing obstructing rings, make this type of mask difficult to recommend for the project.

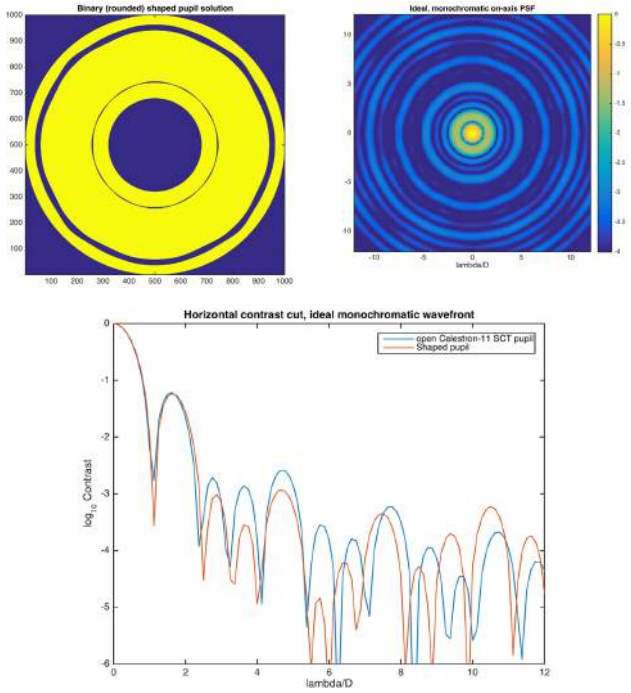

Figure 27. A concentric ring mask (top-left), its PSF (top-right), and a radial contrast cut (bottom).

Solutions with Bowtie-Shaped Search Zones

When the optimization program constrains the contrast only below some fixed polar angle in the image quadrant, the result is a mask with a bowtie-shaped search zone. With 90-degree wedges, by trial and error we found that the inner working angle has an absolute lower limit of $1.2\,\lambda/D$ (0.5 as at 550 nm). For a contrast goal of$10^{-2.7}$, the solution is simply two large obstructions. Each obstruction is connected to either the interior or exterior edges of the aperture. At larger contrasts, for example $10^{-3.0}$, the mask geometry becomes more complicated, with more free-standing islands, and the fraction of open area drops. In Figure 28, we show the shaped pupil solution, PSF, and horizontal contrast cut for the $1.2\,\lambda/D$ IWA, $10^{-2.7}$ contrast design.

As the contrast curve (measured in the horizontal cut extending from the center of the image) shows, this shaped pupil pushes down the first sidelobe of the ideal telescope PSF by over an order of magnitude. Therefore, it may offer a significant boost in the binary star target sample available to the telescope. The relatively simple mask layout is another compelling feature.

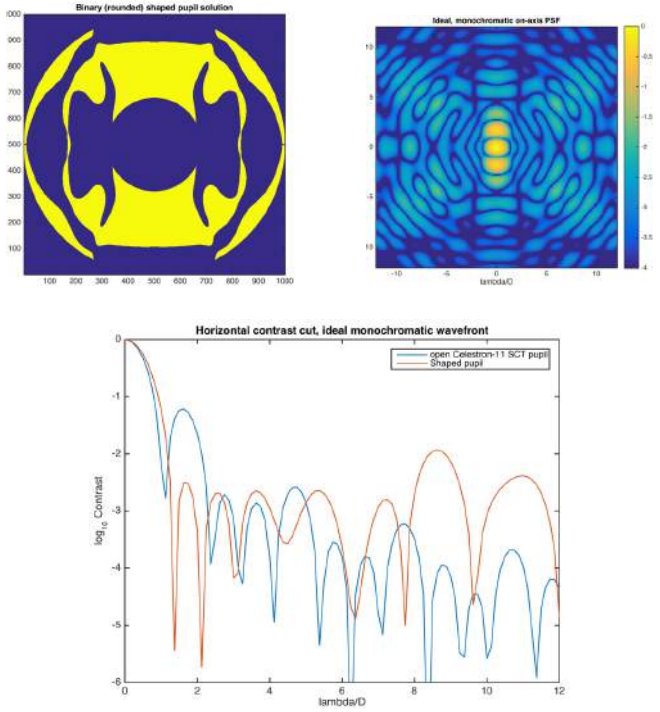

Figure 28. A bowtie mask (top-left), its PSF (top-right), and a horizontal contrast cut (bottom).

Considering its simple shape alongside its strong performance, the bowtie mask is a good choice to pursue alongside the double Gaussian mask. The double Gaussian mask has deep contrast but a large inner working angle; the bowtie mask has somewhat less contrast but a very small inner working angle. The two complement one another well and should elucidate whether contrast or inner working angle is easier to maintain in practice.

Testing

With two qualified mask designs, the next step is to construct the masks and perform basic tests to ensure the shaped-aperture approach is viable. The bowtie mask shows great promise in simulations, but we choose to begin with the double Gaussian mask because of its particularly distinctive hourglass-shaped diffraction pattern. The double Gaussian mask, cut out of 1/8-inch-thickness newsboard material with the aid of a laser cutter, is seen attached to the C11 in Figure 29. A beam had to be added across the center of the mask for structural contiguity. This beam contributes a vertical spike to the diffraction pattern.

Rowe simulated the results from this configuration with his Atmospheric Seeing Distortion program (ASD), which takes into account atmospheric phase distortion and camera sensitivity as it performs speckle interferometry on simulated images. Figure 30 shows the simulated autocorrelation result of a binary star system before and after the application of the double Gaussian mask.

Speckle interferometry contains an autocorrelation step that appears to form direct images of the stellar system, but this similarity is an illusion. The process duplicates the stars' combined diffraction pattern, producing bright points of light that outnumber the actual stars in view. Still, the angle and separation of stars can be determined—in this case, measured from the center of the image to one of the two bright points of light on the horizontal axis. These bright points are more distinct with the simulated mask than without it, making the measurement more robust and suggesting that the physical mask may improve practical measurements in a similar fashion.

Figure 29. The double Gaussian mask applied to the Celestron C11 telescope. The mask's outer gear teeth are designed to interface with an automatic rotation mechanism (not pictured).

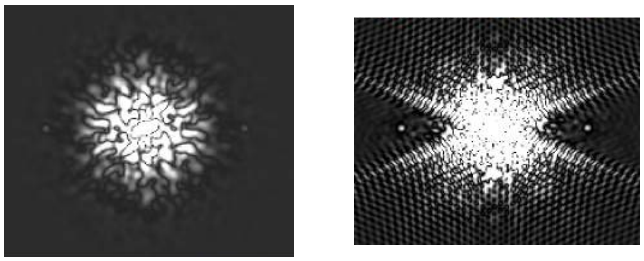

Figure 30. Rowe's simulated speckle interferometry results for a synthetic binary system viewed without a mask (left) and with a double Gaussian mask (right).

Jimmy Ray performed the double Gaussian mask's first test, in which he observed Rigel and its companion, Rigel B (Figure 31). The expected hourglass shape is quite visible, with notably dark discovery zones toward the image's left and right sides. The test confirms the mask's basic functionality.

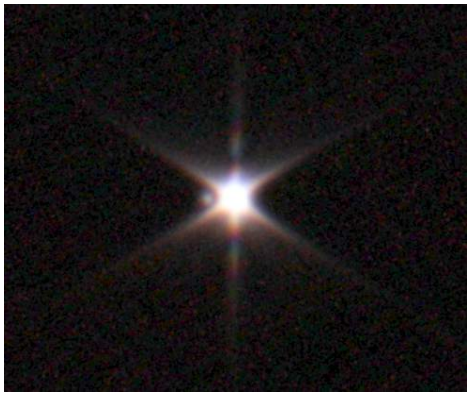

Figure 31. Rigel as captured by Ray using a double Gaussian mask. Rigel B, in Rigel's discovery zone, is visible just to the left of center. This image does not use speckle interferometry.

Rigel and Rigel B were an easy target because they were separated by 9 arcseconds. Future tests will explore the resolving capacity of the double Gaussian mask as well as the bowtie mask. We will use a CCD camera with speckle interferometry as we work toward progressively more challenging targets. It is our hope that these masks will prove to enhance the ability of small, ground-based telescopes to observe binary stars.

Acknowledgements

We wish to extend our thanks to Jimmy Ray for performing our astronomical testing and enthusiastically supporting the project; to Jeremy Kasdin for providing crucial feedback on an early version of this paper; to James Daley for sharing his hands-on experience with aperture masks; and to Robert Argyle for contributing sources that would otherwise be very hard to find. We also thank the faculty and staff of California Polytechnic State University for facilitating this research and supporting the scientific process through the University's "learn by doing" philosophy. Genet thanks California Polytechnic State University Office of Research and Economic Development for support through their Extramural Funding Initiative, and the W. M. Keck Foundation for support through the Concordia University Undergraduate Education Program. We all thank Vera Wallen for editorial suggestions.

References

2008. Andor Luca-S 658M specifications. *Andor Technology*.

Carlotti, A., Vanderbei, R., & Kasdin, J. 2011. Optimal pupil apodizations of arbitrary apertures for high-contrast imaging. *Journal of the Optical Society of America.*

Carlotti, A., Kasdin, J., Vanderbei, R., & Delorme, J. R. 2013. Optimized shaped pupil masks for pupil with obscuration. *Society of Photo-Optical Instrumentation Engineers (SPIE) Conference Series*, 8442.

2013. Cost estimate of the James Webb space telescope. NASA.gov.

Daley, J. 2014. LSO double star measures for the year 2012. *Journal of Double Star Observations*, 10, 136–138.

Debes, J., Ge, J., & Chakraborty, A. 2002. First high-contrast imaging using a Gaussian aperture pupil mask. *The Astrophysical Journal*, 572, L165–L168.

Debes, J. & Ge, J. 2004. High-contrast imaging with Gaussian aperture pupil masks. *Publications of the Astronomical Society of the Pacific*, 116(821), 674–681.

Dupuy, T., Liu, M., Bowler, B., Cushing, M., Helling, C., Witte, S., & Hauschildt, P. 2010. Studying the physical diversity of late-m dwarfs with dynamical masses. *The Astrophysical Journal*, 721(2), 1725–1747.

Haguenauer, P., Serabyn, E., Mennesson, B., Wallace, J., Gappinger, R., Troy, M., Bloemhof, E., Moore, J., & Koresko, C. 2006. Astronomical near-neighbor detection with a four-quadrant phase mask (FQPM) coronagraph. *SPIE Proceedings*, 62651G.

Hecht, E. 2002. *Optics*, 4. Reading, MA: Addison-Wesley, 540.

Herschel, J. 1847. Results of astronomical observations made during the years 1834, 5, 6, 7, 8, at the Cape of Good Hope; being the completion of a telescopic survey of the whole surface of the visible heavens, commenced in 1825. London: Elder Smith, 165.

2012. Hertzsprung–Russell diagram. *Encyclopaedia Britannica*.

Kasdin, J. 2014. Speckle, masks, and adaptive optics for large delta magnitudes. E-mail.

Kasdin, J., Vanderbei, R., Spergel, D., & Littman, M. 2003. Extrasolar planet finding via optimal apodized-pupil and shaped-pupil coronographs. *The Astrophysical Journal*, 582, 1147–1161.

Oppenheimer, B. 2003. Coronography, American Museum of Natural History.

Richmond, M. 2011. Continuous spectra. Rochester Institute of Technology. Web. Licensed under Creative Commons license CC BY-NC-SA 2.0.

Rouan, D., Riaud, P., Boccaletti, A., Clénet, Y., & Labeyrie, A. 2000. The four-quadrant phase-mask coronagraph. *Publications of the Astronomical Society of the Pacific*, 112, 777, 1479–1486.

Sheehan, W. 1995. Disappointments and triumphs. In *The Immortal Fire Within: The Life and Work of Edward Emerson Barnard.* Cambridge: Cambridge University Press, 347.

Sinnot, R. & Ashford, A. 2005. The martian moons in 2007–08. *Sky and Telescope.*

Sivaramakrishnan, A., Koresko, C., Makidon, R., Berkefeld, T., & Kuchner, M. 2001. Ground-based coronography with high-order adaptive optics. *The Astrophysical Journal*, 552, 397–408.

Slepian, D. 1965. Analytic solution of two apodization problems. *Journal of the Optical Society of America*, 55, 9, 1110–1114.

Smith, R. & Marsh, J. 1974. Diffraction patterns of simple apertures. *Journal of the Optical Society of America*, 64, 6, 798–803.

Turner, N., ten Brummelaar, T., McAlister, H., Mason, B., Hartkopf, W., & Roberts, L Jr. 2001. Search for faint companions to nearby solar-like stars using the adaptive optics system at Mount Wilson Observatory. *The Astronomical Journal*, 121, 3254–3258.

Vanderbei, R., Spergel, D., & Kasdin, J. 2003a. Spiderweb masks for high-contrast imaging. *The Astrophysical Journal*, 590, 593–603.

Vanderbei, R., Spergel, D., & Kasdin, J. 2003b. Circularly symmetric apodization via star-shaped masks. *The Astrophysical Journal*, 599, 686–694.
Vanderbei, R., Kasdin, J., & Spergel, D. 2004. Checkerboard-mask coronagraphs for high-contrast imaging. *The Astrophysical Journal*, 615, 555–561.

Measurements of Double Stars Using a 280 mm Reflector and an EM-CCD: 2014-2015 Report

Jocelyn Sérot
Observatory Clermon-Ferrand, France

Abstract This paper presents the measurements of 296 visual binary stars obtained between October 2014 and July 2015 with an 11" reflector telescope and an EM-CCD camera, using speckle interferometry.

Introduction

Following the work described by Serot (2011a, 2011b, 2014), we present the measurements of 296 visual binary stars obtained between Oct 2014 and Jul 2015 with an 280 mm reflector telescope and an EM-CCD camera. The total number of measurements was 307, with magnitudes and separation ranging between 2.5 and 13.6 and 0.4″ and 25″ respectively.

Equipment

The telescope used for the reported measurements was a 280 mm Schmidt-Cassegrain reflector (Celestron C11). The observatory is located in a garden, protected by a roll-off shed (Figure 1) at the periphery of Clermont-Ferrand, a mid-sized town in the center of France (45°47'N Lat., 3°04'E Long.).

The camera was a Raptor Kite EM-CCD (Raptor Photonics) equipped with a Texas Instruments TC247SPD sensor. The high sensitivity offered by this type of device allows imaging of faint stars with short exposure times (10-40 ms typically) in order to "freeze" the effects of turbulence for subsequent reduction either by lucky imaging or speckle interferometry (Serot 2011a, 2011b, and 2014). Technical data for this camera are summarized in Table 1. The camera was connected to the computer running the acquisition software through a high-speed CameraLink cable.

The native focal length of the telescope (2.8 m, F/D=10) was augmented to 11m using a telecentric amplifier (Televue Powermate 5x), resulting in a scale factor of 0.13''/pixel (pixel size = 10 µm).

An atmospheric dispersion corrector, using a simple pair of Risley prisms (Pierro Astro), was inserted in the optical path (Figure 2) to compensate for the effects of atmospheric dispersion when imaging stars were not close to the zenith. An IR-cut filter (rejecting all wavelength above 700 nm) was also systematically used.

Image Acquisition and Reduction

Acquisition was carried out with a dedicated software, Genika Astro 6 from (Airylab). Acquisition sequences (between 1000 and 2000 images, depending on the seeing conditions and/or star brightness) were stored in .SER format before being converted to FITS format for further processing. Except for very bright stars, the electron-multiplying gain was generally set between 3000 and 3200 (the range is 0-3500). Exposure time for individual images typically ranged from 10 to 40 ms (longer exposure times tended to blur the speckle patterns in most of seeing conditions).

Precise on-sky scale and orientation calibration was performed each observing night using a pair of calibration stars taken from a list available from the SAF website (Maury et al. 2007).

Selection of the binaries to measure was carried out using the latest, online version of the WDS catalog (Mason et al. 2015) with the help of a dedicated software, developed by the author and called

WdsPick. Selection criteria include the position (hour, angle, and declination), the magnitude of the components, their last known separation, the total number of measurements, and the date of the last measure. The goal was to restrict measurements to binaries with brightness and separation within the capabilities of the equipment on the one hand, and to favor measurements of binaries which have not been measured for a significant time on the other hand. Figure 3-a shows the selection window of WdsPick. After selection, the navigation window (Figure. 3-b) can be used to navigate within the list and view both the data extracted from the WDS and the date of all previous measurements. The WdsPick software can connect to a sky catalog and mount control softwares such as SkyChart Chevally so that a simple click on the GoTo button under the former automatically points the telescope to the corresponding star (this only requires that the latter includes the WDS catalog and can physically control the telescope mount.). A flip-mirror and a crosshair eyepiece allows visual inspection of the target field for finely adjusting the telescope position if necessary (the camera field of view is only 80″ x 60″). With this set-up, it is possible to measure up to twenty binaries per hour. WdsPick can also access the databases of all existing measurements of the observer and display if a selected binary has already been measured and, if yes, when and with which instrument.

Figure 1. The Celestron C11 in observational position.

Image pre-processing and reduction was carried out with the Reduc software (version 4.7), developed by F. Losse (2015). Pre-processing essentially consisted of bias substraction. Two measurement methods were used : lucky imaging and speckle interferometry. Lucky imaging proceeds by selection, re-centering, and addition of the best images of the sequence (typically, between 10 and 50 images, i.e. around 1-3%). It is used essentially to get a direct image of the binary, in order to overcome the quadrant ambiguity of the other method and, exceptionally, when the other method fails because the companion is too faint. Speckle interferometry relies on the computation of the auto-correlation of the whole sequence, post-filtering using a local adaptive filter to improve contrast and measurement of the relative positions of the two auto-correlation peaks. This is performed using dedicated functions in Reduc 4.7.

Figure 2. Optical train for measurements. From left to right: focuser (Crayford), flip-mirror (with crosshair eyepiece), filter wheel, Powermate, Raptor Kite EM-CCD (with power supply and CameraLink cables). The ADC is not present here. It is normally mounted just before the Powermate.

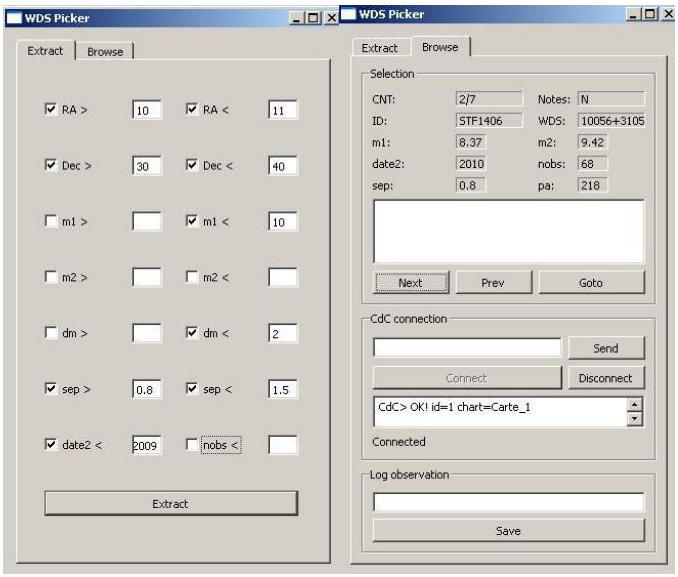

Figure 3. The WdsPick software. Left: Criteria selection window. Right: Browsing and control window.

Figure 4 shows some examples of images obtained during the reduction process. For each example, we give the magnitude of both components and the measured separation. The left image is the one obtained by lucky imaging (with 10-30 images added) and the right image is the auto-correlogram (computed on 1000 images), after post-filtering.

Measures obtained with Reduc were then entered into the dedicated database (also developed by the author) for archiving, analysis, and publication. The complete database is available online at *http://www.pierro-astro.com/materiel-astronomique/accessoires-optiques/correcteurs-reducteurs/a-d-c-correcteur-de-dispersion-atmospherique_detail.*

Sensor	Texas Instruments TC247-SPD
Sensor type	1/2" Frame Interline Transfer
Active pixels	658x496 pixels
Pixel size	10 μm x 10 μm
Active area	6,58 x 4,96 mm
Full Well capacity	24000 e-
Non linearity	< 1%
Readout noise	<1 e- with EM gain on <20 e- with EM gain off
Dynamic range	87 dB
Peak QE	52% @ 530nm
Spectral response	350-1100 nm
Refroidissement	Intégré. -20°C pour t=+20°C
Dark current	< 1^e- / pixel / sec
Output format	16 bit CameraLink
Dimensions	97 mm x 68 mm x 61 mm
Weight	550 g

Table 1. Technical specifications of Raptor Kite EM-CCD camera used for the measurements.

Target Selection

The choice of the binaries to measure was dictated by the intrinsic capabilites of the experimental setup : angular resolution (0.42″ in our case), sensor sensitivity, and overall signal-to-noise ratio on the one hand, and average seeing on the other hand. Our experience has led us to retain the following limits:

1. $h \geq 30°$
2. magnitude m1 of the primary component ≤ 10.5
3. magnitude m2 the secondary component ≤ 13
4. difference in mag. between the components ≤ 2
5. separation between 0,4″ and 2″

Criteria 1 derives from the correction range of our ADC. Moreover, under 30°, the impact of the turbulence is generally too strong to get usable images.

Criteria 2 and 3 derive from the intrinsic sensitivity of our camera, taking into account the local seeing. In fact, even with an EM-CCD, the brightness of measurable stars is still limited in the end by the local sky background. This background has a significant impact on the photon (shot) noise. Contrary to the thermal noise and the readout noise, which are negligible – thanks to the short exposure times and the EM gain respectively – the background noise largely dominates in an urban site.

Criteria 4 and 5 result from both from experience and utility considerations. Obtaining reliable measures with dM>2 is very difficult except for well separated pairs. Moreover, these well separated pairs rarely need to be re-measured because of their very slow apparent motion.

Some measures outside the aforementioned limits have, on exception, been included in the selection, either because they have a specific interest (e.g. large dM, pair with a known orbit) or just because they appear to be near another selected pair.

Figures 5, 6, and 7 show the distribution of all measurements according to the magnitude and separation of the components.

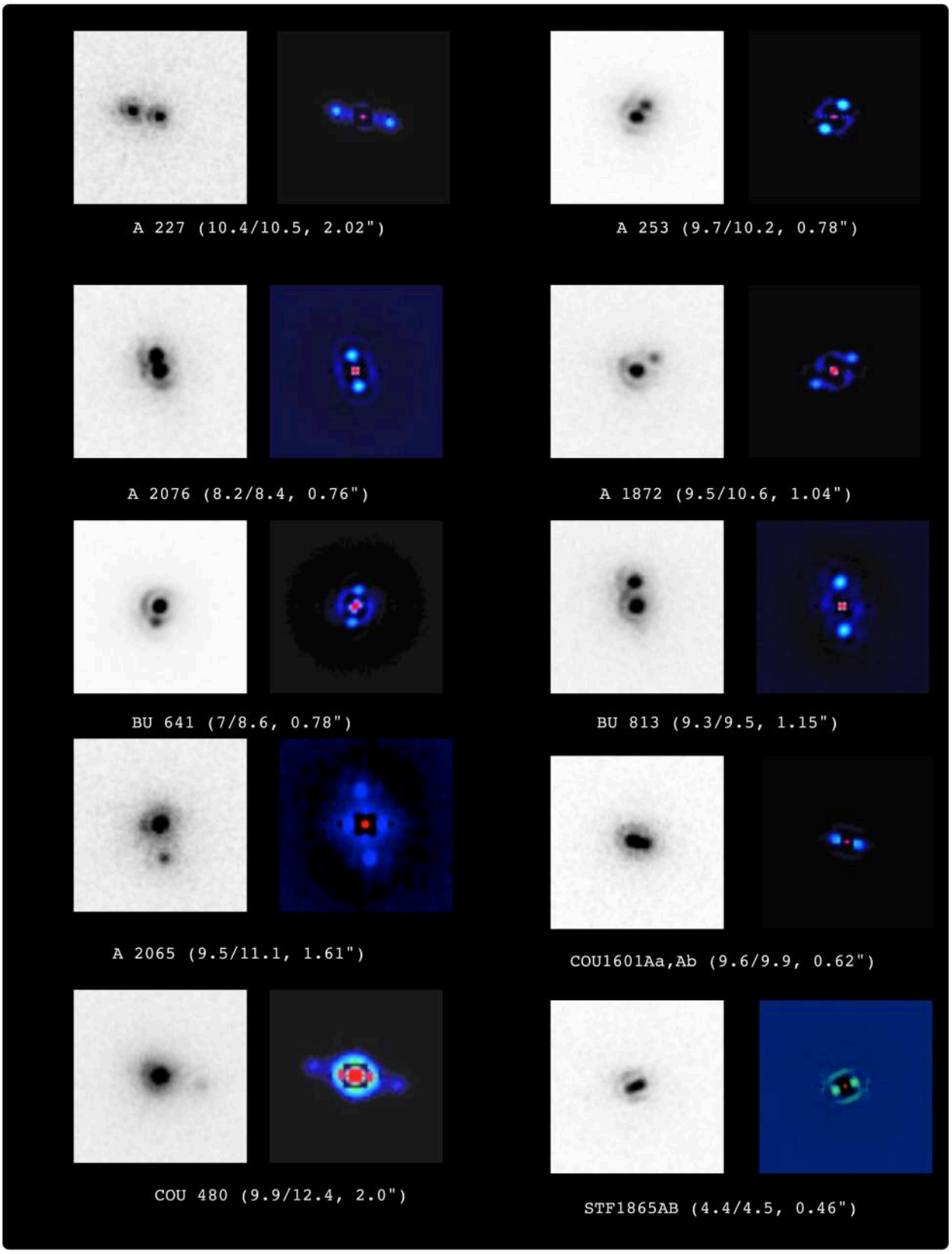

Figure 4. Examples of processed images (left : addition of N best frames, right : auto-correlogram).

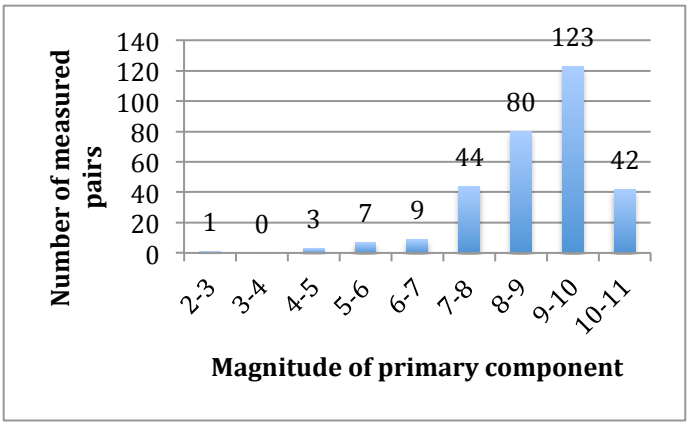

Figure 5. Distribution of measurements according to the magnitude of the primary component.

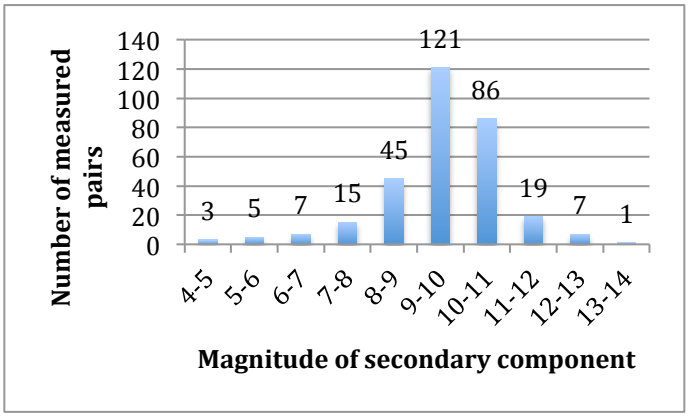

Figure 6. Distribution of measurements according to the magnitude of the secondary component.

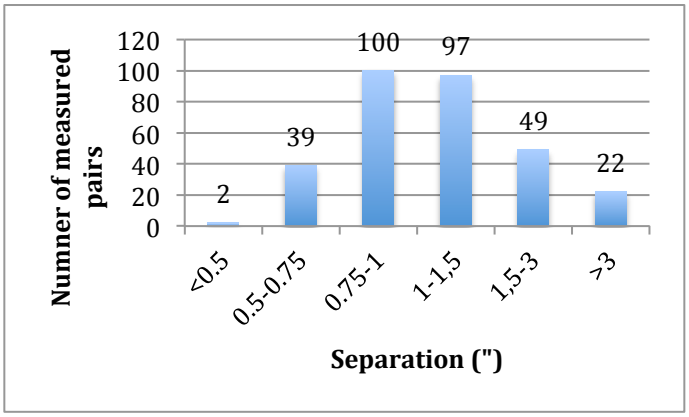

Figure 7. Distribution of measurements according to the separation of components.

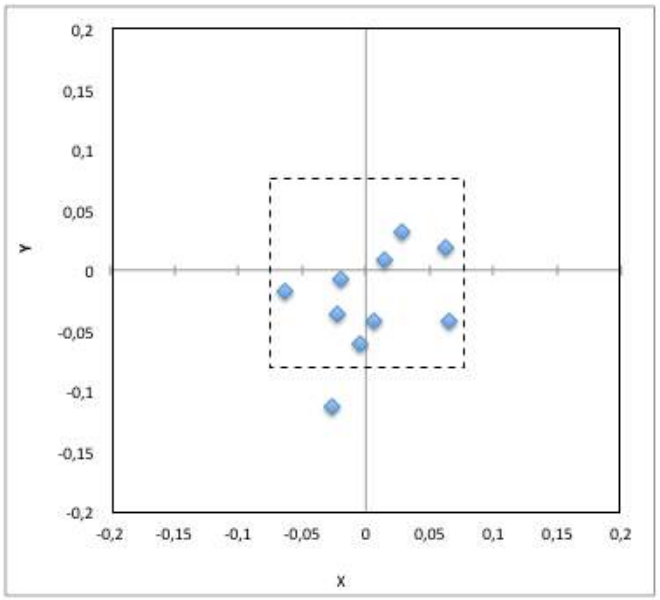

Figure 8. O-C residuals plotted in rectangular coordinates for pairs having an orbit graded 1-3. The dash-lined square represents a pixel in the used instrumental setup.

Results

The reported measures were obtained during 26 nights, between Nov 2014 and Jul 2015. The total number was 307 measures, involving 296 binaries (among these, 36 had a published orbit).
The measures are summarized in Table 2, provided after the References section on page 199.

For pairs having a known orbit, Table 3 (also provided after References section, page 210) gives the O-C residuals, computed from the ephemerids published in the 6th orbit catalog (Hartkopf & Mason 2009).

For pairs having an orbit graded 1-3, the residuals are plotted in Figure 8 using a polar to rectangular conversion, in order to assess the precision of the measurements.

Acknowledgments

This research has made use of the Washington Double Star and 6th Orbit catalogs maintained at the U.S. Naval Observatory.

The author would like thank F. Losse, developer of the Reduc software, for the quality and usefulness of this tool and for his kind and very valuable support.

References

AiryLab. http://www.airylab.com/index.php?option=com_content&view=article&id=50&Itemid=89.

Astro(spacehere)Surf. http://www.astrosurf.com/legalet/MesuresDoubles/mesures.html.

Chevalley, P. SkyChart. http://www.api.net/skychart/start?id=en/start.

Hartkopf, W.I., & Mason, D.B. 2009. *Sixth Catalog of Orbits of Visual Binary Stars*. USNO. http://www.usno.navy.mil/USNO/astrometry/optical-IR-prod/wds/orb6.

Losse, F. 2015. Reduc, v4.7. http://www.astrosurf.com/hfosaf.

Mason, D.B., Wycoff G.L., &Hartkopf, W.I. 2015. *Washington Double Stars Catalog*. USNO. http://www.usno.navy.mil/USNO/astrometry/optical-IR-prod/wds/WDS.

Mauroy, F., Mauroy, P., & Morleterase, G. 2007. Liste de 32 couples étalons. O&T. Available online at http://saf.etoilesdoubles.free.fr/documents/COUPLES%20ETALONS%20Guy%20-%20Pascal.pdf.

Pierro(spacehere)Astro. http://www.pierro-astro.com/materiel-astronomique/accessoires-optiques/correcteurs-reducteurs/a-d-c-correcteur-de-dispersion-atmospherique_detail.

Raptor Photonics. http://www.raptorphotonics.com/product/kite-30.

Sérot, J. 2011a. Mesures d'étoiles doubles avec un télescope de 150mm et une caméra EM-CCD. *Observations et Travaux*, 78.

Sérot, J., Trégon B., & Grasse, F. 2011b. Mesures d'étoiles doubles à la lunette de 50cm de Nice et au télescope de 60cm du Pic du Midi de Bigorre. *Observations et Travaux*, 78.

Sérot, J. 2014. Mesures d'étoiles doubles : campagne 2014-2014. *Observations et Travaux*, 83. In preparation.

.

Table 2. Measurements.

NAME	RA+DEC	MAGS	PA	SEP	DATE	N	NOTES
A 2016	02287+0840	9.5,9.7	178.6	0.61	2014.888	1	
A 2413	02572+0153	8.2,8.6	164.9	0.54	2014.888	1	1
HO 502	03150+3543	9.5,10.1	13.6	0.77	2014.888	1	
A 2224	03163+1920	8.2,9.6	332.2	0.86	2015.044	1	
STF 377AB	03206+1911	8.7,9.3	109.9	1.1	2015.044	1	
STF 381	03233+2058	7.5,8.7	108.2	1.01	2015.044	1	
A 2344AB	03261+2015	9,9.7	195	1.22	2015.044	1	
STF 395	03286+2904	8.6,9.8	89.3	1.83	2015.044	1	
A 1931	03318+0749	8.7,9.5	55.7	0.84	2014.888	1	
BU 533AB	03356+3141	7.5,7.7	222.5	1.01	2015.044	1	
BU 536AB	03463+2411	8.1,9.3	177.9	1	2015.044	1	
STT 66	03521+4048	8.1,8.5	144.6	0.99	2015.044	1	
STF 520	04182+2248	8.2,8.4	79.3	0.68	2015.044	1	1
STT 82AB	04227+1503	7.3,8.6	330.8	1.17	2015.044	1	
HO 15	04245+3007	10,10	147.9	0.78	2015.044	1	
A 1005	04256+3210	9,9.8	245.8	0.77	2015.044	1	
HU 608	04262+3544	10,9.9	48.2	0.71	2015.044	1	1
A 1837	04284+3826	9.4,10.8	132.3	1.51	2015.044	1	
STF 567	04367+1930	9,9.2	344.2	2.05	2015.044	1	1
BU 404	04561+0908	9.6,9.7	290.7	1.65	2015.044	1	
HU 1091	04567+3917	9.7,9.9	36.4	0.83	2015.044	1	
STF 899	06228+1734	7.4,8	18.1	2.05	2015.03	1	
J 690	06308+1004	9.3,10.8	359.2	1.7	2015.047	1	
STF3117	06414+0944	9.1,9.7	76.5	0.9	2015.047	1	
J 697	06436+1109	9.1,10.5	182	1.96	2015.047	1	
AG 119	06446+2327	8.9,9.1	83.4	1.51	2015.047	1	

A 2731AB	06487+0737	8.2,9.5	68.3	1.35	2015.047	1	
COU 917AB	06487+1913	9.1,9.6	250.3	0.89	2015.047	1	
J 56	06526+0314	9.3,9.7	333.9	1.5	2015.047	1	
STF 981	06555+3010	8.7,8.9	299.7	0.96	2015.047	1	1,2
HO 342	07028+1305	7.9,8.7	86.5	1.14	2015.047	1	
STF1037AB	07128+2713	7.2,7.2	305.6	0.86	2015.03	1	
A 2525	07138+1756	8.4,9.8	99.8	0.86	2015.047	1	
KU 28	07162+0535	9,10	323.7	1.04	2015.047	1	
BU 330	07196-0055	8.7,9.8	214	1.3	2015.047	1	
A 2863	07202-0001	9.2,9.4	288.2	1.18	2015.047	1	
STF1074AB	07205+0024	7.4,7.8	172	0.8	2015.047	1	
HU 706	07251+1956	9.1,9.5	209.7	0.42	2015.047	1	
A 2868	07292+1253	8.5,8.9	21.9	0.69	2015.047	1	
STF1116	07345+1218	7.8,8.5	95.6	1.76	2015.047	1	
STT 182	07527+0323	7.8,7.9	10.6	0.82	2015.047	1	
A 2954AB	08005+0955	8.4,8.9	341.3	0.59	2015.047	1	
A 2954AB,C	08005+0955	7.9,12	47.4	3.49	2015.047	1	
STF1175	08024+0409	7.8,9.1	283.4	1.34	2015.047	1	1
STT 186	08033+2616	7.7,7.9	72.25	0.96	2015.0385	2	
A 1971	08061-0047	9.2,9.4	4.9	0.91	2015.047	1	1
HU 849	08091+3714	9.6,9.8	283.1	1.17	2015.112	1	
STF1196AB	08122+1739	5.3,6.2	21.8	1.09	2015.047	1	
STF1196AB	08122+1739	5.3,6.2	21.9	1.13	2015.112	1	
STF1196AC	08122+1739	5.3,5.8	61.7	6.4	2015.047	1	
STF1196AC	08122+1739	5.3,5.8	61.8	6.47	2015.112	1	
STF1196BC	08122+1739	6.2,5.8	69	5.58	2015.047	1	
STF1196BC	08122+1739	6.2,5.8	69.3	5.63	2015.112	1	
STF1197	08127+2933	9,9.6	99.5	1.83	2015.112	1	
PRT 3	08138+1538	8.6,9.9	339.7	1.5	2015.112	1	
HU 625	08175+3250	9.6,10.9	355.2	1.78	2015.112	1	

HU 855	08224+1309	9.8,10.5	254.4	0.85	2015.112	1
HDS1213Aa,Ab	08296+5203	9.2,9.6	323.3	0.93	2015.192	1
BU 209	08432+3849	8.7,9	9.5	1.25	2015.112	1
A 2546	08437+1654	9.7,10	220.3	1.14	2015.112	1
A 2472	08444+1555	9.1,9.2	256.5	0.75	2015.047	1
STF1279	08500+3935	9.1,9.2	87.5	1.23	2015.112	1
STF1271	08501+5612	9.4,10.2	80.7	0.93	2015.192	1
PER 1	08512+0820	8.3,9.5	353.7	0.84	2015.047	1
STF1275AB	08514+5732	8.6,8.8	198.2	1.87	2015.192	1
STF1291AB	08542+3035	6,6.3	310.1	1.55	2015.192	1
STF3120AB	08561+4341	8.4,8.9	1	1.35	2015.192	1
A 2968	08571+1045	9,9.4	132.4	1.11	2015.047	1
A 2968	08571+1045	9,9.4	130.9	1.09	2015.112	1
A 1973	08581+2634	9.4,10.7	103.7	1.12	2015.047	1
STF1296	08593+3457	9,9.9	75.8	1.76	2015.192	1
BU 211	09020+0240	7.3,8.7	264.5	0.95	2015.047	1
HU 720	09033+4740	8.6,9.2	139.9	0.72	2015.192	1
COU2619	09088+4416	9.5,10.5	240.3	1.13	2015.192	1
STF1339	09210+3643	9.1,9.8	65.4	1.38	2015.112	1
AG 165	09233+2211	9.9,10.1	15.2	1.27	2015.112	1
STT 201AB	09239+2754	8.4,9.4	206.1	1.21	2015.112	1
HU 869	09252+1449	9.8,9.7	267	0.72	2015.112	1
A 4	09263+3109	9.5,10.6	35.3	0.84	2015.112	1
A 1985	09300+4216	8.6,8.7	24.2	1.57	2015.192	1
A 2053	09444+4047	9.4,10.6	86.3	0.73	2015.112	1
STF1381	09513+6037	8.9,9.2	186.4	0.77	2015.192	1
STF1397	09567+2503	9.3,10.6	96.3	1.13	2015.112	1
A 2482	09599+1610	9.2,10	47.3	0.7	2015.112	1
STT 210	10026+4622	8.5,9	255.7	1.23	2015.192	1
HU 631	10040+3239	8,9.3	255.1	0.7	2015.112	1

STF1406	10056+3105	8.3,9.4	220.8	0.8	2015.112	1	
A 2142	10057+4103	7.9,8.8	296.1	1	2015.192	1	
A 2564	10083+0802	9.8,9.9	276.4	0.77	2015.189	1	
STT 213	10131+2725	8.6,9.8	121.7	1.07	2015.112	1	1
STT 215	10163+1744	7.2,7.4	176.3	1.49	2015.279	1	1
A 1990	10234+2630	9.4,9.6	290.5	1.48	2015.112	1	
STF1429	10250+2437	9,9.3	156.2	0.78	2015.112	1	1
HU 877	10255+3647	9.1,10.4	249.6	1.69	2015.112	1	
STT 217	10269+1713	7.8,8.5	146.3	0.73	2015.112	1	1
STF1439	10301+2048	8.3,8.8	71.1	1.34	2015.189	1	
STF1457	10387+0544	7.6,8.1	334.6	1.8	2015.189	1	1
STT 228	10473+2235	8.1,8.9	169.3	0.68	2015.189	1	
BU 597	10548+2345	9.2,10.1	46.9	0.92	2015.189	1	
STF1501	11023+3049	9.8,10.1	186.3	1.33	2015.189	1	
A 1590	11035+5432	8.9,9.6	328.9	1.45	2015.192	1	1
A 1590	11035+5432	8.9,9.6	329.7	1.47	2015.266	1	1
STF1504	11040+0338	7.9,8	122.9	1.16	2015.189	1	
HO 378AB	11050+3825	8.2,9.1	236.2	0.98	2015.192	1	
STF1517AB	11137+2008	7.5,8	318.1	0.73	2015.189	1	
STF1519	11156+5947	9,9.9	289.7	1.43	2015.266	1	
STF1523AB	11182+3132	4.3,4.8	176.4	1.79	2015.189	1	
STF1555AB	11363+2747	6.4,6.7	151.3	0.76	2015.192	1	
STT 237AB	11390+4109	8.1,9.3	243.7	2.03	2015.266	1	
STT 243	11598+5324	9,9.6	9.1	1	2015.192	1	
STT 243	11598+5324	9,9.6	7.8	1.14	2015.266	1	
STF1606	12108+3953	7.4,7.9	151.2	0.58	2015.258	1	1
STF1613	12126+3546	9.2,9.3	7.2	1.13	2015.192	1	
STF1613	12126+3546	9.2,9.3	10.7	1.08	2015.258	1	
STT 251	12291+3123	8.3,9.2	61	0.77	2015.192	1	1
STT 251	12291+3123	8.3,9.2	61.4	0.66	2015.258	1	1

STF1647	12306+0943	8,8.3	247.9	1.22	2015.258	1	1
A 1600	12329+5448	8.5,9.8	7.8	0.77	2015.26	1	
COU 595	12340+2650	9.4,10.3	182.5	0.92	2015.258	1	
COU 595	12340+2650	9.4,10.3	187	0.9	2015.26	1	
STF1667AB	12396+6440	9.4,9.9	38.4	1.13	2015.192	1	
J 432	12454+0331	9,9.7	250.6	0.91	2015.26	1	
COU 397	12575+2457	9,9.7	63.4	0.7	2015.258	1	
STF1709	13025+2330	7.8,10	251.6	2.69	2015.353	1	
HO 257	13058+2614	10.3,10.9	154.5	1.97	2015.299	1	
STF1730	13121+3655	9.2,10.4	338.3	1.84	2015.299	1	
STT 263	13166+5034	9.5,9.7	137	1.75	2015.299	1	
HU 644AB	13198+4747	9.1,9.8	87.9	0.78	2015.26	1	
A 565	13222+2710	9.8,10.2	16.3	0.85	2015.282	1	
HO 260	13235+2914	9.6,9.9	88.4	1.66	2015.299	1	1
AG 187	13272+2028	10.4,10.7	306.9	1.56	2015.299	1	
A 1610	13333+4526	9.7,10	268.75	0.875	2015.2905	2	
A 1792	13340+0847	8.4,9.5	309	0.76	2015.282	1	
STF1771	13367+6947	8.7,9.3	81.7	1.74	2015.266	1	
A 1611	13368+0650	8.9,9	118.8	0.79	2015.282	1	
STF1770	13377+5043	6.9,8.1	122.4	1.73	2015.266	1	
STF1781	13461+0507	7.8,8.1	196	0.98	2015.282	1	1
STF1781	13461+0507	7.8,8.1	198.4	0.88	2015.299	1	1
A 685	13512+2948	9.9,10.3	25	0.77	2015.282	1	
STT 273AB	13563+0517	8.6,8.8	109.3	0.93	2015.282	1	
BU 937	13571+3426	9,9.4	135.6	0.91	2015.26	1	
A 1614	13577+5200	8.9,9.1	120	1.41	2015.26	1	1
STF1794	13598+1953	9.4,9.6	125.9	1.9	2015.299	1	
A 687	14002+2826	10.4,10.5	312.7	1.15	2015.299	1	
HWE 29AB	14033+0557	9.9,9.8	236.9	1.23	2015.282	1	
A 2064	14034+1740	9.6,11	179.3	0.97	2015.373	1	

HDS1980Aa,Ab	14068+5946	9.7,11.4	258.3	1.41	2015.373	1	
A 346	14078+2443	10.3,10.4	310.1	0.87	2015.299	1	
STT 276AB,C	14082+3645	8.4,10.6	71.5	9.61	2015.282	1	
STT 276AB,C	14082+3645	8.4,10.6	72.2	9.5	2015.373	1	2
A 2065	14083+1644	9.5,11.1	341.9	1.61	2015.373	1	
COU 480	14127+2547	9.9,12.4	72.8	2	2015.353	1	
BU 224	14135+1234	8.9,9.3	94.8	0.65	2015.282	1	1
KUI 66	14148+1006	5.4,8.4	111.4	0.84	2015.373	1	
STF1819AB	14153+0308	7.7,7.9	167.4	0.9	2015.282	1	
BU 1272AB	14178+4845	9.4,10.3	321	23.43	2015.373	1	3
HJ 2710AC	14178+4845	9.4,9.7	138	1.33	2015.373	1	4
HU 901	14184+3412	9.7,9.8	43.4	0.69	2015.282	1	
BU 1273	14185+4755	9.5,10.8	174.6	1.31	2015.373	1	
STF1834	14203+4830	8,8.2	103.8	1.65	2015.373	1	1
COU 482	14213+3050	9.9,9.9	124.4	0.77	2015.373	1	
A 148	14220+5107	8.3,8.9	189.5	0.58	2015.373	1	
A 149AB	14234+4736	9.4,9.8	124	0.78	2015.373	1	
STF1848	14278+3257	8.6,11.6	356.7	3.13	2015.353	1	
A 688	14333+2725	9.9,10.2	12.7	0.8	2015.373	1	
COU 406	14403+2549	9,12	18.4	3.48	2015.353	1	
STF1865AB	14411+1344	4.4,4.5	287.3	0.46	2015.353	1	
STF1877AB	14450+2704	2.5,4.8	343.5	2.89	2015.353	1	
COU 608	14499+3200	9.2,11.8	201.5	1.7	2015.373	1	
HU 1153	14516+1519	8.5,11.2	296.1	3.07	2015.353	1	
STT 289	14560+3218	6.2,10.2	110.4	4.82	2015.353	1	
STF1909	15038+4739	5.2,6.1	65.4	0.89	2015.282	1	1
STF1908AB	15049+3428	9.2,10.3	152.1	1.29	2015.282	1	
HEI 378	15054+1338	9.6,10.7	352.2	1.63	2015.425	1	
STF1907	15056+1138	9.1,9.1	348.5	0.87	2015.373	1	
STF1911	15077+1158	10,10.4	291.2	1.98	2015.425	1	

A 1116	15116+1007	8.8,8.6	53.7	0.76	2015.425	1	
A 1366	15162+3418	9.3,12.2	78	3.82	2015.353	1	
STF1937AB	15232+3017	5.6,5.9	207.3	0.7	2015.4	1	
HU 909	15232+6100	8.5,10.6	281.6	1.4	2015.4	1	
HU 149	15246+5413	7.4,7.6	272.3	0.72	2015.4	1	
COU 974	15306+3504	10.5,11.3	337.7	1.54	2015.425	1	
COU 610	15329+3122	4.2,6.2	205.1	0.79	2015.353	1	
HU 746	15344+3201	8.8,11.5	216.4	2.02	2015.353	1	
LEO 33	15352+1456	10.4,10.4	258	1.55	2015.425	1	
STT 298AB	15360+3948	7.1,8.4	185.5	1.19	2015.4	1	
HU 652	15361+4849	9.2,9.5	185.9	1.16	2015.4	1	
HU 1167AB	15382+3615	8,9.8	81.7	1.34	2015.4	1	5
STF1964AC	15382+3615	8,8	861	4.99	2015.4	1	6
STF1964AD	15382+3615	8,9	80.8	15.69	2015.4	1	6
STF1964CD	15382+3615	8,9	20.2	1.56	2015.4	1	6
HU 579	15404+2123	9,9.3	138.2	0.72	2015.4	1	7
A 2076	15405+1840	8.2,8.4	185.9	0.76	2015.4	1	1
COU 617	15514+2921	9.5,12.5	97.2	4.77	2015.353	1	
HO 399	15554+2932	7.6,10.4	117.4	3.66	2015.353	1	
HU 154	16004+5431	7.8,10.8	298.4	1.39	2015.4	1	
HEI 240	16027+1257	9.8,10.7	115.4	1.19	2015.458	1	
STF2004	16032+2851	9.5,10.3	278	1.81	2015.458	1	
A 1642	16137+4638	8.8,9.3	180.6	0.82	2015.4	1	1
A 348	16161+2936	9,10.9	152.5	0.96	2015.4	1	
A 226	16273+2653	9.4,11.8	94.4	1.01	2015.4	1	
BU 813	16280+2632	9.3,9.5	177	1.15	2015.4	1	
STF2057AB	16316+1917	10.4,10.6	268.3	4.92	2015.458	1	
YNG 1	16316+5746	8.5,9.7	216.2	1.25	2015.4	1	
STF2058AB	16317+1919	10.3,10.5	351.8	2.06	2015.458	1	
STF2058AC	16317+1919	10.3,12.3	141.1	15.31	2015.458	1	

BU 817	16326+2314	9.3,9.5	328.6	0.88	2015.458	1	
HU 486	16395+2244	10.2,10.8	163.8	1.17	2015.458	1	
A 227	16469+2701	10.4,10.5	237.3	2.02	2015.458	1	
A 575	16509+4259	9.6,10.2	148.6	0.73	2015.4	1	
HU 1278	16522+1535	10,10	358.8	1.22	2015.458	1	
A 350	16540+2906	9.4,9.6	150	0.64	2015.4	1	
HEI 70	16557+1544	10,12.1	318.1	1.23	2015.458	1	
HEI 71AB	16569+1540	10.3,11.4	253.1	1.26	2015.458	1	
A 1872	16578+4344	9.5,10.6	119.9	1.04	2015.4	1	
HU 1279	16598+1319	10.4,11.6	156.4	1.64	2015.458	1	
STT 322	16598+3655	7.9,10.1	205.3	1.4	2015.4	1	
COU1290	17007+3951	10.4,10.5	34.2	0.79	2015.463	1	
HU 489	17155+2007	10.3,10.8	36.3	1	2015.474	1	
HO 414AB	17222+2605	9.4,9.7	103.4	0.78	2015.474	1	
COU 112	17228+2428	10,11.8	23.8	1.38	2015.474	1	
HO 415	17231+2545	8.8,9.6	344.6	0.85	2015.474	1	
STF2163	17234+4209	10.2,10.4	73.2	1.43	2015.504	1	
HU 671	17238+2155	8.7,9.7	259.4	0.82	2015.474	1	
STF2162	17239+3627	9.3,9.5	283.9	1.28	2015.504	1	
A 2089	17249+4701	9.9,10.1	330.3	0.72	2015.474	1	
HU 923	17344+4913	9.4,9.9	105.2	0.93	2015.463	1	
A 694	17383+4242	9.7,11.3	102.3	1.1	2015.474	1	
STF2203	17412+4139	7.7,7.8	293.6	0.75	2015.463	1	
D 16BC	17433+4345	10.1,11.6	149.9	0.9	2015.474	1	8
STF2214AB	17433+4345	9.6,10.1	211.5	19.66	2015.474	1	9
HO 560AB	17434+3357	8.8,9.1	262.9	1.38	2015.493	1	
HU 1284	17436+1257	9.5,10.7	63.3	0.93	2015.504	1	
HU 1285	17436+2237	8.8,9.1	214.7	0.61	2015.463	1	1
STF2206	17445+1900	8.8,9.8	247.9	0.9	2015.463	1	
COU 631	17455+2950	10.4,13.6	51.3	5.64	2015.504	1	

HU 1287	17456+1553	10,10.2	63.3	1.91	2015.463	1	
STF2205	17457+1743	9.3,9.5	9.4	0.87	2015.463	1	1
AC 7BC	17465+2743	10.2,10.7	289.2	0.75	2015.493	1	10
BAR 8	17486+2339	8.6,10.4	238.2	1.15	2015.474	1	
TDT 536	17513+1723	10.3,10.7	61.8	0.99	2015.504	1	
STT 338AB	17520+1520	7.2,7.3	162.7	0.74	2015.463	1	
COU1599	17531+4212	9.7,9.7	143.4	0.68	2015.463	1	
STF2243	17533+3605	9.1,9.4	38.4	1.06	2015.493	1	
AC 9	17541+2949	9,9.1	242	1.01	2015.474	1	
COU1601Aa,Ab	17555+4108	9.6,9.9	63.8	0.62	2015.493	1	
BU 417	17562+3926	8.2,10	319.3	0.89	2015.493	1	
COU 999	17566+3045	10,10.6	311.6	1.42	2015.493	1	
HU 1184	17569+3236	9.4,10.2	205	0.86	2015.493	1	
HO 424	17577+2815	8.4,10.7	203.7	1.43	2015.493	1	
COU1002	17587+3538	7.1,9.7	169	0.75	2015.504	1	
HO 563AB	17599+5304	10.1,10.4	184.3	0.73	2015.493	1	
BU 1127AB	18025+4414	7.3,9.2	47.4	0.74	2015.488	1	
J 1220	18056+1242	10.2,10.2	128.8	1.5	2015.51	1	
HU 674	18097+5024	7.6,8.6	212.9	0.77	2015.488	1	1
STF2289	18101+1629	6.6,7.2	217.9	1.23	2015.493	1	1
HU 317	18113+1713	9.6,9.6	205.3	1.47	2015.493	1	
A 238	18114+2519	8.5,9.5	74.6	0.68	2015.493	1	
STF2292	18121+2739	8.3,8.6	272.7	0.81	2015.51	1	
LEO 1	18121+4015	10.3,11.3	145.8	1.47	2015.493	1	
BU 1091	18126+3836	8.6,9.2	320.8	0.66	2015.504	1	1
BU 641	18218+2130	7,8.6	341.3	0.78	2015.488	1	
AG 222AB	18222+1413	9.4,9.7	145.6	1.44	2015.488	1	
HO 83	18233+2731	10.1,10.3	115.5	0.85	2015.493	1	
STF2315AB	18250+2724	6.5,7.7	114.3	0.61	2015.488	1	
BU 134	18253+4653	7.9,9.7	126	1.03	2015.51	1	

HU 66BC	18253+4846	8.4,8.2	26.6	0.82	2015.493	1	
STT 351AC	18253+4846	7.9,8.2	26.1	0.83	2015.493	1	11
COU2278	18276+4926	9.6,10.3	16.4	1.38	2015.51	1	
STF2320	18278+2442	7.1,8.9	0.8	0.87	2015.51	1	
A 246	18305+2519	10,11	166	1.39	2015.504	1	
STT 359	18355+2336	6.3,6.6	4.4	0.79	2015.504	1	1
A 249	18361+2452	10.1,10.2	275.4	1.05	2015.504	1	
STF2356	18384+2842	8.7,9.2	62.6	1	2015.504	1	
L 25	18387+2847	10.1,10.7	253.9	1.28	2015.504	1	
A 1380AB	18390+5559	10.5,10.3	20.3	0.92	2015.51	1	
COU 641	18406+2636	10.2,10.3	56.7	0.64	2015.504	1	
HU 324	18408+2142	9.4,9.9	108.5	0.85	2015.504	1	
A 253	18437+3141	9.7,10.2	134.3	0.78	2015.493	1	1
HU 755	18448+5201	9.7,9.9	126.7	0.6	2015.488	1	
HU 756	18466+5142	9.7,11.1	261.9	0.8	2015.493	1	
STF2402	18497+1041	8.9,9.2	207.7	1.48	2015.493	1	
BU 265	18502+1131	7.3,9.2	230.8	1.39	2015.504	1	
STF2409AB	18517+1331	8.4,9.6	21.6	0.94	2015.493	1	
BU 421AB	18517+4323	9.8,9.8	296.4	1.21	2015.493	1	
HU 199	18521+1148	9,9.5	344.8	0.86	2015.493	1	
STF2412	18526+1400	8.9,9	56.6	1.41	2015.504	1	
BU 137AB	18540+3723	8.6,9	163.2	1.62	2015.504	1	
COU1932	18549+4437	10.2,10.3	295.3	0.86	2015.504	1	
COU1016	18570+2747	10.3,11.1	129.7	1.05	2015.504	1	
STF2422	18571+2606	7.9,8.2	69	0.76	2015.504	1	
A 260	18576+3209	9.1,9.6	244.4	0.81	2015.504	1	
AG 366	18581+4711	8.5,8.6	186.4	1.43	2015.504	1	
STF2430	18594+2936	9,9.1	186.9	1.54	2015.504	1	
STF2437	19019+1910	8.4,8.8	2	0.63	2015.488	1	1
STT 371AB	19159+2727	7,7.5	160.7	0.87	2015.488	1	

STT 368AB	19160+1610	7.5,8.4	219.3	1.12	2015.488	1	
COU2520	19161+4407	10.2,10.8	232.7	0.9	2015.488	1	
A 157	19163+3723	10,10.5	149.2	1.47	2015.488	1	
COU1158	19174+3159	8.7,11	70.3	1.43	2015.488	1	
STT 377AB	19363+3540	9.3,9.4	34.5	0.91	2015.488	1	
STT 377BC	19363+3540	9.4,10.2	154.7	25.47	2015.488	1	
STT 378AB	19365+4101	7.7,8.9	285.9	1.39	2015.488	1	
A 598AB	19365+4124	9.9,10.1	192.6	0.98	2015.488	1	
COU2406	19371+4108	10.4,10.7	4.4	0.82	2015.488	1	
A 1241AB	23380+1253	9,9.7	9	0.66	2014.888	1	
HU 1325	23401+1258	9.8,10	41.7	0.82	2014.888	1	1

Notes:
[a]Pair having an entry in the 6th Orbit Catalog (see Table 3)
[b]Sep(AB)<0.5"
[c]AC=HJ 2710
[d]AB=BU 1272
[e]AC=STF1964
[f]AB=HU1167
[g]mB seems largely south estimated in the WDS (probably fainter than 10)
[h]AB=STF2214
[i]BC=D16
[j]A,BC=STF2220
[k]AB=HU66

Table 3. O-C Residuals for pairs having an known orbit.

NAME	RA+DEC	DATE	O-C(PA,SEP)		GRADE	REF
A 2413	02572+0153	2014,888	1,2	-0,04	3	Hrt2010a
STF 520	04182+2248	2015,044	-2,9	0,07	3	Hrt2001b
HU 608	04262+3544	2015,044	-4,2	0,12	5	Hrt2009
STF 567	04367+1930	2015,044	1,2	0,02	5	USN2002
STF 981	06555+3010	2015,047	6,3	-0,01	5	Hop1971
STF1175	08024+0409	2015,047	-7,3	-0,05	5	Ole2001
A 1971	08061-0047	2015,047	-354	0,09	5	Ole1993
STT 213	10131+2725	2015,112	1	0	4	Sca2008e
STT 215	10163+1744	2015,279	-2,1	-0,07	4	Zae1984
STF1429	10250+2437	2015,112	-0,7	0,02	5	Zul1981
STT 217	10269+1713	2015,112	-2,2	-0,05	3	Sca2013b
STF1457	10387+0544	2015,189	1,1	-0,04	4	RAO2014
A 1590	11035+5432	2015,192	-2,9	-0,06	5	Baz1985b
A 1590	11035+5432	2015,266	-2,1	-0,04	5	Baz1985b
STF1606	12108+3953	2015,258	5,6	0,03	4	Msn1999a
STT 251	12291+3123	2015,192	-0,2	0,09	5	Sca2003c
STT 251	12291+3123	2015,258	0,1	-0,02	5	Sca2003c
STF1647	12306+0943	2015,258	-3,7	-0,02	4	Hop1970
HO 260	13235+2914	2015,299	1,1	0,03	3	Zir2013a
STF1781	13461+0507	2015,282	1,2	0	3	Alz2007
STF1781	13461+0507	2015,299	3,6	-0,1	3	Alz2007
A 1614	13577+5200	2015,26	0	0,02	3	RAO2014
BU 224	14135+1234	2015,282	-5	0,01	4	Lin1985c
STF1834	14203+4830	2015,373	0,1	0,07	3	USN2000c
STF1909	15038+4739	2015,282	-2,6	-0,05	2	Zir2011
A 2076	15405+1840	2015,4	0,5	0,03	4	Zir2014a
A 1642	16137+4638	2015,4	0,2	0,04	4	Hrt2001b
HU 1285	17436+2237	2015,463	2,8	0,11	4	USN2002
STF2205	17457+1743	2015,463	0,4	-0,11	4	Cve2008a
HU 674	18097+5024	2015,488	3,9	0,29	5	USN2002
STF2289	18101+1629	2015,493	2,3	-0,01	4	Hop1964b
BU 1091	18126+3836	2015,504	1,8	-0,1	5	Zir2012b
STT 359	18355+2336	2015,504	0,3	0,04	3	Sca2009a
A 253	18437+3141	2015,493	-1,3	0,16	4	Baz1987d
STF2437	19019+1910	2015,488	-3,2	0,07	4	Sca2008c
HU 1325	23401+1258	2014,888	11,5	-0,05	5	Sca2003a

About the Editors

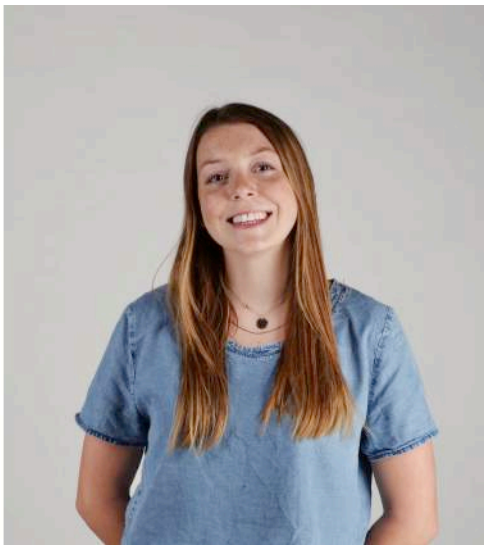

The four Editors and Editorial Consultant, Jolyon Johnson, pose for a photo. Left to right: Eric Weise (recent graduate, Mathematics and Physics, University of California, San Diego), Dr. Vera Wallen (retired School District Superintendent), Jolyon Johnson (graduate student, Science Education, University of Washington), Dr. R. Kent Clark (Emeritus Professor of Physics, University of South Alabama), and Dr. Russell Genet (Research Scholar in Residence, California Polytechnic State University). Pictured on the right: Meghan Legg, Associate Editor (Graphic Communication senior, California Polytechnic State University).